

Cluster-based redox activity in Endohedral Metallofullerenes: Electrochemical and EPR studies

Dissertation

zur Erlangung des akademischen Grades

Doctor rerum naturalium (Dr. rer. nat.)

vorgelegt der Fakultät Mathematik und Naturwissenschaften

der Technischen Universität Dresden

von M. Sc. **Nataliya Samoylova**

geboren am 13.05.1990 in Woronezh, Russland

Die Dissertation wurde in der Zeit von 10 / 2013 bis 04 / 2017 im Leibniz Institute for Solid State and Materials Research (IFW Dresden) angefertigt

Eingereicht am 17.05. 2017

Wissenschaftlicher Betreuer:

1. Prof. Dr. Gotthard Seifert, Technische Universität Dresden
2. Dr. Alexey Popov, Leibniz Institute for Solid State and Materials Research (IFW Dresden)

Gutachter:

1. Prof. Dr. Gotthard Seifert, Technische Universität Dresden
2. Prof. Dr. Biprajit Sarkar, Freie Universität Berlin

Tag der öffentlichen Verteidigung:

Table of contents

Abstract	5
Chapter 1. Introduction and background	6
1.1. Endohedral fullerenes	6
1.2. Synthesis and isolation of endohedral fullerenes	9
1.2.1. <i>Synthesis and extraction</i>	9
1.2.2. <i>Selected EMF families: synthesis and structures</i>	11
1.2.3. <i>HPLC as a main method of EMF separation</i>	16
1.2.4. <i>Alternative methods of EMFs separation</i>	19
1.3. Electrochemistry of EMFs	27
1.3.1. <i>Methods of Cyclic voltammetry and Square Wave Voltammetry</i>	27
1.3.2. <i>Cyclic voltammetry as applied to EMFs</i>	30
1.3.3. <i>Endohedral and cluster-based redox activity in different EMF families</i>	33
1.4. EPR spectroscopy	44
1.4.1. <i>Basic principles of the method</i>	44
1.4.2. <i>EPR spectroscopy applied to EMFs: several examples</i>	47
Chapter 2. Redox-active metal-metal bonds in dimetallofullerenes $M_2@C_{82}$ and comparison to sulfide clusterfullerene $Er_2S@C_{82}$ and carbide $M_2C_2@C_{82}$ analogues.	51
2.1. $M_2@C_{82}$: synthesis and isolation	51
2.2. Molecular structure determination of the $M_2@C_{82}-C_{3v}$ and $M_2@C_{82}-C_5$ EMFs	53
2.2.1. <i>Vis-NIR absorption spectroscopy</i>	53
2.2.2. <i>Vibrational spectroscopy</i>	54
2.2.3. <i>NMR spectroscopy</i>	56
2.3. Charge distribution and electronic structure	58
2.4. Electrochemistry	63
2.4.1. <i>$M_2@C_{82}$ dimetallofullerenes with $C_{82}-C_{3v}$ cage isomer</i>	65
2.4.2. <i>$M_2@C_{82}$ dimetallofullerenes with $C_{82}-C_5$ cage isomer</i>	67
2.4.3. <i>Mixed metal $M_2@C_{82}$ and $M_2C_2@C_{82}$ compounds</i>	69
2.5.1. <i>EPR spectroscopy of $Sc_2@C_{82}-C_{3v}$ cation-radical</i>	72
2.5.2. <i>SQUID Magnetometry</i>	78
2.6. Chapter summary	81
Chapter 3. Single-occupied metal bonding orbital in $M_2@C_{80}(CH_2Ph)$: electrochemical and EPR studies	82
3.1. Unique $M_2@C_{80}(CH_2Ph)$ EMFs: synthesis and structure	82

3.2. The electronic structure of neutral $Y_2@C_{80}(CH_2Ph)$ compounds: EPR investigation	84
3.3. Electrochemical studies	88
3.4. Changing of the spin states in $Y_2@C_{80}(CH_2Ph)$, upon redox activity: EPR investigations.....	94
3.5. Chapter summary	98
Chapter 4. Titanium based redox activity in $M_2TiC@C_{80}$ and $M_2TiC_2@C_{80}$ clusterfullerenes.....	99
4.1. $M_2TiC@C_{80}$ and $M_2TiC_2@C_{80}$ EMFs: structure and background	99
4.2. Electronic structure and redox behavior	101
4.3. Chapter summary	109
Chapter 5. Experimental details.....	110
Summary.....	122
References.	124
List of Publications.....	142
Acknowledgements	144

Abstract

Endohedral fullerenes are closed carbon shells encapsulating molecular or ionic species in their inner space. Obtained for the first time in 1985, endohedral metallofullerenes (EMFs) remain in focus of research for many years with a broad variety of metal atoms, endohedral cluster and cage sizes being reported.

Electrochemical studies of endohedral metallofullerenes are of particular interest because of the more complex redox behavior in comparison to empty fullerenes. The EMF molecules can be considered as a combinations of positively charged cluster and negatively charged carbon shell “ligand”, and both constituents can be redox active. A cage-based electrochemical activity is more common, in particular, the most abundant nitride clusterfullerenes generally have redox-active cages. Cluster-based electrochemical activity is less common and can be revealed via unexpected redox behavior (e.g., shifted potential when compared to analogous molecules, potential metal dependence) and with the use of spectroscopic methods.

Here we report electrochemical and EPR studies of three EMF families: (i) $M_2@C_{82-C_{3v}}$ and $M_2@C_{82-C_5}$ dimetallofullerenes with a covalent bonding between two metal atoms, (ii) $M_2@C_{80}(CH_2Ph)$ dimetallofullerene derivatives with single-occupied metal-bonding orbital, and (iii) $M_2TiC@C_{80}$ EMFs with endohedral Ti(IV) (M is either Sc or Y or a lanthanide). For the first two families, the metal-metal bonding orbital has been found to be redox active: in $M_2@C_{82}$, the double-occupied M-M bonding orbital is involved in the first oxidation process, while in $M_2@C_{80}(CH_2Ph)$ the unoccupied component of single-occupied metal-bonding orbital acts as the LUMO, accepting one electron during the first reduction step. Thus, single electron transfer reactions in both cases lead to the changes in the magnetic properties of EMFs, which is especially well revealed by EPR spectroscopy. For the series of $M_2TiC@C_{80}$ EMFs, the first reduction predominantly occurs on internal Ti atom and can be described as Ti^{IV}/Ti^{III} redox process. Due to the variation of the size of the Ti ion in different oxidation states, reduction changes the inner strain of the cluster, leading to a large variability of the Ti^{IV}/Ti^{III} reduction potential in dependence on the size of the formally inert lanthanide metal in $M_2TiC@C_{80}$.

Chapter 1. Introduction and background

1.1. Endohedral fullerenes

Along with diamond, graphite, lonsdaleite and graphene, fullerenes, hollow spherical molecules consisting of carbon pentagons and hexagons, present themselves as one of the solid carbon allotropes. Fullerenes were obtained for the first time in 1985¹ as an unexpected product of high temperature graphite vaporization, which was a part of the research activities of several astrophysicists and spectroscopists to explain formation mechanisms of long-chain carbon molecules in circumstellar shells. The Nobel Prize in Chemistry for this discovery has been awarded jointly to Robert F. Curl Jr., Sir Harold W. Kroto and Richard E. Smalley in 1996.

The concept of enclosing some particles inside the fullerene cage was suggested in the same year as the fullerenes were discovered. James R. Heath and his collaborators (working in the group of Richard Smalley) demonstrated, that addition of LaCl_3 to the vaporized graphite results in formation of C_nLa compound series, where n is an even number from 44 to more than 76². Sufficiently high stability of these new complexes approved the suggestion that the metal atom is “captured” inside the carbon shell.

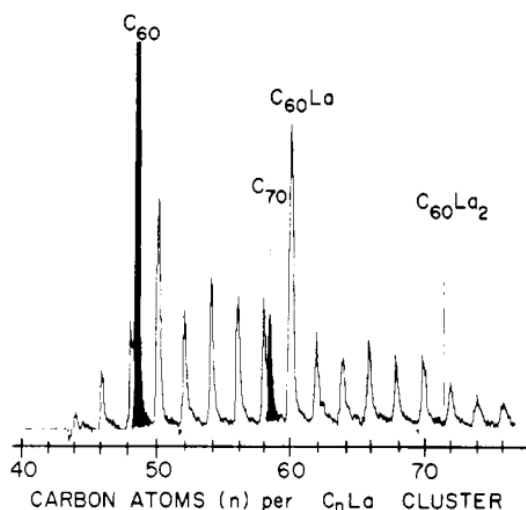


Figure 1.1. Fragment of time-of-flight mass spectrum of C_nLa cluster complexes (open peaks) and bare C_n clusters (blackened peaks) produced by laser vaporization of a lanthanum-impregnated graphite disk in a pulsed supersonic nozzle. Reproduced with permission from².

That was the first mention of Endohedral Metallofullerenes (EMFs) – fullerenes with encapsulated metal species. Nowadays the symbol @, first suggested for EMFs by Smalley in

1991³, is commonly used for their designation. This symbol is written after the formulae of the encapsulated species and before the cage formula: e.g. $Sc_3N@C_{78}$ transcription indicates that the endohedral cluster consisting of three scandium and one nitrogen atom is placed inside the C_{78} fullerene cage.

In principle there is a large number of possible ways to build fullerene cage from carbon atoms, but experimentally observed fullerenes generally consist on pentagon and hexagon rings. (Only few fullerene structures, containing also heptagons⁴⁻⁷, are known, and most of them were obtained from “normal” fullerenes under relatively harsh reaction conditions).

For a fullerene polyhedron C_n , comprising only pentagon and hexagon faces, the number of pentagons is always 12, whereas the number of hexagons is $n/2-10$, which is imposed by the Euler’s theorem. The most stable in this case are fullerenes, which obey the so-called Isolated Pentagon Rule (IPR): each pentagon should be surrounded with 5 hexagons, whereas pentagon-pentagon edges are forbidden. Structures involving adjacent pentagons were shown to exhibit various degrees of strain-related instability⁸.

In 80s and 90s the common opinion of fullerene researchers was that only IPR-cages can exist both for empty cages and endohedrals. But in 2000 at once two independent studies showed that EMFs with the cages violating IPR can be synthesized and isolated^{9,10}, and a number of non-IPR EMF structures had been described in the following years¹¹⁻¹⁵.

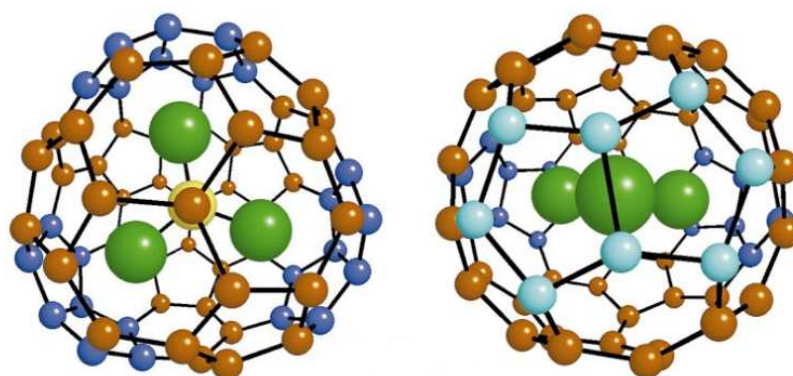


Figure 1.2. Two orthogonal views of the non-IPR $Sc_3N@C_{68}$; two adjacent pentagons are highlighted with light-blue color. Reproduced with permission from⁹.

Thus, we can say that the Isolated Pentagon Rule is not strictly obeyed in case of EMFs, although all most stable endohedral fullerenes, characterized by high synthesis yields, are IPR-isomers.

With increasing of the number of cage atoms the number of all possible isomers (both IPR and non-IPR) grows dramatically. As a consequence, the nomenclature issue becomes particularly important.

The most general approach is based on the Fowler-Monopoloulos spiral algorithm^{16,17}: starting with a sequence of three mutually adjacent faces, new faces are added to the string such that the next face is adjacent to the previous one, and that has neighboring faces left which are still not part of the spiral string. As a result, one obtains a string of length of 12 pentagons and F-12 hexagons.

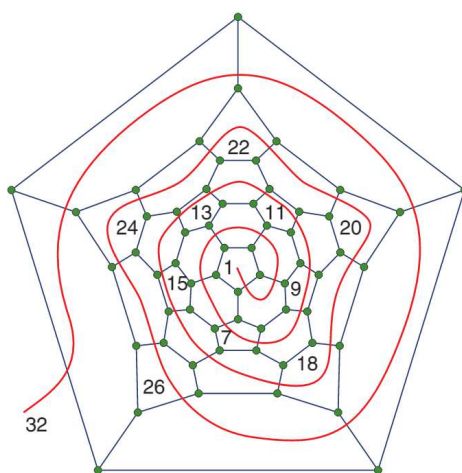


Figure 1.3. Canonical spiral of C_{60-I_h} ¹⁸

The Spiral string is then abbreviated as a list of the 12 pentagon positions, called the face spiral pentagon indices (FSPI). The lexicographically smallest of all successful spirals is the canonical spiral of the fullerene. For example, for C_{60-I_h} we have the canonical FSPI of {1, 7, 9, 11, 13, 15, 18, 20, 22, 24, 26, 32} as shown in figure 1.3.

To number different isomers of a fullerene with the same number of cage carbons, at first one should find the canonical spiral of each isomer. Then the spirals are ranged in ascending order: the isomer with lexicographically smallest canonical spiral gets the number “1” and so on.

A short form of numbering system, in which only IPR isomers are numbered was adopted during the early period of fullerene research, when non-IPR EMFs were not considered to exist. Nowadays this form is still commonly used to simplify the numbering. For example, the IPR isomer of C_{80} , which is usually labeled as $C_{80-I_h}(7)$ is $C_{80-I_h}(39712)$ in the full notation system¹⁹. However, an increasing number of the non-IPR isomers EMFs, published during the last decade, requires the use of the extended notation, which includes all possible isomers for

a given number of carbon atoms. In this work we will use the following scheme, which is successfully employed in many publications nowadays: the full notation is used for non-IPR isomers, the short notation - for IPR isomers¹⁹.

Another common practice is to label the isomers of EMF by their symmetry point group, or, to be more precise, by symmetry point group of the carbon cage. For example, $Sc_3N@C_{80-I_h}$ transcription means, that Sc_3N -cluster is encapsulated inside the C_{80} of icosahedral symmetry. The actual symmetry of the whole EMF molecule in this case is lower and hard to establish due to the internal cluster rotation.

In full notation of EMFs the symmetry point group symbol is generally hyphenated after the " C_{2n} " transcription, and the number of isomer is written in brackets in the end of transcription, e.g. $Er_2S@C_{82-C_{3v}}(8)$.

All metal atoms in EMFs are positively charged, and their valence electrons are transferred to the carbon cage atoms. In case of clusterfullerenes, the negative charge is distributed between carbon shell and internal non-metal atoms.

1.2. Synthesis and isolation of endohedral fullerenes

1.2.1. Synthesis and extraction.

There are many different approaches for endohedral fullerene synthesis, suggested during more than three decades of intensive research. In general, three principle strategies can be distinguished: the first one is vaporization of graphite, including laser ablation^{2,3,20}, arc discharge synthesis²¹⁻²³, resistive heating^{24,25}, and thermal plasma dissociation of hydrocarbons^{26,27}, the second one is implantation of the atoms through the walls of the already existing carbon cages (ion bombarding^{28,29}, high pressure treatment^{30,31}, explosion-induced penetration³²) and the third group includes chemical approaches via opening the orifices in the fullerenes (so called "fullerene surgery")^{33,34}. In practice the absolute majority of EMFs is nowadays produced with Krätschmer-Huffman arc discharge approach, so we will focus mainly on this group of methods.

Krätschmer-Huffman procedure²², which is also called direct current (DC) arc-discharge method, was invented in 1990. This synthesis approach is based on evaporation of graphite rods in the electric arc, under inert atmosphere of helium to avoid the oxidation of carbon. The general construction of the DC arc discharge machine is illustrated in figure 1.4.

It consists of a cylindrical water-cooled chamber with two electron inlets connected to a power source. During the synthesis procedure, two hollow graphite rods, filled with a mixture

of metals or metal oxides and organic dopants, are fixed inside the generator with the help of specific holders and used as anode and cathode in DC arc discharge process, which induces carbon evaporation from the anode. Normally, during the synthesis the anode and cathode are switched several times to efficiently evaporate both rods and prevent excess carbon depositing on the cathode. The arc current is varied in ranges of 100-200 amperes.

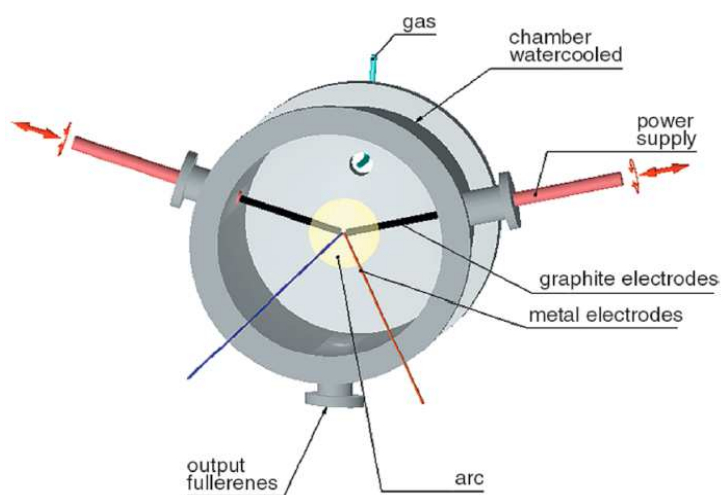


Figure 1.4. Schematic view of a Krättschmer–Huffman machine used at IFW-Dresden, which is the representative DC arc discharge apparatus used in many groups nowadays.¹⁹The technical parameters used for the fullerene synthesis can be found in the Chapter 5.

Before and after each procedure the chamber is pumped out. Products of the reaction in the form of a black soot are deposited in the cold zones of the generator, then collected and prepared for further treatment. The main components of this soot are insoluble amorphous carbon particles and graphite and a total yield of the fullerenes (including empty cages) in EMFs synthesis is limited by several mass %.

There is a number of methods for extraction of the fullerenes from the primary soot, obtained by arc-discharge synthesis. The most standard one is hot solvent Soxhlet extraction through a porous cellulose thimble with using carbon disulfide, toluene or *o*-dichlorobenzene as a solvent. Often it is preceded with 2-3 hour acetone pre-extraction to rinse the soot from most of the non-fullerene organic products. There have been also several attempts for separating EMFs from empty fullerenes and different EMFs from each other already at the step of extraction: extraction with polar solvent^{35–37}, multi-step extraction³⁸, high-temperature high-pressure extraction³⁹, and solid-phase extraction⁴⁰ (see also *Section 1.2.4. Alternative methods of EMFs separation*).

1.2.2. Selected EMF families: synthesis and structures.

During the first years after EMFs discovery research was focused mainly on *monometallofullerenes*: their synthetic procedures have been evolving step by step as more knowledge and experience have been accumulated⁴¹. The most efficient approach occurred to be the Krätschmer-Huffman arc-discharge evaporation of graphite rods²², filled with metal oxide dopants, as described above. The primary soot in such syntheses contained empty cages and several monometallofullerenes with dominating $M^{III}@C_{82}-C_{2v}$ compound. Generally the total yield of the endohedral fullerenes is less than 1%.

In monometallofullerenes, metal usually adopts the oxidation state of +2 or +3, transferring all valence electrons to the cage, so the total charge distribution can be written as $M^{x+}@C_{2n}^{x-}$.

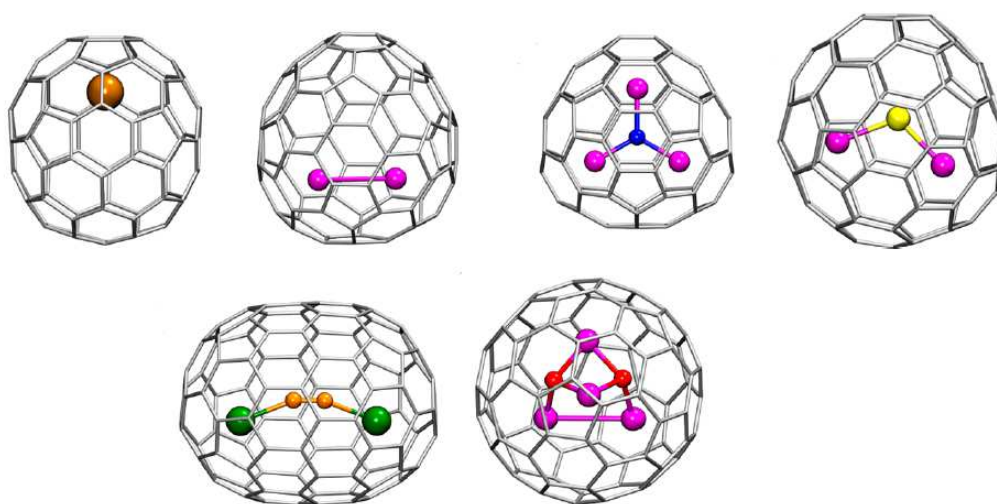


Figure 1.5. Molecular structures of different EMFs types (left to right, top to bottom): $La@C_{82}-C_{2v}(9)$; $Sc_2@C_{82}-C_{3v}(8)$; $Sc_3N@C_{80}-I_h(7)$; $Sc_2S@C_{82}-C_{3v}(8)$; $Y_2C_2@C_{100}-D_5(450)$; $Sc_4O_2@C_{80}-I_h(7)$. Carbon atoms in the fullerene cage are grey; endohedral carbon atoms are shown in orange, nitrogen is blue, oxygen is red, sulfur is yellow, Sc atoms are magenta, La is dark orange, Y is dark green.

In 1999 Steven Stevenson and his colleagues demonstrated that introducing a small amount of nitrogen gas into the Krätschmer-Huffman generator during vaporization of graphite rods containing metal oxides leads to a new clusterfullerene, $Sc_3N@C_{80}-I_h$ ⁴². Discovery of this nitride clusterfullerene was the beginning of the “Nitride era” in EMF research.

In M_3N -clusterfullerenes, metals are in the oxidation state +3, wherein one electron is donated to internal nitrogen and two electrons - to the carbon shell. Thus, the formal charge distribution in the molecule is $(M^{3+})_3N^{3-}@C_{2n}^{6-}$. This is the highest value of the negative charge

on the carbon cage, which can be adopted in EMFs to date. So far as stability of different fullerene cages is substantially determined by their charge state, the combination with M_3N cluster allows to catch those cages, which are not available as empty fullerenes or monometallofullerenes. In particular, the fullerenes from $M_3N@C_{80-I_h}$ family occur to be extremely stable, whereas neither empty C_{80-I_h} fullerene, nor monometallofullerene with the C_{80-I_h} cage of icosahedral symmetry has ever been isolated⁴³.

Synthetic procedure suggested by Stevenson et al in 1991 has been later modified. In 2002 the group of Lothar Dunsch developed a new Reactive Gas method⁴⁴: introducing small amounts of NH_3 to the Krätschmer–Huffman generator of local design led to formation of nitride clusterfullerenes as the *main* fullerene products, while the relative yield of the empty fullerene and conventional metallofullerenes was less than 5%. Further advance on this way was employment of solid nitrogen source such as guanidium thiocyanate, guanidinium hydrochloride, urea or melamine^{45,46}. This method also allows to suppress formation of empty fullerene and synthesize nitride clusterfullerenes with high yield.

The cage distribution is metal size dependent: for the smallest Sc, the soot contains $Sc_3N@C_{80-I_h}$ as the main fullerene product (in case of mixed metal systems it turns to mixture of different $Sc_x(M')_{3-x}N$ -based compounds, where $x=0, 1, \dots, 3$), substantial amounts of the second isomer of C_{80} -cage EMF, $Sc_3N@C_{80-D_{5h}}$, as well as $Sc_3N@C_{78-D_{3h}}$, $Sc_3N@C_{68-D_3}$, $Sc_3N@C_{82-C_{2v}(9)}$, and some empty fullerenes. In case of medium size metals such as, for example Er, Lu and Dy, the clusterfullerenes with higher cages ($C_{84}-C_{88}$) can be isolated as well, although nitride clusterfullerene with C_{80-I_h} cage isomer is still the main EMF product⁴⁷. For such lanthanides as La, Ce, Pr and Nd the cage size distribution is shifted to larger cages. In particular, for Nd-based NCFs, $Nd_3N@C_{88}$ was the dominating EMF product of the synthesis, while only small amount of C_{80-I_h} EMF was formed⁴⁸. In case of La, the distribution is further shifted to $La_3N@C_{92}$ and $La_3N@C_{96}$ as the main EMF products⁴⁹. The total relative yield of EMFs in these cases is substantially decreased. Wherein in mixed metal systems, such as Gd/Sc, Nd/Sc and La/Sc, and several other mixed-metal nitrides $M_x(M')_{3-x}N@C_{80-I_h}$ have been formed with good yield^{50,51}.

Dimetallofullerenes have been observed in mass spectrum of primary soot in parallel to monometallofullerenes since the very first years of EMF research, but their yields have been usually considerably lower, that complicated their isolation and further characterization⁴¹. As it has been demonstrated in several recent works^{52,53} dimetallofullerenes can also be obtained

as minor products in arc-discharge procedures with nitrogen source. In this case dimetallofullerenes are eluted in the higher nitrides region after the main fraction of $M_3N@C_{80-I_h}$ fullerenes.

The first dimetallofullerene, $La_2@C_{80}$, was isolated as an individual compound in 1991⁵⁴, and the $I_h(7)$ isomer was suggested for its cage structure, based on quantum chemical calculations, but unambiguous confirmation, based on ^{13}C NMR and ^{139}La NMR was reported only six years later⁵⁵. Subsequently C_{80-I_h} dimetallofullerenes with other metals such as Ce, Pr and also mixed dimetallofullerene have been successfully separated and structurally elucidated⁵⁶⁻⁵⁸. For Ce- and La-based dimetallofullerenes also minor $C_{80-D_{5h}}$ cage isomers have been found, similarly to nitride clusterfullerenes^{58,59}.

For C_{82} -based dimetallofullerenes there are also several different cage isomers, that have been isolated and characterized: $M_2@C_{82-C_s}(6)$, $M_2@C_{82-C_{3v}}(8)$ and the minor $M_2@C_{82-C_{2v}}(9)$. For the first two, the structures were determined by single-crystal X-ray diffraction of Er-based dimetallofullerenes in 2002^{60,61}. For the C_{3v} isomer there are also ^{13}C NMR data, obtained for $Y_2@C_{82-C_{3v}}$ and $Sc_2@C_{82-C_{3v}}$ samples. Structure of the less-abundant $M_2@C_{82-C_{2v}}(9)$ isomer was established by UV-vis-NIR absorption spectra comparison. So far as EMFs absorption behavior is mostly determined by the $\pi \rightarrow \pi^*$ excitation of the carbon cage π -electrons, fullerenes with the same cage isomer (and in the same charge state) but different internal cluster usually have quite similar shape of their UV-vis-NIR spectra. This phenomenon is especially pronounced in case of $C_{82}EMF_s$: the spectra of three different isomers of $Er_2@C_{82}$ are virtually identical to those of $Er_2C_2@C_{82}$ and $Y_2C_2@C_{82}$ ⁶² (figure 1.6). Thus, the $C_{82-C_{2v}}$ structure was suggested for the third minor isomer of $Er_2@C_{82}$, based on the structure of the corresponding carbide clusterfullerene, $Y_2C_2@C_{82}$, established earlier by ^{13}C NMR. Similarity of the UV-vis-NIR spectra has also allowed to establish the structures of different isomers of $Tm_2@C_{82}$ and $TmHo@C_{82}$, synthesized by mixed Ho/Tm arc/discharge synthesis in 2000⁶³.

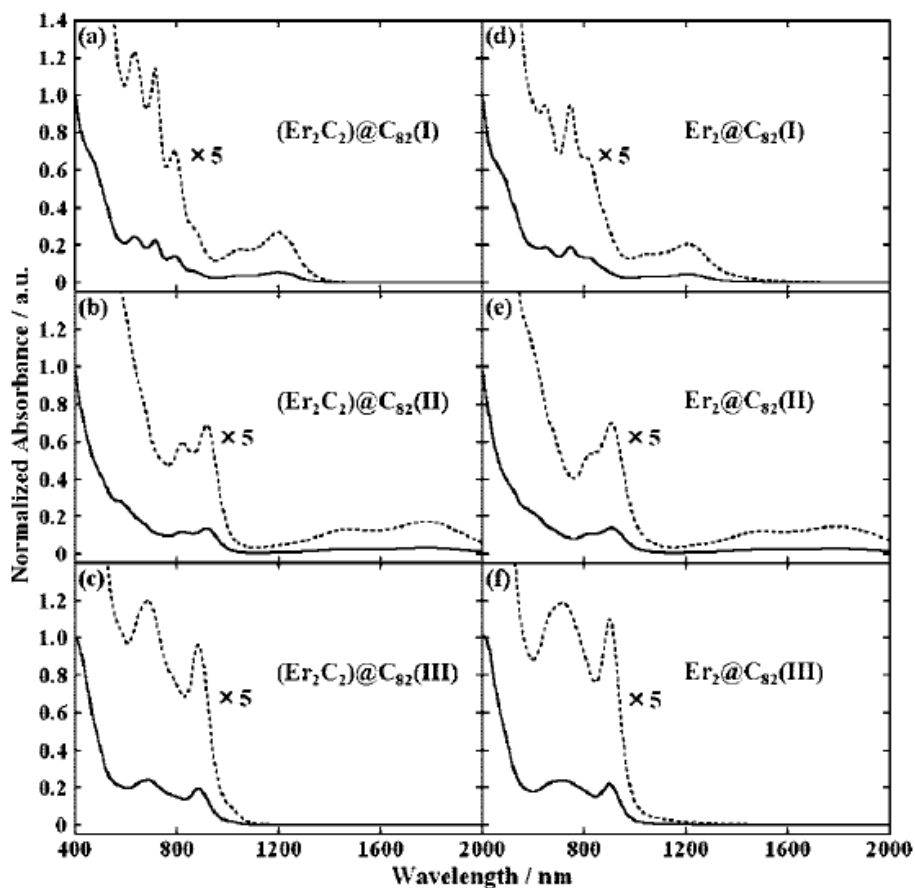


Figure 1.6. UV-vis-NIR absorption spectra of $(Er_2C_2)@C_{82}$ and $Er_2@C_{82}$ isomer I (C_s), II (C_{2v}) and III (C_{3v}) in CS_2 solvent at room temperature. These spectra are normalized with the absorbance at 400 nm, respectively. Isomers in original work are numbered in order of their elution from the column. Reproduced with permission from⁶².

Generally dimetallofullerenes are characterized by a wide diversity of cage sizes. In addition to the $M_2@C_{80}$ and $M_2@C_{82}$ families, a list of other dimetallofullerenes have been isolated and characterized, among them: non-IPR $Sc_2@C_{66}-C_{2v}$ (4059), non-IPR $La_2@C_{72}-D_2$ (10611) and $Ce_2@C_{72}-D_2$ (10611), $La_2@C_{78}-D_{3h}$ (5) and $Ce_2@C_{78}-D_{3h}$ (5), $Sm_2@C_{88}-D_2$ (35), $Sm_2@C_{90}-C_1$ (21), and $Sm_2@C_{92}-D_3$ (85) and $Sm_2@C_{104}-D_{3d}$ (822), the largest structurally characterized EMF to date.

When metals in dimetallofullerene adopt the highest oxidation state +3, the charge distribution is $(M^{3+})_2@C_{2n}^{6-}$, similar to nitride clusterfullerenes. Such dimetallofullerenes are often stabilized with the same cage isomers, as nitride clusterfullerenes do, e.g. $C_{80}-I_h$, $C_{80}-D_{5h}$, $C_{78}-D_{3h}$. At the same time, for C_{82} -based EMFs to date there has been no common opinion about metal and carbon cage charge state. In chapter 2 of the present work we will provide our line of arguments and experimental proofs concerning this issue.

Similarly to dimetallofullerenes and monometallofullerenes, *carbide clusterfullerenes* have been obtained in synthesis without nitrogen source since the early period of EMF research. Acetylide group in carbide clusterfullerene molecules is carrying the charge of 2-, so the charge distribution in dimeatllcarbide is $(M_2C_2)^{4+}@C_{2n}^{4-}$.

Mass-spectroscopy does not allow to distinguish the peak of carbide clusterfullerene $M_2C_2@C_{2n}$ from the peak of dimetallofullerene $M_2@C_{2n+2}$, so these two classes have been sometimes mixed up, especially in the first years of fullerene studies. Later, when the amount of accumulated material allowed to involve such methods as NMR and single-crystal or powder XRD, some “dimetallofullerenes” have been found to be actually carbide clusterfullerenes. The first example is $Sc_2C_2@C_{84-D_{2d}}(23)$, which was initially thought to be “ $Sc_2@C_{86}$ ”: in 2001, Shinohara et al. demonstrated, that this compound exhibits 11 lines in the range of C-sp² atoms in ¹³C NMR spectra⁶⁴. Such a spectral pattern could not be assigned to any of the IPR isomers of the C₈₆cage, but switching to C₈₄ cages provided perfect fit with the C₈₄-D_{2d}(23) isomer. This structure was also confirmed by powder synchrotron X-ray studies with Rietveld/MEM analysis, which revealed additional electron density due to the rapidly rotating acetylide group⁶⁴, and later by single-crystal XRD⁶⁵.

Several years later the structures of clusterfullerenes from the “ $M_2@C_{84}$ ” family have been similarly reassigned to carbide clusterfullerenes $M_2C_2@C_{82}$. In 2004, ¹³C NMR spectroscopic studies of the three isomers of “ $Y_2@C_{84}$ ” revealed, that these EMFs were in fact isomers of $Y_2C_2@C_{82}$ with C_s(6), C_{3v}(8), and C_{2v}(9) carbon cages⁶⁶. The structure of dominating $Y_2@C_{82}-C_{3v}(8)$ isomer was also approved by powder synchrotron Rietveld/MEM X-ray analysis⁶⁷. For $Sc_2C_2@C_{82}$ a close similarity of UV-vis-NIR absorption spectra of “ $Sc_2@C_{84}$ ” and “ $Dy_2@C_{84}$ ” EMFs with the spectra of already known isomers of $Y_2C_2@C_{82}$ revealed that the first two also have carbide clusterfullerene structure. Analogous comparison allows one to assign three isomers of $Er_2C_2@C_{82}$ as $Er_2C_2@C_{82}-C_s(6)$, $Er_2C_2@C_{82}-C_{3v}(8)$ and $Er_2C_2@C_{82}-C_{2v}(9)$ ⁶², as has been already discussed above in dimetallofullerenes section.

The structure of the $Sc_2C_2@C_{82}-C_{3v}(8)$ main isomer was confirmed two years later by ¹³C NMR spectroscopy⁶⁸ and by powder synchrotron X-ray diffraction with Rietveld/MEM analysis, which uncovered an additional electron density in the center of the cage corresponding to the acetylide group⁶⁹. Single crystal XRD confirmation of the structure was not achieved for a long time due to disorder of the $Sc_2C_2@C_{82}$ molecules in the crystal lattice, although in 2007 Nagase et al obtained good quality crystals of $Sc_2C_2@C_{82}-C_{3v}(8)$ adamantylidene adduct. In 2012 the

same group finally managed to gain well-ordered crystal of nonderivatized $\text{Sc}_2\text{C}_2@\text{C}_{82}\text{-C}_{3v}(8)$ via cocrystallization with $\text{Co}(\text{OEP})$.

The structure of the $\text{Sc}_2\text{C}_2@\text{C}_{82}\text{-C}_5$ isomer was confirmed in 2011. Akasaka et. al. have found the signal from the acetylide group (244.4 ppm) in the ^{13}C NMR spectrum of a ^{13}C -enriched sample; single crystal XRD experiment results for the $\text{Sc}_2\text{C}_2@\text{C}_{82}\text{-C}_5(6)$ pyrrolidine derivative have been published in the same work, that unambiguously confirmed the structure of this isomer.

In 2010 group of Lothar Dunsch has demonstrated that in case of arc-discharge synthesis with guanidium thiocyanate as a nitrogen source, some sulfur-containing fullerenes could be found in the primary soot⁷⁰. Authors have managed to isolate several compounds with common formula $\text{M}_2\text{S}@\text{C}_{82}$ ($\text{M}=\text{Sc}, \text{Y}, \text{Dy}$ and Lu), comparison of UV-vis-NIR absorption spectra has uncovered the $\text{M}_2\text{S}@\text{C}_{82}\text{-C}_{3v}(8)$ structure for all EMFs. This conclusion was also supported by quantum chemical calculations and, in case of $\text{Sc}_2\text{S}@\text{C}_{82}$, by vibrational spectroscopy. The same year Ning Chen from the group of Luis Echegoyen has developed a new synthetic method based on the use of SO_2 /helium atmosphere in the Krätschmer–Huffman arc-discharge reactor⁷¹. This approach allowed to increase the yield of sulfide clusterfullerenes, wherein formation of other EMFs was suppressed.

During the following years several sulfide clusterfullerenes such as $\text{Sc}_2\text{S}@\text{C}_{82}\text{-C}_5(6)$ ⁷², $\text{Sc}_2\text{S}@\text{C}_{82}\text{-C}_{3v}(8)$ ⁷², $\text{Sc}_2\text{S}@\text{C}_{72}\text{-C}_5(10528)$ with non-IPR cage¹¹, synthesized from SO_2 /helium arc discharge processes, have been isolated and their structures have been determined by method of single-crystal XRD.

In sulfide clusterfullerenes the sulfur adopts the oxidation state 2-, so the total charge distribution is similar to carbide clusterfullerenes: $(\text{M}_2\text{S})^{4+}@\text{C}_{2n}^{4-}$. Cage size and structure are also quite similar, that implies in similar set of cages for corresponding EMF families: the most abundant sulfide clusterfullerenes also have $\text{C}_{82}\text{-C}_{3v}(8)$ and $\text{C}_{82}\text{-C}_5(6)$ cage isomers.

1.2.3. HPLC as a main method of EMF separation

The most powerful approach for the fullerene separation is High Performance Liquid Chromatography (HPLC), based on different distribution of compounds between a stationary phase (chromatography column) and a mobile phase (flowing solvent), that results in the difference of their retention times. This difference in distribution is determined by such properties as boiling temperature, polarity, electric charge (for ionic compounds), size of the molecule, and some others.⁷³

The most suitable stationary phase for fullerenes HPLC-analysis and separation was proved to be silica gel, modified with different aromatic groups. Herein, there are two main mechanisms, providing retention: the π - π interaction between aromatic rings of the column and π -electron density of the fullerene cage and charge transfer interaction between the stationary phase and induced dipole moment produced from the charge transfer inside the fullerene cage^{19,74}.

In particular, *Cosmosil* has invented several columns for fullerenes (see figure 1.7): *Cosmosil Buckyprep* is the simplest one and is intended for the separation of empty cages, *Cosmosil Buckyprep-M* is specified for EMFs separation and *Cosmosil Buckyprep-D* with more polar addends is specified for the separation of empty and endohedral fullerene derivatives⁷⁵.

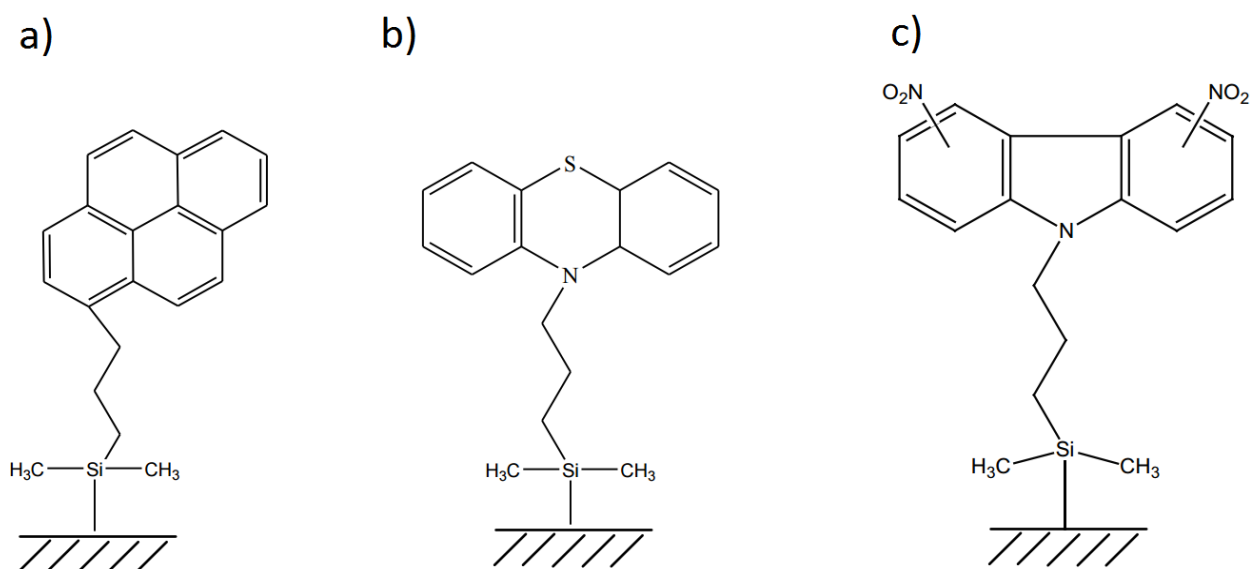


Figure 1.7. Stationary phase modifiers of different columns exploited for HPLC separation of fullerenes: dimethyl-3-(1-pyrenyl)-propyl – *Cosmosil Buckyprep* column (a); dimethyl-3-(N-phenothiazinyl)propyl – *Cosmosil Buckyprep-M* column (b); dimethyl-3-(N-dinitrocarbazolyl)propyl – *Cosmosil Buckyprep-D* column (c)⁷⁵.

The choice of mobile phase is determined by several criteria, such as the chemical inertness with response to stationary phase, low viscosity and reasonable solubility of fullerenes. The most frequently used solvents are toluene, *o*-dichlorobenzene, hexane and their mixtures.

Detection of different EMF compounds eluted from the HPLC column is usually provided by UV-vis-NIR absorbance detector. Collected data (chromatogram) is presented as a dependence of selected wavelength absorbance from retention time; each peak represents (in ideal separation conditions) an individual compound. Both qualitative and quantitative information about mixture composition can be concluded from the HPLC- chromatogram.

Usually, EMF primary soot is a comprehensive mixture of quite similar components and in the HPLC-trace we can observe many overlapping peaks. As a consequence, HPLC isolation of individual components becomes non trivial and time consuming task. The retention behavior is mostly determined by the cage structure, that makes separation of fullerenes with identical cages (e.g. mixed nitride clusterfullerenes^{50,76,77}, dimetallofullerenes and related metal carbides⁶⁹) especially difficult.

In majority of cases, multi-step HPLC separation is needed for isolation of individual EMFs: the fractions collected by the first chromatographic procedure and containing several different EMFs undergo further HPLC stages to get the individual compounds. The final separation step often involves the recycling chromatographic technique as an effective approach for the separation of compounds with minimal difference in retention time.

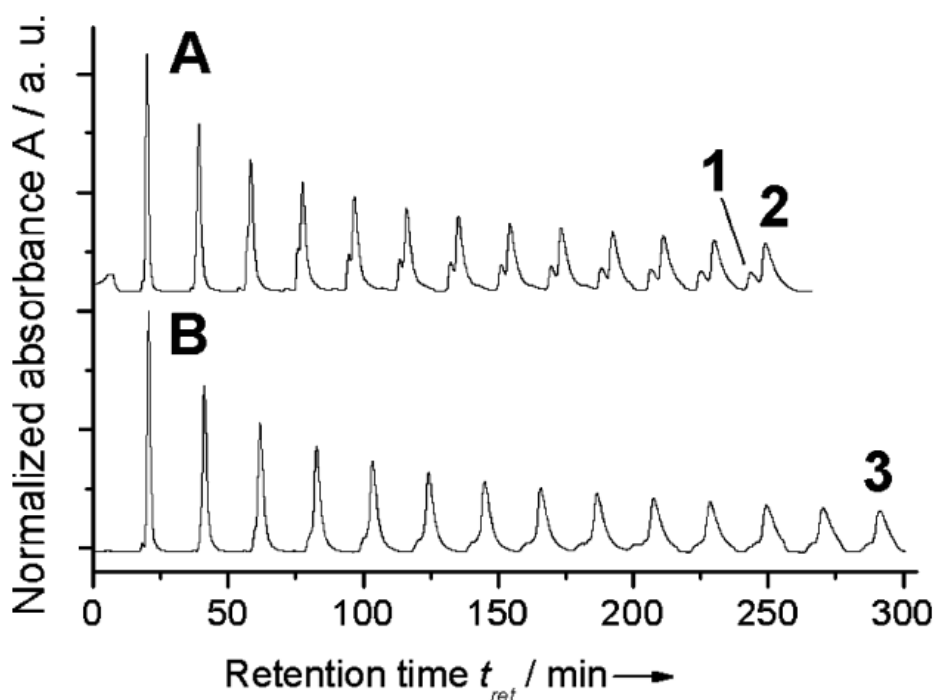


Figure 1.8. Recycling HPLC chromatograms of two fractions A and B containing mixture of $Gd_xSc_{3-x}N@C_{80}$ EMFs (I_h , $x = 0-2$) which was first isolated by conventional HPLC as the first-step separation. Reproduced with permission from⁵⁰.

Compared to the classical one-cycle process, in recycling technique the compounds are passed through the same column several times, providing increased effective path. The sample passes in the column wherein the difference of retention times $t_{R1}-t_{R2}$ can be enhanced after n cycle-procedure up to value of $n*(t_{R1}-t_{R2})$ until sufficient resolution is achieved.

1.2.4. Alternative methods of EMFs separation

So far, as multistep HPLC-isolation of individual EMFs is rather time and labor-consuming, in the last decades many research groups have been looking for alternative separation techniques. Today we know several approaches, allowing to avoid or sufficiently simplify the HPLC-separation procedure.

In 1991 Chaj *et al*³ suggested a method of fractional sublimation, based on difference in sublimation energies (ΔH_{sub}), that can be successfully utilized for separation endohedral fullerenes from empty fullerenes^{3,78,79}.

Intensive studies of the EMFs chemical behavior during the last decade have revealed significant differences of their reactivity in comparison to empty cages, as well as between different types of EMFs⁸⁰. This phenomenon has been used in several separation approaches. In 2005 Dorn demonstrated substantial difference in fullerene reactivity with respect to Diels-Alder reaction with cyclopentadienyl functionalized resins⁸¹, which was employed to develop a scalable separation procedure. Passing toluene solution of standard Sc_2O_3 /graphite arc discharge synthesis extract through the column packed with cyclopentadienyl functionalized resins resulted in isolation of $\text{Sc}_3\text{N}@C_{80}$ -*I* isomer with 60% purity^{81,82}. Further purification was performed with help of HPLC. Reacted fullerenes were recovered from the column by treating with hot maleic anhydride/toluene mixture. Later in 2013 C. Wang and his colleagues used well known Prato dipolar cycloaddition following by selective retro-reaction of pyrrolidine group to simplify the separation of nitride clusterfullerenes with Sc, Lu, Ho from empty fullerenes⁸³.

Another fundamental approach to non-chromatographic separation of EMFs employs the differences in their electrochemical properties. Here two groups of techniques can be distinguished: direct electrolysis-assistant separation and using of selective redox agents.

The first electrolysis-based approach of the EMF separation was proposed in 1998 by Diener and Alford⁸⁴. The authors synthesized Gd-EMFs and used sublimation technique followed by dissolution of the sublimate in *o*-xylene. Mass-spectrometric analysis indicated that initial sublimate contained some fullerenes which were not detected in the *o*-xylene extract – most of them were monometallofullerenes such as $\text{Gd}@C_{60}$ and $\text{Gd}@C_{74}$. Electrolysis of the insoluble part suspended in benzonitrile at -1.0 V versus Ag/AgNO_3 reference resulted in dissolution of the 98% of the particles. Mass-spectroscopic measurements of the reoxidized sample showed the presence of the “missing” EMFs. Thus, authors have unexpectedly revealed

a new method for separation of those fullerenes, which are not accessible with standard extraction techniques.

In 2004 Akasaka and coworkers developed an effective separation technique⁸⁵, based on electrochemical reduction of the fullerene extract in o-DCB at the potential of saturated calomel electrode (-0.60 V versus $\text{Fe}(\text{Cp})_2^{+/0}$ pair). At this potential mono- and dimetallofullerenes (such as $\text{La}@\text{C}_{82}$ and $\text{La}_2@\text{C}_{80}$) are reduced, whereas empty fullerenes with more negative reduction potentials stay neutral. After electrolysis the solvent was evaporated and the solid residue was treated by polar acetone/ CS_2 mixture, to dissolve anionic EMFs, while neutral empty fullerenes remained insoluble.

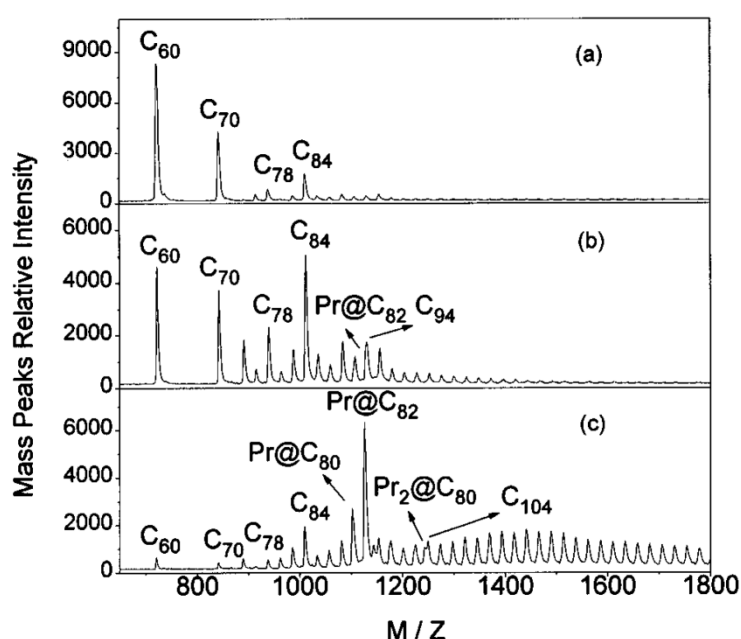


Figure 1.9. Mass spectra of extracts from the soot, produced by the arc-discharge of Pr_6O_{11} /carbon rods: (a) toluene Soxhlet extract at its boiling point, (b) toluene extract at high temperature, high pressure, (c) pyridine extract at high temperature, high pressure. Reproduced with permission from³⁹.

Selective reduction or oxidation of EMFs can be achieved also with the help of redox reagents or even the solvent used for the fullerene extraction. Since the early studies of EMFs the extraction with some N-containing solvents (such as N,N-dimethylformamide^{36,38,86}, pyridine^{35,39,87,88} and aniline^{37,89}) has been shown to be powerful method for getting extracts, enriched with EMFs.

It has been revealed, that molecules of solvent in these experiments act as a donor⁹⁰, providing effective charge transfer to EMFs; the resulting extract is then a solution of EMFs anions (that can be later reoxidized). Due to this phenomenon, better extraction of EMFs from the soot can be achieved. Furthermore, it allows extraction of the EMFs which are not

extractable by standard solvent (e.g., M@C₆₀ compounds are efficiently extracted only with aniline⁸⁹). In 2006 the group of Akasaka have demonstrated the same mechanism of dimethylformamide (DMF) extraction of La-containing EMF mixture^{36,91}. Solubility of empty non-charged fullerenes in DMF is very low, so this solvent extract predominantly La-EMFs as anions. Such La-EMF DMF extracts can be then dissolved in polar acetone/CS₂ mixture in a similar way to the electrolysis-assisted separation described in their previous work.

A separation procedure based on selective oxidation was developed by Bolskar et al. and successfully applied for Gd-EMFs^{78,92}. The procedure employed three oxidants of different strength: Ag⁺ salts ($E^{+/0} +0.65$ V versus Fe(Cp)₂^{+/0}), tris(4-bromophenyl) aminium hexachloroantimonate (also known as “magic blue”, $E^{+/0}+0.70$ V versus Fe(Cp)₂^{+/0}) and AlCl₃ ($E^{+/0}=+ 1.1$ V versus Fe(Cp)₂^{+/0}) and subsequent separation based on the different solubility of neutral and charged species. The authors have divided the typical extract of Gd@C_{2n} EMFs into three different fractions, from one of those Gd@C₈₂ was further chromatographically separated in one step.

The first EMF, isolated by the method of selective oxidation was *I_h* isomer of Sc₃N@C₈₀ (separated from the mixture with Sc₃N@C₈₀-*D_{5h}* by Echevoyen et al. in 2005⁹³). Authors have demonstrated that due to the difference in oxidation potentials of two isomers (which is 0.27 V more cathodic for the Sc₃N@C₈₀-*D_{5h}*), a selective reagent could be found to oxidize only the second isomer, while the first will stay neutral. This procedure also can be employed for the separation of pure Sc₃N@*I_h*-C₈₀ from the standard extract of Sc-based EMFs⁹⁴.

In 2010 Shinohara et.al. used selective oxidation with tris-(4-bromophenyl) salt to isolate Li@C₆₀ from empty C₆₀⁹⁵. The product was finally crystallized as [Li@C₆₀]⁺(SbCl₆)⁻, allowing to determine its structure by XRD.

Remarkable progress in non-chromatographically separation of EMFs was made by the group of Professor Steven Stevenson from Indiana-Purdue University Fort Wayne. In 2006 Stevenson first invented so-called “Stir and Filter approach”⁹⁶ (“SAFA”). Fullerene extract is added to the modified silica gel suspension, stirred, and then passed through a filter. Different fullerenes are interacting with amine-functionalized silica, which traps more reactive compounds, while less reactive ones remain in the filtrate. Making first experiments with standard Sc₂O₃/graphite arc discharge extract, authors have found, that reactivity with response to amino silica is decreasing in the series C₇₆> C₇₈> C₇₀> C₈₄> C₆₀> M₃N@C₆₈>

$M_3N@C_{78} > M_3N@C_{80-D5h} > M_3N@C_{80-Ih}$. Variation of different types of silica gel and the stirring time enabled isolation of pure I_h isomer of $Sc_3N@C_{80}$ (recovery up to 93%)^{96,97}.

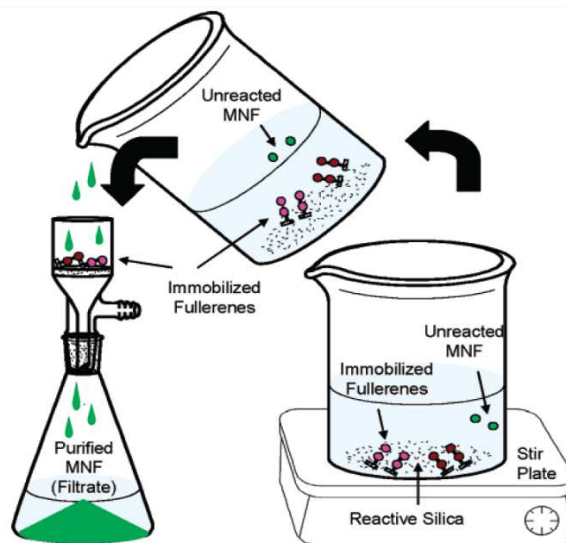


Figure 1.10. Schematic of the “Stir and Filter Approach” (SAFA) separation of EMFs. Reproduced with permission⁹⁶.

SAFA method is following the same concept, which has been used earlier by group of Dorn in their experiments with cyclopentadienyl functionalized resins. However, reaction with amino-silica (i.e., electron transfer and addition) was found to be more selective than Diels-Alder 4+2 cycloaddition, used by Dorn et. al.

Later authors expanded their “SAFA” experiments to Er- and Gd-containing fullerene mixtures and managed to separate pure $Er_3N@C_{80-Ih}$ and a fraction, enriched with $Gd_3N@C_{80-Ih}$ ⁹⁸.

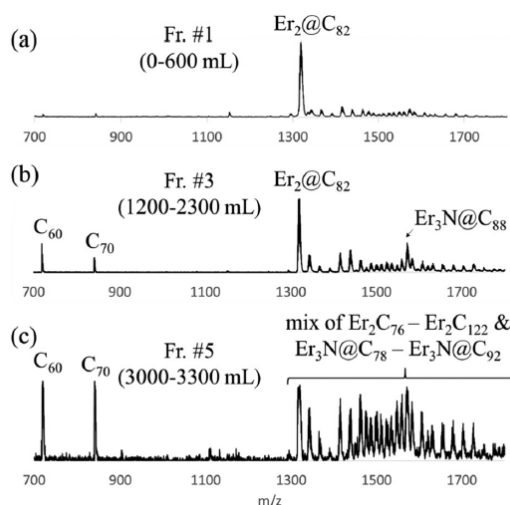
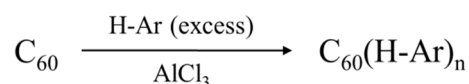


Figure 1.11. MALDI mass spectra showing selectivity of release and fractionation of different types of Er metallofullerenes for samples obtained upon addition of (a) 0–600 mL, (b) 1200–2300 mL, and (c) 3000–3300 mL of CS_2 eluent. Reproduced with permission from⁹⁸.

In the same work it has been demonstrated, that trapped fullerenes can be released from the silica precipitate by CS₂ washing. Moreover, sufficient selectivity has been observed during multi step washing of the reacted silica, very first fractions contain different fullerenes when comparison to those obtained by long washing. In particular, Er₂@C₈₂ dimetallofullerene (about 90% pure, mixture of isomers) has been isolated as a first fraction washed from reacted silica.

In parallel to the SAFA method, the group of Stevenson has been developing another approach for HPLC-free EMF separation: selective oxidation with Lewis acids. Reactions of Lewis acids with fullerenes have been known from the very first years of fullerene research. In 1991 Olah et al. reported AlCl₃-catalyzed polyarylation of empty cage fullerenes (either pure C₆₀ or a mixture of C₆₀/C₇₀, benzene solution)⁹⁹:



The authors have noted that single electron transfer (SET) can also take place in redox processes for Lewis acid halides that are more easily reducible. These experiments revealed different reactivity of C₆₀ and C₇₀ to Lewis acids. (C₇₀ was shown to be more reactive). In 1994 groups of Olah and Bucsi employed this reactivity differences to develop a scalable separation method¹⁰⁰. Addition of AlCl₃ to CS₂ solution of fullerene mixture resulted in precipitation of more reactive C₇₀, while most of C₆₀ remained in solution. After filtration, the filtrate was shown to be pure C₆₀ (>99.8%, 73% recovery). The Precipitate consisted of a mixture of C₆₀ and C₇₀ charge-transfer complexes with AlCl₃. The authors also demonstrated that complexation is reversible and both fullerenes can be successfully recovered from the precipitate.

In 2009 Stevenson et al performed the first reactions of Lewis acids with EMFs¹⁰¹. Starting with standard Sc-arc discharge extract containing scandium nitrides Sc₃N@C₆₈, Sc₃N@C₇₈, Sc₃N@C_{80-D5h}, Sc₃N@C_{80-Ih}, scandium oxide Sc₄O₂@C_{80-Ih} and empty cages C₆₀ and C₇₀ as main components. The authors revealed that all the EMFs were much more reactive than empty fullerenes.

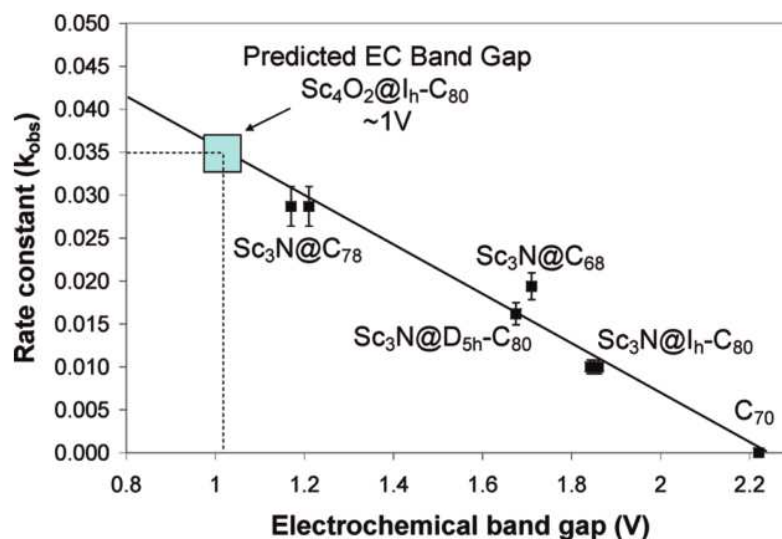


Figure 1.12. Correlation of the rate constants from metallofullerene reactions with Lewis acids versus the electrochemical band gap. Blue square shows area of the predicted electrochemical band gap of $Sc_4O_2@C_{80-I_h}$. Reproduced with permission from¹⁰¹.

Wherein the reactivity decreased in series of $Sc_4O_2@C_{80-I_h} > Sc_3N@C_{78} > Sc_3N@C_{68} > Sc_3N@C_{80-D_{5h}} > Sc_3N@C_{80-I_h} > C_{70} > C_{60}$, that was related to the value of electrochemical band gap. Interestingly, the author have employed this correlation to predict the value of $Sc_4O_2@C_{80}$ band gap (figure 1.12). This prediction is in a good agreement with experimental value of 1.10 V, observed later by Popov and colleagues¹⁰².

These chemical reactivity differences were manipulated into effective separation method. Using two different Lewis acids (stronger $FeCl_3$ and weaker $AlCl_3$) and tuning the reaction time, authors managed to separate primary metallofullerene extract into several fractions, each containing different type of EMFs, including isomeric pure fraction of $Sc_3N@C_{80-I_h}$. The recovery of precipitate was carried out with serial treatment by ice water, sodium bicarbonate, and excess of CS_2 . As a non-chromatographic method, Lewis acids-based purification approach requires no special columns and no HPLC fraction collection.

In 2012 group of Shinohara¹⁰³ reported interactions of Lewis acids with other types of endohedral fullerenes, such as mono- and dimetallofullerenes and carbide clusterfullerenes. After trying several Lewis acids finally authors have found $TiCl_4$ as the best agent for quick and effective separation of fullerene mixtures. In only 10 minutes, EMFs can be complexed, precipitated, and isolated from unreacted lower empty-cages (e.g., C_{60} , C_{70}).

Herewith the EMF first oxidation potential was demonstrated to be the crucial factors for efficient purification: all fullerenes, having first oxidation potentials lower than 0.50–0.60 V can be equally well separated and purified in a single reaction step. The one with lower potential will precipitate first, that can be also employed in separation methodic. In particular, a mixture of $\text{Ce}_2@\text{C}_{80}$ ($E^{+/0} = + 0.55$ V versus $\text{Fe}(\text{Cp})_2^{+/0}$) and $\text{Ce}@\text{C}_{82}$ ($E^{+/0} = + 0.08$ V versus $\text{Fe}(\text{Cp})_2^{+/0}$) can be separated into $\text{Ce}_2@\text{C}_{80}$ as a filtrate and fraction, enriched with $\text{Ce}@\text{C}_{82}$ as a precipitate.

Also in 2012, the same group reported the mechanism of EMF - TiCl_4 interactions¹⁰⁴. These results have confirmed that reactivity of empty fullerenes and endohedrals with TiCl_4 is a function of the first oxidation potentials. Formation of the metallofullerene- TiCl_4 complex proceeds with one electron transfer from the endohedral to Lewis acid molecule.

In 2013 Stevenson et al⁵³ have demonstrated that using of CuCl_2 as a weaker Lewis acid than AlCl_3 or TiCl_4 , allows to lower the precipitation threshold from +0.62 V to +0.19 V (we are using potential values given versus $\text{Fe}(\text{Cp})_2^{+/0}$ throughout this discussion). Thus, one can separate highly reactive ($E^{+/0} < 0.19$ V) EMFs from the less reactive ($E^{+/0} > 0.19$ V) ones. In particular $\text{Sc}_4\text{O}_2@\text{C}_{80-I_h}$ can be isolated from the mixture with other metallic oxide endohedrals; $\text{Sc}_3\text{C}_2@\text{C}_{80}$ ($E^{+/0} = -0.04$ V,) can be isolated as a dominating EMF from the mixture with other metallic carbide endohedrals; $\text{Sc}_3\text{N}@\text{C}_{78}$ ($E^{+/0} = 0.12$ V¹⁰⁵) can be easily separated from $\text{Sc}_3\text{N}@\text{C}_{68}$ ($E^{+/0} = 0.33$ V¹⁰⁶) and from both D_{5h} ($E^{+/0} = 0.34$ V¹⁰⁷) and I_h ($E^{+/0} = 0.62$ V¹⁰⁸) isomers of $\text{Sc}_3\text{N}@\text{C}_{80}$.

Moreover, in this work non-HPLC separation of different Er-based dimetallofullerenes was demonstrated for the first time. Authors started with the standard Er_2O_3 -based arc-discharge synthesis extract. After separating of $\text{Er}_3\text{N}@\text{C}_{80-I_h}$ with help of SAFA method, mixture contained two dimetallofullerenes, $\text{Er}_2@\text{C}_{82-C_5}(6)$ and $\text{Er}_2@\text{C}_{82-C_{3v}}(8)$, as main EMF products and some empty cage fullerenes (see fig. 1.13a). Addition of CuCl_2 as a first step of separation resulted in precipitation of mainly C_5 isomer, while most of C_{3v} isomer remained in the solution and was precipitated with addition of AlCl_3 at the second step. At that time no information about redox properties of $\text{Er}_2\text{C}_2@\text{C}_{82-C_5}(6)$ has been available, while Anderson et al⁸⁸ have reported the first oxidation potential of $\text{Er}_2\text{C}_2@\text{C}_{82-C_{3v}}(8)$ as +0.19 V obtained from Square Wave Voltammetry experiment in pyridine. Nevertheless this experiments have demonstrated, that oxidation behavior of these two isomers is different, $\text{Er}_2\text{C}_2@\text{C}_{82-C_5}(6)$ being easier to oxidize.

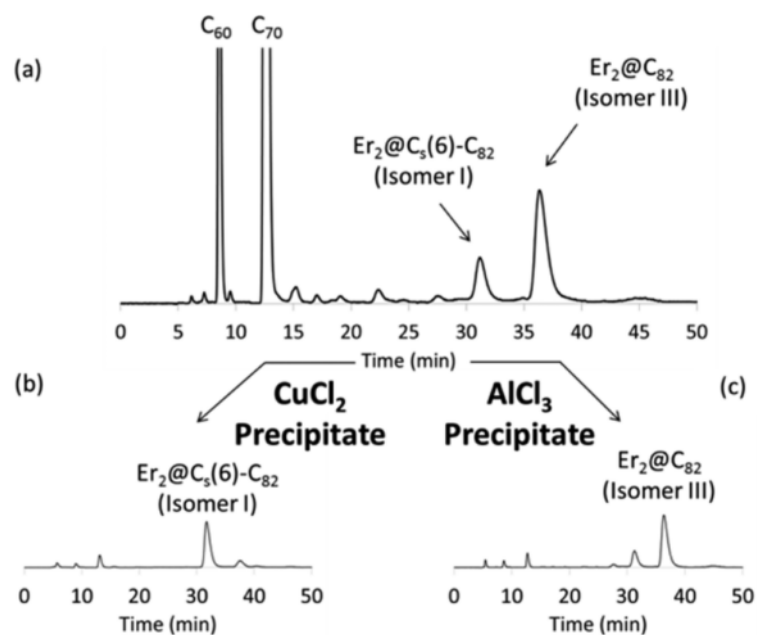


Figure 1.13. Scheme of $Er_2C_2@C_{82-C_5(6)}$, $Er_2C_2@C_{82-C_{3v}(8)}$ separation (a) HPLC chromatogram before reaction with $CuCl_2$ or $AlCl_3$, (b,d) HPLC chromatograms of the decomplexed precipitates obtained after 44 min of reaction time when using (b) $CuCl_2$ or (c) $AlCl_3$. Reproduced with permission from⁵³.

In 2014, Stevenson et al¹⁰⁹ compared reactivity of 11 different Lewis acids in experiments with Gd_3N -based EMFs. The goal was to determine a range of precipitation thresholds and find the matching agent for selective precipitation of targeted Gd endohedrals. Authors found $CaCl_2$ and $ZnCl_2$ to be the weakest Lewis acids of the 11 tested, that could provide the most selective separation.

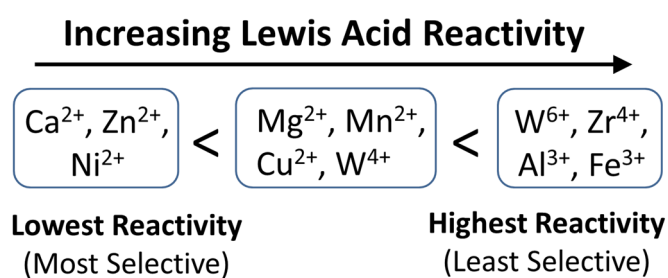


Figure 1.14. Selectivity and reactivity of Gd-based metallofullerenes with a variety of Lewis acids. Reproduced with permission from¹⁰⁹.

In particular, matching these weak Lewis acids with the very low 1st oxidation potential of $Gd_3N@C_{88}$ ($E^{+/0} = 0.06$ V¹¹⁰) allowed selective precipitation of $Gd_3N@C_{88}$ from Gd soot extract. Further in 2016 this fullerene was separated by $ZnCl_2$ complexation and finally purified with SAFA method, that allowed to determine its structure with single-crystal XRD¹¹¹.

1.3. Electrochemistry of EMFs

1.3.1. Methods of Cyclic voltammetry and Square Wave Voltammetry

Cyclic voltammetry (CV) is a type of potentiodynamic electrochemical measurement, generally applied for solutions. In a cyclic voltammetry experiment three electrode scheme is employed. The working electrode potential is scanned linearly until reaching of some switching potential value and then back to the initial potential. These cycles of scans in potential may be repeated several times.

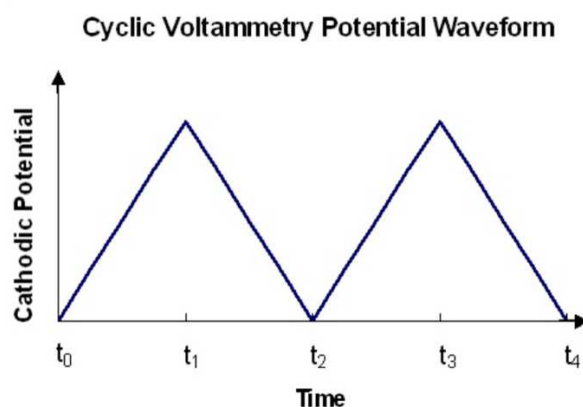
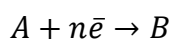


Figure 1.15. The linear potential scan versus time

In cyclic voltammetry the current between the working electrode and the counter electrode is plotted versus the applied potential. In absence of redox activity this graph represents itself a plain curve with small contribution of capacitive current (range from -0.2 to $0V$ at the figure 1.16). This current, also called "non-faradaic" or "double-layer" current, does not involve any charge transfer reactions, but is responsible for accumulation (or removal) of electrical charges on the electrode surface and in the electrolyte solution near the electrode. When the potential is close to the redox potential of the target substance, one can observe the peak of the current due to the charge transfer between molecules in solution and working electrode (so called Faraday current, area of 0 to $+0.3V$ at the figure 1.16.). When the redox process is reversible, the peak of the reversed charge transfer can be observed during the back potential scan as well.

The simplest Faradaic electrode reaction is the heterogeneous charge transfer in which, dependent on the given electrode potential, compound A is reduced to compound B (electron-transfer mechanism: E mechanism):



The charge-transfer process in the near-electrode area is described by the Butler-Volmer equation¹¹²:

$$j_A(0, t) = \frac{i}{nFA} = C_A(0, t)k_0 e^{-a\frac{nF}{RT}(E-E_0)} - C_B(0, t)k_0 e^{(1-a)\frac{nF}{RT}(E-E_0)} \quad (\text{Eq. 1.1})$$

where k_0 is rate constant of heterogeneous charge transfer, a is transfer coefficient, A is electrode area, j is flux at the electrode interface, F is Faraday constant, C_A and C_B are concentrations.

The other process, that can influence the voltammogram peak shape is diffusional mass transport, that occurs because of the difference between the resulting potential-dependent surface concentrations $C_A(0, t)$ and $C_B(0, t)$ and the bulk concentrations in the rest of the solution. The concentration gradient at the electrode surface is directly proportional to the charge flux:

$$J_A(0, t) = -D_A \left(\frac{\partial C_A}{\partial x} \right)_{x=0} = D_B \left(\frac{\partial C_B}{\partial x} \right)_{x=0} \quad (\text{Eq. 1.2})$$

Depending on the ratio of these two processes rates, three main types of processes can be distinguished:

1) *Reversible process*. $k_0 > 10^{-1} \text{sm/s}$. At high rates of heterogeneous charge transfer, the current at the electrode surface is limited by the diffusion mass transport process, which is hence the slowest step (hence diffusion control). Dynamic equilibrium is established at the phase boundary. The Butler-Volmer equation is reduced to the Nernst equation, i.e. the surface concentrations $C_A(0, t)$ and $C_B(0, t)$ are determined only by the actual electrode potential and are no longer influenced by heterogeneous kinetic effects:

$$E = E_0 + \frac{RT}{nF} \ln \left(\frac{C_A}{C_B} \right) \quad (\text{Eq. 1.3})$$

This case is titled reversible because a thermodynamic equilibrium between anodic and cathodic forms exists at the phase boundary. On the voltammogram we can observe the peak of forward process and peak of reverse process with equal current values. The equilibrium potential is then measured as a half-sum of the forward and reversed potentials. A peak-to-peak separation at standard conditions (298K) is 0.059 V for a single-electron transfer reaction, which is determined by the formula:

$$\Delta E_p = \frac{|E_r + E_f|}{2} = 2.3 \frac{RT}{nF} \quad (\text{Eq. 1.4})$$

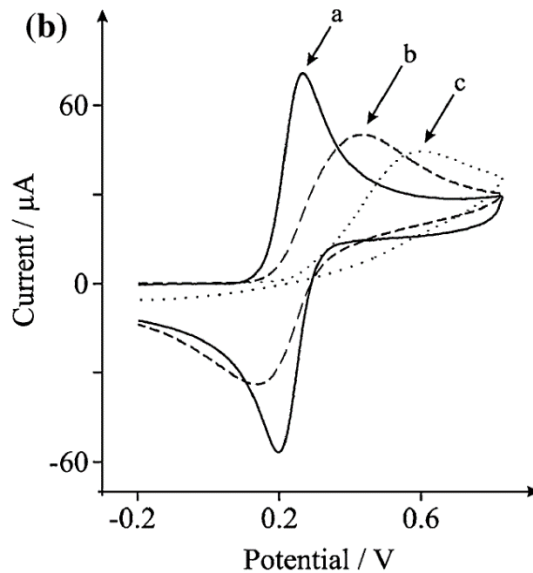


Figure 1.16. Cyclic voltammograms for the reversible (a), quasi-reversible (b) and irreversible (c) charge transfer processes.

2) *Irreversible process*: $k_0 < 10^{-5} \text{sm/s}$. When charge transfer at the electrode is slow it becomes the limiting stage that determines the current. Depending on the potential, only one of the cathodic and anodic heterogeneous reactions has a measurable rate. No backward peak can be observed. The Nernst equation is not satisfied in this conditions, moreover the values of the peak potential formally cannot be compared with thermodynamic equilibrium potentials measured in reversible processes that must be considered in analyzing of electrochemical data.

3) *Quasi-reversible process*. At intermediate charge transfer rates both the charge transfer and the mass transport determine the current. The Nernst equation is satisfied only approximately. On the voltammograms we can observe the reverse peak, but the peak-to-peak difference significantly exceeds the value of 0.059 V.

Another voltammetry technique, frequently employed for EMF studies is *Square Wave Voltammetry (SWV)*. In SWV experiments the working electrode potential is varied as a square wave function of time, and the current is measured at the end of each half-wave, just prior to potential change (see Figure 1.17). The voltammogram then shows a dependence of the

difference between reverse and forward current as a function of the applied potential. As a result, the contribution to the current signal resulting from capacitive current is minimal, that provides increase of sensitivity in comparison with standard voltammetry technique. The main disadvantage of this method is inability to distinguish the process reversibility.

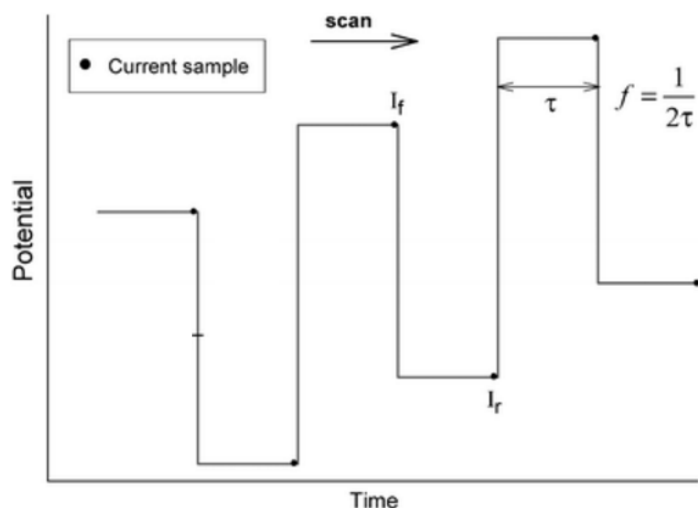


Figure 1.17. The square wave voltammetry potential scan versus time. I_f and I_r points indicate the sampling of forward and reversed current respectively.

1.3.2. Cyclic voltammetry as applied to EMFs

Voltammetry experiments with EMFs are generally limited with small amounts (0.1 mg or less) of the sample available. To overcome these difficulties, specific miniature cavities and electrode systems are constructed, that allows to decrease the solution volume and reach high EMF concentration in the near-electrode area. The design of such cell does not support employment of any standard reference electrode such as Standard hydrogen electrode or others. Generally, thin silver wire, covered with silver chloride, is used as a pseudo reference electrode, while all potentials are recalculated with respect to some internal standard. The most abundant internal standard in EMF electrochemistry is Ferrocene-Ferrocenium couple $\text{Fe}(\text{Cp})_2^{+/0}$, which undergoes reversible one-electron oxidation at 0.64 V^{113} versus the Standard hydrogen electrode. Electrochemical experiments with EMFs are typically carried out in glovebox to protect redox species from reactions with water and oxygen. The most commonly used solvent is o-dichlorobenzene, although in some cases THF and toluene/acetonitrile mixtures are applicable as well. In some earlier works⁸⁸ redox behavior of EMFs was studied in pyridine

solutions, but later it was demonstrated that due to the donor-acceptor relationship between pyridine and fullerene, the observed potentials values were shifted.

Scheme of the electrode system, employed in the present work and all the experimental details can be found in Chapter 5.

1.3.2. EMF redox processes

Electrochemical properties of endohedral metallofullerenes (EMFs) have been in focus of the researchers since mid-1990s, when the first isomerically pure samples became available^{114,115}. Today almost any new isolated EMF or EMF derivative is characterized electrochemically. Studies of redox behavior provide information about the EMF electronic properties and stability. In particular, potentials of the first oxidation and reduction steps ($E_{1/2}(+/0)$ and $E_{1/2}(0/-)$) are associated with correspondingly HOMO and LUMO level of the molecule. The value of HOMO-LUMO gap (gap_{EC}), defined as the difference between $E_{1/2}(+/0)$ and $E_{1/2}(0/-)$ values in the electrochemical experiment, can be used, along with the optical gap, as a measure of the kinetic stability of fullerenes.

Fullerene cages are known as good electron acceptors and can undergo multiple electrochemically-reversible single-electron redox processes in solution. E.g. electrochemical studies of C_{60} have demonstrated that it is able to reversibly accept up to 6 electrons¹¹⁶. Similar cathodic behavior is exhibited by higher fullerenes¹¹⁷⁻¹²⁰. At the same time, oxidation of empty fullerenes generally occurs at relatively high positive potentials, making it difficult to achieve the reversible process in standard electrochemical experiment, there are only several works that describe the oxidation of empty fullerenes (C_{76} , C_{78} , C_{82} , C_{84} etc.)^{117,119}.

Encapsulation of species inside the carbon shell results in more complex redox behavior of EMFs than that of empty fullerenes. The carbon cage in the EMF molecule can be considered as a special type of π -ligand, similar to those in organometallic complexes (e.g. as in ferrocene). In terms of organometallic electrochemistry, the ligand can be “non-innocent”, when it exhibits its own redox activity, or “innocent”, when it does not take part in the redox process. In a similar fashion, both the fullerene cage and the endohedral species can be redox active.

Figure 1.18 shows two extremes of such redox behavior. In the first case, only the carbon cage is redox-active, meaning that the valence and spin state of endohedral species remains constant during electrochemical processes (i.e. fullerene behaves as a “non-innocent”

ligand). In the second case, the endohedral cluster is the redox-active species, whereas the carbon shell behaves as an inert cavea, transparent to electrons. In terms of organometallic electrochemistry, here the fullerene cage behaves as an innocent ligand, even though the electron transfer occurs across the metal/ π -system interface. This type of electron transfer is described as an endohedral (or *in cavea*) electron transfer process¹²¹. Endohedral redox activity is generally determined by the energy level of the metal-based molecular orbitals (MOs), which should be the frontier MOs (HOMO or LUMO) of the EMF molecule.

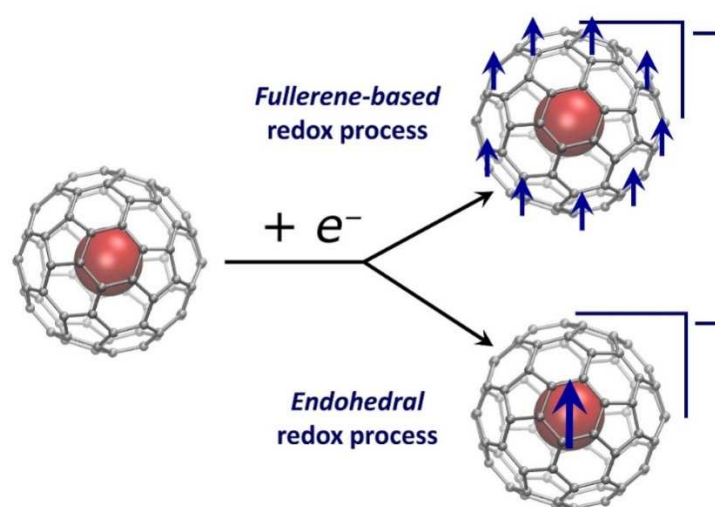


Figure 1.18. Schematic description of the fullerene-based (up) and cluster-based (down) redox processes. In the first one, reduction the surplus charge and spin density are delocalized over the fullerene cage, whereas in the latter the spin state of the endohedral cluster is altered, whereas the fullerene remains intact. Reproduced with permission from¹²¹.

Experimentally, the endohedral redox processes can be revealed via unusual redox behavior (e.g., shifted potential when compared to molecules with same cage isomer, metal dependence of the potential). Importantly, cluster-based reductions are usually electrochemically reversible, that also can serve as their indicator in some cases. Spectroelectrochemical methods such as electron spin resonance or nuclear magnetic resonance spectroelectrochemistry also allow to recognize endohedral activity^{19,120}. Cluster-based EMF cation and anion radicals demonstrate rich hyperfine structure of the ESR spectra that will be discussed in more details in ESR section. Modern methods of quantum chemical calculations also serve as a powerful instrument in revealing endohedral redox activity, as far as they reliably predict localization of the HOMO and LUMO.

1.3.3. Endohedral and cluster-based redox activity in different EMF families

Monometallofullerenes. In monometallofullerenes, metal atoms donate all valence electrons to the carbon cage. Generally the energies of metal-based electronic states appear to be far from the frontier MOs and both HOMO and LUMO are completely localized on the fullerene cage. Herewith monometallofullerene redox behavior is mostly determined by the structure and charge state of the fullerene cage. As a result, redox properties are not strongly dependent on a particular metal, and can be described using the separation into three groups: monovalent, divalent and trivalent metals. Wherein all monometallofullerenes exhibit electrochemically reversible reduction and oxidations.

Among monometallofullerenes with encapsulated M^I metal, Li@C_{60} is the only one produced in sufficient amounts for electrochemical experiment. In a neutral state Li@C_{60} is paramagnetic, and its stable form is the cation $[\text{Li@C}_{60}]^+$. It has been demonstrated that reduction behavior of $[\text{Li@C}_{60}]^+$ is similar to that of empty C_{60} but all reduction steps are shifted to the cathodic region by ca 0.6 V^{122} (figure 1.19). Such a shift can be rationalized taking into account Coulomb interaction of electrons delocalized over the fullerene with the positive charge located in the internal cluster.

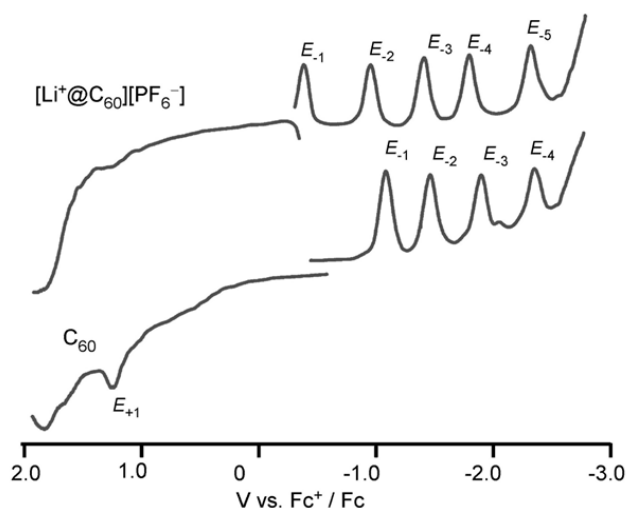


Figure 1.19. Square wave voltammetry of the $[\text{Li}^+\text{@C}_{60}][\text{PF}_6^-]$ salt compared to that of fullerene C_{60} ; Reproduced with permission from¹²³

Voltammetry curve of $[\text{Li@C}_{60}]^+$ can be also described as that of neutral Li@C_{60} . In this case the first reduction of $\text{Li}^+\text{@C}_{60}$ is assigned as the first oxidation of Li@C_{60} . If considered this

way, Li@C₆₀ appears to be extremely easy to oxidize (−0.38 V) and easy to reduce (−0.95 V) due to an unpaired electron delocalized over the cage¹²³.

M^{II}@C_{2n} monometallofullerenes (M^{II} = Ca, Sm, Eu, Tm, Yb; 2n = 74–94) are diamagnetic in the neutral state with closed-shell electronic structure. The first reduction potentials of all these EMFs are qualified in the range from −0.8 V to −1 V, that resembles empty cages with their electron acceptor behaviour^{124–126}. At the same time the oxidation potentials of M^{II}@C_{2n} monometallofullerenes are usually within the reach of standard conditions¹²⁴. Comparing redox potentials of several Yb and Sm mono-EMFs with C₈₂ cages (Table 1.1), one can see that the variation of redox potentials due to the carbon cage isomerism can exceed 0.5 V, while variation of the metal has a minor influence (generally less than 0.05 V).

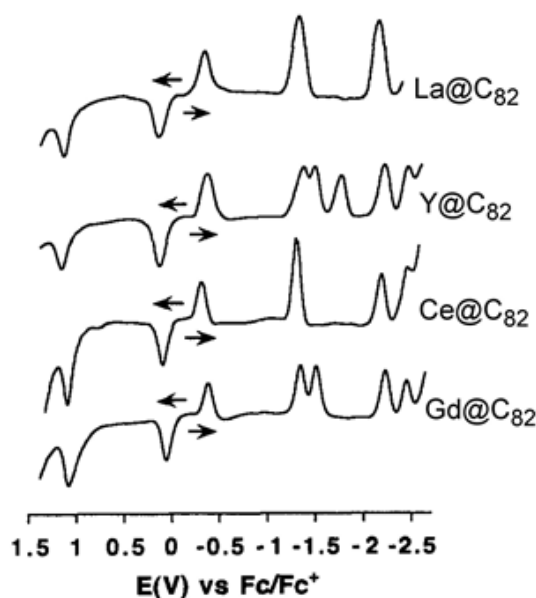


Figure 1.20. Square wave voltammetry of monometallofullerenes M^{III}@C_{82–C_{2v}(9)} with trivalent lanthanides measured in *o*-dichlorobenzene. Reproduced with permission from ¹¹⁵

The electrochemical behavior of the most abundant M^{III}@C_{2n} family mono-EMFs (M^{III} is Sc, Y, La, Ce, Pr, Nd, Gd-Er, Lu) is substantially different from that of M^I@C_{2n} and M^{II}@C_{2n} EMFs because M^{III}@C_{2n} molecules are radicals in the neutral state, having an unpaired electron delocalized over the fullerene cage. As a result, their gap_{EC} values are usually very small (close to 0.5 V), and such EMFs are normally much easier to reduce or oxidize than empty fullerenes¹⁹.

The most well-studied are M^{III}@C_{82–C_{2v}(9)} monometallofullerenes : in 1996 Suzuki et al have published the SQW results for La, Y, Ce and Gd-EMFs¹¹⁵. Comparison of the redox potentials reveals that potential values remain almost constant regardless the encapsulated

metall. Isomerism of the cage again (like it was for $M^{II}@C_{2n}$ EMFs) has stronger influence: for instance, $C_5(6)$ isomer of $La@C_{82}$ is easier to oxidize than $C_{2v}(9)$ isomer by 0.14 V¹¹⁵. Interestingly, $M^{II}@C_{82-C_{2v}(9)}$ and $M^{III}@C_{82-C_{2v}(9)}$ have very similar reduction potentials, but oxidation of the second group is almost 0.5 V more cathodic.

Dimetallofullerenes. Whereas mono-EMFs exhibit only cage-based redox activity, the encapsulation of two metal atoms inside the fullerene cage can lead to the cluster-based redox processes.

Quantum chemical calculations show, that dimetallofullerenes with six-fold charged cages, such as $La_2@C_{80}$, have cage-based HOMO and endohedral LUMO, so one can expect to see untypical metal-based reduction, while the oxidation will be cage-based.

This suggestion is supported by experimental data. Cyclic voltammetry studies of Ce- and La-based dimetallofullerenes $La_2@C_{2n}$ ($2n = 72, 78, 80$) demonstrate that these EMFs exhibit 2-3 reversible single-electron reduction steps^{127,128}. The first reduction occurs at notably positive potentials and is metal dependent – for Ce di-EMFs potentials are systematically negatively shifted by up to 0.13 V with respect to the corresponding isomer of La di-EMFs. For instance, the first reduction of $La_2@C_{80-Ih}$ occurs at -0.31 V, and the first reduction of related Ce EMF – at -0.39 V¹²⁹. Smaller cages are reduced at more negative potentials (table 1.1), but still above -1V, that is more positive than for EMFs with fullerene-based reduction. At the same time their first oxidations occur at typical for these processes range of +0.2— +0.6V (table 1.1) and the metal dependence is not expressed that much as in case of first reduction, which is typical for cage-based processes.

Another indication of the metal-based reduction activity in La and Ce di-EMFs is the large gap between the first and the second reductions (1.2-1.4V). For two consequent cage-based redox process the difference is usually within 0.4–0.5 V range (see table 1.1.) An endohedral redox process results in a much larger potential difference for the consequent redox steps, since these steps are either based on the cluster MO (which has a much higher on-site Coulomb interaction than in the fullerene cage) or affect different MOs (one on the cluster and one on the carbon cage)^{12,58}.

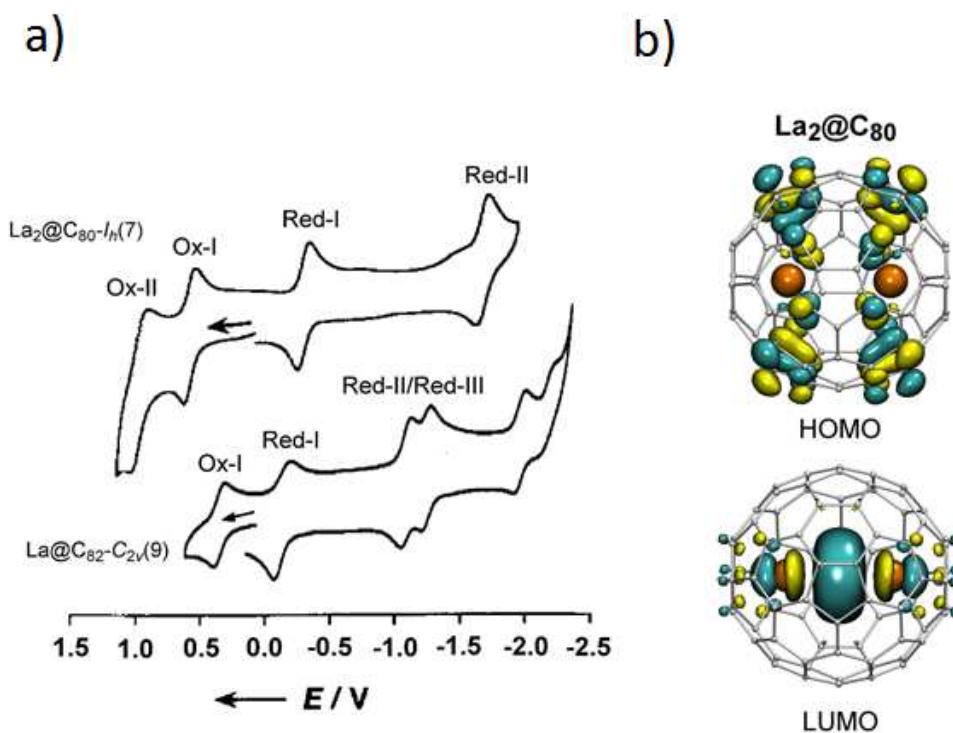


Figure 1.21. a) cyclic voltammetry of $\text{La}_2@C_{80}\text{-I}_h(7)$ compared to that of $\text{La}@C_{82}\text{-C}_{2v}(9)$; scan rate 20 mV/s, *o*-dichlorobenzene solution. Reproduced with permission from¹²⁷; b) Frontier molecular orbitals (HOMO and LUMO) of $\text{La}_2@C_{80}\text{-I}_h(7)$.

The electrochemical investigations of the $\text{M}_2@C_{82}$ family are not thorough up to date: there is only a single work so far, describing redox behavior of these interesting EMFs. In 2012 group of Akasaka demonstrated that the first oxidation potential of $\text{Sc}_2@C_{82}\text{-C}_{3v}(8)^{130}$ is +0.05V, substantially more negative than that of the corresponding isomer of carbide $\text{Sc}_2\text{C}_2@C_{82}\text{-C}_{3v}(8)$. (+0.47 V), which is associated with difference in HOMO energies (-4.89 eV in case of dimetallofullerenes versus -5.30 eV in case of carbide clusterfullerenes). At the same time, in LUMO energies as well as in the reduction potentials, the difference between two compounds is not so expressed.

For Er_2C_{82} -dimetallofullerenes from works of Anderson⁸⁸ and Stevenson⁹⁸ one can suppose that both isomers $\text{Er}_2@C_{82}\text{-C}_s(6)$ and $\text{Er}_2@C_{82}\text{-C}_{3v}(8)$ have first oxidation potentials below +0.2 V, wherein the C_s isomer is easier to oxidize. In the chapter 2 of the present work we will discuss electrochemical behavior of $\text{M}_2@C_{82}$ dimetallofullerene family in more details.

Table 1.1. Redox potentials of selected monometallofullerenes and dimetallofullerenes

EMF	ox-II	ox-I	red-I	red-II	red-III	gap _{EC}	Ref.
Li ⁺ @C ₆₀ -I _h (1)			-0.39	-0.98	-1.44		95
Yb@C ₈₂ -C ₂ (5)	0.90	0.38	-0.86	-0.98		1.24	124
Sm@C ₈₂ -C ₂ (5)		0.42	-0.84	-1.01	-1.51	1.26	126
Yb@C ₈₂ -C ₅ (6)		0.34	-0.62	-0.92	-1.81	0.96	124
Sm@C ₈₂ -C _{3v} (7)		0.56	-0.94	-1.25	-1.79	1.50	125
Yb@C ₈₂ -C _{2v} (9)		0.61	-0.46	-0.78		1.07	124
Sm@C ₈₂ -C _{2v} (9)		0.52	-0.42	-0.77	-1.60	0.94	125
La@C ₈₂ -C ₅ (6)	1.08	-0.07	-0.47	-1.40	-2.01	0.40	114
La@C ₈₂ -C _{2v} (9)	1.07	0.07	-0.42	-1.37	-1.53	0.49	114
Ce@C ₈₂ -C _{2v} (9)	1.08	0.08	-0.41	-1.41	-1.53	0.49	131
Gd@C ₈₂ -C _{2v} (9)	1.08	0.09	-0.39	-1.38	-2.22	0.48	131
Ce ₂ @C ₇₂ -D ₂ (10611)	0.82	0.18	-0.81	-1.86		0.99	12
La ₂ @C ₇₈ -D _{3h} (5)	0.62	0.26	-0.40	-1.84	-2.28	0.66	132
Ce ₂ @C ₇₈ -D _{3h} (5)	0.79	0.25	-0.52	-1.86	-2.23	0.77	133
La ₂ @C ₈₀ -D _{5h} (6)	0.78	0.22	-0.36	-1.72		0.58	59
Ce ₂ @C ₈₀ -D _{5h} (6)	0.66	0.20	-0.40	-1.76	-2.16	0.60	59
La ₂ @C ₈₀ -I _h (7)	0.95	0.56	-0.31	-1.72		0.87	128
Ce ₂ @C ₈₀ -I _h (7)	0.95	0.57	-0.39	-1.71	-	0.96	129
Sc ₂ @C ₈₂ -C _{3v} (8)		0.05	-1.10			1.15	130

Potentials are listed in Volt versus the [Fe(Cp)₂]⁺⁰ pair, "ox" stands for oxidation, "red" stands for reduction, gap_{EC} is an electrochemical gap defined as the difference of the first reduction and oxidation potentials.

Clusterfullerenes. Electrochemical behavior of clusterfullerenes i.e. endohedral metallofullerenes whose endohedral species consist of both metal and non-metal atoms, may be significantly different depending on the formal charges and spatial localization of frontier MOs. We will discuss here two main groups of clusterfullerenes: cluster⁺⁴@cage⁴⁻ EMFs (such as carbide clusterfullerenes M₂C₂@C_{2n}, sulfide clusterfullerenes M₂S@C_{2n}, oxide clusterfullerenes M₂O@C_{2n}) and cluster⁺⁶@cage⁶⁻ (mostly nitride clusterfullerenes M₃N@C_{2n}, methano-CF Sc₃CH@C₈₀, oxide CF Sc₄O₂@C₈₀, and many other EMFs).

Nitride Clusterfullerenes. Figure 1.23 demonstrates DFT-calculated frontier MOs of nitride clusterfullerenes $\text{Sc}_3\text{N@C}_{80-I_h}$ and $\text{Y}_3\text{N@C}_{80-I_h}$. The last one with fullerene-based both HOMO and LUMO represents a typical situation for a majority of nitride clusterfullerenes. In this molecule, both HOMO and LUMO are localized on the carbon cage. On the contrary, high electronegativity of Sc atoms results in rather unique MO distribution in case of $\text{Sc}_3\text{N@C}_{80}$: HOMO is still located on the cage, but LUMO has a substantial cluster contribution.

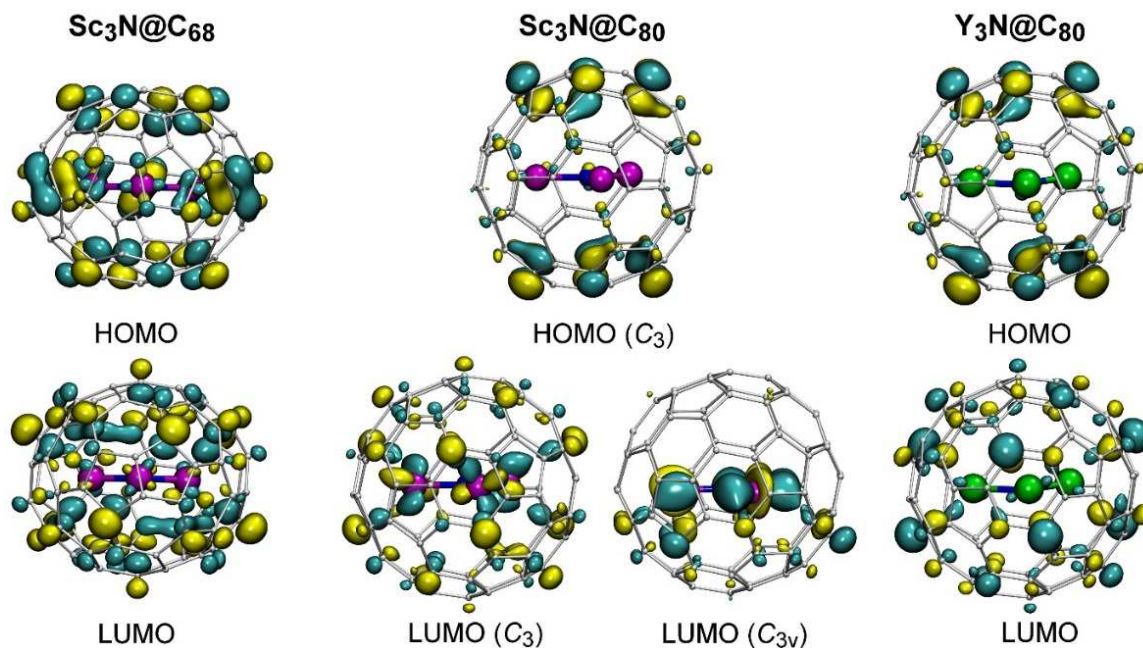


Figure 1.22. DFT-computed frontier molecular orbitals (HOMO and LUMO) of $\text{Sc}_3\text{N@C}_{68-D_3(6140)}$, $\text{Sc}_3\text{N@C}_{80-I_h(7)}$, and $\text{Y}_3\text{N@C}_{80-I_h(7)}$. The LUMO of $\text{Sc}_3\text{N@C}_{80}$ is shown for two conformers: C_3 -conformer is the lowest energy for the neutral state, whereas C_{3v} -conformer is the lowest energy for the anion. For $\text{Y}_3\text{N@C}_{80}$, C_3 -conformer has the lowest energy in both neutral and anionic states.

Based on the calculated frontier MO distribution, similar anodic and different cathodic behavior of $\text{Sc}_3\text{N@C}_{80-I_h}$ and $\text{Y}_3\text{N@C}_{80-I_h}$ isomers can be expected. Indeed, both EMFs have similar oxidation potential near 0.6 V, but noticeably different reduction potentials: -1.26 V in case of $\text{Sc}_3\text{N@C}_{80}$ and -1.41 V in case of $\text{Y}_3\text{N@C}_{80}$ ^{93,134}. The endohedral reduction of $\text{Sc}_3\text{N@C}_{80-I_h}$ nitride clusterfullerene was also demonstrated by the EPR spectrum of its anion radical¹³⁵.

$\text{Y}_3\text{N@C}_{80}$ in its turn exhibits predominantly cage-based reduction, and its first reduction potential can be considered as a reference point for cage-based reduction of C_{80-I_h} cage EMFs. Further experiments demonstrated, that LUMO position affects not only the potential value, but also the reversibility of the process. At standard voltammetric scan rates of 0.1-1V/s both EMFs exhibit electrochemically irreversible but chemically reversible reduction. However,

increasing of the potential scan rate up to several V/s allows to reach electrochemical reversibility in case of $\text{Sc}_3\text{N}@C_{80}$, whereas for $\text{Y}_3\text{N}@C_{80}$ and many other nitride clusterfullerenes with cage/based LUMO the first reduction remains electrochemically irreversible up to the scan rates of at least 70 V/s¹³⁶.

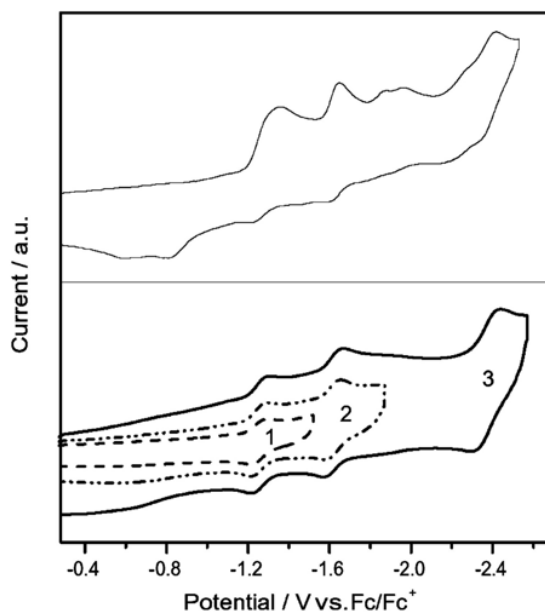


Figure 1.23. Cyclic voltammograms of $\text{Sc}_3\text{N}@C_{80}\text{-I}_h(7)$ in *o*-dichlorobenzene at scan rates of 100 mV/s in the upper panel, and 6 V/s (1), 10 V/s (2), and 20 V/s (3) in the lower panel. The different scan rates for each reduction reflect the scan rate necessary to achieve full electrochemical reversibility. Reproduced with permission from⁹³.

Electrochemical properties of nitride clusterfullerenes were studied in a lot of details, with variable cage sizes and different metals in mono/metal and mixed metal nitride clusters. Among the Sc-based nitride clusterfullerenes, $\text{Sc}_3\text{N}@C_{80}\text{-I}_h$ exhibits the highest oxidation potential, whereas the first oxidation potential of another isomer, $\text{Sc}_3\text{N}@C_{80}\text{-D}_{5h}$, is 0.25 V more cathodic¹⁰⁷. Redox behavior of $\text{Sc}_3\text{N}@C_{68}$ was studied especially carefully, and cage-based reduction and oxidation were confirmed by EPR spectroelectrochemistry in agreement with DFT-predicted localization of HOMO and LUMO on the carbon cage¹⁰⁶ (figure 1.22). $\text{Sc}_3\text{N}@C_{82}\text{-C}_{2v}(9)$ has been thought to be not sufficiently stable for a long time, but in 2015 group of Shangfeng Yang managed to isolate it in sufficient amounts for spectral and electrochemical characterization¹³⁷. Cyclic voltammetry studies have revealed two electrochemically reversible oxidations at 0.0 and 0.37 V and several irreversible reductions. Such a low value of the first oxidation potential can be one of the reason for the low kinetic stability of the compound.

For medium size metals such as Gd, Er, or Dy, nitride clusters cages from C_{78} to C_{88} can be isolated in sufficient amounts and studied electrochemically. In particular for Gd_3N -clusterfullerenes, the whole family from C_{82} to C_{88} has been examined with cyclic voltammetry (see table 1.2. and note that C_{78} and C_{82} cage isomers for Sc_3N and Gd_3N are different). Even larger cages, up to C_{96} , can be studied in case of large lanthanides such as La or Ce¹³⁸⁻¹⁴⁰. Redox behaviour of all these NCFs is more or less similar to that demonstrated by the $C_{80-I_h(7)}$ nitride. The first (and also the second, when it can be detected) oxidation step is generally reversible, while all reduction steps are electrochemically irreversible. Shifts of redox potentials for clusterfullerenes with different metals but the same cage isomer generally do not exceed 0.05-0.1 V¹¹⁰.

With variation of the carbon cages, reduction potentials of EMFs are also not changing significantly, whereas oxidation potentials seem to be shifted negatively with the increase of the cage size, so that the electrochemical gap is decreasing for larger cages (from 2.0 V for $M_3N@C_{78-C_2(22010)}$ to 1.7 V for $M_3N@C_{96}$)¹³⁸⁻¹⁴⁰. Redox behaviour of $M_3N@C_{88-D_2(35)}$ clusterfullerene falls apart from the row, since it is the only group of NCFs which exhibits electrochemically reversible reductions and oxidations.

Mixed-metal nitride clusterfullerenes with redox-active metals. Nitride clusterfullerenes family present itself a convenient platform for a design of redox-active endohedral clusters via formation of the mixed-metal clusters with redox-active metals. Three such metals have been implemented to nitride CFs so far: Ce, Ti, and V.

Ce is different from all other lanthanides in that its Ce^{IV} valence state is accessible and known for a plenty of inorganic and organometallic compounds. Herewith, the redox potential of the Ce^{IV}/Ce^{III} couple can vary in a broad range, depending on chemical environment¹⁴¹. However, redox behavior of Ce-based mono- and di-EMFs with trivalent Ce as well as Ce_3N -nitride clusterfullerenes has not exhibit any unusual activity, suggesting that Ce^{III} in fullerene cage is electrochemically inert. The first indication that endohedral Ce^{III} can be oxidized to Ce^{IV} was obtained in 2010 with isolation of $CeLu_2N@C_{80-I_h}$ ¹⁴². Its first oxidation potential was 0.01 V, almost 0.6 V more negative than expected for a cage-based oxidation in $M_3N@C_{80-I_h}$ nitride clusterfullerenes. DFT computational study also showed that removal of the $4f^1$ electron from Ce in $CeLu_2N@C_{80-I_h}$ molecule is more energetically favorable than removal of an electron from the carbon cage.

In further studies, Sc and Y have been chosen to vary the size of the M_3N -cluster in the $CeM_2N@C_{80-I_h}(7)$ series (Shannon's radii of Sc^{3+} , Lu^{3+} , and Y^{3+} ions are 0.745, 0.86, and 0.90 Å, respectively)¹⁴³. $CeM_2N@C_{80}$ clusterfullerenes demonstrate one electrochemically reversible oxidation step with the potential in the range from -0.07 V for $CeY_2M@C_{80-I_h}(7)$ to $+0.33$ V for $CeSc_2N@C_{80-I_h}(7)$. This behavior has been explained due to the geometrical reasons: with increasing the cluster size from $CeSc_2N$ to CeY_2N the inner strain in the EMF molecule is also increasing. As the Ce^{III}/Ce^{IV} oxidation is accompanied by a decrease of the strain (ionic radius of Ce^{4+} , 0.87 Å, is considerably smaller than that of Ce^{3+}), in case of big clusters this process is more thermodynamically favorable. Therefore, the oxidation of $CeM_2N@C_{80-I_h}$ occurs at lower potentials for larger M^{3+} ions.

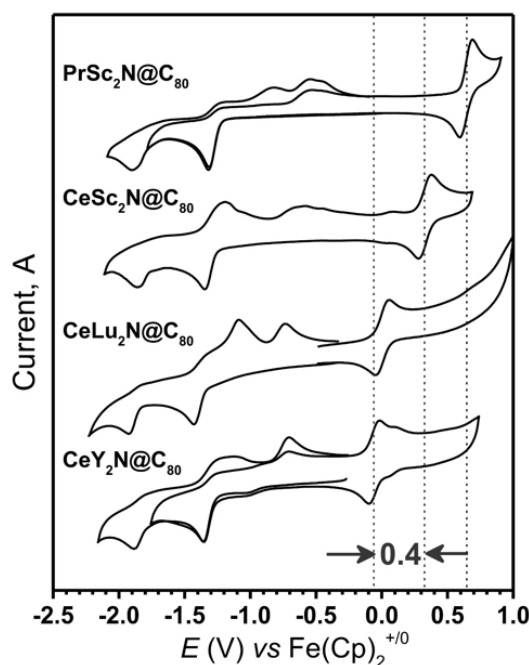


Figure 1.24. Cyclic voltammetry $PrSc_2N@C_{80-I_h}(7)$ and $CeM_2N@C_{80-I_h}(7)$ ($M = Sc, Lu, \text{ and } Y$). Reproduced with permission from¹⁴³.

The concept of the strain-driven Ce^{III}/Ce^{IV} endohedral redox couple was further developed in the studies of $Ce_xM_{3-x}N@C_{2n}$ nitride clusterfullerenes with different cages and cluster configuration. ($x = 1, 2$; $M = Sc$ or Y ; $2n = 78, 84, 86, 88$), performed by group of Duncsh¹⁴⁴. Redox potentials were determined for a series of twelve Ce-containing nitride EMFs and then compared to the non-Ce analogues. The cluster-induced strain was found to be weaker for larger cages that made cage-based reductions in some cases more thermodynamically favorable. Thus, the preference of an endohedral Ce^{III}/Ce^{IV} or a cage-based

oxidation is determined on whether the inner strain is high enough to render a Ce-based oxidation below the oxidation potential of the fullerene cage¹⁴³.

Both titanium and vanadium cannot form nitride clusterfullerenes as the only metals, but can be implemented into the mixed-metal nitride clusterfullerenes. Recently such EMFs as $\text{TiSc}_2\text{N}@C_{80-I_h}(7)$, $\text{TiY}_2\text{N}@C_{80-I_h}(7)$, $\text{VSc}_2\text{N}@C_{80-I_h}(7)$, and $\text{V}_2\text{ScN}@C_{80-I_h}(7)$ have been synthesized and isolated^{145,146}. Comparison of the redox potentials of Ti- and V-containing nitride clusterfullerenes to those of $\text{Y}_3\text{N}@C_{80-I_h}(7)$ reveals that their electrochemical behavior is changed substantially. In particular, Ti-containing EMFs exhibit both reversible oxidations and reductions. Herewith the oxidation potentials occur to be sufficiently more negative, and reduction potentials – more positive than those of $\text{Y}_3\text{N}@C_{80}$, that indicates the endohedral nature of both processes. So, we can conclude, that Ti^{III} in the neutral state can change the valence state to Ti^{II} in the anion form or to Ti^{IV} in the cation form. Nitride EMFs, containing trivalent V also exhibit reversible endohedral oxidation and reduction steps. Oxidation of $\text{V}_2\text{ScN}@C_{80}$ at +0.60 V (see table) is the only process which cannot be reliably assigned to the cage or transition metal¹⁴⁵.

Other clusterfullerenes with six-fold charged cage. For majority of clusterfullerenes with six-fold charged cluster, $C_{80-I_h}(7)$ cage isomer is the dominating, or even the only available cage that has been isolated. Matching redox potentials of these EMFs with the corresponding oxidation and reduction potentials of $\text{Y}_3\text{N}@C_{80-I_h}$ (see table 1.2) one can see, that the cluster-based reduction is typical for all of them. All potentials of the first reduction are sufficiently more positive than –1.41 V reported for $\text{Y}_3\text{N}@C_{80-I_h}$ and span rather broad range, from –1.21 V for $\text{Sc}_3\text{CH}@C_{80}$ ¹⁴⁷ to –0.42 V in the aforementioned $\text{VSc}_2\text{N}@C_{80-I_h}(7)$ ¹⁴⁵. At the same time, the first oxidation potentials for a majority of C_{80-I_h} clusterfullerenes is about +0.6 V that reveals the fullerene-based process. Only two exceptions are breaking this “rule”: $\text{Sc}_4\text{C}_2@C_{80}$ and $\text{Sc}_4\text{O}_2@C_{80}$, in which oxidation is also a cluster-based process.

In case of $\text{Sc}_4\text{O}_2@C_{80}$, both HOMO and LUMO are mainly localized on the oxide moiety. Experimentally, $\text{Sc}_4\text{O}_2@C_{80}$ exhibits reversible reduction and oxidation at 0.00 and –1.10 V, respectively, which is different from the typical values of the cage-based redox potentials¹⁰². For recently isolated and characterized $\text{Sc}_4\text{C}_2@C_{80}$, the HOMO is localized on the Sc_4C_2 cluster, so the first oxidation potential is 0.01 V, whereas the LUMO has large cage component, and the first reduction step occurs at the potential of –1.53 V, which is even more negative, than cage-

based reduction of $Y_3N@C_{80}$ ^{134,148}. Note that in some cases frontier MO can be evenly distributed between cluster and the cage. Origin of such mixed orbitals can be explained as follows: the cage and the cluster MOs have roughly equal energies, and hence they are efficiently “hybridized”. For such compounds, redox potentials of EMFs are usually more close to those for EMFs with cage-based redox activity. (Table 1.2).

Table 1.2. Redox potentials of selected clusterfullerenes with six-fold charged clusters

EMF	ox-II	ox-I	red-I	red-II	red-III	gap _{EC}	Ref.
Sc ₃ N@C ₆₈ -D ₃ (6140)	0.85	0.33	-1.45	-2.05		1.78	106
Sc ₃ N@C ₇₈ -D _{3h} (5)	0.68	0.21	-1.56	-1.91		1.77	140
Sc ₃ N@C ₈₀ -D _{5h} (6)		0.34	-1.33			1.68	107
Sc ₃ N@C ₈₀ -I _h (7)	1.09	0.59	-1.26	-1.62	-2.37	1.85	93
Sc ₃ N@C ₈₂ -C _{2v} (9)	0.37	0.00	-1.35	-1.52	-1.78	1.35	137
Y ₃ N@C ₈₀ -I _h (7)		0.64	-1.41	-1.83		2.05	134
Gd ₃ N@C ₈₀ -I _h (7)		0.58	-1.44	-1.86	-2.13	2.02	110
Gd ₃ N@C ₈₂ -C _s (39663)		0.38	-1.53	-1.87		1.91	151
Gd ₃ N@C ₈₄ -C _s (51365)		0.32	-1.37	-1.76		1.69	110
Gd ₃ N@C ₈₆ -D ₃ (17)		0.33	-1.39	-1.72		1.82	151
Ce ₃ N@C ₈₈ -D ₂ (35)	0.63	0.08	-1.30	-1.57		1.38	138
Ce ₃ N@C ₉₂ -T(92)		0.32	-1.48	-1.64		1.80	139
Ce ₃ N@C ₉₆ -D ₂ (186)	0.67	0.18	-1.50	-1.84		1.68	49
TiSc ₂ N@C ₈₀ -I _h (7)*		0.16	-0.94	-1.58		1.10	152
TiY ₂ N@C ₈₀ -I _h (7)*		0.00	-1.11	-1.79		1.11	146
VSc ₂ N@C ₈₀ -I _h (7)*		0.44	-0.42	-0.66	-1.33	0.86	145
V ₂ ScN@C ₈₀ -I _h (7)*		0.60	-0.77	-2.38	-	1.37	145
CeY ₂ N@C ₈₀ -I _h (7)		-0.07	-1.36	-1.88		1.30	143
CeSc ₂ N@C ₈₀ -I _h (7)		0.33	-1.31	-1.83		1.64	143
Sc ₄ O ₂ @C ₈₀ -I _h (7)	0.79	0.00	-1.10	-1.73		1.10	102
Sc ₄ C ₂ @C ₈₀ -I _h (7)		0.01	-1.53	-1.97		1.54	148

Potentials are listed in Volt versus the $[Fe(Cp)_2]^{+0}$ pair, “ox” stands for oxidation, “red” stands for reduction, gap_{EC} is an electrochemical gap defined as the difference of the first reduction and oxidation potentials. Redox potentials of selected clusterfullerenes with four four-fold charged cluster will be given in table 2.3 in comparison with related dimetallofullerenes.

Clusterfullerenes with four-fold charged clusters. For EMFs with +4 charge on the internal cluster, the most abundant cages are two isomers of C_{82} : $C_{3v}(8)$ and $C_s(6)$. In these molecules, the HOMO is dominantly localized on the cage, while LUMO has different cluster and cage contribution for different EMFs: the LUMO of $Sc_2O@C_{82}$ is localized on the fullerene, the LUMO of $Sc_2S@C_{82}$ is also largely cage-based but has noticeable cluster contribution, whereas the LUMO of $Sc_2C_2@C_{82}$ is predominantly localized on the carbide cluster. In the row of $C_{82}-C_{3v}(8)$ EMFs the absolute value of the first reduction potentials decreases with increasing of the cluster contribution to LUMO: the most negative value is reported for $Sc_2O@C_{82}$ (-1.17 V)¹⁴⁹ followed by $Sc_2S@C_{82}$ (-1.04 V)⁷² and the smallest absolute value was detected for $Sc_2C_2@C_{82}$ (-0.94 V)¹⁵⁰. At the same time, their first oxidation potentials are quite close and fall into the range of 0.47-0.54 V. Similar correlations between redox potentials and frontier MO distribution can be revealed for $C_{82}-C_s(6)$ clusterfullerenes. (see table 2.3.).

1.4. EPR spectroscopy

1.4.1. Basic principles of the method

Electron Paramagnetic Resonance (EPR) sometimes referred to as Electron Spin Resonance (ESR) spectroscopy is a method for studying of materials with unpaired electrons. The EPR phenomenon was discovered in 1944 independently by Yevgeny Zavoisky at the Kazan State University, and by Brebis Bleaney at The University of Oxford.

The method is based on the Zeeman effect of electron energy levels splitting in the presence of a static magnetic field: for a single electron with a spin $S=1/2$ in the presence of external static magnetic field B_0 , the electron's magnetic moment aligns itself either parallel (spin projection $m_s=+1/2$) or antiparallel (spin projection $m_s=-1/2$) to the field, each alignment having a specific energy:

$$E = m_s g_e \mu_B B_0 \quad (\text{Eq. 1.5})$$

where g_e is the electron's so-called g -factor, μ_B is the Bohr magneton.

In EPR experiment sample is disposed under microwave irradiation with magnetic component B_1 , polarized perpendicularly to B_0 , and frequency ν . Absorbing or emitting a photon of energy $h\nu$, unpaired electron can move between the two energy levels.

Interaction of electron with magnetic moments with surrounding nuclei provides an additional energy levels splitting. In external static field nuclear magnetic moment I can have

$2I + 1$ different projections to the field direction m_I ($m_I = -I, -I+1 \dots I$). (see figure 1.25) The resonance field, determined as:

$$B = B_0 - a m_I \quad (\text{Eq. 1.6})$$

Where a is a coupling constant, can take $2I + 1$ different values. Thus each nucleus of spin I additionally splits each of the two electron spin levels into $2I + 1$ sublevels. Possibility of transitions between different levels is regulated by the *selection rules*:

$$\Delta m_s = 1; \quad \Delta m_I = 0 \quad (\text{Eq. 1.7})$$

Herewith the resonance conditions should be obeyed, i.e. the energy difference between spin sublevels, calculated as:

$$\Delta E = \Delta m_s g_e \mu_B B_0 = g_e \mu_B B \quad (\text{Eq. 1.8})$$

should be equal to the photon energy $h\nu$ that leads us to the fundamental equation of EPR spectroscopy:

$$h\nu = g_e \mu_B B \quad (\text{Eq. 1.9})$$

In practice, the resonance conditions are search for by varying the magnetic field B at constant microwave frequency. EPR spectrum presents itself as a dependence of the first derivatives of the microwave absorbance on the field B . Each peak in the spectrum complies one spin excitation.

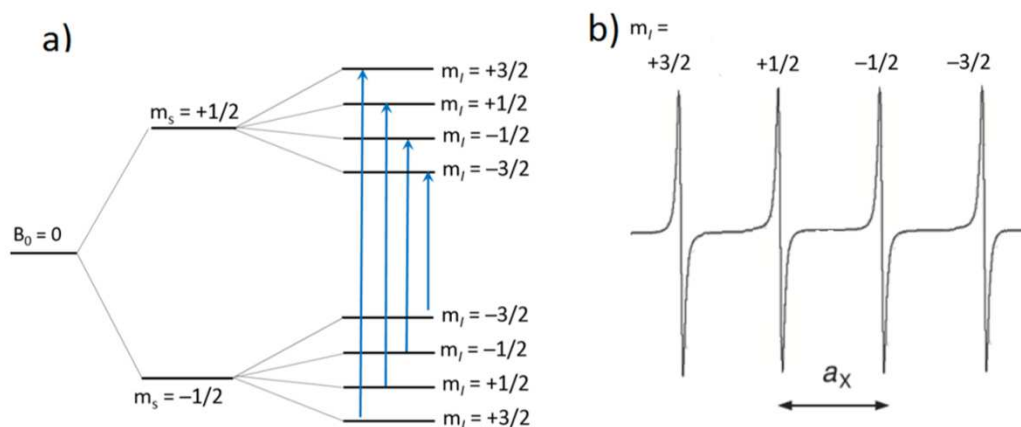


Figure 1.25. Energy levels splitting of an unpaired electron interacting with nuclear spin $I=3/2$, all placed in a static magnetic field B_0 , blue arrows indicate possible electron transitions (a), EPR spectrum of system with unpaired electron interacting with nuclear spin $I=3/2$, black arrow indicates coupling constant a_x (b).

Thus, analyzing the multiplicity of EPR spectrum we can consider, where the electron is localized and with which nucleus it is interacting. Moreover there are several parameters that we can get from the EPR spectrum:

Electron g-factor g_e (dimensionless) provides information about paramagnetic center's electronic structure. The g -factor of a free electron is 2.0023, and the g -factor values of most organic radicals are very close to this value, since the unpaired electron has very small orbital contribution to the magnetic moment (spin-orbital interaction is weak). On the other hand, g -factor for ESR spectra of d- and f-elements can differ greatly from 2.00, because of the spin-orbit coupling.

Hyperfine coupling constant a (measured in magnetic induction units) is a parameter of the spectral line spacing and, in the simplest case, is the spacing itself. This parameter characterizes the degree of interactions between the unpaired electron spin and nuclear spins in its vicinity. The value of the isotropic coupling constant is directly proportional to the spin density in the nucleus.

Line width (measured in magnetic induction units) is measured along the x axis of an EPR spectrum, from a line's center to a chosen reference point of the line.

In general, both the g -factor and *hyperfine coupling constant* a are second-rank tensor including 9 numbers arranged in a 3x3 matrix. Such types of matrix can be diagonalized with help of Euler angle transformation of the magnetic field vector into the molecular coordinate system, thereby reducing the components number to 3: g_{xx} , g_{yy} and g_{zz} ; a_{xx} , a_{yy} and a_{zz} .

If the temperature is high enough and paramagnetic molecules are tumbling fast in solution, any anisotropic property is completely averaged out. Only the isotropic parts of all interactions are observable, which is the isotropic g factor and the isotropic hyperfine coupling constants.

$$g_{iso} = \frac{1}{3}(g_{xx} + g_{yy} + g_{zz}) \quad (\text{Eq. 1.10})$$

$$a_{iso} = \frac{1}{3}(a_{xx} + a_{yy} + a_{zz}) \quad (\text{Eq. 1.11})$$

The spectrum consists of a series of symmetric lines with equal widths. This is the case, for example, for many radicals in solutions at room temperature.

At low temperatures, the paramagnetic molecules are immobilized. There is neither translational nor rotational motion (so called "rigid limit" - figure 1.26). The EPR spectra exhibit

the full anisotropy of all interactions. This is generally the case in powder materials, glasses, and frozen solutions. In crystals, the components of g -factor are determined by the number of crystallographically equivalent orientations of the EPR spin. For example in rhombic lattice the number of g -factor component is reduced to two: $g_{xx} = g_{yy} = g_{\perp}$, $g_{zz} = g_{\parallel}$.

Between these two extremes, there are dynamic regimes where the rotational motion is present but is too slow to completely average the anisotropic interactions, but fast enough to visibly affect the spectrum. In particular, in so called “the fast-motion regime”, the rotational motion is fast enough so that the spectrum still looks similar to the isotropic solution spectrum, although line widths value are affected by both anisotropic hyperfine coupling ΔA and g shift Δg and can be substantially different from line to line.

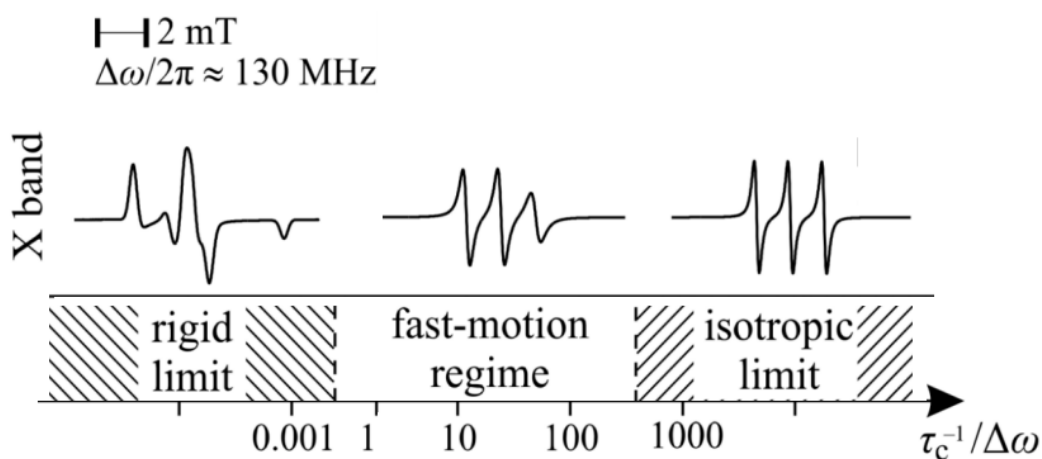


Figure 1.26. Schematic depiction of the nitroxide radical X-band EPR spectra in the low/temperature regime (rigid limit) regime, intermediate fast motional regime and high temperature isotropic regime¹⁵³.

1.4.2. EPR spectroscopy applied to EMFs: several examples

To exhibit EPR activity, the analyzed compound should be paramagnetic. Thus EMFs studied by EPR spectroscopy can be classified into two groups: (a) EMFs, which are paramagnetic in their pristine (neutral) states, and (ii) EMFs, which are diamagnetic in their pristine (neutral) states but can be transformed into paramagnetic forms with help of chemical or electrochemical redox reactions¹⁹.

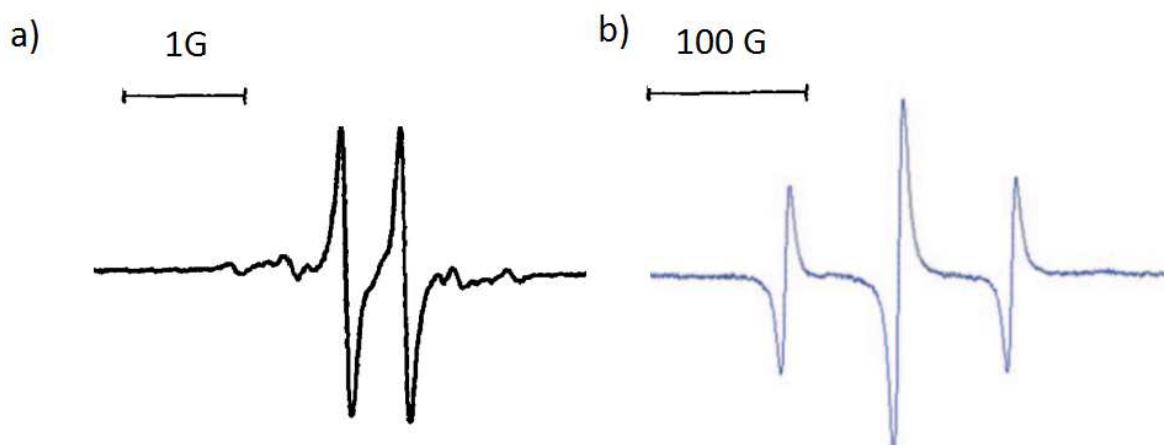


Figure 1.27. a) EPR spectrum of $Y@C_{82}$, measured in solution at room temperature¹⁵⁴; b) EPR spectrum of $Y_2@C_{79}N$, measured in solution at room temperature¹⁵⁵.

The first group is less numerous and includes mainly $M^{III}@C_{2n}$ monometallofullerenes (usually with Sc, Y, and La) and their derivatives^{142,154}. In addition, EPR experiment data has been published for $Sc_3C_2@C_{80-I_h}$ ^{156,157} and its derivatives^{158–160}, dimetallic endohedral heterofullerene $M_2@C_{79}N$ (Y, Gd, “pseudo- I_h ” isomer)^{155,161} and several nitride clusterfullerenes: $ErSc_2N@C_{80-I_h}$ ¹⁶², $TiSc_2N@C_{80-I_h}$ ¹⁵², and $TiY_2N@C_{80-I_h}$ ¹⁴⁶. Although the list of paramagnetic EMFs is much broader, for a majority of lanthanide-based EMFs, the EPR studies are complicated because of the fast spin–lattice relaxation. Figure 1.27 shows EPR spectra of $Y@C_{82-C_{2v}}$ and $Y_2@C_{79}N$. Nuclear spin of ^{89}Y is $\frac{1}{2}$. Therefore, monometallofullerene exhibits a typical doublet ($2N \cdot I + 1 = 2 \cdot \frac{1}{2} + 1 = 2$) with the coupling constant of 0.48 G and g-factor of 1.9999¹⁵⁴. The small coupling constant indicates that the spin density is mainly localized on the fullerene cage.

Dimetallic endohedral heterofullerene $Y_2@C_{79}N$ in solution exhibits a triplet ($2N \cdot I + 1 = 4 \cdot \frac{1}{2} + 1 = 3$) with the $a(^{89}Y)$ coupling constant of 81.23 G and g-factor of 1.9740¹⁵⁵. Thus, the coupling constant is more than 150 larger than in $Y@C_{82}$, which is an indication of the metal-based radical. DFT calculations also gave a similar value of coupling constant revealing that the large part of the spin density is localized between the two Y atoms.

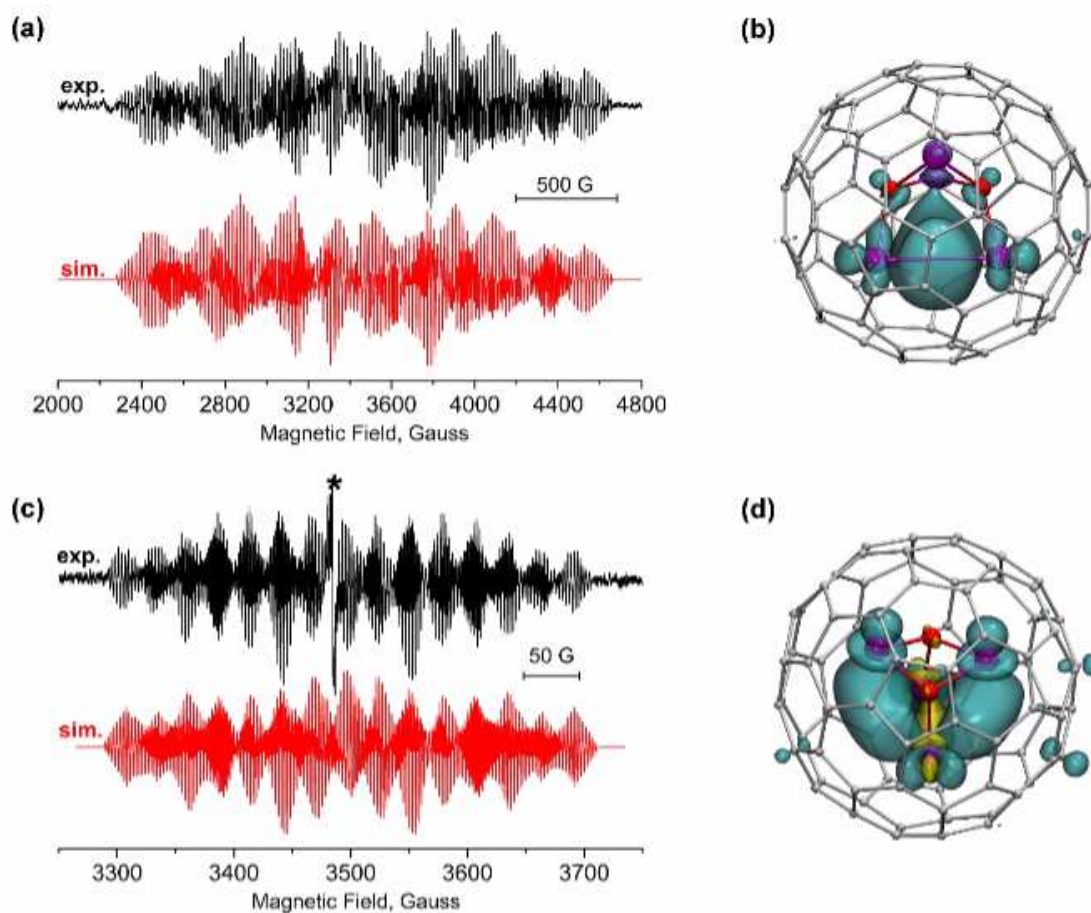


Figure 1.28. (a) Experimental (*exp.*) and simulated (*sim.*) EPR spectra of cation radical $Sc_4O_2@C_{80}^+$; (b) Spin-density distribution in $Sc_4O_2@C_{80}^+$; (c) Experimental (*exp.*) and simulated (*sim.*) EPR spectra of anion radical $Sc_4O_2@C_{80}^-$; (d) Spin-density distribution in $Sc_4O_2@C_{80}^-$. Reproduced with permission from¹⁰².

The second group - diamagnetic EMFs, which can be transformed into paramagnetic anions or cations – is more numerous and includes dimetallofullerenes as well as different carbide nitride and oxide clusterfullerenes. It is important, that only EMFs with reversible redox activity can form EPR active ion-radicals. Herewith, the EPR spectra of EMFs with cluster-based redox activity are of particular interest, because the spin density will be located on the internal cluster.

One of the illustrative examples of the cluster-based ion-radicals is provided by charge states of the oxide clusterfullerene $Sc_4O_2@C_{80-I_h}(7)$. As it has been mentioned above, both HOMO and LUMO of the molecule are localized on the internal cluster¹⁰². Reversible behavior of the compound in both oxidation and reduction confirms that cation and anion radicals are stable enough and could be studied *in situ* by EPR spectroscopy. The molecule has rather complex electronic structure with two non-equivalent pairs of Sc atoms. Two atoms bonded to

two oxygens each have a formal state of Sc^{3+} , whereas those two bonded to only one oxygen each have a formal state of Sc^{2+} and form a $\text{Sc}^{2+}\text{--Sc}^{2+}$ bond. The nuclear spin of each Sc is $7/2$, resulting in a complicated EPR spectrum for 2 equivalent pairs of Sc (figure 1.28). Complex hyperfine patterns of the radicals can be simulated by considering two pairs of Sc atoms, with substantially different coupling constants. The $a(^{45}\text{Sc})$ values of 2×2.6 and 2×27.4 G in the anion, 2×150.4 and 2×19.0 G in the cation have been assigned to Sc^{2+} and Sc^{3+} pairs respectively, with the help of extended DFT calculations and molecular dynamics simulations. Spin density in both species is localized on the Sc_4O_2 cluster (Figure 1.28b,d), leading to large *hfc* values and second order features in the hyperfine structure. The large value of the coupling constant of the Sc^{2+} atoms in the cation radical (150.4 G) can be explained due to the M–M bonding nature of the HOMO. Thus, EPR spectroscopy confirmed that $\text{Sc}_4\text{O}_2@C_{80}$ exhibits cluster-based redox behavior in both reduction and oxidation.

Chapter 2. Redox-active metal-metal bonds in dimetallofullerenes $M_2@C_{82}$ and comparison to sulfide clusterfullerene $Er_2S@C_{82}$ and carbide $M_2C_2@C_{82}$ analogues.

2.1. $M_2@C_{82}$: synthesis and isolation

In this chapter we will demonstrate the detailed spectroscopic and electrochemical investigations of a series of $M_2@C_{82}-C_{3v}$ and $M_2@C_{82}-C_5$ dimetallofullerenes to reveal variation of the redox behavior in different metal and cages combinations. In particular, $Er_2@C_{82}$, $ErSc@C_{82}$, $Sc_2@C_{82}$, $Lu_2@C_{82}$ and $YLu@C_{82}$ EMFs with $C_{3v}(8)$ isomer together with $Lu_2@C_{82}$ and $Er_2@C_{82}$ with $C_5(6)$ isomer have been isolated and characterized. Comparison to their clusterfullerene analogues such as $Er_2S@C_{82}$ sulfide clusterfullerenes and several carbide clusterfullerenes has been performed as well.

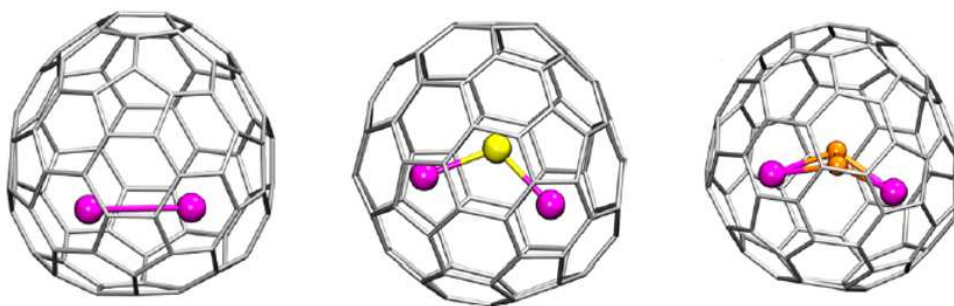


Figure 2.1. Molecular structures of $Sc_2@C_{82}$, $Sc_2S@C_{82}$ and $Sc_2C_2@C_{82}$, all with $C_{3v}(8)$ cage isomer. Carbon atoms in the fullerene cage are grey; endohedral carbon atoms are shown in orange, sulfur is yellow, Sc atoms are magenta.

All listed EMFs have been obtained from the minor fractions of different arc-discharge syntheses. In particular Er_2 - and Er_2S -clusterfullerenes have been obtained from the Er-based arc-discharge synthesis with guanidium thiocyanate as a nitrogen source (Fig. 2.2). $Er_2S@C_{82}-C_5(6)$ and $Er_2S@C_{82}-C_{3v}(8)$ EMFs have been isolated for the first time. Sulfur atoms from guanidium thiocyanate have been encapsulated inside the fullerene cage as a part of metal Er_2S sulfide cluster, as it has been observed earlier for Sc and Lu sulfide clusterfullerenes⁷⁰. The yield of both sulfide clusterfullerenes has been found to be lower with respect to the corresponding isomers of dimetallofullerenes, obtained in the same synthesis. Wherein the yield of $Er_2@C_{82}-C_{3v}(8)$ is about two times bigger than that of $Er_2@C_{82}-C_5(6)$, in case of $Er_2@C_{82}$ EMFs the yields of two isomers are approximately equal.

$\text{Lu}_2@C_{82}$ dimetallofullerenes have been obtained as a minor products of Lu/Ti/ NH_3 and Lu/Ti/melamine arc-discharge syntheses⁵², performed in our group in period of 2012-2013; mixed metal-dimetallofullerene YLu@ C_{82} EMF has been obtained from Lu/Y/ NH_3 arc discharge synthesis¹⁶³; carbides YSc $_2@C_{82-C_5}$ (6) and Y $_2C_2@C_{82-C_5}$ (6) have been obtained from the Y/Sc/ NH_3 arc-discharge syntheses; Sc $_2C_2@C_{82-C_5}$ (6) has been obtained from the Sc/Ti/ CH_4 arc/discharge syntheses¹⁶⁴. Mixed metal-dimetallofullereneErSc@ $C_{82-C_{3V}}$ (8)EMF has been obtained from Er/Sc/guanidium thiocyanate arc-discharge syntheses.

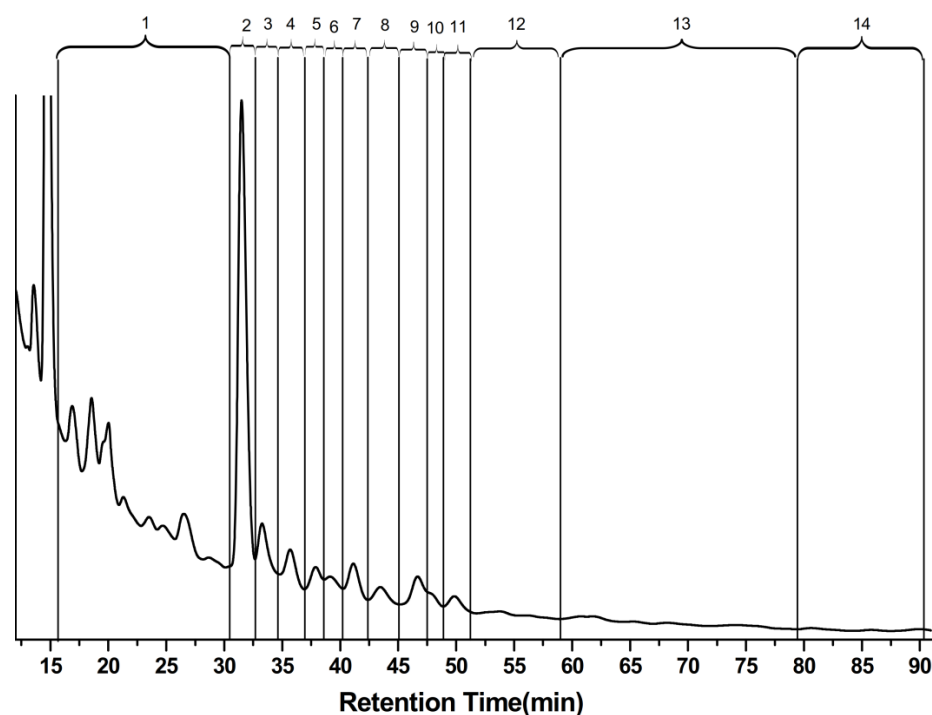


Figure 2.2. HPLC profile of Er-GNT primary extract. Fraction 3 contains $\text{Er}_3\text{N}@C_{80-D_{5h}}$ and $\text{Er}_2\text{S}@C_{82-C_5}$ EMFs; fraction 4 contains $\text{Er}_2@C_{82-C_5}$ EMF; fraction 5 contains $\text{Er}_3\text{N}@C_{82}$ and $\text{Er}_2\text{S}@C_{82-C_{3V}}$ EMFs; fraction 7 contains $\text{Er}_2\text{S}@C_{82-C_{3V}}$ EMF. Further separation was performed with help of recycling HPLC. (For more details, see Chapter 5).

All listed above EMFs have been isolated as individual compounds with help of recycling HPLC technique (for more details, see Chapter 5.) The composition purity has been confirmed with laser desorption time-of-flight (LD-TOF) mass spectrometry.

Sc $_2@C_{82-C_{3V}}$ (8) and additional amounts of $\text{Er}_2@C_{82-C_{3V}}$ (8) and $\text{Er}_2@C_{82-C_5}$ (6) have been synthesized and isolated by our colleagues from the group of Professor Stevenson in Indiana-Purdue University Fort Wayne. They have employed original non-Chromatographic “Catch and Release” approach: at first fullerene Er and Sc-based extracts have been fractionated with described above SAFA method (Section 1.2.4), wherein both Er_2 - and Sc $_2$ -dimetallofullerenes

have been immobilized onto the aminosilica. During the second step the spent reactive silica has been washed several time with different solvents, resulting in isolation of individual compounds of $\text{Sc}_2\text{@C}_{82}\text{-C}_{3v}(8)$ and $\text{Er}_2\text{@C}_{82}\text{-C}_{3v}(8)$.

2.2. Molecular structure determination of the $\text{M}_2\text{@C}_{82}\text{-C}_{3v}$ and $\text{M}_2\text{@C}_{82}\text{-C}_s$ EMFs

2.2.1 Vis-NIR absorption spectroscopy

Molecular structures of two $\text{Er}_2\text{@C}_{82}$ dimetallofullerenes with $\text{C}_s(6)$ and $\text{C}_{3v}(8)$ carbon cage isomers were determined earlier by single crystal X-ray diffraction^{60,61}. Molecular structure of the other EMFs can be assigned using comparison of vis-NIR absorption spectroscopy data.

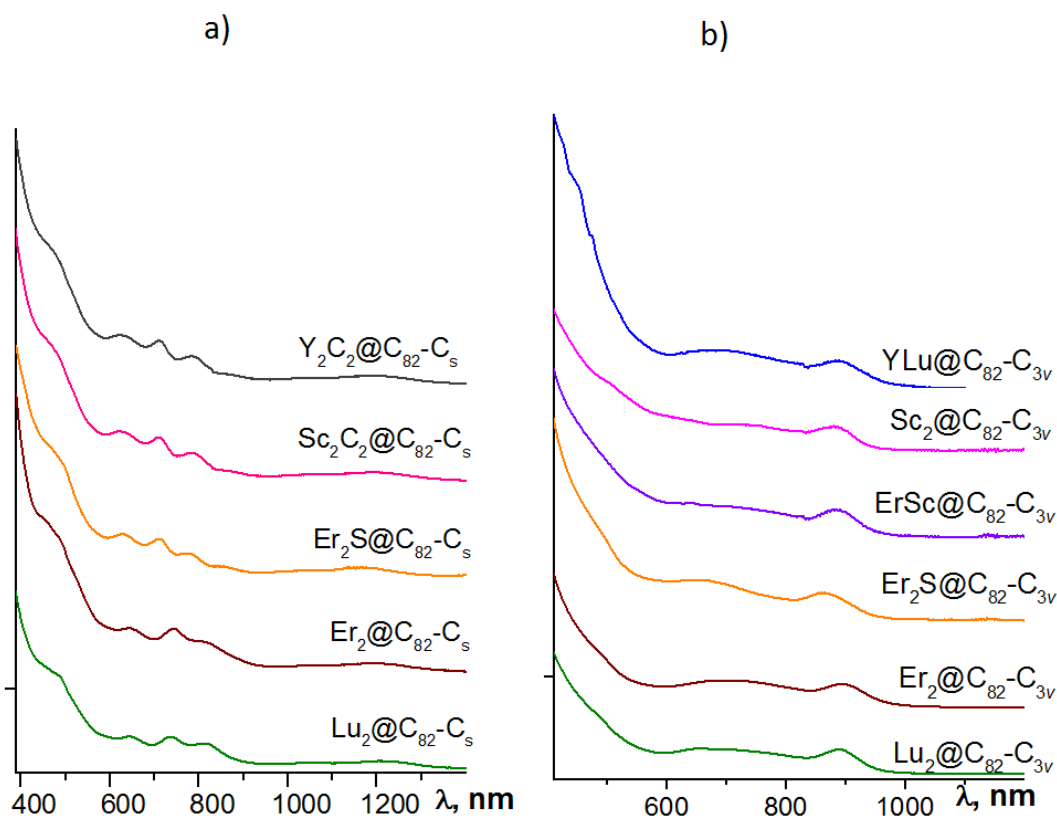


Figure 2.3. Vis-NIR absorption spectra of EMFs: (a) isomer I, $\text{C}_{82}\text{-C}_s(6)$ and (b) isomer II, $\text{C}_{82}\text{-C}_{3v}(8)$, toluene, $l=1$ cm. For $\text{Er}_2\text{@C}_{82}\text{-C}_{3v}(8)$, the molar extinction coefficients at 379 nm, 477 nm, and 899 nm were determined to be $23.4 \cdot 10^3$, $7.2 \cdot 10^3$, and $2.7 \cdot 10^3$, respectively.

Figure 2.3 demonstrates, that absorption spectra of all compounds discussed in this chapter can be classified into two groups with very similar spectral shapes – one for $\text{C}_{82}\text{-C}_s(6)$ EMFs and another one for $\text{C}_{82}\text{-C}_{3v}(8)$ EMFs. Variation of endohedral species composition has almost no influence on the spectra shape. Figure 2.3a. shows the spectra of the isomer I, identified

by its absorption pattern as $C_{82}-C_5(6)$; these spectra are also very similar to the spectra of $Sc_2C_2@C_{82}-C_5(6)$,⁴⁸ $Sc_2S@C_{82}-C_5(6)$ ⁴⁹ and $Y_2C_2@C_{82}-C_5(6)$ ⁶⁶. Figure 2.3b. shows the spectra of the isomer II, identified as $C_{82}-C_{3v}(8)$; very similar spectra have been also reported for $Sc_2S@C_{82}-C_{3v}(8)$ ^{49, 51} or carbide clusterfullerenes $M_2C_2@C_{82}-C_{3v}(8)$ ($M = Sc, Y, Er$)^{62,66,69,130}.

As mentioned in the Chapter 1, the absorption behavior of EMFs is dominated by the $\pi-\pi^*$ transitions in the π -system of the carbon cage. It is also known, that the same carbon cage isomer can demonstrate different π -electron structure depending on its formal charge state, that results in different absorption behavior: for example, absorption pattern of $C_{82}-C_{2v}(9)$ cage trianion in $M^{III}@C_{82}-C_{2v}(9)$ monometallofullerenes¹⁶⁵ is different from that of the corresponding dianion in $Sm^{II}@C_{82}-C_{2v}(9)$ ¹⁶⁶ and tetraanion in $Y_2C_2@C_{82}-C_{2v}(9)$ ⁶⁶. Thus, the shape the vis-NIR absorption spectra of EMFs are very sensitive not only to the isomeric structure, but to the formal charge distribution as well.

Hereof we can conclude, that all EMFs, been assigned as $C_{82}-C_{3v}(8)$, also have the same formal charge state of the cage of 4-. Whereas the C_{82}^{4-} state is natural for the $Er_2S@C_{82}$ taking into account the formal 3+ charge of the erbium ion and the 2- charge of the sulfide ion, for the $M_2@C_{82}$ molecules the 4-fold charge of the cage indicates that the metal atoms have to be assigned a formal charge of 2+.

For $C_{82}-C_5(6)$ EMF family with Er and Lu we can use the same line of arguments. The cluster charge in dimetallofullerenes $Lu_2@C_{82}-C_5(6)$ and $Er_2S@C_{82}-C_5(6)$ should be +4, the same to that of $Er_2S@C_{82}$ and carbide clusterfullerenes $Y_2C_2@C_{82}-C_5(6)$, $YScC_2@C_{82}-C_5(6)$ and $Sc_2C_2@C_{82}-C_5(6)$. Thus in this family of dimetallofullerenes, each of the metal atoms also donates two electrons to the carbon cage, leaving one valence electron for the metal-metal bond formation.

2.2.2. Vibrational spectroscopy

For $C_{3v}(8)$ isomers of $Lu_2@C_{82}$, $Er_2@C_{82}$, and $Er_2S@C_{82}$ the cage structure has been also confirmed with IR transmittance spectroscopy and Raman spectroscopy.

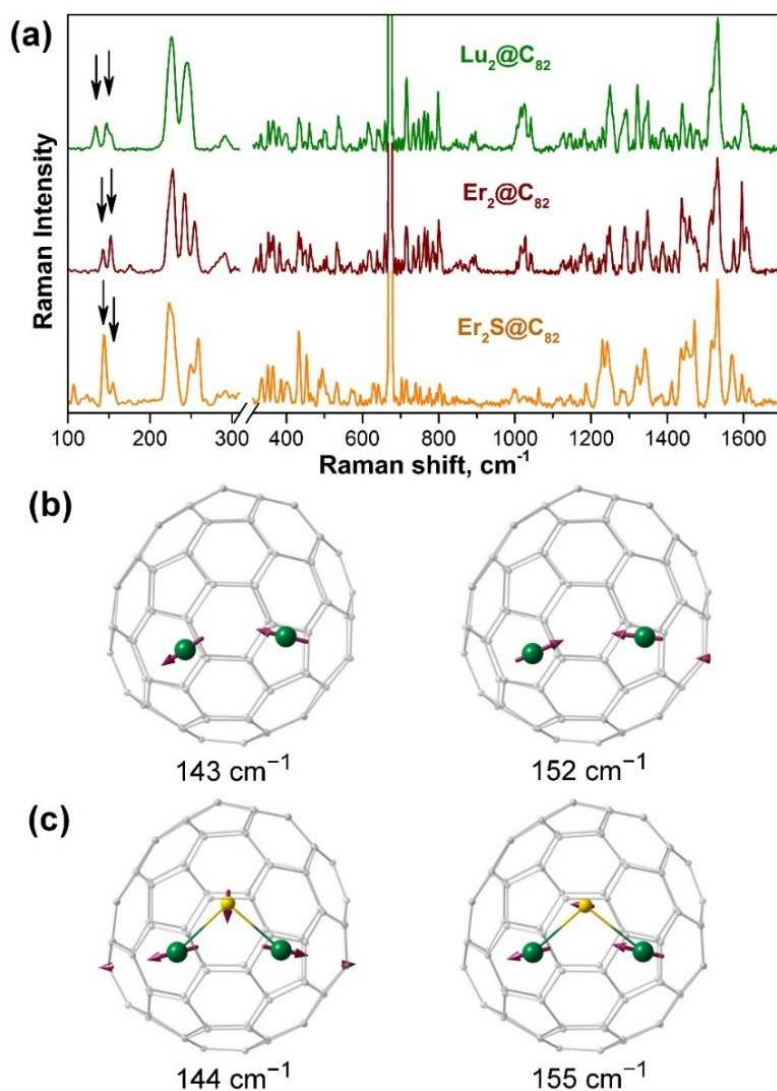


Figure 2.4. (a) Raman spectra of $\text{Lu}_2@C_{82-C_{3v}}$, $\text{Er}_2@C_{82-C_{3v}}$, and $\text{Er}_2\text{S}@C_{82-C_{3v}}$ measured at 78 K and excited with 647 nm laser line of the Kr^+ laser; note the change of the frequency scale at 310 cm^{-1} . Black arrows denote the peaks corresponding to the “metal-cage stretching” vibrations; the strong peak at 672 cm^{-1} is an instrumental artifact. (b) and (c) show atomic displacement patterns and frequencies for such vibrations in $\text{Er}_2@C_{82}$ (b) and $\text{Er}_2\text{S}@C_{82}$ (c) obtained from DFT calculations of Lu analogues.

All listed EMFs are characterized by low-frequency metal-based modes and the isomer-specific cage vibrational patterns. Figure 2.4 demonstrates Raman spectra of $\text{Lu}_2@C_{82}$, $\text{Er}_2@C_{82}$, and $\text{Er}_2\text{S}@C_{82}$ clusterfullerenes. Close similarity of the cage vibrations in the $200\text{--}1700\text{ cm}^{-1}$ frequency range has been observed, especially between the two dimetallofullerenes. Very close analogy has been also uncovered for the IR spectra of $\text{Lu}_2@C_{82}$ and $\text{Er}_2@C_{82}$ (figure 2.5), which represents an additional prove of the same fullerene cage in the same formal charge state in both compounds.

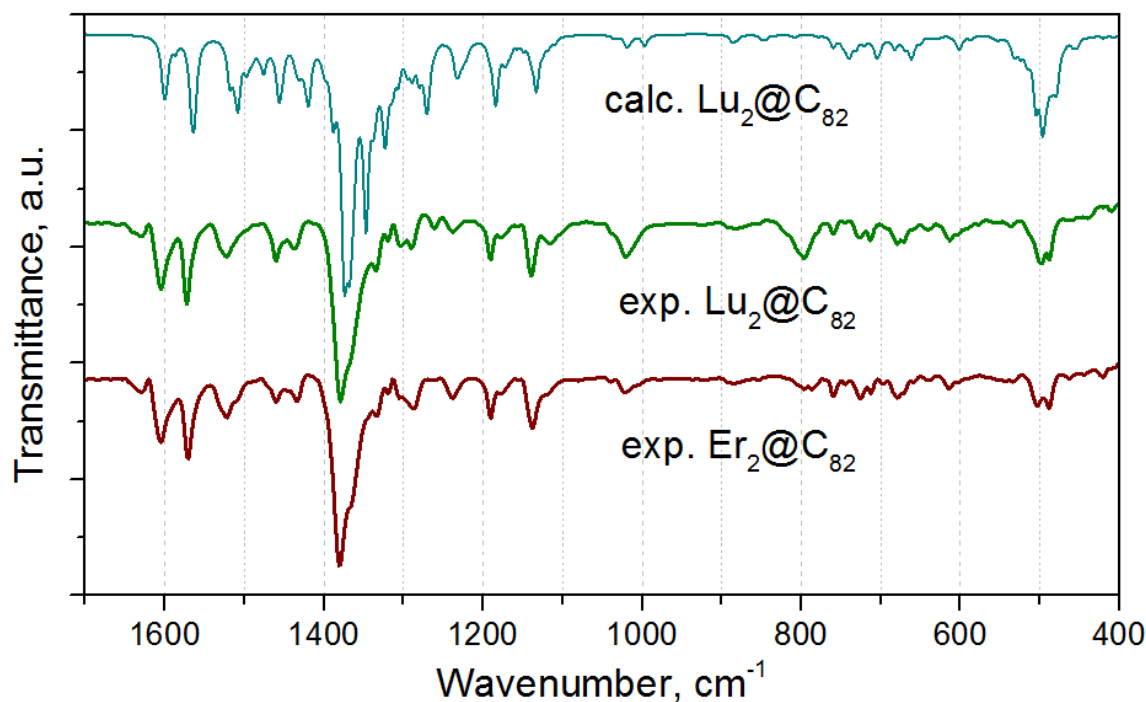


Figure 2.5. Experimental IR spectra of $Er_2@C_{82-C_{3v}}$ and $Lu_2@C_{82-C_{3v}}$ compared to the computed spectrum for $Lu_2@C_{82-C_{3v}}$ (calculations were performed at the PBE/TZ2P level of theory)

For all three EMFs, the so-called “metal-cage stretching” vibrations are observed in the range of near 150 cm^{-1} . The two peaks can be assigned to the in-phase and out-of-phase motions of metal atoms normal to the fullerene surface (Figure 2.5.b-c). In the spectrum of Lu_2 -dimetallofullerene, the frequencies of these two modes are somewhat lower ($134/147\text{ cm}^{-1}$) than in that of $Er_2@C_{82}$ ($143/152\text{ cm}^{-1}$), which is mainly caused by differences in atomic mass. Interestingly, very similar frequencies for these modes (around $144/155\text{ cm}^{-1}$) can also be observed for the $Er_2S@C_{82}$, i.e. the presence of the Er–S bonding has no pronounced effect on the frequencies.

2.2.3. NMR spectroscopy

Further confirmation of the molecular structure of $Lu_2@C_{82-C_{3v}}$ has been made with help of ^{13}C NMR spectroscopy. For fullerene with $C_{82-C_{3v}(8)}$ cage, one can expect 17 ^{13}C NMR signals: 11 signals with 6-fold intensity for 66 atoms in general position, 5 signals with 3-fold intensity for 15 atoms, located on the symmetry mirror planes and 1 signal with 1-fold intensity for atom in the pyramid apex. In the experimental spectrum of $Lu_2@C_{82-C_{3v}}$ (Figure 2.6.) we have found and assigned all 6-fold and 3-fold intensity peaks, whereas the low-intensity peak due to the single carbon has not been identified with available signal-to-noise ratio. Similar but

not identical ^{13}C NMR spectral patterns have been already reported for other dimetallofullerenes with $\text{C}_{82}\text{-C}_{3v}(8)$ cage isomer: $\text{Y}_2@C_{82}\text{-C}_{3v}$ ⁶ and $\text{Sc}_2@C_{82}\text{-C}_{3v}$ ⁵⁰. The range of the ^{13}C shift tends to decrease with the increase of the metal size.

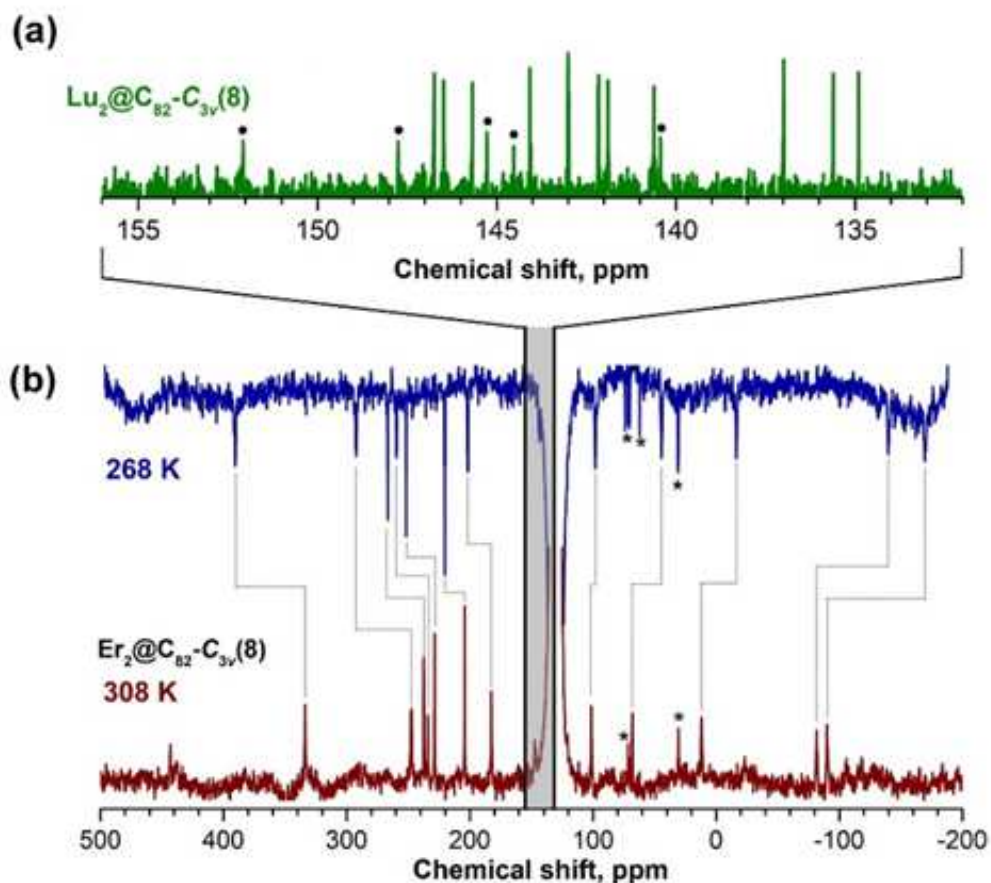


Figure 2.6. (a) ^{13}C NMR spectrum of $\text{Lu}_2@C_{82}\text{-C}_{3v}(8)$; half-intensity peaks are marked with dots. (b) ^{13}C NMR spectra of $\text{Er}_2@C_{82}\text{-C}_{3v}(8)$ measured at 268 and 308 K, temperature shifts of the peaks are marked with grey lines. Asterisks denote the peaks assigned to impurities due to the lack of the temperature dependence; the strong peak at 131 ppm is due to the solvent (d^4 -*o*-dichlorobenzene). Shaded area denotes the range of the chemical shift in diamagnetic $M_2@C_{82}\text{-C}_{3v}(8)$ molecules.

Together with the results of UV-vis-NIR spectroscopy and MS spectroscopy, information from NMR experiment unequivocally confirms that $\text{Lu}_2@C_{82}$ is dimetallofullerene with $\text{C}_{82}\text{-C}_{3v}(8)$ cage. A carbide clusterfullerene $\text{Lu}_2\text{C}_2@C_{80}$ or another isomer of $\text{Lu}_2@C_{82}$ with lower symmetry can be totally excluded by the spectroscopic data.

^{13}C NMR spectra have been also measured for $\text{Er}_2@C_{82}\text{-C}_{3v}$. Due to the paramagnetic influence of endohedral Er ions, ^{13}C chemical shifts in $\text{Er}_2@C_{82}$ broadening of the spectra has occurred: signals span the range of several hundred ppm. 13 out of 17 expected peaks could be identified with high degree of certainty after variable-temperature NMR measurements in

d^4 -o-dichlorobenzene (Figure 2.6.b). Pronounced temperature dependence of the chemical shifts has been detected due to the paramagnetic chemical shifts imposed by endohedral Er ions.

2.3. Charge distribution and electronic structure

The structural studies discussed in the previous section revealed that Sc, Er and Lu in both $M_2@C_{82-C_{3v}}$ and $M_2@C_{82-C_s}$ do not adopt their highest 3+ oxidation state. Moreover, quantum chemical calculations demonstrate¹⁶⁷, that those two valence metal electrons (one from each metal atom), which are not transferred to the cage, form the metal-metal covalent bonding. Thus instead of $(M^{3+})_2@C_{82}^{6-}$ the formal charge distribution in $M_2@C_{82}$ can be described as $(M^{2+}-M^{2+})@C_{82}^{4-}$.

The charge distribution of $M_2@C_{82}$ EMFs with C_{82}^{4-} carbon cage instead of C_{82}^{6-} is in a good agreement with several independent DFT studies which have proved high stability of $C_{82-C_{3v}(8)}$, and $C_{82-C_s(6)}$ tetra-anions^{70,168,169}. In particular in 2008 Valencia *et al.* performed DFT calculations for a series of different C_{82} cage isomers within the confines of ionic model, implying the transfer of four electrons from the encapsulated cluster to the carbon cage. These calculation found the $C_{82-C_{3v}(8)}^{4-}$ tetraanion to be the most stable with $C_{82-C_{2v}(9)}^{4-}$ and $C_{82-C_s(6)}^{4-}$ following it¹⁶⁸.

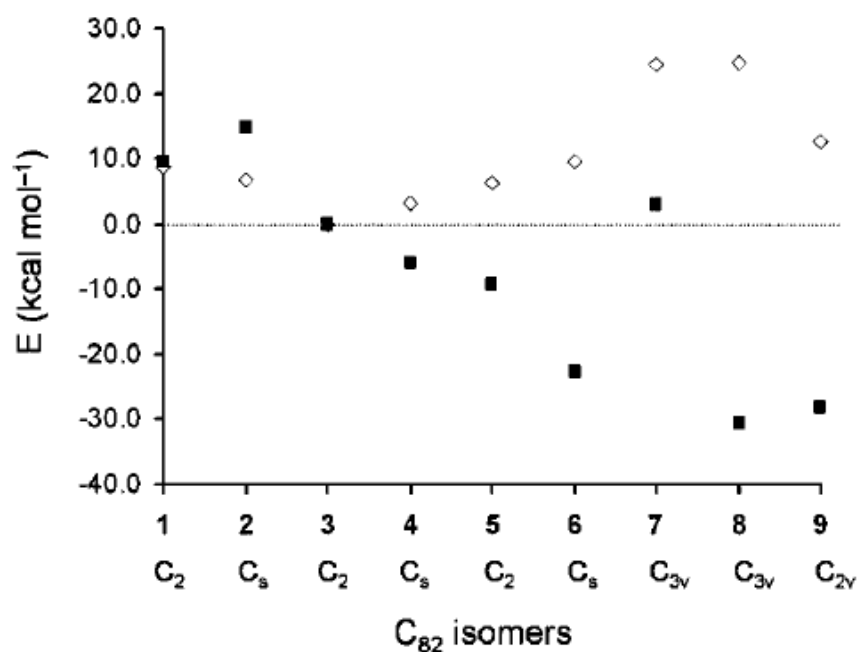


Figure 2.7. Energies (in kcal mol⁻¹) of C_{82} (empty diamonds) and C_{82}^{4-} isomers (filled squares) relative to $C_{82-C_2(3)}$ isomer. Reproduced with permission from¹⁶⁸.

Moreover, authors demonstrated, that among the 1267 examined IPR structures from C_{60} to C_{100} the $C_{82}-C_{3v}$ isomer displays the most favorable electronic structure to accept four electrons and can be named a kind of “archetype cage” for encapsulating clusters with the charge of 4+, similarly to that $C_{80}-I_h(7)$ is an “archetype cage” for encapsulating clusters with the charge of 6+.

Experimentally observed $C_{82}-C_{3v}(8)$ EMFs generally present themselves as metal carbide^{62,66,68} or metal sulfide^{70,71} clusterfullerenes, both with the cage charge of 4-, confirming that $C_{82}-C_{3v}^{4-}$ state is more thermodynamically favorable than $C_{82}-C_{3v}^{6-}$; $C_{82}-C_s(6)$ cage also exhibits predisposition to form tri- and tetra-anions instead of hexa-anions^{53,62,66}. No single nitride clusterfullerene or other EMF with cluster charge of 6+ with $C_{82}-C_{3v}(8)$ or $C_{82}-C_s(6)$ carbon cage has ever been isolated (Synthesized in 2008, $(Gd_3N)^{6+}@C_{82}^{6-}-C_s$ has another C_s isomer of C_{82} , non-IPR $C_{82}-C_s(39663)^{151}$).

Thus, the four-fold-charged state of $C_{82}-C_{3v}(8)$ and $C_{82}-C_s(6)$ carbon cages is logical and conventional case in EMF chemistry. At the same time, M_2 cluster with the charge of 4+ (that means actually a formal charge of 2+, assigned to each metal atom) at first sight represents a quite unusual situation for such lanthanides as Er and Lu as well as for Sc: these metals are usually trivalent in EMFs (monometallofullerenes and nitride clusterfullerenes^{80,170}).

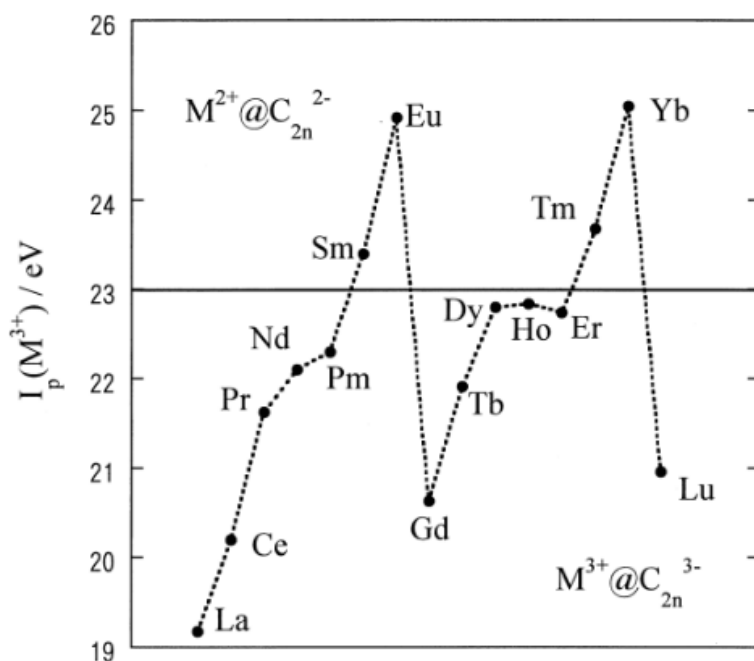


Figure 2.8. The third ionization potentials of the lanthanide elements. Metals, placed above the horizontal line can be adopting the oxidation state of 2+ in monometallofullerenes; metals, placed below the horizontal line are adopting the oxidation state of 3+ in monometallofullerenes. Reproduced with permission from¹⁷⁰.

In particular in 2001 group of Shinohara studied¹⁷⁰ the predisposition of different lanthanides to adopt oxidation state of 2+ or 3+ in monometallofullerenes and demonstrated, that divalent state is typical for metals with higher values of the third ionization potential, such as Sm, Eu; Tm and Yb. The third ionization potentials of Er and especially Lu metals has been demonstrated to be sufficiently low for adopting the oxidation state of 3+ in EMFs.

Obviously, the correlation with the third ionization potential, explaining perfectly the behavior of different metals in monometallofullerenes, seems to be not valid in case of dimetallofullerenes. Recent theoretical investigations demonstrated that $M_2@C_{2n}$ molecule should be considered as a combination of carbon cage with enclosed metal dimer species rather than a combination of carbon cage with two isolated metal atoms, so that the possibility of metal-metal bonding should be taken into account^{167,171}. Thus dimetallofullerene molecules exhibit an interesting situation: on the one hand, two positive metal ions undergo strong Coulomb repulsion, but on the other hand they are placed in the confined space of the hollow carbon cage and in some cases it is favorable to form intermetallic covalent bonds.

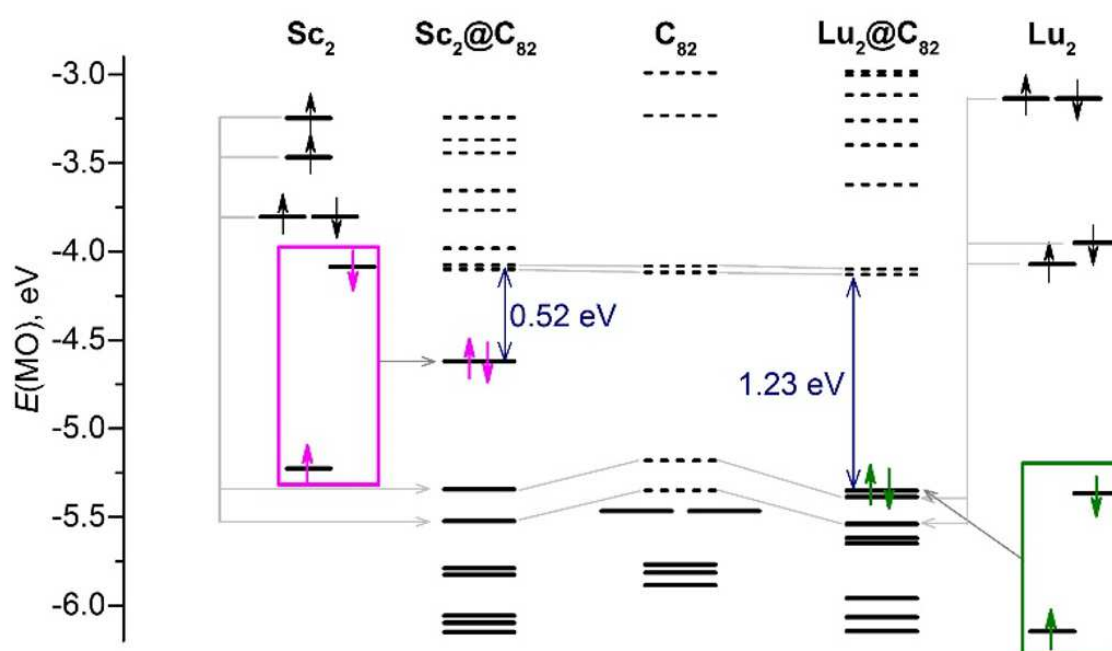


Figure 2.9. DFT-computed molecular orbital levels of the metal dimers Sc_2 and Lu_2 , dimetallofullerenes $Sc_2@C_{82}$ and $Lu_2@C_{82}$, and the empty fullerene C_{82} ; all fullerenes have $C_{3v}(8)$ cage isomer. Occupied levels are shown as solid lines, whereas unoccupied ones - as dashed lines. Electrons at the $(ns)\sigma_g^2$ MOs in the M_2 dimers and corresponding $M-M$ bonding orbital in the $M_2@C_{82}$ molecules are highlighted in magenta for Sc) and green for Lu).

Finally in 2012 our colleagues performed comprehensive DFT analysis of several dimetallofullerenes and concluded, that charge distribution in dimetallofullerenes is

determined by an energy matching between the frontier carbon cage orbitals and the M–M bonding metal dimer orbital¹⁶⁷.

Figure 2.9 shows how the M–M bonding orbitals in $Sc_2@C_{82}-C_{3v}$ and $Lu_2@C_{82}-C_{3v}$ dimetallofullerenes are developed from the molecular orbitals of Sc_2 and Lu_2 dimers, respectively. The ground state of the Sc_2 dimer is a quintet $(4s)\sigma_g^2(3d)\pi_u^2(3d)\sigma_g^1(4s)\sigma_u^1$, whereas Lu_2 is a triplet $(6s)\sigma_g^2(6s)\sigma_u^2(5d)\pi_u^2$ (the high spin states result in a significant splitting of the spin-up and spin-down orbitals of the same type)^{172,173}. The energy levels of the four highest-energy single-occupied MOs in both metal dimers are sufficiently higher than the LUMO and LUMO+1 energy levels of the empty $C_{82}-C_{3v}(8)$ cage, that is why in the $M_2@C_{82}-C_{3v}(8)$ fullerene these four electrons are transferred from the metal dimer to the cage. At the same time, the last pair of valence electrons, which occupy the $(4s)\sigma_g^2$ MO in Sc_2 and the $(6s)\sigma_g^2$ MO in Lu_2 , remains intact in di-EMFs because the energy of the corresponding MO is lower, than the energy of the LUMO+2 of the empty C_{82} fullerene. As a result, we have $M_2@C_{82}-C_{3v}$ molecules with the 4-fold charged carbon cage and the M–M bonding HOMO resembling the $(ns)\sigma_g^2$ MO of the corresponding metal dimer. (The empty $C_{82}-C_s$ carbon cage has its LUMO and LUMO+1 levels comparable to that of $C_{82}-C_{3v}$, so the final MO structure will be generally the same).

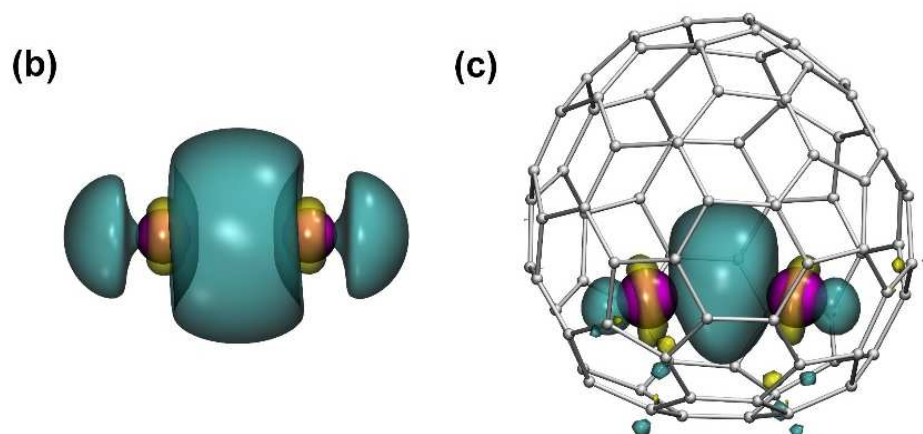


Figure 2.10. (b) $(4s)\sigma_g^2$ MO in the Sc_2 dimer. (c) The HOMO of the $Sc_2@C_{82}$ with the Sc–Sc bonding character. In (b) and (c), Sc atoms are magenta, carbons are light grey, MO isosurfaces are shown in cyan and dark yellow.

Thus, we have concluded that the HOMO energy level in $M_2@C_{82}$ is largely determined by the energy level of the $(ns)\sigma_g^2$ orbital in the M_2 dimer, which in due turn inversely correlates with the $ns^2(n-1)d^1 \rightarrow ns^1(n-1)d^2$ excitation energy of the free metal atom: the higher the free atom excitation energy, the lower the energy of the $(ns)\sigma_g^2$ MO will be. For instance, in the row

La – Sc – Lu the $ns^2(n-1)d^1 \rightarrow ns^1(n-1)d^2$ excitation energies increase from 0.33 eV in La to 1.43 eV in Sc to 2.34 eV in Lu¹⁷⁴.

The $(6s)\sigma_g^2$ MO in La_2 has such a high energy that the vacant cage MOs are usually more stable and hence La easily gives its electrons to the carbon cage and adopts charge state of 3+. La-based dimetallofullerenes are formed only with hexa-anionic cages; the La–La bonding MO is then the LUMO of the EMF molecule and its low energy provides substantial anodic shift of the first reduction. (For example the first reduction potential of the $\text{La}_2@C_{80}$ is only -0.31 V) Herewith the HOMO in all La-based dimetallofullerenes is cage-based, so the first oxidation occurs in typical potential range for cage-based oxidations of this particular cage isomer.

In Sc_2 the energy of $(4s)\sigma_g^2$ bonding orbital is lower, than that in the La-dimer. If the cage LUMO is still lower, it is more energetically favorable for the Sc_2 dimer to give all six electrons to the cage. If the cage LUMO is located higher than the of $(4s)\sigma_g^2$ bonding orbital of the Sc_2 dimer, it is energetically favorable to retain the metal-metal bond. Thus, Sc can be either 3+ (for example as in $\text{Sc}_2@C_{66}$ ^{10,158}) or 2+ (as in both isomers of $\text{Sc}_2@C_{82}$) depending on the energy level of the empty cage LUMO. Similar behavior can be expected for Y or Er dimetallofullerenes. In the first case, the behavior will be similar to the La-based dimetallofullerenes. In the second case, the $\text{Sc}^{2+}\text{-Sc}^{2+}$ bonding orbital is the HOMO in the dimetallofullerene, but its energy level is sufficiently high (see fig 2.9). So, the first anodic peak of Sc and Er dimetallofullerene voltammograms is expected to be due to the oxidation of the M-M bond, proceeding at relatively low potentials.

In the Lu_2 dimer, the $(6s)\sigma_g^2$ level is the lowest among other considered M_2 dimers. Bonding orbital in Lu_2 is so stabilized that it is not favorable to give electrons away and Lu always adopts a formal charge state of 2+ and favors tetra-anionic cages. The metal-bonding MO becomes the HOMO, while the LUMO is localized on the cage. Wherein, the energy of the $\text{Lu}^{2+}\text{-Lu}^{2+}$ HOMO is considerably lower than in case of $\text{Sc}^{2+}\text{-Sc}^{2+}$ HOMO in the same EMF isomer

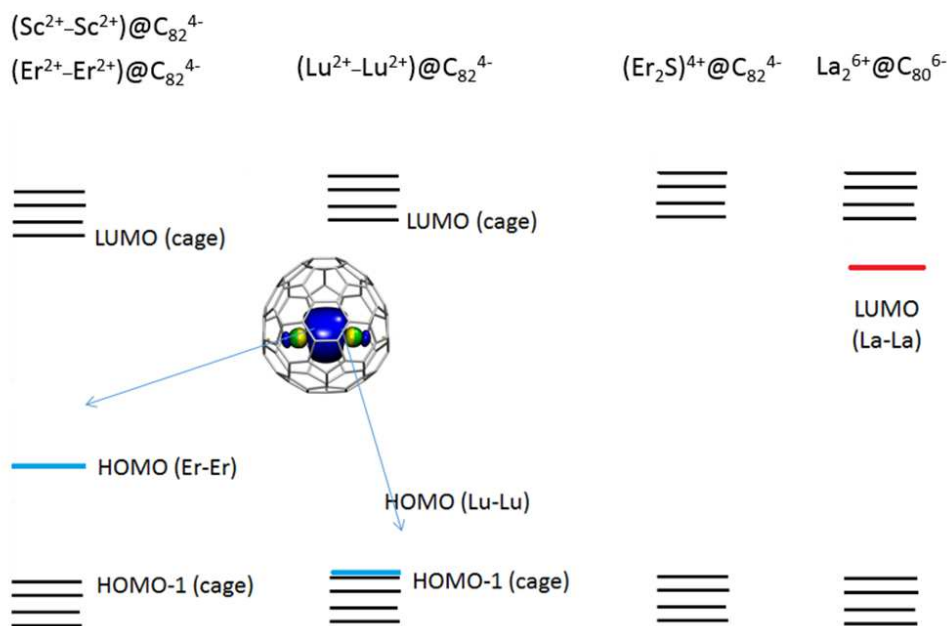


Figure 2.11. Schematic image of frontier MO levels in several dimetallofullerenes in $\text{Er}_2@\text{C}_{82}$ the metal bonding MO is the HOMO with relatively high energy; in $\text{Lu}_2@\text{C}_{82}$ the metal bonding MO is the HOMO with lower energy; in $\text{La}_2@\text{C}_{80}$, the metal La-La bonding MO is the LUMO.

It should be noted, that the evidence of the $\text{M}^{2+}\text{-M}^{2+}$ bonding in EMFs has been predicted not only in our group: during the last decade there has been a list of independent theoretical works concerning this issue.^{155,167,171,175-178} In early 2000 Huang et al. performed ab initio DV cluster method calculations, exposing metal-metal interaction in $\text{Er}_2@\text{C}_{82}$ ¹⁷⁵. Later presence of covalent metal-metal interactions in case of Er^{178} - and Y-dimetallofullerenes¹⁷¹ as well as Y-trimetallofullerenes¹⁷⁶ have been uncovered with help of different quantum-chemical calculation methods. At the same time all experimentalists, working with dimetallofullerenes to date have seemed to completely disallow this concept. There are several works, describing unique properties of dimetallofullerenes^{62,66,130}, but none of them actually describes these properties taking into account the possibility of bonding between two metal atoms. Moreover, even the charge state of metal atoms in the $\text{M}_2@\text{C}_{82}$ molecules is a matter of debate. In the present work we are for the first time trying to explain the properties of $\text{M}_2@\text{C}_{82}$ dimetallofullerenes in terms of metal-metal bonding.

2. 4. Electrochemistry

Comparison of the redox potentials in the series of different di-EMF and clusterfullerenes with the same cage isomer is a straightforward method to experimentally reveal the metal-metal bonding in the EMF.

Molecular orbital analysis shows that the HOMO of $M_2@C_{82}$ both isomers is the $M^{2+}-M^{2+}$ bonding orbital. Therefore, at the first oxidation step, the electron should be removed from this orbital. Since the energy of the EMF HOMO correlates with the bonding energy of the corresponding metal dimer, the oxidation potential in the $M_2@C_{82}$ compounds should be metal dependent. In particular, Lu_2 -dimetallofullerenes with their low energy of the $Lu^{2+}-Lu^{2+}$ bonding HOMO are expected to have higher oxidation potential values than the Sc_2 - and Er_2 -dimetallofullerenes. On the other hand, the LUMO of $M_2@C_{82-C_{3v}}$ and $M_2@C_{82-C_5}$ is predominantly localized on the carbon cage, and hence the first reduction potential of $M_2@C_{82}$ should be a metal-independent property of the cage.

In other words, one can expect all three $M_2@C_{82-C_{3v}}$ dimetallofullerenes with Lu, Sc and Er to have different values of the first oxidation potential, but almost similar values of the first reduction potentials. And the same predictions can be done in case of two $M_2@C_{82-C_5}$ dimetallofullerenes.

Two isomers of Er_2S sulfide clusterfullerenes were employed as a kind of “reference points” in these electrochemical investigations. In both isomers of $M_2S@C_{82}$ sulfides the frontier orbitals are mostly located on the cage with minor cluster contribution. So in the anodic region we expect sulfide clusterfullerene to have the highest values of the first oxidation potential in comparison with $M^{2+}-M^{2+}$ oxidation of dimetallofullerenes, while the comparison of the first reduction potential of $M_2@C_{82}$ with corresponding isomer of $M_2S@C_{82}$ can confirm the cage-based character of the LUMO.

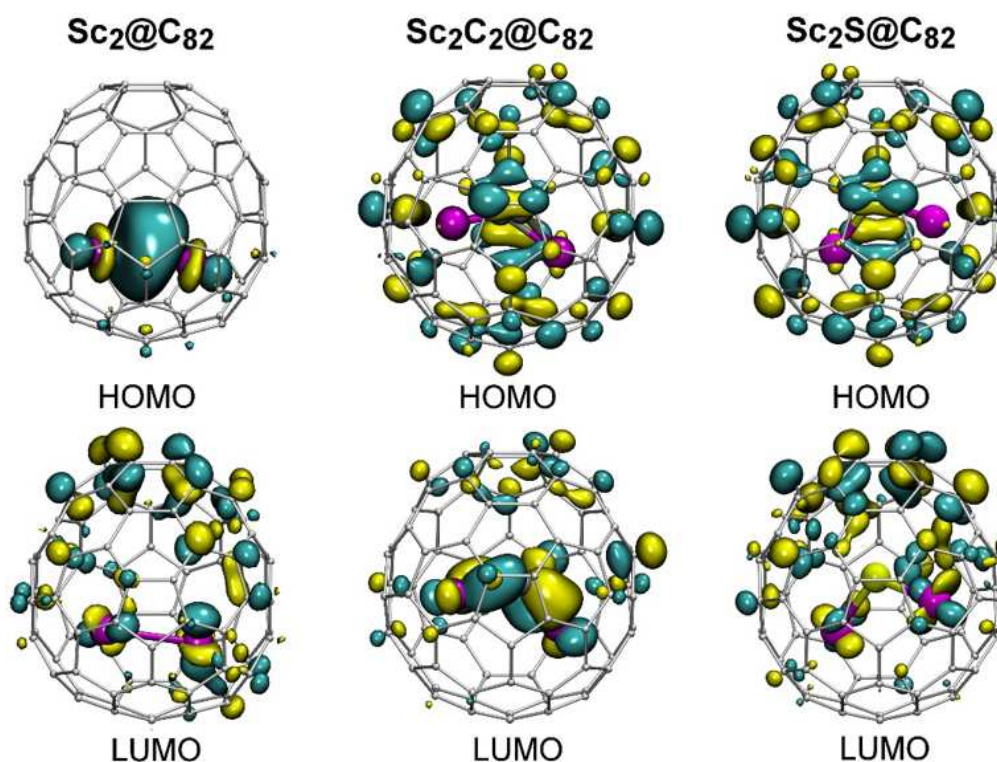


Figure. 2.12. DFT-computed frontier molecular orbitals of $Sc_2@C_{82}$, $Sc_2C_2@C_{82}$, $Sc_2O@C_{82}$, and $Sc_2S@C_{82}$, all with $C_{3v}(8)$ fullerene cage.

The cyclic voltammograms of $C_{82}-C_{3v}$ and $C_{82}-C_5$ families of EMFs are shown at the figures 2.13 and 2.14 respectively, and all the potential data is summed up in Table 2.1 and Table 2.2

2.4.1. $M_2@C_{82}$ dimetallofullerenes with $C_{82}-C_{3v}$ cage isomer

The first reduction of $M_2@C_{82}-C_{3v}$ is at about -1.1 V and proceeds irreversibly (re-oxidation peak appears at about -0.70 V). At more negative potentials it is followed by the broad double peak of the second reduction at about -1.4 V. (We are using potential values, given versus $Fc(Cp)_2^{+/0}$ couple throughout this discussion). For Sc_2 - and Er_2 -EMFs this second process is also irreversible, but for $Lu_2@C_{82}$ the reversed peak can be observed with the forward-reversed current ratio of about 0.92. Furthermore, in case of $Lu_2@C_{82}-C_{3v}$ the experimental conditions allowed to detect the third reversible reduction step at about -1.71 V.

$Er_2S@C_{82}-C_{3v}$ demonstrates analogous reduction pattern; both reduction peaks as well as the reoxidation one are positively shifted by 0.10-0.15 V, that can be due to the cluster contribution to the unoccupied molecular orbitals.

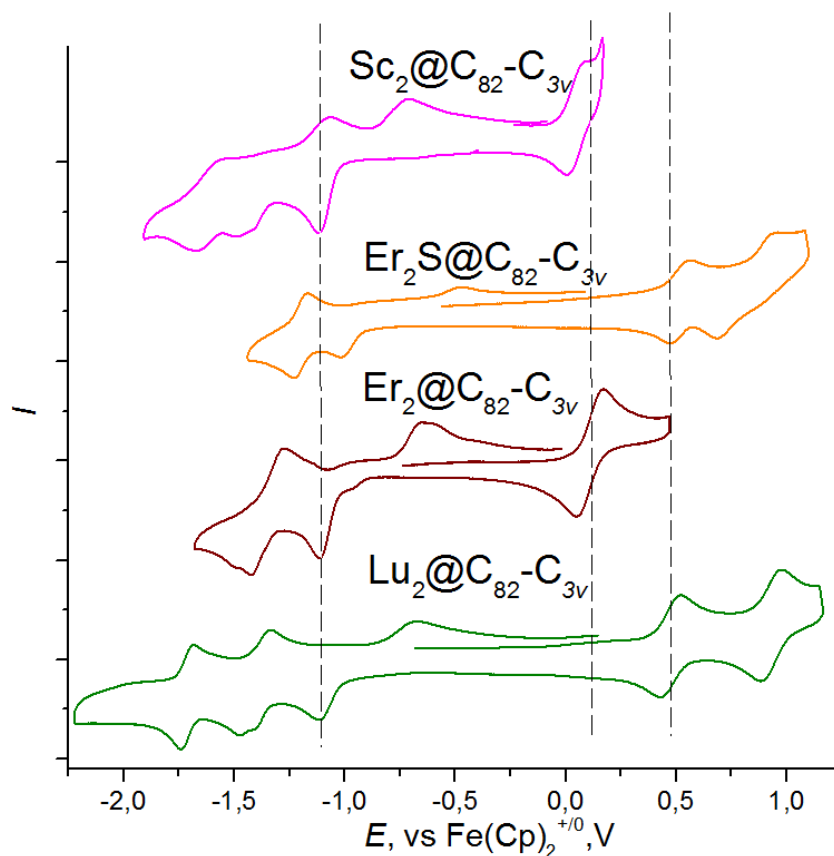


Figure 2.13. Cyclic voltammetry of $\text{Lu}_2@C_{82}$, $\text{Er}_2@C_{82}$, $\text{Sc}_2@C_{82}$ and $\text{Er}_2\text{S}@C_{82}$ with $C_{3v}(8)$ cage isomer. Measurements are performed at room temperature in *o*-dichlorobenzene/TBABF₄ with the scan rate 100 mV/s. To guide an eye, vertical dotted lines denote the first oxidation potentials of $\text{Lu}_2@C_{82}$ and $\text{Er}_2@C_{82}$ and the first reduction potential of $\text{Lu}_2@C_{82}$

At the same time, anodic behavior of $\text{M}_2@C_{82}-C_{3v}$ dimetallofullerenes exhibit pronounced metal-dependence, as it can be expected for the metal-based HOMO. The least positive potential, +0.02 V, has been recorded for $\text{Sc}_2@C_{82}$ (similar results were also reported for this molecule by Akasaka et al.¹³⁰). $\text{Er}_2@C_{82}$ is the next in a row with the potential value of +0.13 V. The first oxidation of $\text{Lu}_2@C_{82}$ occurs at the much more positive potential of +0.48 V (and the second one can be observed at +0.93). Similar value of +0.50 V has been observed also for $\text{Er}_2\text{S}@C_{82}$ at its first oxidation step, confirming that the energy of the $\text{Lu}^{2+}-\text{Lu}^{2+}$ bonding orbital is very close to that of the cage-based orbitals. In all cases, the peak current ratios I_r/I_f are close to unity, that demonstrates stability of the EMF species with partial occupancy of the metal-metal bonding orbital towards any follow-up chemical reactions, at least within the cyclic voltammetry (CV) timescale.

It is interesting to make the comparison with redox properties of Sc-clusterfullerene series from the literature data (see table 2.2). The potential matching reveals, that first reduction potentials of $\text{Sc}_2\text{S}@C_{82}-C_{3v}$ (−1.04 V⁷²), and $\text{Sc}_2\text{C}_2@C_{82}-C_{3v}$ (−0.94 V¹⁵⁰) are somewhat

more positive than those of $M_2@C_{82}-C_{3v}$ similarly to how it is in the case of $Er_2S@C_{82}-C_{3v}$ (-0.99V), while recently published $Sc_2O@C_{82}-C_{3v}$ has the most negative first reduction potential at -1.17 V¹⁴⁹. The span of these values agrees with the metal contributions to the LUMOs, from negligible in $Sc_2O@C_{82}$ to the dominant in $Sc_2C_2@C_{82}$ (Fig. 2.10.) Thus, we can postulate that -1.17 V is the intrinsic reduction potential of the $C_{82}-C_{3v}^{4-}$ cage in EMFs with the 4-fold charge cluster, and more positive values evidence for the certain contribution of the metal atoms to the LUMO. Reduction potentials of $M_2@C_{82}-C_{3v}$ are found in the range from -1.11 to -1.16 V, i.e. weak metal-dependence can be detected. So, we can see, that the cluster exhibits a small contribution to the LUMO of these di-EMFs. Whereas the first oxidation step of $Er_2S@C_{82}-C_{3v}$ and all Sc-based clusterfullerenes with $C_{82}-C_{3v}$ isomer occur at about $+0.5$ V, and this potential may be considered as the intrinsic property of the $C_{82}-C_{3v}$ fullerene cage.

Table 2.1. Selected electrochemical parameters for several EMFs with $C_{82}-C_{3v}(8)$ cage isomer.

		E^*, V	$\Delta E_{F-R}, V$	I_R/I_F	character
$Lu_2@C_{82}-C_{3v}$	ox-I	+0.48	0.08	0.92	reversible
	ox-II	+0.93	0.09	0.97	reversible
	red-I	-1.10	-	-	irreversible
	red-II	-1.48	0.08	0.92	reversible
	red-III	-1.71	0.06	0.92	reversible
$Er_2@C_{82}-C_{3v}$	ox-I	+0.12	0.11	0.94	reversible
	red-I	-1.11	-	-	irreversible
	red-II	-1.42	-	-	irreversible
$Er_2S@C_{82}-C_{3v}$	ox-I	+0.50	0.08	0.88	reversible
	red-I	-1.01	-	-	irreversible
	red-II	-1.29	0.06	0.95	reversible
$Sc_2@C_{82}-C_{3v}$	ox-I	+0.05	0.08	0.91	reversible
	red-I	-1.10	-	-	irreversible
	red-II	-1.41	-	-	irreversible

Potentials are listed in Volt versus the $[Fe(Cp)_2]^{+/0}$ pair, "ox" stands for oxidation, "red" stands for reduction, "reox-I" stands for a new reoxidation peak, appearing after the second reduction, " ΔE_{F-R} " stands for difference of the forward and reversed peak potentials, " I_R/I_F " stands for the ratio of the forward and reversed peak current.

2.4.2. $M_2@C_{82}$ dimetallofullerenes with $C_{82}-C_s$ cage isomer

The first reduction potentials of the $M_2@C_{82}-C_s$ dimetallofullerenes are at -1.00 V (Lu) and -1.01 V (Er). Importantly, in both EMFs the first reduction step is reversible as well as the second one near -1.30 V. Reversible third reduction at -1.77 V is also observed for $Lu_2@C_{82}-C_s$. Thus, the $M_2@C_{82}$ isomers are an interesting example of the isomer-dependent reversibility of the reduction behavior. The anodic behavior of $M_2@C_{82}-C_s$ follows the same trend as it was for

$M_2@C_{82}-C_{3v}$ isomers. The first oxidation is electrochemically reversible and the potential is metal-dependent, $Er_2@C_{82}-C_5$ being noticeably easier to oxidize than $Lu_2@C_{82}-C_5$ (+0.02 V versus +0.34 V). In case of Lu-dimetallofullerene, the second reversible oxidation can be observed at +0.72 V.

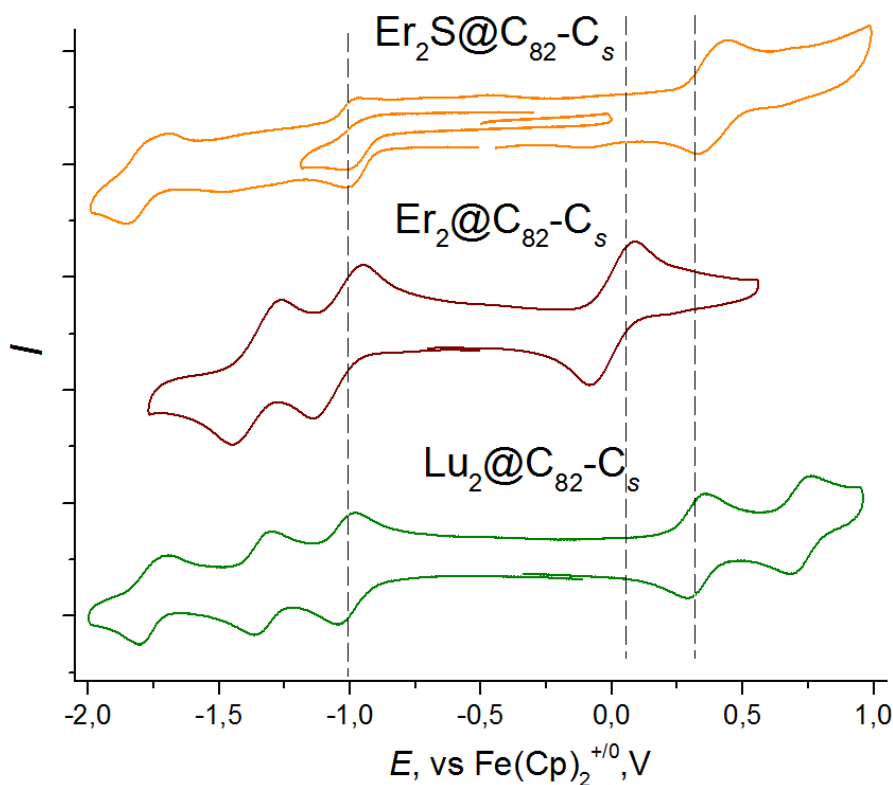


Figure 2.14. Cyclic voltammetry of $Lu_2@C_{82}$, $Er_2@C_{82}$ and $Er_2S@C_{82}$ with the $C_5(6)$ cage isomer. Measurements are performed at room temperature in *o*-dichlorobenzene/ $TBABF_4$ with the scan rate 100 mV/s. To guide an eye, vertical dotted lines denote the first oxidation potentials of $Lu_2@C_{82}$ and $Er_2@C_{82}$ and the first reduction potential of $Lu_2@C_{82}$

The first reduction potential of $Er_2S@C_{82}-C_5$ is -0.99 V and the process proceeds irreversibly (the reoxidation peak at about -0.95 V appears only after extending of the potential sweep down to reach the second reduction peak). There is a large gap between the first and the second reduction steps: the last one is observed at -1.7 V, near the third reduction of $Lu_2@C_{82}$. Herewith the first reduction of other $C_{82}-C_5$ clusterfullerenes such as Sc_2S- , Sc_2C_2- and Sc_2O- EMFs also occurs in the range from -0.93 to -1.01 V^{72,179}, but none of Sc-based clusterfullerenes demonstrates such a pronounced gap between the first and the second reduction. So we can conclude, that the structure of the higher unoccupied orbitals in case of $Er_2S@C_{82}-C_5$ sulfide is different to that of corresponding dimetallofullerenes as well as other clusterfullerenes (table 2.2.)

The first oxidation of $\text{Er}_2\text{S}@C_{82}\text{-}C_5$ is reversible and occurs at +0.39 V, similarly to oxidation of the Sc-based clusterfullerenes (0.35 V-0.42 V, see table 2.2). Notable, that in case of the C_5 isomer the difference between metal-based oxidation in $\text{Lu}_2@C_{82}$ and cage-based oxidations in $\text{Er}_2\text{S}@C_{82}$ is more pronounced: 0.06 V versus 0.02 V for corresponding pair of C_{3v} isomers. Therefore for $C_{82}\text{-}C_5$ we can observe noticeable difference between the $\text{Lu}^{2+}\text{-}\text{Lu}^{2+}$ HOMO and the nearest cage-based orbitals.

Table 2.2. Selected electrochemical parameters for several EMFs with $C_{82}\text{-}C_5(6)$ cage isomer

		E, V^*	$\Delta E_{F-R}, \text{V}$	I_R/I_F	character
$\text{Lu}_2@C_{82}\text{-}C_5$	ox-I	+0.33	0.06	0.97	reversible
	ox-II	+0.72	0.07	0.97	reversibly
	red-I	-1.01	0.06	0.97	reversible
	red-II	-1.34	0.05	0.91	reversible
	red-III	-1.74	0.09	0.88	reversible
$\text{Er}_2@C_{82}\text{-}C_5$	ox-I	+0.02	0.17	0.98	reversible
	red-I	-1.04	0.18	0.96	reversible
	red-II	-1.36	0.18	0.93	reversible
$\text{Er}_2\text{S}@C_{82}\text{-}C_5$	ox-I	+0.39	0.09	0.97	reversible
	red-I	-0.99	-	-	irreversible
	red-II	-1.79	0.11	0.86	reversible

Potentials are listed in Volt versus the $[\text{Fe}(\text{Cp})_2]^{+/0}$ pair, "ox" stands for oxidation, "red" stands for reduction, "reox-I" stands for a new reoxidation peak, appearing after second reduction, " ΔE_{F-R} " stands for difference of the forward and reversed peak potentials, " I_R/I_F " stands for the ratio of the forward and reversed peak current.

2.4.3. Mixed metal $M_2@C_{82}$ and $M_2C_2@C_{82}$ compounds

The revealed metal dependence of the dimetallofullerene oxidation potential made us wonder how the HOMO will behave in a mixed-metal system, especially when two metals with different electronic properties are combined in one molecule.

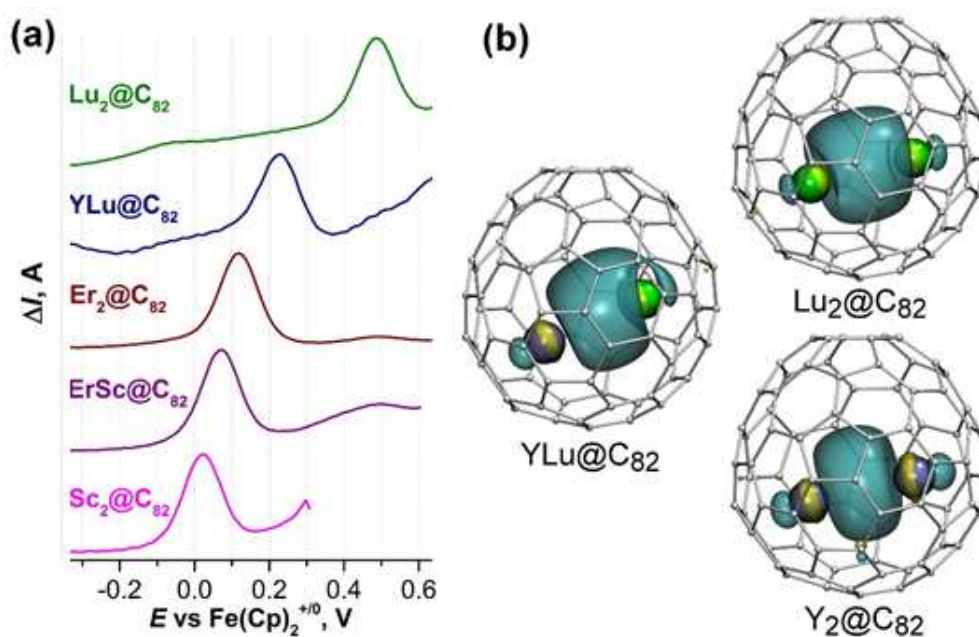


Figure 2.15. (a) Square wave voltammetry of $\text{Lu}_2@C_{82}$, $\text{YLu}@C_{82}$, $\text{Er}_2@C_{82}$, $\text{ErSc}@C_{82}$, and $\text{Sc}_2@C_{82}$, all with $C_{3v}(8)$ cage, in the anodic range; (b) Isosurfaces of the HOMO in $\text{Lu}_2@C_{82-C_{3v}}$, $\text{YLu}@C_{82-C_{3v}}$, and $\text{Y}_2@C_{82-C_{3v}}$.

To clarify this question, we have isolated small amounts of $\text{YLu}@C_{82-C_{3v}}$ and $\text{ErSc}@C_{82-C_{3v}}$ dimetallofullerenes that was enough to perform Square Wave Voltammetry experiment. Unfortunately, all our attempts to isolate $\text{Y}_2@C_{82-C_{3v}}$ have occurred to be fruitless. Although the compound has been observed in the fullerene mixture according to mass-spectral analysis, we have not succeed to isolate any noticeable amount of individual EMF that may be due to its low stability. It should be noted that fullerenes with low oxidation potential which include $\text{Y}_2@C_{82}$ are characterized by highly intense peaks in the positive mode of mass spectrum, even in case when their concentration in the mixture is very low, so it is difficult to estimate the dimetallofullerene amount with only a mass-spectrum in hand.

DFT calculations show that the HOMO energy of the $\text{Y}_2@C_{82-C_{3v}}$ (-4.426 eV at the PBE/TZ2P level) is even higher than that of $\text{Sc}_2@C_{82-C_{3v}}$ (-4.676 eV), so for the first dimetallofullerene an oxidation potential near 0.0 V or more negative can be expected. Square-wave voltammetry shows that $\text{YLu}@C_{82}$ is oxidized at $+0.23$ V (Fig. 2.15), almost exactly in the middle between the oxidation potential of $\text{Lu}_2@C_{82-C_{3v}}$ and expected potential of $\text{Y}_2@C_{82-C_{3v}}$. Likewise, the HOMO energy of $\text{YLu}@C_{82}$ (-4.962 eV) is close to the mean value of the HOMO energies of $\text{Y}_2@C_{82-C_{3v}}$ (-4.426 eV) and $\text{Lu}_2@C_{82-C_{3v}}$ (-5.332 eV). Interestingly, the shape of the HOMO of $\text{YLu}@C_{82}$ has pronounced asymmetry: the electron density is shifted towards Lu atom. (Fig. 2.15). Similar electrochemical behavior is observed in the mixed Er-Sc system: the

first oxidation potential of $\text{ErSc}@C_{82}\text{-C}_{3v}$ dimetallofullerene (+0.08 V) has been found exactly between the corresponding potentials of $\text{Sc}_2@C_{82}$ (+0.02 V) and $\text{Er}_2@C_{82}$ (+0.13 V). At the same time the reduction potentials of all listed dimetallofullerenes, measured in square wave voltammetry experiment, are much closer and vary from -1.16 V to -1.11 V. It should be noted, that these values are a little more cathodic with respect to those, measured in cyclic voltammetry experiment. This can be explained due to the irreversibility of the process. For comparison, in case of reversible first oxidation of $C_{82}\text{-C}_s$ family there is almost no difference between cyclic voltammetry and square wave voltammetry potentials.

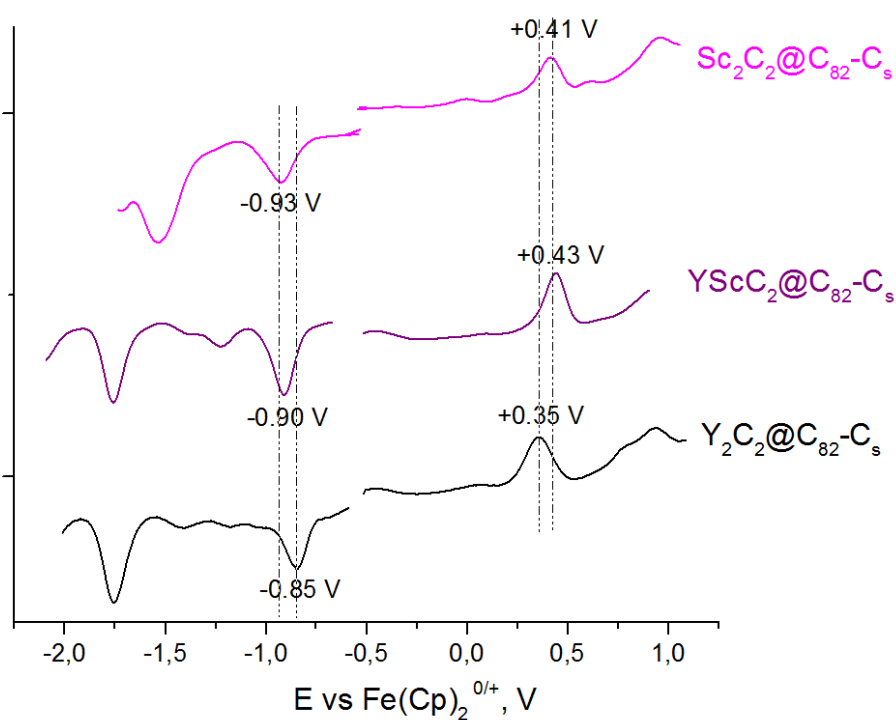


Figure 2.16. Square wave voltammetry $\text{Sc}_2\text{C}_2@C_{82}$, $\text{YScC}_2@C_{82}$ and $\text{Sc}_2\text{C}_2@C_{82}$, all with $C_s(6)$ cage. Measurements are performed at room temperature in *o*-dichlorobenzene/TBAPF₄ with the scan rate of 100 mV/s. To guide an eye, vertical dotted lines denote oxidation and reduction potentials of $\text{Sc}_2\text{C}_2@C_{82}$, and $\text{Y}_2\text{C}_2@C_{82}$.

We also have separated and studied three $C_{82}\text{-C}_s$ metal carbides: $\text{Sc}_2\text{C}_2@C_{82}\text{-C}_s$, $\text{YScC}_2@C_{82}\text{-C}_s$ and $\text{Y}_2\text{C}_2@C_{82}\text{-C}_s$. The square wave voltammetry experiment has revealed, that the first reduction potential of these EMFs is to some extent metal dependent, Y carbides being easier to reduce. In particular the first reduction potential of $\text{Y}_2\text{C}_2@C_{82}$ is -0.85 V, which is the most positive value in the whole $C_{82}\text{-C}_s$ family. The first reduction potential of $\text{YScC}_2@C_{82}\text{-C}_s$ (-0.90 V) can be observed between the oxidation potentials of $\text{Sc}_2\text{C}_2@C_{82}$ and $\text{Y}_2\text{C}_2@C_{82}$. As to the oxidation potentials, no pronounced metal-dependence has been detected: $\text{Y}_2\text{C}_2@C_{82}$ has

the lowest oxidation potential of +0.35V, but those of YScC₂- and Sc₂C₂-clusterfullerenes are much closer, the mixed-metal carbide even being slightly more difficult to oxidize.

These experiment confirm, that in M₂C₂@C₈₂-C₅ EMFs the internal M₂C₂ cluster has contribution to the both LUMO and HOMO and the first one is more pronounced.

Table 2.3. Redox potentials of selected dimetallofullerenes and clusterfullerenes.

EMF	ox-I	red-I	red-II	red-III	gap _{EC}	link	EMF
Er ₂ @C ₈₂ -C ₅ (6)	0.65	0.02	-1.01	-1.31		1.03	t.w.
Lu ₂ @C ₈₂ -C ₅ (6)	0.74	0.34	-1.00	-1.32	-1.77	1.34	t.w.
Er ₂ S@C ₈₂ -C ₅ (6)		0.39	-1.01	-1.85	-2.21	1.40	t.w.
Sc ₂ C ₂ @C ₈₂ -C ₅ (6)	0.64	0.42	-0.93	-1.30	-	1.35	179
Sc ₂ O@C ₈₂ -C ₅ (6)	0.72	0.35	-0.96	-1.28	-1.74	1.31	72
Sc ₂ S@C ₈₂ -C ₅ (6)	0.65	0.39	-0.98	-1.12	-1.73	1.37	72
Sc ₂ @C ₈₂ -C _{3v} (8)		0.02	-1.16	-1.53	-1.73	1.18	t.w.
ErSc@C ₈₂ -C _{3v} (8)		0.08	-1.11	-1.49	-1.72	1.19	t.w.
Er ₂ @C ₈₂ -C _{3v} (8)		0.13	-1.14	-1.41	-1.83	1.27	t.w.
Lu ₂ @C ₈₂ -C _{3v} (8)	0.95	0.50	-1.16	-1.46	-1.77	1.66	t.w.
YLu@C ₈₂ -C _{3v} (8)		0.23	-1.13			1.36	t.w.
Er ₂ S@C ₈₂ -C _{3v} (8)	0.88	0.51	-0.98	-1.21	-1.70	1.49	t.w.
Sc ₂ C ₂ @C ₈₂ -C _{3v} (8)	0.93	0.47	-0.94	-1.15	-1.60	1.41	150
Sc ₂ O@C ₈₂ -C _{3v} (8)	1.09	0.54	-1.17	-1.44	-1.55	1.71	149
Sc ₂ S@C ₈₂ -C _{3v} (8)	0.96	0.52	-1.04	-1.19	-1.63	1.56	72

Potentials are listed in Volt versus the [Fe(Cp)₂]⁺⁰ pair, "ox" stands for oxidation, "red" stands for reduction, gap_{EC} is an electrochemical gap defined as the difference of the first reduction and oxidation potentials. All potentials obtained in this work have been measured in the SWV experiment and can be slightly to that measured in the CV experiment.

2.5. Magnetic behavior of the M-M bonding electrons.

2.5.1. EPR spectroscopy of Sc₂@C₈₂-C_{3v} cation-radical

Reversible oxidation of Sc₂@C₈₂ and Er₂@C₈₂ demonstrated in the electrochemical experiments proves the stability of their cation radicals and opens the possibility for detailed studies of their properties. We have chosen EPR spectroscopy as a powerful tool that can provide information about compound structure spin density localization

The first oxidation step of the $M_2@C_{82}$ is a removal of one electron from the M–M bonding MO, which results in the cation radical with the unpaired electron localized between two metal atoms. The M–M bonding MO has a pronounced *spd*-hybrid character with substantial s-contribution from the $(ns)\sigma_g^2$ orbital of the M_2 dimer. Partial s-character is of particular importance because of the orbital shape: it is the only type of orbital without a nodal point in nucleus. Thus the s-orbitals contribution provides the high spin density on the M nucleus in $M_2@C_{82}$, which leads to large values of isotropic hyperfine coupling constants in the EPR spectra. For instance, huge $a(^{139}\text{La})$ *hfc* constant in the anion radical $\text{La}_2@C_{80-I_h}$ as well as its paramagnetic derivatives prove the presence of the single-occupied La–La bonding MO in these species¹²⁸.

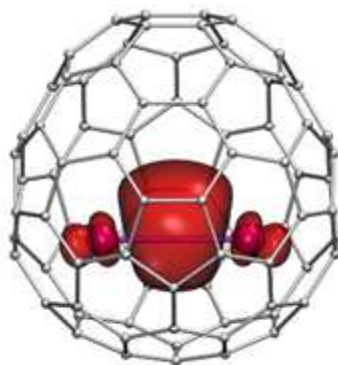


Figure 2.17. DFT-computed spin density distribution in $\text{Sc}_2@C_{82}^+$

The cation radical $\text{Sc}_2@C_{82}^+$ has been generated by chemical oxidation of $\text{Sc}_2@C_{82}-C_{3v}(8)$ with tris(4-bromophenyl) aminium hexachloroantimonate in *o*-dichlorobenzene solution in the dry nitrogen atmosphere. This compound (also known as “Magic blue” due to the saturated dark blue color of the solutions) exhibits reversible one-electron oxidation at $E^{+/0}=+0.70$ V versus $\text{Fe}(\text{Cp})_2^{+/0}$, that is between the first and the second oxidation steps of $\text{Sc}_2@C_{82}$ dimetallofullerene. Thus addition of approximately equimolar amount of magic blue results in removing of one electron from the metal-metal bonding HOMO of $\text{Sc}_2@C_{82}$.

The EPR spectrum of $\text{Sc}_2@C_{82}^+$ cation radical measured at room temperature (Fig. 2.18) revealed a complex multi-line hyperfine structure spanning the range of 2800 G. Due to the large spectrum width and relatively narrow line width of 1–3 G (requiring the use of small modulation amplitude), acquisition of the spectrum took 2 days. After that, intensity of the signal started to decrease, revealing the cation radical degradation.

The nuclear spin of ^{45}Sc is $7/2$; so the total spin of the system with two equivalent Sc nucleus is calculated as $I = I_1 + I_2$ and spans all integer values from 0 to 7. If only the first order of perturbation is considered, positions of resonance lines in the EPR spectrum are dependent only on the projection of the total momentum, m_I , and one can expect to see the $2 \cdot I + 1 = 15$ lines in the EPR spectrum of Sc_2 dimer, corresponding to $m_I = 0, \pm 1, \dots, \pm 7$, position of each resonance being determined by formula:

$$B = B_0 - am_I \quad (\text{Eq. 2.1})$$

However, the experimental spectrum of $\text{Sc}_2@C_{82}^+$ is much more complex and has as many as 64 lines. The reason is that for the large value of hyperfine coupling constants, the resonance positions are also dependent on the total momentum I . The equation 2.1 for the resonance field actually includes other terms, but when the value of a hfc constant is small with respect to B_0 , their contribution is negligible.

$$B = B_0 - am_I - \frac{a^2}{2B_0} [I(I+1) - m_I^2] + \dots \quad (\text{Eq.2.2})$$

The formula (Equation 2.2) splits m_I -dependent lines into lines with different $|I, m_I\rangle$ values. In case of $\text{Sc}_2@C_{82}^+$, the total spin I spans integer values from 0 to 7, and each value of spin projection m_I can be achieved for $(7+1-|m_I|)$ different values of I . For instances, the resonances with $m_I = 7$ and $m_I = -7$ can be achieved only with $I = 7$, while the resonance resonances with $m_I = 6$ and $m_I = -6$ can be achieved for two different values of the total spin I : 7 and 6, and so on. Thus, two resonances at the lowest and the highest magnetic fields correspond to non-degenerate $m_I = \pm 7$ states, the next two states with $m_I = \pm 6$ are split into two signals each, and the central line with $m_I = 0$ is split into 8 lines. The total number of resonances is then $1+2+3+4+5+6+7+8+7+6+5+4+3+2+1=64$. Figure 2.18 shows assignment of all observed

lines and indicates positions expected in the first order (blue lines) and their splitting in the higher orders of perturbation theory according to different l values (red lines).

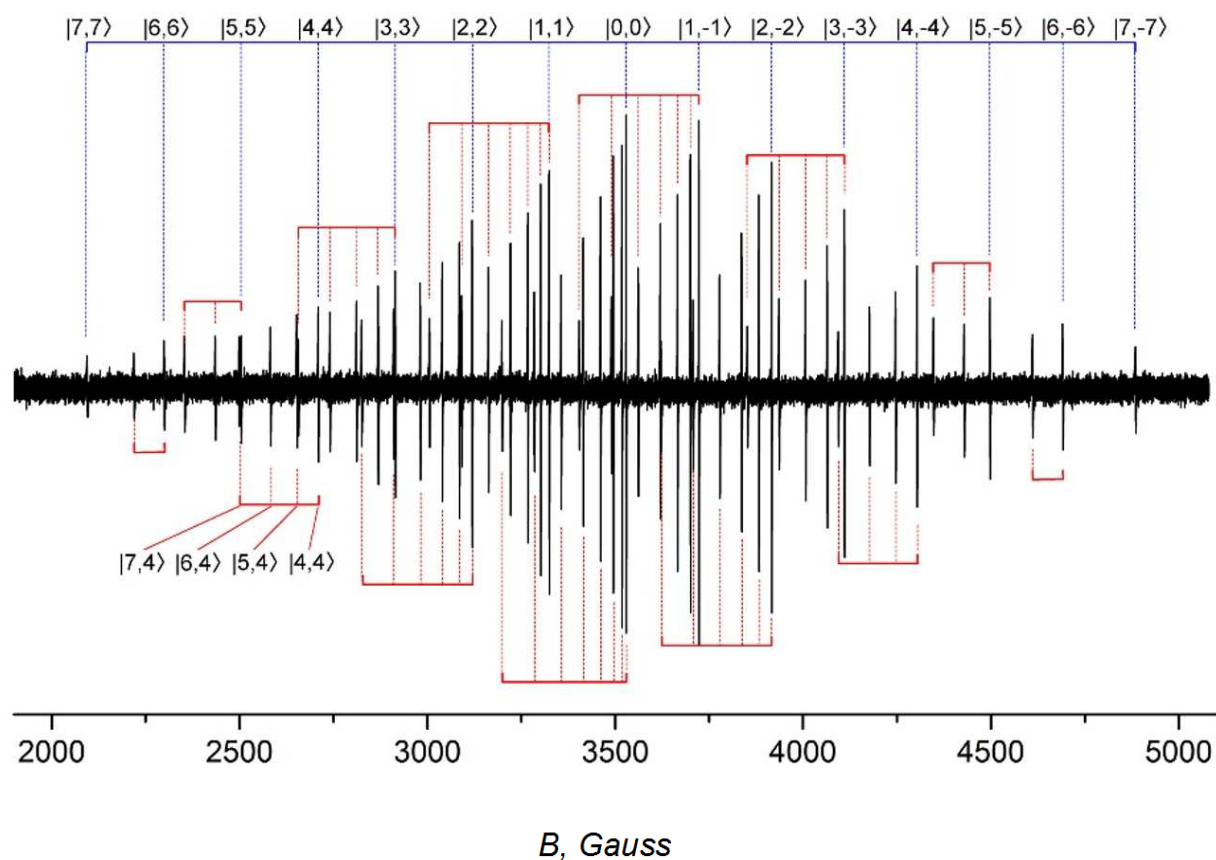


Figure 2.18. EPR of the cation radical $\text{Sc}_2@\text{C}_{82}^+$. Assignment of the peaks to $|I, m_l\rangle$ states is shown in blue and red lines. Blue lines denote the states with $l = |m_l|$, red lines show groups with identical m_l values and $l \geq |m_l|$.

Despite the seemingly complex hyperfine pattern, positions of all resonances can be perfectly reproduced with a single $a(^{45}\text{Sc})$ constant of 199.2 G equal for two Sc atoms and a g -factor of 1.994. The $a(^{45}\text{Sc})$ constant in $\text{Sc}_2@\text{C}_{82}^+$ is the largest among all Sc-based EMF compounds and is one of the largest among all Sc-based compounds in general.

The value of isotropic coupling constant a_{Sc} can be employed to estimate the contribution of s -orbitals of Sc to the Sc–Sc bonding orbital. ScO radical with $a(^{45}\text{Sc})$ value of 630 G is known to be a pure Sc- $4s^1$ system¹⁸⁰. Taking it as a reference, we can determine the contribution of Sc atomic $4s$ -orbitals to the spin density in $\text{Sc}_2@\text{C}_{82}^+$ as 32%, that is in good agreement with the spd -hybrid orbital composition of the spin density distribution, calculated by DFT (Figure 2.17).

So far as resonance lines with different l , but the same m_l have been resolved, there degeneracy of the spectrum is lifted. So one can expect the intensity of all 64 resonance lines in the isotropic spectrum to be identical. The experimental data (Fig. 10) at first sight does not follow this prediction: the peaks close to the center have considerably higher height. The reason is the variation of the line width across the spectrum from 1.1 G for the central lines to 2.2/3.4 G on the high- and low-field areas, which is caused by the incomplete rotational averaging (tumbling).

In 1961 Kivelson et al. demonstrated, that in the fast-motional regime the linewidth is determined as a quadratic or cubic function from m_l ¹⁸¹.

$$\text{Width} = \alpha + \sum_i (\beta_i m_l + \gamma_i m_l^2 + \dots) \quad (\text{Eq. 2.3})$$

Here α , β and γ coefficients are depending from g -factor and coupling constant anisotropy and rotation time.

For our system with a strong second order effect we hypothesized that line-width in the fast-motional regime depends quadratically on both m_l and l . To check this suggestion at first we selected 15 points with same values of $|m_l|=l$ and verified that the linewidth exhibits quadratic dependence on m_l

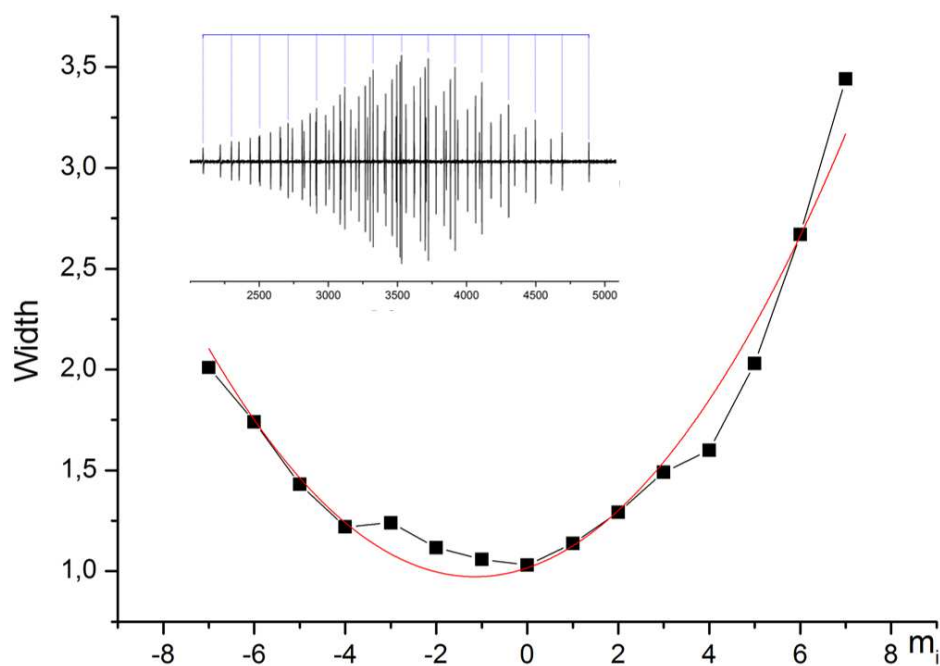


Figure 2.19. Linewidth of the 15 resonance lines with $|m_l|=l$ in the EPR spectrum of $Sc_2@C_{82}^+$ as a quadratic function of m_l . The inset exhibits the position of selected resonances at the spectrum.

For the resonance lines with zero m_l values the quadratic dependence has also been found on the total momentum l :

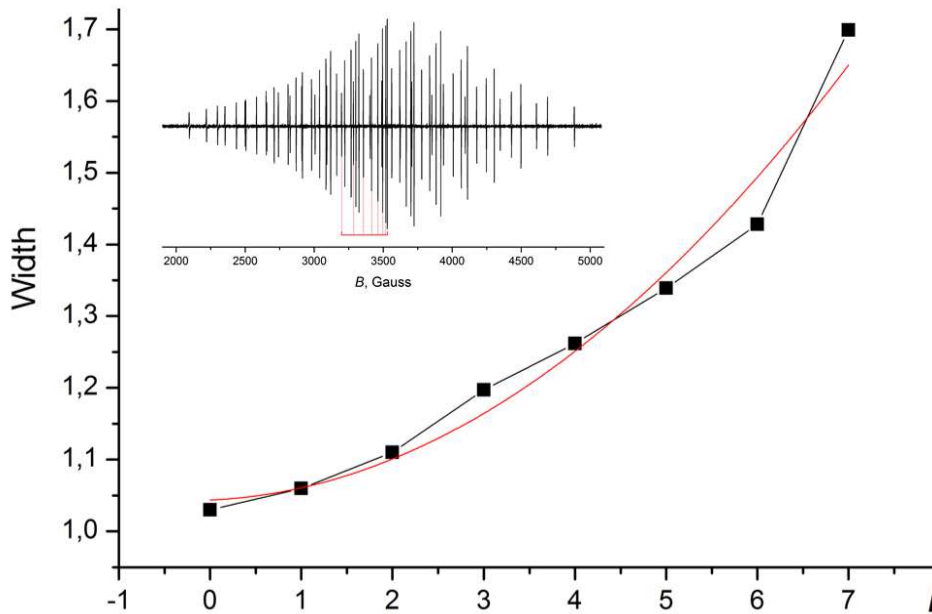


Figure 2.20. Linewidth of the 8 resonance lines with $m_l=0$ in the EPR spectrum of $Sc_2@C_{82}^+$ as a quadratic function of m_l . The inset exhibits the position of selected resonances at the spectrum.

Final two-parameter (m_l and l) fit of all 64 resonances line-width in the fast-motional regime revealed square dependence on both m_l , and l , including also a mixed term $m_l \cdot l$. (Figure 2.21).

$$\text{Width} = \alpha + \beta_1 m_l + \beta_2 l + \gamma_{10} m_l^2 + \gamma_{01} l^2 + \gamma_{11} m_l l \quad (\text{Eq. 2.4})$$

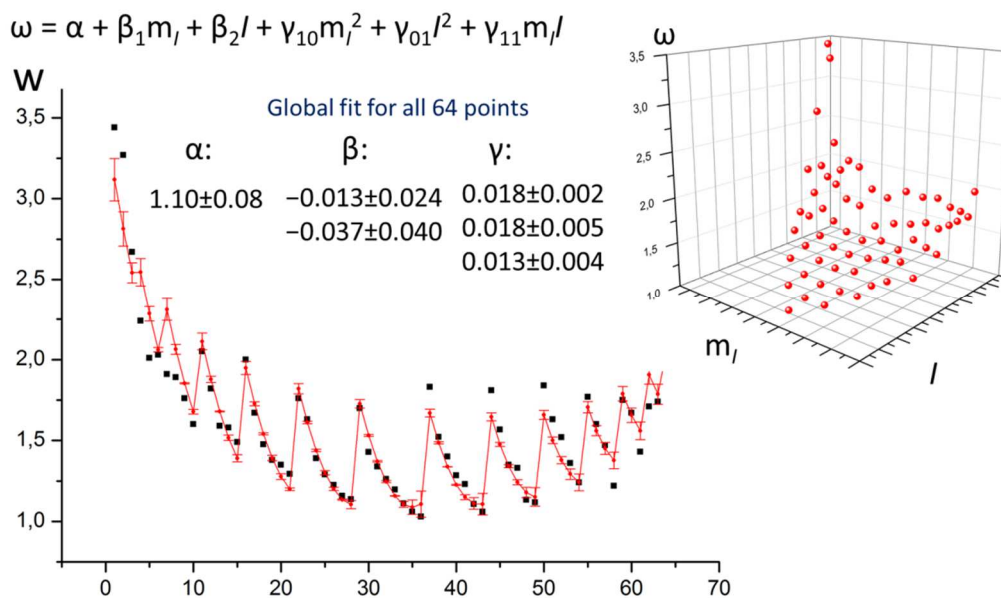


Figure 2.21. Linewidth in the EPR spectrum of $Sc_2@C_{82}^+$ as a function of I and m_I and the fit of the whole set of data using quadratic function of both parameters

It is interesting, that the contribution of the two linear terms $\beta_1 m_I$ and $\beta_2 I$ have been determined worse with respect to three quadratic terms $\gamma_{10} m_I^2$, $\gamma_{01} I^2$ and $\gamma_{11} m_I I$. At the same time the contribution of the first ones also is much smaller. On the whole the fitting error has been found to be low (see figure 2.21).

After adjusting the calculated line widths values to the simulation algorithm the experimental spectrum can be perfectly reproduced by a simulated one.

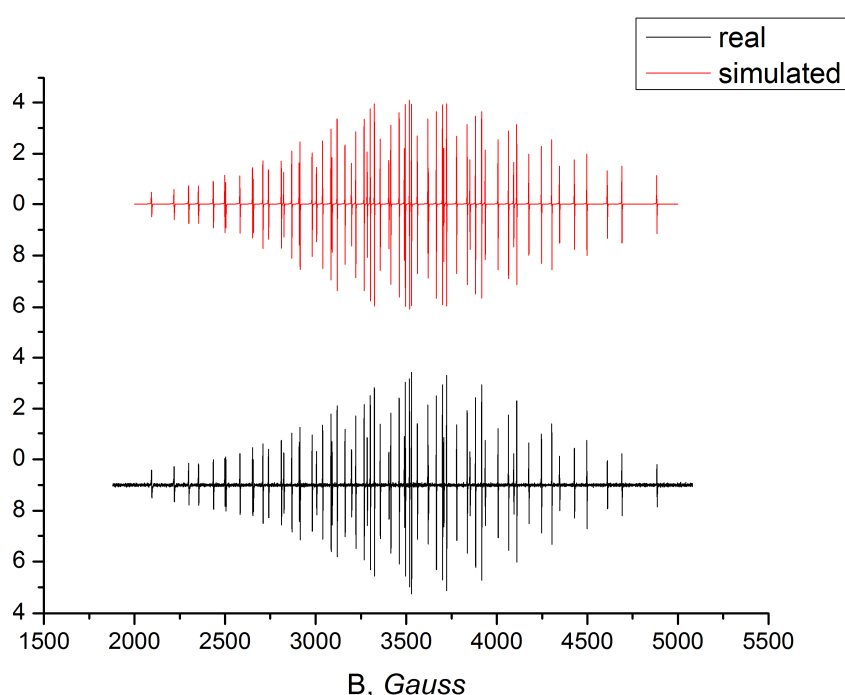


Figure 2.22. Comparison of experimental (black) and simulated (red) EPR spectra of $Sc_2@C_{82}^+$. For the sake of comparison, noise reduction was applied to the experimental spectrum by filtering high frequency part in the Fourier-transformed spectrum. Positions of the lines in simulated spectrum were obtained using XSope software, linewidth are from the fit described above.

2.5.2. SQUID Magnetometry

Because of the strong lanthanide-induced broadening of the resonance lines, EPR spectra of $Er_2@C_{82}^+$ cation radicals cannot be measured in solution at room temperature. In the absence of EPR indication of the spin localization in these dimetallofullerene cations, we have addressed this question using SQUID magnetometry. One can expect, that changing from the double-occupied Er–Er bonding orbital in the neutral $Er_2@C_{82}$ molecule to the single-occupied orbital in $Er_2@C_{82}^+$ cation-radical will also adjust the Er–Er exchange coupling. This

should result in the changes in the magnetization behavior of the compound, which can be revealed with the help of SQUID magnetometry measurements.

Similar to $\text{Sc}_2@\text{C}_{82}^+$, the $\text{Er}_2@\text{C}_{82}^+$ cation radical has been prepared by oxidation of $\text{Er}_2\text{S}@\text{C}_{82}\text{-C}_{3v}$ EMF with an excess of tris(4-bromophenyl)aminium hexachloroantimonate in *o*-dichlorobenzene solution. After the reaction the solvent has been evaporated and the residue has been washed with acetonitrile to remove the excess of oxidant and with toluene to remove rest of unreacted dimetallofullerene and then redissolved in *o*-dichlorobenzene.

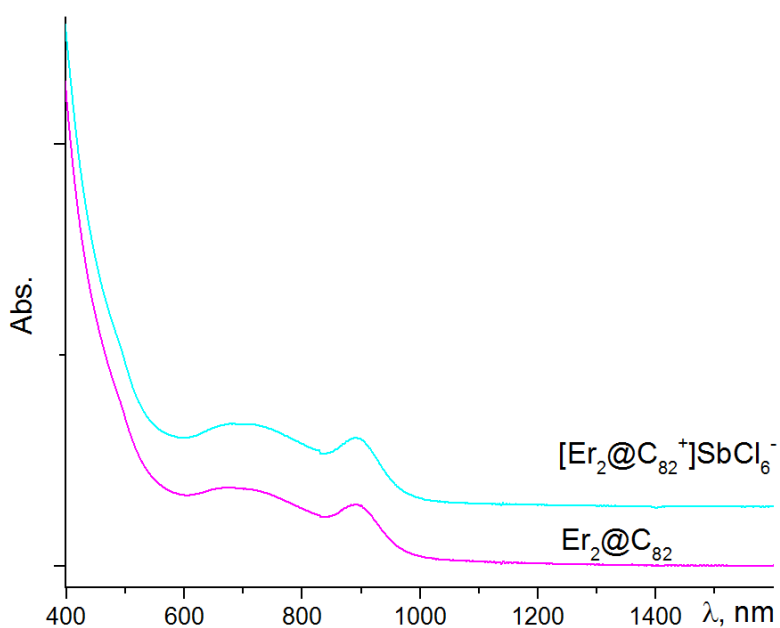


Figure 2.23. Vis-NIR absorption spectra of $[\text{Er}_2@\text{C}_{82}]^+\text{SbCl}_6^-$ and $\text{Er}_2@\text{C}_{82}$ with $\text{C}_{82}\text{-C}_{3v}(8)$ cage isomer, *o*-dichlorobenzene, $l=1$ cm.

The Vis-NIR spectra of final $[\text{Er}_2@\text{C}_{82}]^+\text{SbCl}_6^-$ is very similar to that of the parent $\text{Er}_2@\text{C}_{82}$ EMF (figure 2.23). So far as shape of Vis-NIR is mostly determined by the $\pi \rightarrow \pi^*$ excitation of the cage π -electrons, we can conclude, that the electronic structure of the $\text{Er}_2@\text{C}_{82}$ carbon cage is not changed upon oxidation. This fact additionally confirms the cluster-based nature of the HOMO in these EMFs.

Figure 2.24 demonstrates normalized magnetization curves measured for the powder samples of pristine $\text{Er}_2@\text{C}_{82}$, $\text{Er}_2@\text{C}_{82}^+$ salt as well as for the same isomer of $\text{Er}_2\text{S}@\text{C}_{82}$. The $\text{Er}_2@\text{C}_{82}$ and $\text{Er}_2@\text{C}_{82}^+$ samples exhibit strongly different magnetization saturation behavior in the magnetic field area of below 2 T. With the increase of the external magnetic field the magnetization grows much faster in case of the cation-radical than in case of parent dimetallofullerene. This effect cannot not be caused by the rest of tris(4-bromophenyl)aminium

hexachloroantimonate influence: saturation curve of the last one has been measured at the same conditions and demonstrates the magnetization growth much slower than both EMFs samples. Thus, normalized magnetization curve for non-interacting mixture of tris(4-bromophenyl)aminium hexachloroantimonate and $\text{Er}_2@C_{82}$ would be also reaching saturation slower than $\text{Er}_2@C_{82}$. Similarly, in case when oxidation does not influence the metal-metal interaction but only creates an additional spin of 1/2 localized on the carbon cage, saturation of the $\text{Er}_2@C_{82}^+$ cation radical would be reached slower with respect to the pristine $\text{Er}_2@C_{82}$ dimetallofullerene. This line of arguments has confirmed that the difference in the magnetization curves of $\text{Er}_2@C_{82}$ and $\text{Er}_2@C_{82}^+$ is not caused by an additional spin 1/2 center weakly interacting with the spin system of Er_2 unit, but has to have a lanthanide-based nature.

Thus one can conclude that oxidation of $\text{Er}_2@C_{82}$ with tris(4-bromophenyl)aminium hexachloroantimonate strongly influences the spin state in the endohedral M_2 unit, supposedly transforming it into a three-center $[M-e-M]$ spin system with stronger exchange interactions. SQUID measurements have confirmed that metal-metal bonding in $\text{Er}_2@C_{82}^+$ cation-radical is substantially modified with respect to neutral dimetallofullerene. Interestingly, magnetization saturation curve of $\text{Er}_2@C_{82}^+$ at 2 K is almost similar to that of the $\text{Er}_2S@C_{82}$.

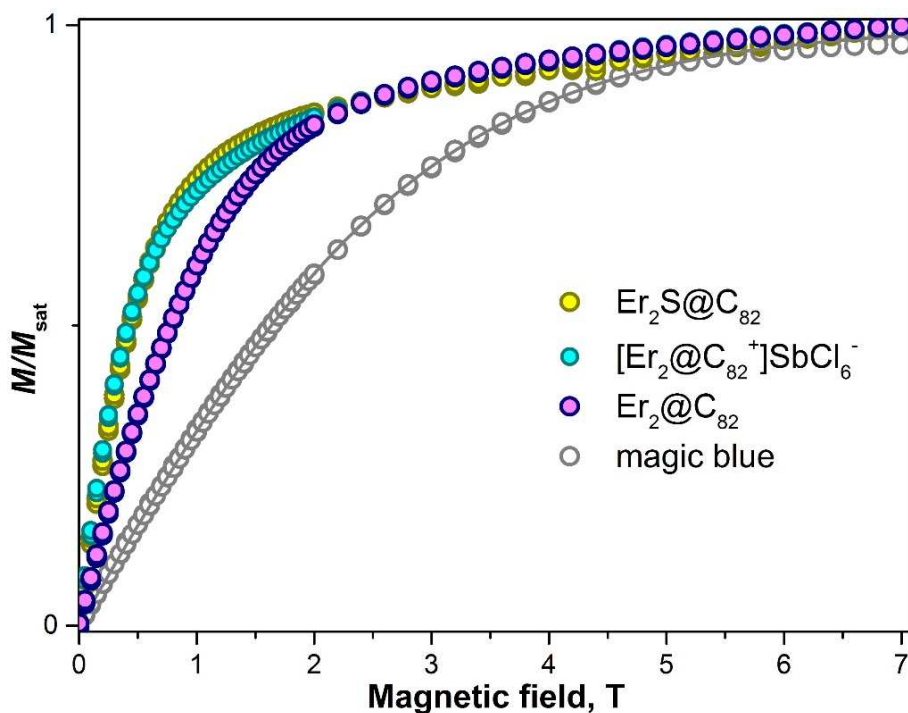


Figure 2.24. Magnetization curves of $\text{Er}_2S@C_{82}$, $\text{Er}_2@C_{82}$, $[\text{Er}_2@C_{82}^+]\text{SbCl}_6^-$, and magic blue at $T = 2$ K (all EMFs are with $C_{82}-C_{3v}(8)$ cage). For each sample, the curve was normalized to the value measured at 7 T. The line shows Brillouin function with the spin $S=1/2$ fitting the data points for magic blue.

2.6. Chapter summary

1. Two series of $M_2@C_{82-C_{3v}}$ and $M_2@C_{82-C_s}$ dimetallofullerenes as well of corresponding sulfide and carbide clusterfullerenes have been isolated and characterized. For both cage isomers dimetallofullerenes have non-trivial structure with a metal-metal bonding between two metal atoms, which has been proved with several spectroscopic techniques as well as DFT calculations.

2. The $M^{2+}-M^{2+}$ bonding orbital is the HOMO orbital of the dimetallofullerene molecule, that strongly influences the oxidation behavior of dimetallofullerene in comparison with corresponding isomers of clusterfullerenes.

3. The EPR spectrum of $Sc_2@C_{82}$ cation radical shows a giant isotropic ^{45}Sc hyperfine coupling constant of 199.2 G due to the large contribution of 4s atomic orbitals of Sc to the Sc–Sc bonding MO in $Sc_2@C_{82}$.

4. For $Er_2@C_{82}$, the metal-based oxidation leads to the formation of a unique spin system, in which local magnetic moments of Er ions derived from 4f electrons are coupled to each other via a single unpaired spin delocalized between two ions. The oxidation of $Er_2@C_{82}$ to $Er_2@C_{82}^+$ hence results in the strong changes in the magnetization behavior.

Chapter 3. Single-occupied metal bonding orbital in $M_2@C_{80}(CH_2Ph)$: electrochemical and EPR studies

3.1. Unique $M_2@C_{80}(CH_2Ph)$ EMFs: synthesis and structure

In the previous chapter we have demonstrated, that such metals as Er, Lu and Sc can adopt the charge state of 2+ in dimetallofullerenes and form stable EMFs with 4-fold charged cages $C_{82}-C_s$ and $C_{82}-C_{3v}$, although lower lanthanides as Ce and La adopt charge state of 3+ and can be stabilized with 6-fold charged cages. However there is a third variant of the electronic configuration of the M_2 cluster, which can be realized for Y and a list of medium lanthanides such as Dy, Tb and Gd. For all this metals no dimetallofullerene with 6-fold $C_{80}-I_h$ cage has ever been isolated, whereas a dimetallofullerene with 4-fold $C_{82}-C_{3v}$ cage has been found only in case of Y. $Y_2@C_{82}-C_{3v}$ is characterized by low first oxidation potential and low stability⁶⁶.

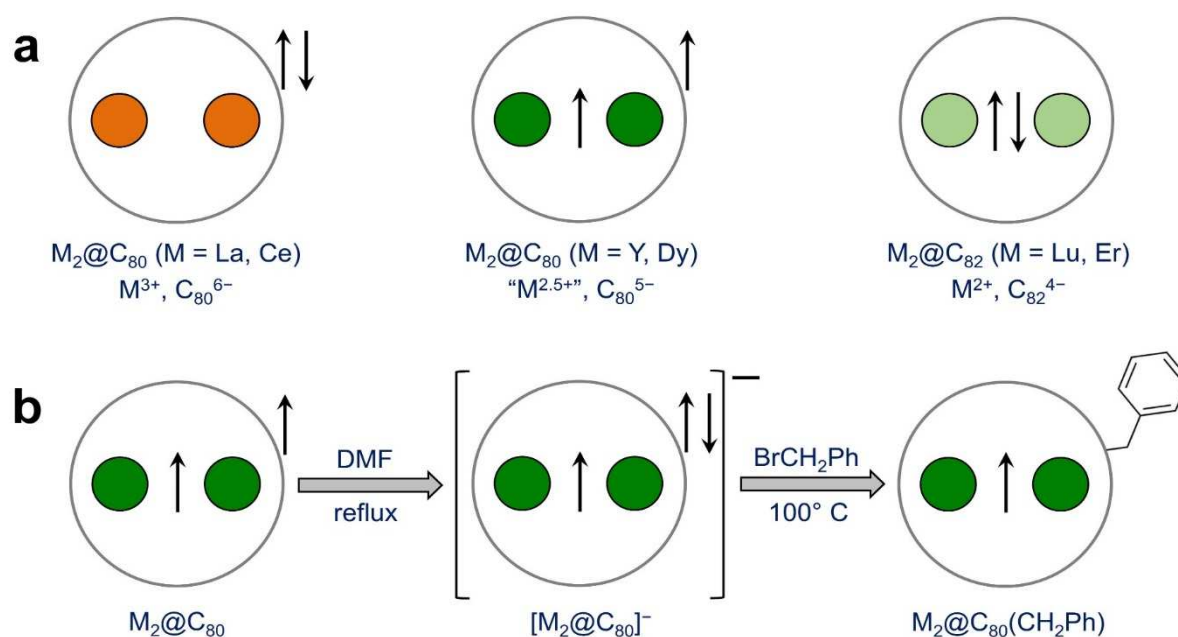


Figure 3.1. Schematic depiction of dimetallofullerenes and derivatives. **(a)** Comparison between different types of dimetallofullerenes. **(b)** Description of the synthetic route for $M_2@C_{80}$ with single-electron M–M bond.

Calculations made by group of Shinohara in 2014 have revealed that the ground state of $M_2@C_{80}$ molecule (M = Y, Gd) is a triplet with one unpaired electron on the M–M bonding MO, and another one unpaired electron being delocalized over the carbon cage (Figure 3.1a)¹⁸². In this way, the M_2 cluster actually donates 5 electrons to the carbon cage that can be called an intermediate situation between 4 electrons in case of Er, Sc and Lu and 6 electrons in case

of La and Ce. This statement is confirmed by isolation of $Y_2@C_{79}N$ and $Gd_2@C_{79}N$ azafullerenes, in which the formal charge of the mixed $C_{79}N$ cage is 5-. Moreover EPR studies of neutral $Y_2@C_{79}N$ and $Gd_2@C_{79}N$ have revealed an unpaired electron delocalized between two metal atoms¹⁵⁵.

Thus, $M_2@C_{80}$ dimetallofullerenes with unpaired electrons in the metal bonding orbital are biradicals in the ground state. These EMFs are extremely unstable and cannot be extracted from the primary soot using the ordinary extraction (with CS_2 , halogen aromatics, etc.). There have been several attempts to extract such EMFs as anions^{37,183} using donor solvents such as pyridine and DMF or to transform them into stable chemical derivatives (in particular, by adding a CF_3 group with the formation of $M_2@C_{80}(CF_3)$ mono adduct)^{182,184,185}, although in both cases products have not been isolated individually.

During the last year Dr. Liu from our group has investigated and developed the ingenious two-step procedure to extract such dimetallofullerenes from the standard metal oxide/graphite arc-discharge primary soot. During the first step, solid EMFs are transferred to anionic form with DMF extraction: this solvents acts as a donor, providing an additional electron to dimetallofullerene molecules. As a result we have $M_2@C_{80}$ anions, in which all cage electrons are coupled, and only one unpaired electron remains on the metal-bonding orbital. Such anions are more stable in comparison with parent biradical dimetallofullerenes and can be efficiently dissolved in polar DMF (Figure 3.1 b). This ionic solution is then treated with excess of $BrCH_2Ph$, that finally leads to a mixture of different $M@C_{2n}(CH_2Ph)$ and $M_2@C_{78,80}(CH_2Ph)$ benzyl monoadducts. These compounds are stable on air and soluble in toluene. The reaction with $BrCH_2Ph$ proceeds via formal nucleophilic substitution of Br^- with $M_2@C_{80}^-$ anion. Wherein the cage electron pair forms the bonding between fullerene and CH_2Ph moiety. Consequently, in the final monobenzyl derivative $M_2@C_{80}(CH_2Ph)$, the only unpaired electron is located on the metal-bonding orbital, while all other electrons are coupled. It should be noted, that formation of benzyl monoadduct is not common in fullerene chemistry: generally in case of monovalent addends EMFs as well as empty fullerenes form derivatives with even number of attached groups. Formation of stable derivative with one attached benzyl moiety also indicates the unusual electronic structure of parent $M_2@C_{80}$ EMFs.

Described above extraction procedure has been shown to be applicable in case of Y, Dy and Tb dimetallofullerenes. Further multi-step HPLC procedure allows to isolate two isomers of

$M_2@C_{80}(CH_2Ph)$ - with C_{80-I_h} and $C_{80-D_{5h}}$ cages. Molecular structure of $Dy_2@C_{80}(CH_2Ph)$ with C_{80-I_h} cage isomer has been confirmed by single-crystal XRD experiment. Molecular structure of $M_2@C_{80}(CH_2Ph)$ with $C_{80-D_{5h}}$ cage isomer has been determined by UV-vis-NIR spectroscopy based on the analogy with the monoadduct of $La_2@C_{80-D_{5h}}$ ¹⁸⁶.

These dimetallofullerene derivatives with single-occupied molecular bonding orbital (SOMO) represent a unique case in EMF research. Unpaired ground state electron between two metals strongly influences both electrochemical and magnetical behavior. In particular SQUID studies of $Dy_2@C_{80}(CH_2Ph)$ with C_{80-I_h} cage isomer have demonstrated that this fullerene is a single molecule magnet with record-high blocking temperature of 22 K. The three-center spin system of molecule can be described as $[Dy^{3+}-e-Dy^{3+}]$, in which all moments are collinear and coupled ferromagnetically to form a single spin unit of $21 \mu_B$ ¹⁸⁷.

In the present work we focus mainly on electrochemical and EPR studies of different $M_2@C_{80}(CH_2Ph)$ EMFs ($M= Y, Dy, Tb, C_{80-I_h}$ and $C_{80-D_{5h}}$ cage isomers), so far as author has been involved only in these parts of the research. For more details about the synthesis, structure and SQUID measurements, see ref¹⁸⁷.

3.2. The electronic structure of neutral $Y_2@C_{80}(CH_2Ph)$ compounds: EPR investigation

The electronic structure of the $Y_2@C_{80}(CH_2Ph)$ derivatives with C_{80-I_h} and $C_{80-D_{5h}}$ cages is confirmed by EPR spectroscopy. The EPR spectrum of neutral $Y_2@C_{80}(CH_2Ph)$ fullerene with C_{80-I_h} cage (Y_2-I_h), measured in solution at room temperature (Figure 3.2) exhibits a broad triplet with the isotropic $a(^{89}Y)$ hyperfine constant of 81.2 G (224 MHz) and an electron g -factor of 1.9733. Such a large value of the ^{89}Y coupling constant confirms the presence of the unpaired electron on the Y-Y bonding molecular orbital. As in case of $Sc_2@C_{82}^+$ cation-radical, this bonding is formed with sufficient contribution of s-orbital that provides high spin density at the nuclei and strong nuclear-spin interaction.

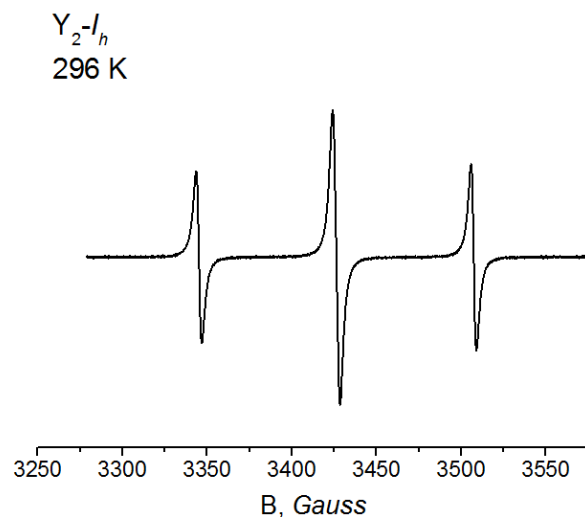


Figure 3.2. EPR spectrum of Y_2-I_h in toluene solution at room temperature

The EPR spectrum of the Y_2-I_h frozen solution at 150 K (Figure 3.3) shows characteristic rhombic pattern with hyperfine tensor components $a_{\perp}(^{89}Y)=75,3$ G (208 MHz) and $a_{\parallel}(^{89}Y)=88,9$ G (246 MHz) respectively, and g -tensor components $g_{\perp}=1.9620$, and $g_{\parallel}=1.9982$. The averaged values of g -factor and hyperfine constant, obtained from the low temperature tensors, are respectively 1.974 and 79.8 G, that is quite closed to experimentally observed isotropic values.

The pronounced anisotropy of both tensors also indicates that a substantial degree of the spin density is localized on the two Y atoms.

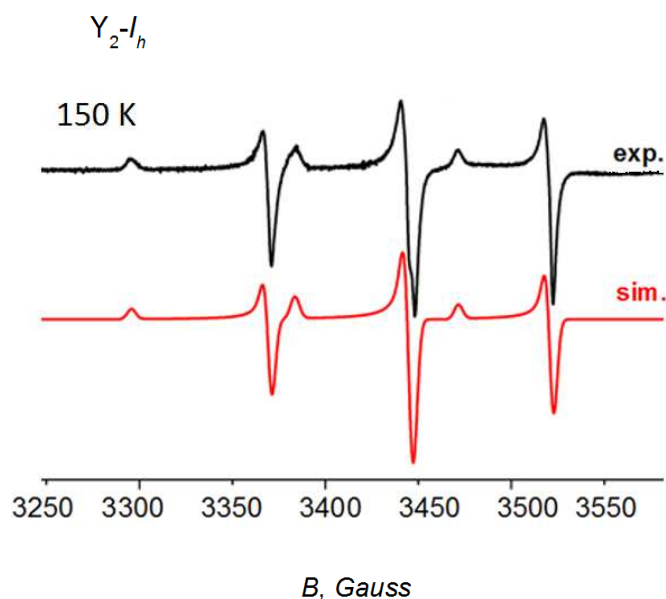


Figure 3.3. Experimental and simulated EPR spectra of Y_2-I_h in frozen toluene solution at 150 K.

At the intermediate temperatures, between 276 and 176 K, the EPR spectra in toluene solution have a shape of an asymmetrically broadened triplet, the broadening degree increasing with the decrease of the temperature. The simulation can be done in the fast motion regime: all the hyperfine tensor components and g -tensor components are fixed as obtained from the simulation for 150 K, the only variable parameter is the correlation time. The linewidth is then calculated from the correlation time. In particular figure 3.4 shows the experimental and simulated spectra for the temperature of 196 K. The value of correlation time decimal logarithm $\text{Log}(t_{\text{corr}})$ is -9.115 .

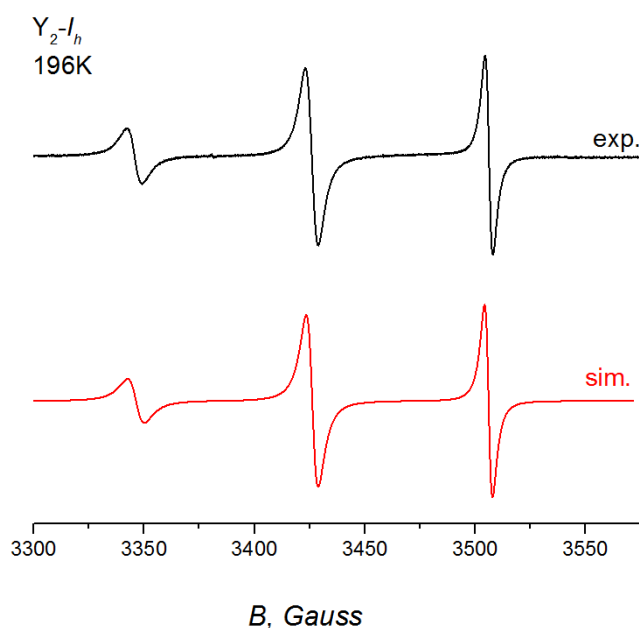


Figure 3.4. Experimental and simulated EPR spectra of Y_2-I_h at 196 K

The EPR parameters of Y_2-I_h are very close to those reported earlier for corresponding isomer of $Y_2@C_{79}N$ azafullerene^{155,161}: both EMF molecules have very similar spin density distribution arising from the single-occupied Y–Y bonding MO. DFT calculations also confirm that the spin density in Y_2-I_h is fully enclosed inside the carbon cage and resembles the spatial distribution of the Y–Y bonding molecular orbital.

In case of Dy_2-I_h and Tb_2-I_h EMFs, the EPR spectroscopy is not applicable, and the electron distribution cannot be confirmed directly. Although, UV–vis–NIR absorption, Raman, and IR spectra of all three M_2-I_h fullerenes are very similar¹⁸⁷, confirming that these compounds have identical molecular and electronic structure. Thus, conclusions, made for Y_2-I_h can be extended to Dy_2-I_h and Tb_2-I_h EMFs as well.

The EPR spectrum of $Y_2@C_{80}(CH_2Ph)$ fullerene with $C_{80}-D_{5h}$ cage isomer (Y_2-D_{5h}) generally follows the same trend as the I_h analogue does, although several noticeable differences have been detected. The EPR spectrum of toluene solution at room temperature (Figure 3.5) can be assigned to the system with two close but inequivalent Y atoms: $a_1(^{89}Y) = 79$ G (218.3 MHz), $a_2(^{89}Y) = 77.1$ G (213 MHz) and g -factor of 1.9738.

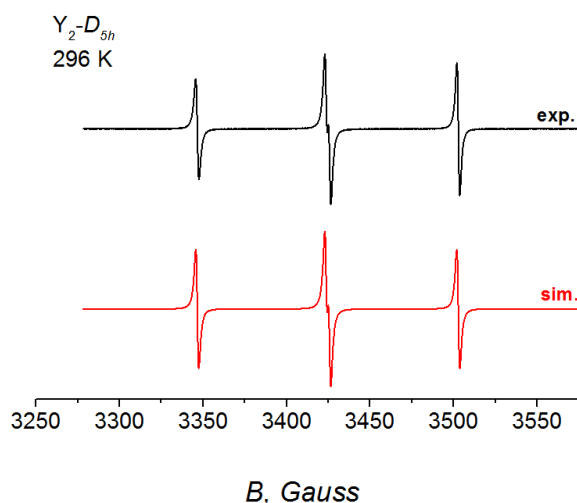


Figure 3.5. EPR spectrum of Y_2-D_{5h} in toluene solution at room temperature

In the EPR spectrum of the frozen solution at 150 K we can observe rhombic pattern of both hyperfine tensor components $a_1(^{89}Y)=[73,3$ G; 87,7 G] and $a_2(^{89}Y)=[73,1$ G; 86,7 G], whereas the g -tensor is fully anisotropic $g=[1.9582; 1.9665; 1.9971]$.

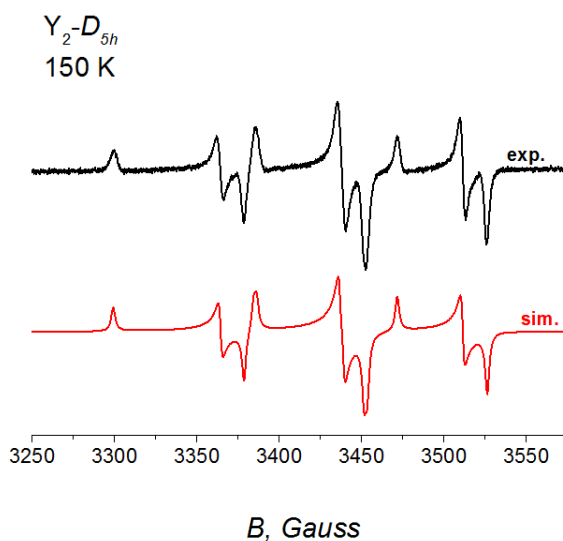


Figure 3.6. Experimental and simulated EPR spectra of Y_2-D_{5h} in frozen toluene solution at 150 K.

The spectrum of Y_2-D_{5h} at 196 K is also a distorted and broadened triplet, it is interesting that unequivalence of Y nuclei is not visible anymore. The value of $\text{Log}(t_{\text{corr}})$, obtained from simulation in the fast motion regime is -9.025, so Y_2-D_{5h} is characterized by somewhat slower rotation in comparison with Y_2-I_h .

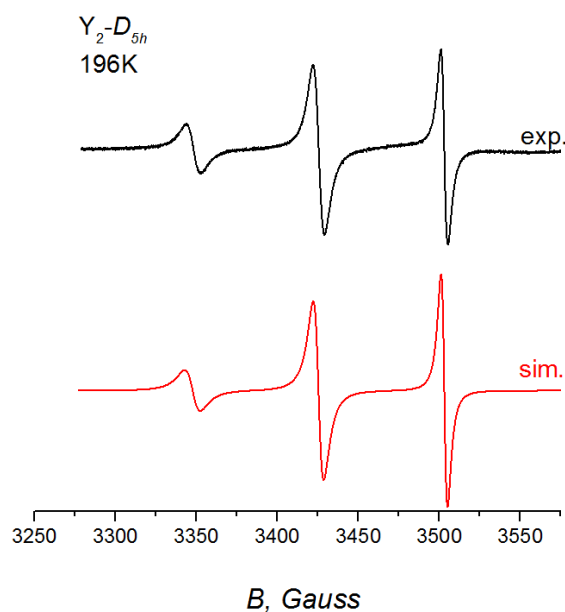


Figure 3.7. Experimental and simulated EPR spectra of Y_2-D_{5h} at 196 K

3.3. Electrochemical studies

Redox behavior of $M_2@C_{80}(\text{CH}_2\text{Ph})$ fullerenes with single-occupied metal-bonding orbitals of particular interest. In the previous chapter we have demonstrated, that in $M_2@C_{82}$ EMFs with Sc, Er and Lu the double-occupied metal bonding orbital is the HOMO, while in $La_2@C_{80}-I_h$ molecule this empty metal-bonding orbital is LUMO. This orbital has both occupied and unoccupied components that hypothetically allows participation in both oxidation and reduction activity. However, DFT calculations (made for Y-based EMF with $C_{80}-I_h$ cage) predict, that the occupied SOMO component has energy level much lower than the cage-based HOMO and hence is not electrochemically active (Figure 3.10). At the same time, the LUMO of $Y_2@C_{80}(\text{CH}_2\text{Ph})$ is the unoccupied counterpart of the Y–Y bonding SOMO, and one can expect the first reduction step to involve this orbital.

Cyclic voltammetry and square wave voltammetry experiments have been executed in standard conditions in o-dichlorobenzene solution under dry N_2 atmosphere. All three Y_2-I_h , Dy_2-I_h and Tb_2-I_h EMFs exhibit completely reversible first reduction and partially reversible second and third reduction steps (Figure 3.8). The first oxidation is also reversible. In case of Y

and Dy EMFs, the second oxidation step can be detected in square wave voltammetry experiment, this process is also partially observed in cyclic voltammetry and most likely proceeds irreversibly.

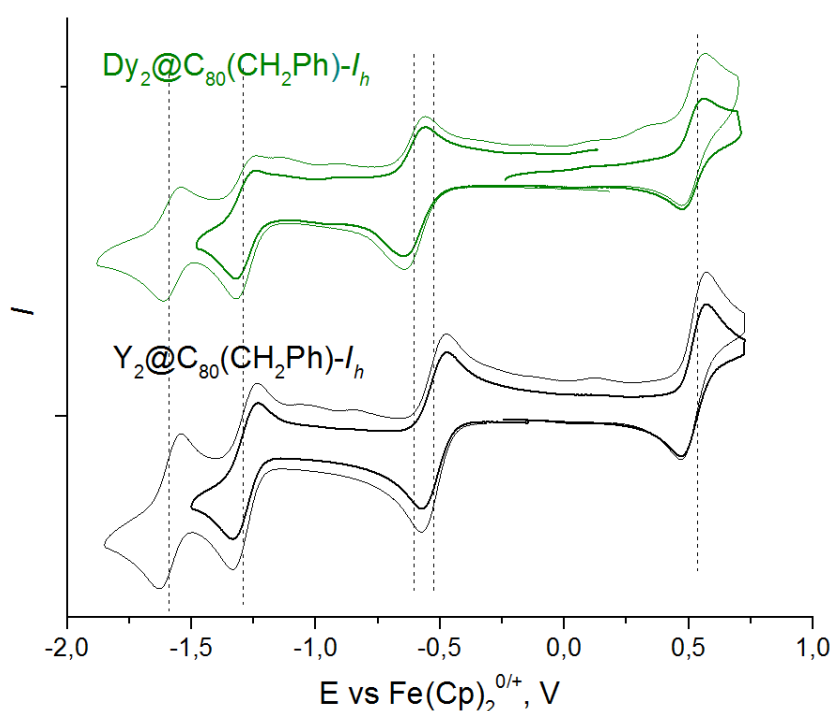


Figure 3.8. Cyclic voltammetry $Y_2@C_{80}(CH_2Ph)$ and $Dy_2@C_{80}(CH_2Ph)$ EMFs with $C_{80}-I_h$ cage isomer. Measurements are performed at room temperature in *o*-dichlorobenzene/TBABF₄ with the scan rate 100 mV/s. To guide an eye, vertical dotted lines denote redox potentials.

The first oxidation potentials of Y_2-I_h , Dy_2-I_h and Tb_2-I_h are virtually identical and placed in the range of +0.51-+0.52 V that is typical for cage-based processes. Metal-independent value of the potential also indicates the cage-based character of the oxidation: internal dimetallic cluster is not involved in the charge transfer, the potential is determined only by the electronic structure of the cage.

At the same time the first reduction potentials are more positive than standard cage-based processes and are characterized by substantial metal-dependence: Y-based EMF is the easiest to reduce (-0.52 V), then comes Dy_2-I_h with -0.60 V and Tb_2-I_h is the hardest to reduce with $E = -0.79$ V. In case of Y- and Dy-based EMFs the second and third reduction potentials as well as the second oxidation potential are also identical, although for Tb_2-I_h both the second and third reduction potentials are negatively shifted by 80 and 130 mV respectively.

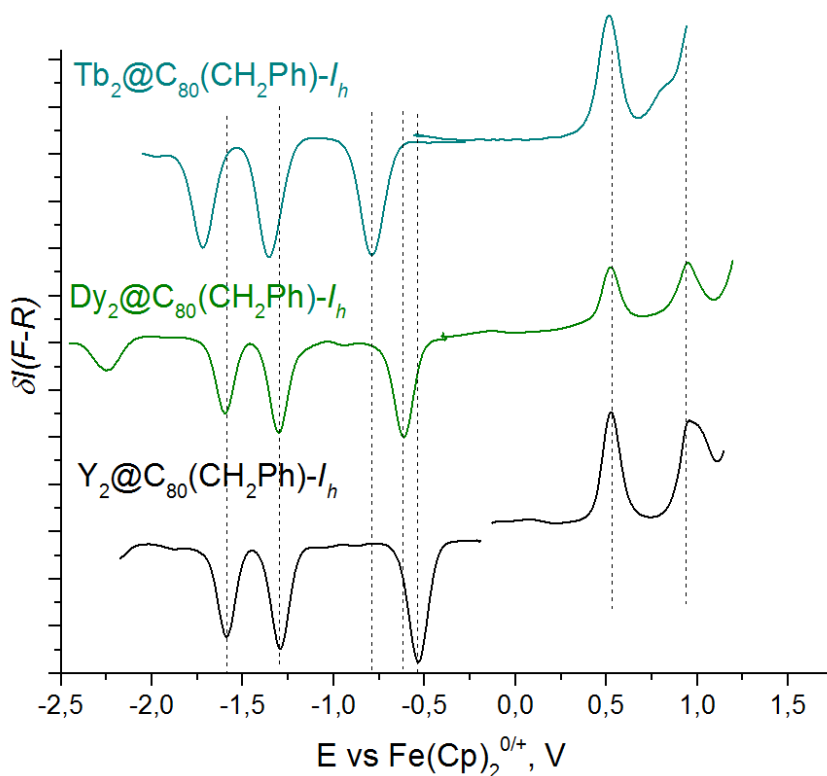


Figure 3.9. Square wave voltammetry of $Y_2@C_{80}(CH_2Ph)$, $Dy_2@C_{80}(CH_2Ph)$ and $Tb_2@C_{80}(CH_2Ph)$ compounds with $C_{80}-I_h$ cage isomer. Measurements are performed at room temperature in *o*-dichlorobenzene/TBAPF₄ with the scan rate 100 mV/s. To guide an eye, vertical lines denote redox potentials of $Y_2@C_{80}(CH_2Ph)-I_h$ and first reduction potentials of $Dy_2@C_{80}(CH_2Ph)-I_h$ and $Tb_2@C_{80}(CH_2Ph)-I_h$

The difference in electronic structure between $M_2@C_{80}(CH_2Ph)$ EMFs and already known $M_2@C_{80}$ dimetallofullerenes with $C_{80}-I_h$ cage make comparing their redox behavior to be meaningless. The only known reference compound for such EMFs is recently synthesized $La_2@C_{80}(CH_2Ph)$ with I_h cage isomer¹⁸⁸. This compound also has a single-occupied La–La bonding MO, that has been proven by EPR experiment. It should be noted, that mechanism of its formation is however different to that of Y, Dy and Tb analogs: the parent $La_2@C_{80}$ (that is stable and soluble in toluene) is treated with $BrCH_2Ph$ under irradiation with light of wavelength $\lambda > 350$ nm. The reaction proceeds via radical mechanism. In the ground state the metal-bonding orbital in $La_2@C_{80}$ is empty, but DFT calculations show, that in the excited state one of electrons can switch to metal-bonding LUMO, forming a triplet. This particle can be further stabilized by bonding with one CH_2Ph radical. The electronic structure of resulting La_2-I_h is similar to that of M_2-I_h EMFs with Y, Tb and Dy: the only unpaired electron is located on the metal-metal bonding orbital. The orbital energy distribution is although directly opposite: in

case of La-based EMF calculation show, that the occupied component of SOMO is HOMO, while the unoccupied component has high energy level and is not electrochemically active.

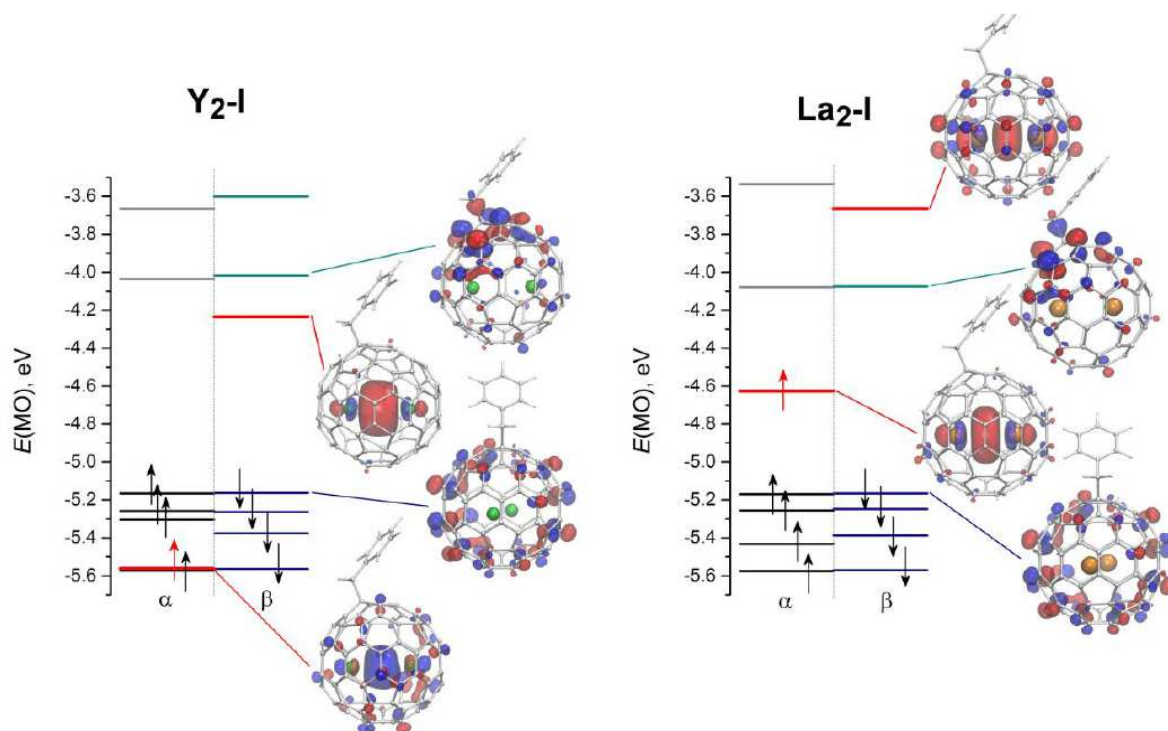


Figure 3.10. DFT-computed molecular orbital levels in Y_2-I_h and La_2-I_h , spin-up (α) and spin-down (β) levels are shown separately, arrows denote electrons in occupied MOs; Metal-based levels are highlighted in red. In Y_2-I_h , HOMO levels are fullerene-based, whereas the lowest unoccupied MO is localized on the Y_2 -fragment. In La_2-I_h , the highest occupied level is localized on La_2 -dimer, whereas LUMO levels are localized on the fullerene core.

Experimentally observed redox potential values for La_2-I_h (ref.¹⁸⁸) are in complete agreement with orbital distribution. La_2-I_h is characterized by a remarkably low first oxidation potential of +0.15 V. From the experiments with Y_2-I_h , Dy_2-I_h and Tb_2-I_h we can set down the first oxidation potential of $C_{80}(CH_2Ph)$ EMF with I_h isomer as approximately +0.5 V. In case of La_2-I_h pronounced negative shift undoubtedly indicates the cluster-based activity.

The first reduction potential of La_2-I_h is -0.82 V, which is the most negative among the Y, Tb and Dy analogs (whereas the second and the third reductions occur at similar potentials, see table 3.1). Taking into account the DFT calculation results, we can consider the value of -0.82 V as the level of cage-based reduction of $C_{80}(CH_2Ph)$ EMF with I_h cage isomer.

So we can conclude, that the first oxidation of Y, Tb and $DyM_2@C_{80}(CH_2Ph)$ EMFs is the cage-based process, while for La_2-I_h it is cluster-based. On the contrary, the first reduction step

for $\text{La}_2\text{-}I_h$ is cage-based, while the first reduction of $\text{Y}_2\text{-}I_h$ and $\text{Dy}_2\text{-}I_h$ is metal-dependent and occurs via the M–M SOMO. The first reduction of $\text{Tb}_2\text{-}I_h$ is the only process that could not be clearly assigned. Somewhat more positive with respect to the $\text{La}_2\text{-}I_h$ potential, it may indicate the cluster-based nature, although the difference is too small to make any definite conclusions. The switching of the redox mechanisms in $\text{M}_2\text{-}I_h$ EMFs on going from Y through Tb to La also can be explained by the higher energy of the $(6s)\sigma_g^2$ MO in the La_2 dimer, which is inherited in dimetallofullerenes in the form of a high-energy La–La bonding orbital.

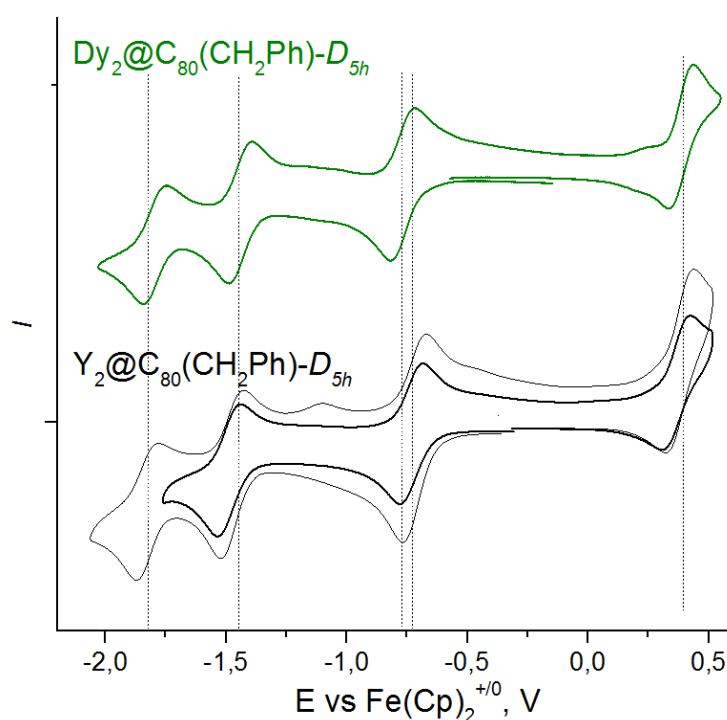


Figure 3.11. Cyclic voltammetry $\text{Y}_2@C_{80}(\text{CH}_2\text{Ph})$ and $\text{Dy}_2@C_{80}(\text{CH}_2\text{Ph})$ EMFs with $C_{80}\text{-}D_{5h}$ cage isomer. Measurements are performed at room temperature in *o*-dichlorobenzene/ TBABF_4 with the scan rate 100 mV/s. To guide an eye, vertical lines denote redox potentials of $\text{Y}_2@C_{80}(\text{CH}_2\text{Ph})\text{-}D_{5h}$

Redox behaviour of $\text{M}_2@C_{80}(\text{CH}_2\text{Ph})$ fullerenes with $C_{80}\text{-}D_{5h}$ cage generally follows the same trend. These EMFs exhibit three reversible reduction and one reversible oxidation steps.

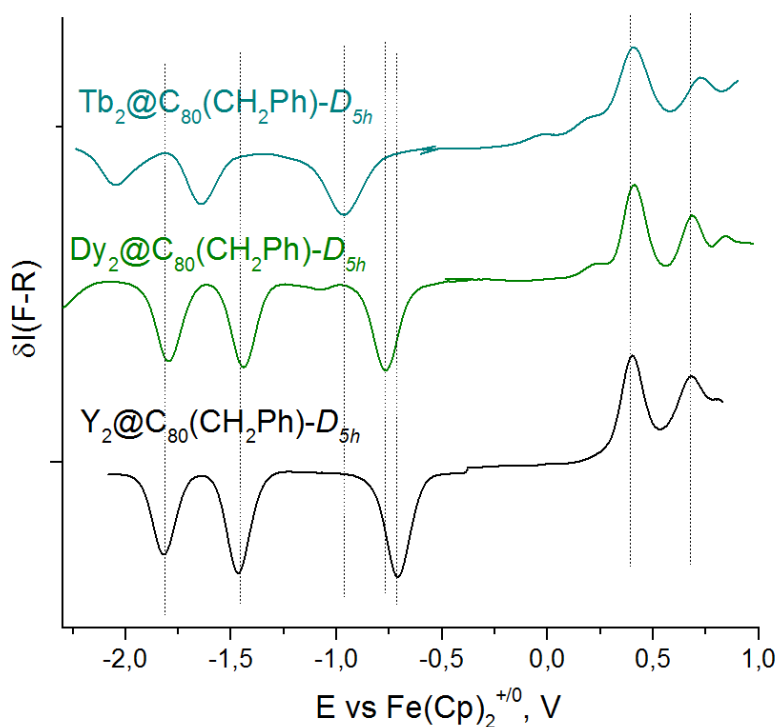


Figure 3.12. Square wave voltammetry of $Y_2@C_{80}(CH_2Ph)$, $Dy_2@C_{80}(CH_2Ph)$, and $Tb_2@C_{80}(CH_2Ph)$ compounds with $C_{80}-D_{5h}$ cage isomer. Measurements are performed at room temperature in *o*-dichlorobenzene/TBAPF₄ with the scan rate 100 mV/s. To guide an eye, vertical lines denote redox potentials of $Y_2@C_{80}(CH_2Ph)-D_{5h}$ and first reduction potentials of $Dy_2@C_{80}(CH_2Ph)-D_{5h}$ and $Tb_2@C_{80}(CH_2Ph)-D_{5h}$

Table 3.1. Redox potentials of selected EMF monobenzyl derivatives

EMF	ox-I	ox-II	red-I	red-II	red-III	gap _{EC}	link
$Y_2@C_{80}(CH_2Ph)-I_h$	+0.52	+0.98	-0.52	-1.29	-1.60	1.04	t.w.
$Dy_2@C_{80}(CH_2Ph)-I_h$	+0.52	+0.98	-0.60	-1.28	-1.58	1.12	t.w.
$Tb_2@C_{80}(CH_2Ph)-I_h$	+0.51	-	-0.79	-1.36	-1.71	1.30	t.w.
$La_2@C_{80}(CH_2Ph)-I_h$	+0.15	-	-0.82	-1.34	-1.64	0.97	188
$Y_2@C_{80}(CH_2Ph)-D_{5h}$	+0.40	+0.68	-0.72	-1.47	-1.82	1.12	t.w.
$Dy_2@C_{80}(CH_2Ph)-D_{5h}$	+0.40	+0.67	-0.77	-1.44	-1.79	1.17	t.w.
$Tb_2@C_{80}(CH_2Ph)-D_{5h}$	+0.40	+0.72	-0.96	-1.64	-2.05	1.36	t.w.

Potentials are listed in Volt versus the $[Fe(Cp)_2]^{+/0}$ pair, "ox" stands for oxidation, "red" stands for reduction, gap_{EC} is an electrochemical gap defined as the difference of the first reduction and oxidation potentials. All potentials obtained in this work have been measured in the SWV experiment and can be slightly to that measured in the CV experiment.

The first oxidation potentials are exactly identical for all three Y_2-D_{5h} , Dy_2-D_{5h} and Tb_2-D_{5h} EMFs (+0.40 V), while the first reduction potential spans the range from -0.72 V for Y to

-0.96 V for Tb. Similarly to I_h isomers we can make a conclusion, that unoccupied component of metal-metal bonding SOMO acts as the LUMO for these molecules, while the HOMO is cage-based.

The whole series of $M_2@C_{80}(CH_2Ph)$ fullerenes with $C_{80}-D_{5h}$ cage isomer is characterized by more negative both oxidation and reduction potentials with respect to their I_h analogs (see Table 3.1). The metal-dependence of the redox behavior is somewhat less pronounced.

3.4. Changing of the spin states in $Y_2@C_{80}(CH_2Ph)$, upon redox activity: EPR investigations

Our next step was the investigation of electronic structure of $Y_2@C_{80}(CH_2Ph)$ cations and anions. As we can conclude from the DFT data and electrochemical experiments, the first reduction occurs predominantly at the metal-bonding SOMO. In this case the unpaired electron at this orbital will be coupled upon reduction, and the resulting $Y_2@C_{80}(CH_2Ph)^-$ anion should be diamagnetic. So, one can expect to see no signal in the EPR spectrum of the $Y_2@C_{80}(CH_2Ph)$ monoanion.

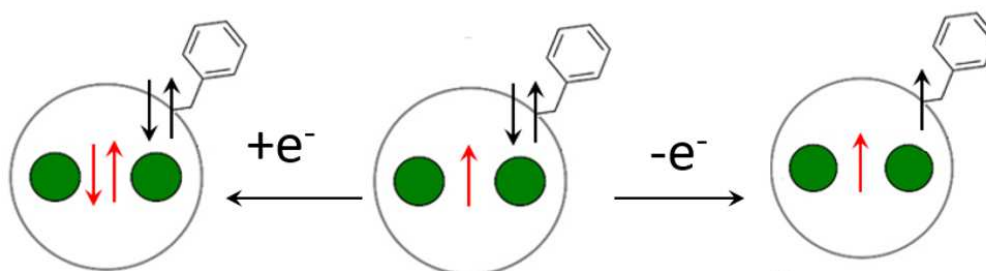


Figure 3.13. Schematic depiction of $M_2@C_{80}(CH_2Ph)$ first reduction and oxidation processes

At the same time, oxidation is the cage-based process, and the first electron will be taken from the cage HOMO, turning parent $Y_2@C_{80}(CH_2Ph)$ to a biradical with one unpaired electron at the metal-bonding SOMO and another one – at the fullerene cage. Such changes in the spin state also will influence the EPR activity of the compound.

To check this suggestion we measured EPR spectra of Y_2-I_h monocation and monoanion. The cation $Y_2-I_h^+$ has been generated by chemical oxidation with tris(4-bromophenyl) aminium hexachloroantimonate (“Magic blue”, $E^{+/0} = +0.70$ V) in *o*-dichlorobenzene solution in the dry nitrogen atmosphere. The anion $Y_2-I_h^-$ has been generated by chemical reduction with excess of decamethylferrocene ($E^{0/-} = -0.51$ V) under the same conditions.

In case of $Y_2-I_h^-$ anion the experiment results are in total agreement with our expectations. Upon addition of decamethylferrocene solution to our sample the EPR signal started to decrease. When the excess of reductant has been added, we could observe the total disappearance of the signal both at room temperature and at 150K.

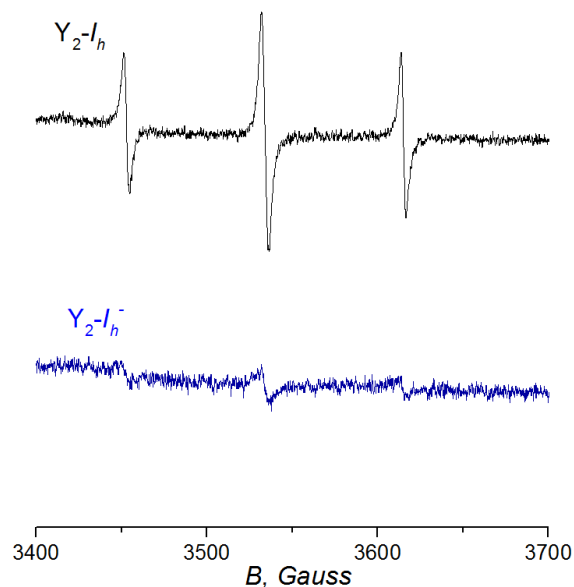


Figure 3.14. EPR spectrum of parent Y_2-I_h and anion $Y_2-I_h^-$ in toluene solution at room temperature.

These data unequivocally confirms, that the first reduction of Y_2-I_h EMF is SOMO-based.

In case of $Y_2-I_h^+$ the interpretation of the EPR experiment is somewhat more complicated. So far as the tris(4-bromophenyl) aminium hexachloroantimonate, used as an oxidant, is also paramagnetic, its signal should be subtracted from the final spectrum. Having done this (for more details see figure 6.X in the experimental section), we can assert, that one electron oxidation of Y_2-I_h radical actually leads to the changes (rather than disappearance) in the EPR signal: the new resonance has appears near the 3470 G, the parent triplet becomes more asymmetric.

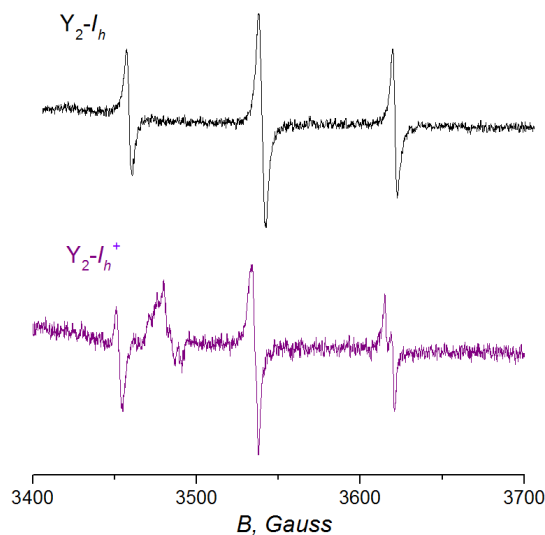


Figure 3.15. EPR spectrum of parent Y_2-I_h and cation $Y_2-I_h^+$ in toluene solution at room temperature.

The spectrum of the frozen solution of the oxidized Y_2-I_h at 100 K is also different from that of the pristine Y_2-I_h .

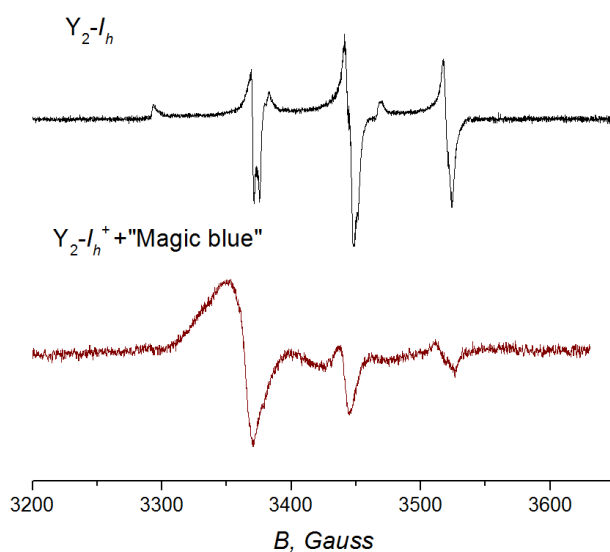


Figure 3.16. EPR spectrum of parent Y_2-I_h and cation $Y_2-I_h^+$ in frozen toluene solution at 100 K.

The shape of biradical EPR spectra is determined by the value of spin-spin interaction constant J . Zero J corresponds to the system of two non-interacting spins. In this case the spectrum is just a combination of two individual spectra corresponding to two separate spin centers of the molecule. Increase of the J value leads to the growth of the spin-spin interaction and consequently, more pronounced distortions at the spectrum. We performed simulation for the several systems with different J values. Other EPR parameters were fixed: we used the g -

tensor components and *hyperfine tensor* components, obtained from the simulation for neutral Y_2-I_h experiment at 150 K. For the second spin center the hyperfine tensor components have been set as zero values.



Figure 3.17. Simulated EPR data for the biradical particle with different values of spin-spin coupling constant J . other EPR parameters such as $a_{\perp}(^{89}Y)=74,3$ G (208 MHz) and $a_{\parallel}(^{89}Y)=87,8$ G (246 MHz), $g_{\perp}=1.9620$, and $g_{\parallel}=1.9982$ are fixed.

From comparing the simulated spectra with real EPR data we can suggest, that observed $Y_2-I_h^+$ cation-biradical is a system with weak spin-spin interactions. ($J < 10$ MHz).

3.5. Chapter summary

1. EPR spectroscopy together with DFT calculations show that $M_2@C_{80}(CH_2Ph)$ EMFs with C_{80-I_h} and $C_{80-D_{5h}}$ cages have very interesting electronic structure with single-occupied molecular orbital in the ground state

2. For all Dy, Y and Tb EMFs unoccupied component of SOMO acts as LUMO of the molecule, while occupied component of the SOMO is not redox active.

3. Redox reactions of $Y_2@C_{80}(CH_2Ph)$ with C_{80-I_h} can influence the spin states, that is revealed in EPR activity. In particular, the first reduction leads to the coupling of the SOMO-electron, and the compound becomes EPR-silent. The first oxidation turns parent $Y_2@C_{80}(CH_2Ph)$ radical to biradical particle with one unpaired electron at the metal-bonding SOMO and another one – at the cage.

Chapter 4. Titanium based redox activity in $M_2TiC@C_{80}$ and $M_2TiC_2@C_{80}$ clusterfullerenes

4.1. $M_2TiC@C_{80}$ and $M_2TiC_2@C_{80}$ EMFs: structure and background

M_2TiC -clusterfullerenes family is a specific type of EMFs, where one Ti atom and two other metal atoms (usually IIIB group: Sc, Y or lanthanide) are connected to the central μ_3 -carbon atom inside the fullerene cage. Single-crystal X-ray diffraction as well as computational studies demonstrate that Ti in this compound is in the (IV) state, donating two electrons to the cage and another two – to the internal carbon^{52,164}. Thus the Ti(IV)= (μ_3 -C) bond is shown to be double, which represents the first example of multiple bond between a metal and the central, non-metal atom of the endohedral cluster.

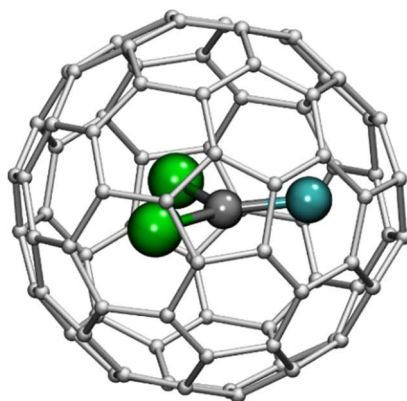


Figure 4.1. DFT-optimized molecular structure of $Lu_2TiC@C_{80-I_h}$, Ti is cyan, Lu is green, internal μ_3 -C is dark grey.

Structure, size and the charge state of the metal- M_2TiC -clusters are quite similar to those of well-known nitride clusters, so most abundant cage isomer of metal-titanium-clusterfullerenes is also $M_2TiC@C_{80-I_h}$.

The molecular structure of M_2TiC_2 -cluster in its turn has some analogues to M_3C_2 , e.g. Sc_3C_2 in $Sc_3C_2C_{80}$ ¹⁸⁹. DFT calculations show that the cluster has two low energy conformations: in the first one C_2 unit is perpendicular to the M_2Ti plane and has μ_2 -coordination with all metal atoms, in the second one it is tilted out of the M_2Ti plane and has μ_2 -coordination with Ti and one lanthanide, and μ_1 -coordination with another lanthanide. For $Sc_2TiC_2@C_{80-I_h}$ the cluster configuration with a tilted arrangement of C_2 was found to be more stable, whereas for

clusterfullerenes with larger metals (i.e. Y, Lu), the lowest-energy configuration corresponds to the more compact structure with the C_2 unit perpendicular to the plane of metal atoms.

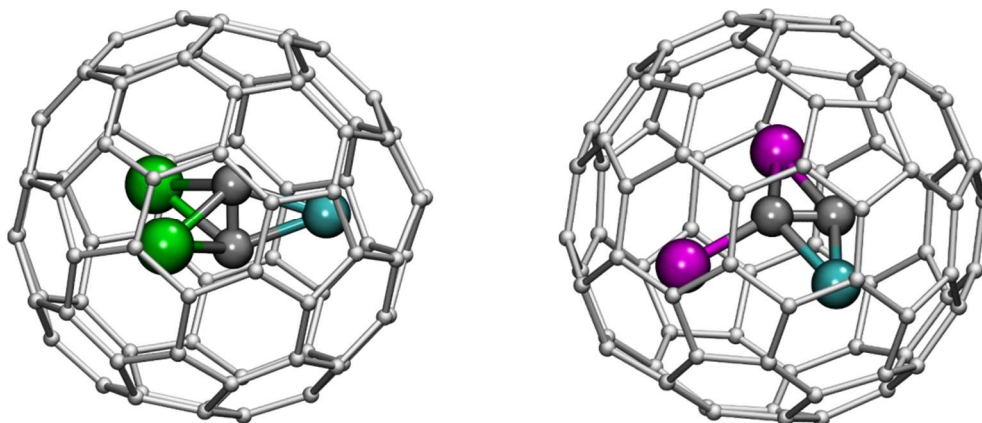


Figure 4.2. DFT-optimized molecular structure of $Lu_2TiC_2@C_{80-Ih}$ and $Sc_2TiC_2@C_{80-Ih}$, Ti is cyan, Lu is green, Sc is magenta, internal carbons are grey.

The first fullerene of the family $Lu_2TiC@C_{80-Ih}$ was discovered in 2013 as a minor product of Lu/Ti/ NH_3 and Lu/Ti/melamine arc discharge syntheses⁵². Cyclic voltammetry experiment exposed one reversible oxidation at + 0.63 V and one reversible Ti(IV) to Ti (III) reduction at -0.91 V. The last one resembles other Ti-based reductions, that have been detected in C_{80-Ih} EMFs: $TiSc_2N@C_{80}$ ¹⁹⁰ and $TiY_2N@C_{80}$ ¹⁴⁶, which are reduced reversibly at respectively -0.94 and -1.11 V (cage-based reductions for C_{80-Ih} EMFs are generally irreversible and proceed at deeper potentials - see table 4.2.).

Later in 2015 our colleagues investigated the new reactive gas method with methane¹⁶⁴, applicable for high selectivity -synthesis of $M_2TiC@C_{80}$ as well as $M_2TiC_2@C_{80}$ clusterfullerenes. This approach has provided us with $M_2TiC@C_{80-Ih}$ with Sc, Lu, Y, Dy, Er and Gd and $M_2TiC_2@C_{80-Ih}$ with Sc and Dy, so we became able to study the electrochemical behavior of this clusterfullerenes family in more details to identify differences and similarities between EMFs with different metals.

4.2. Electronic structure and redox behavior

Computational studies reveal that all $M_2TiC@C_{80-I_h}$ molecules have a cluster-localized LUMO with large contribution of Ti. So, the first cathodic peak of $M_2TiC@C_{80-I_h}$ is expected to be Ti(IV)/Ti(III) reduction. Herein the HOMO is cage-based, similar to nitride clusterfullerenes.

For the $M_2TiC_2@C_{80-I_h}$, both HOMO and LUMO are predominantly localized on the endohedral cluster and have a large contribution of the acetylide fragment. The LUMO of $M_2TiC_2@C_{80}$ is to a large extent localized on Ti, whereas in the HOMO both Ti and lanthanide ions have comparable contributions:

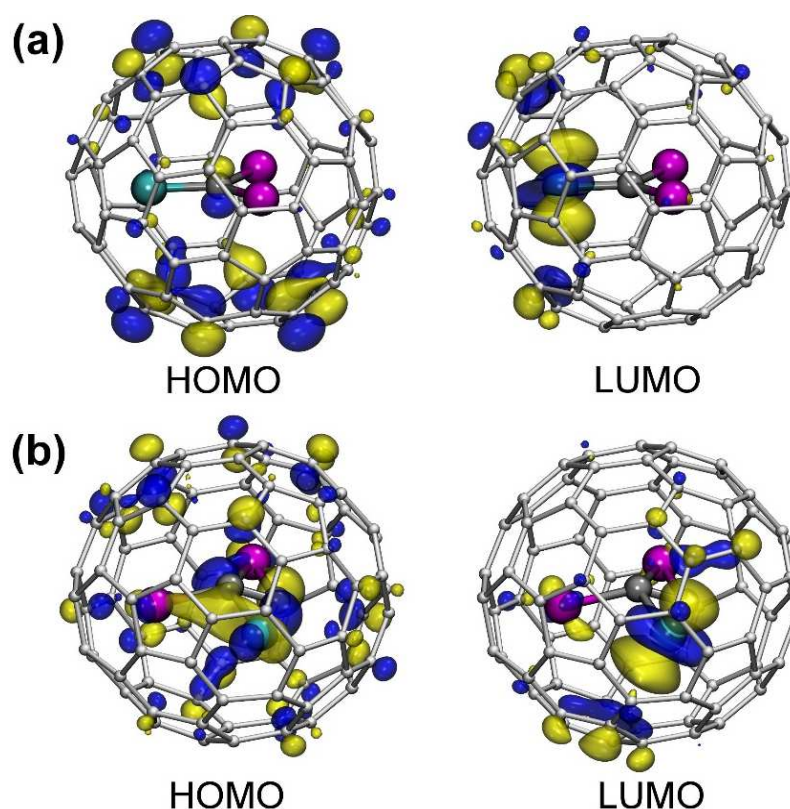


Figure 4.3. DFT-computed frontier molecular orbitals of a) $Sc_2TiC@C_{80-I_h}$ and b) $Sc_2TiC_2@C_{80-I_h}$ computed at the Ti=cyan, Sc=magenta, internal carbons =grey.

Cyclic voltammetry experiments show that the first reduction of $Sc_2TiC@C_{80-I_h}$ (Figure 4.4) is reversible as it was for $Lu_2TiC@C_{80-I_h}$, but proceeds at more positive potential (-0.67 V vs -0.91 V in case of Lu). The process is reversible and the potential value confirms that this peak can be ascribed to the endohedral Ti^{IV}/Ti^{III} redox couple. When monoanion is transformed further to dianion at -1.61 V the process turns to be irreversible. This also influences the

character of the first reduction: reverse peak is decreasing and we can observe a new re-oxidation peak at the potential value of about -0.34 . The first oxidation is reversible and occurs at $+0.66$ V, very close to that of the nitride clusterfullerene, which is in accord with almost identical HOMOs in both molecules.

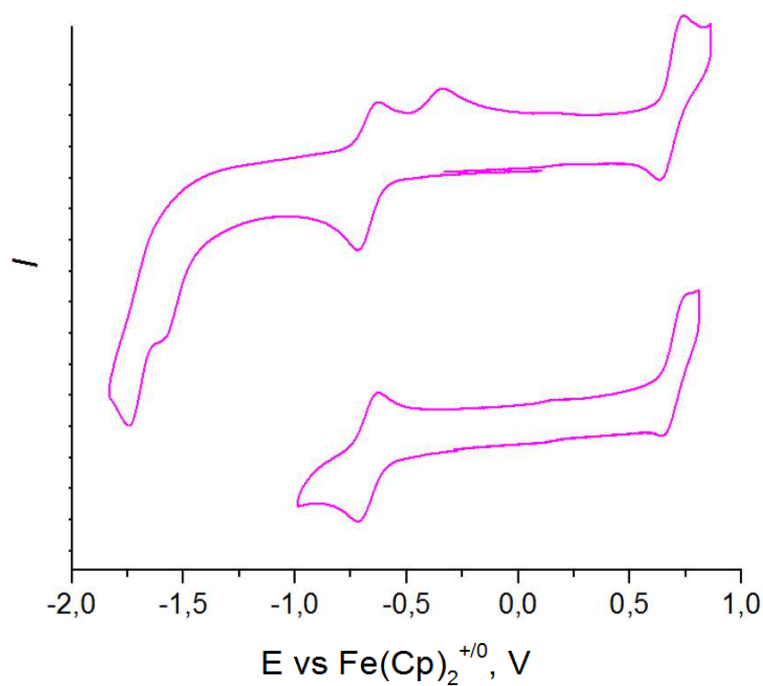


Figure 4.4. Cyclic voltammetry of $Sc_2TiC@C_{80-Ih}$. Measurements are performed at room temperature in *o*-dichlorobenzene/ $TBABF_4$ with the scan rate 100 mV/s.

$Dy_2TiC@C_{80-Ih}$ demonstrates similar electrochemical behavior: the first reduction is reversible (potential is -0.97 , which is more negative, then for Lu and Sc, but still in the range typical for Ti-based reductions of EMFs). Extending of the potential sweep window further to reach the second and third reductions results in irreversible processes and creates a new re-oxidation peak at -0.49 V, in the potential range of the first reduction step. The first oxidation of $Dy_2TiC@C_{80-Ih}$ proceeds reversibly at $+0.61$ V (Figure 4.5).

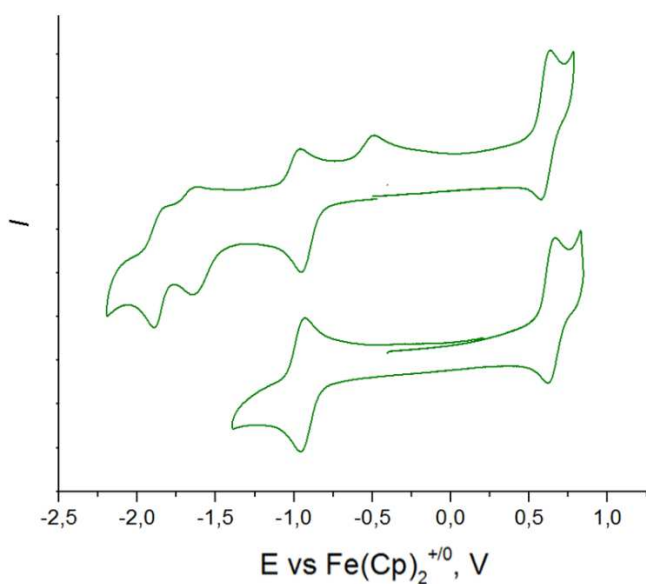


Figure 4.5. Cyclic voltammetry of $Dy_2TiC@C_{80-Ih}$. Measurements are performed at room temperature in *o*-dichlorobenzene/ $TBABF_4$ with the scan rate 100 mV/s

Table 4.1. Selected electrochemical parameters for $Sc_2TiC@C_{80-Ih}$ and $Dy_2TiC@I_h-C_{80}$

		E	ΔE_{F-R}	I_R/I_F	character
$Sc_2TiC@C_{80-Ih}$	ox-I	+0.66	0.10	0.97	reversible
	red-I	-0.68	0.09	0.96	reversible
	reox-I*	-0.34	-	-	-
	red-II	-1.61	-	-	irreversible
	red-III	-1.73	-	-	irreversible
$Dy_2TiC@C_{80-Ih}$	ox-I	+0.61	0.05	0.93	reversible
	red-I	-0.97	0.04	0.95	reversible
	reox-I*	-0.49	-	-	-
	red-II	-1.63	-	-	irreversible
	red-III	-1.88	-	-	reversible

Potentials are listed in Volt versus the $[Fe(Cp)_2]^{+/0}$ pair, "ox" stands for oxidation, "red" stands for reduction, "reox-I" stands for a new reoxidation peak, appearing after second reduction, " ΔE_{F-R} " stands for difference of the forward and reversed peak potentials, " I_R/I_F " stands for the ratio of the forward and reversed peak current.

*peak appears after extending of the potential sweep window further to reach the second reduction.

In case of other $M_2TiC@C_{80-Ih}$ and $M_2TiC_2@C_{80-Ih}$ clusterfullerenes, the amounts synthesized were not sufficient to record well-reserved cyclic voltammograms, so we performed square wave voltammetry experiments. The curves are presented at Figures 4.6 and 4.7, and all the data are summarized up it table 4.2.

Comparison of the first reduction potential through the $M_2TiC@C_{80-I_h}$ family uncovers substantial variability of the endohedral Ti(IV)/Ti(III) redox couple from -0.67 V in $Sc_2TiC@C_{80-I_h}$ to -1.04 V in $Gd_2TiC@C_{80-I_h}$ Figure 4.8 shows that a linear correlation exists between the reduction potential of $M_2TiC@C_{80-I_h}$ and the ionic radius of the non-titanium metal, (herein, the first oxidation potential is metal-independent). Such a strong variation of the Ti-based reduction on the second metal, which is not involved in the LUMO, suggests that the energetics of the reduction is controlled by geometric aspects.

In EMF molecules the endohedral cluster is usually sterically hindered by the external fullerene frame. Stability of the compounds is substantially determined by the value of this inner strain energies, which in its turn directly depends on the geometrical factors.

The ionic radius of Ti is increased when going from Ti(IV) (0.605 Å) to Ti(III) (0.67 Å), thereby the whole M_2TiC -cluster becomes bigger and more strained (we are using Shannon ionic radii throughout this discussion¹⁹¹). When the size of the cluster is relatively small in the pristine EMF, as it is in $Sc_2TiC@C_{80-I_h}$, this increase of the cluster size upon reduction does not result in a dramatic growth of the total strain energy (ΔE_{strain} is relatively small). On the contrary, in $Gd_2TiC@C_{80-I_h}$, the size of the cluster is rather large resulting in a non-negligible steric strain already in the pristine neutral compound. A further increase of the cluster size upon reduction is, therefore, not thermodynamically favorable (ΔE_{strain} is large) and requires additional energy input (e.g., applying more negative potential) to overcome the strain.

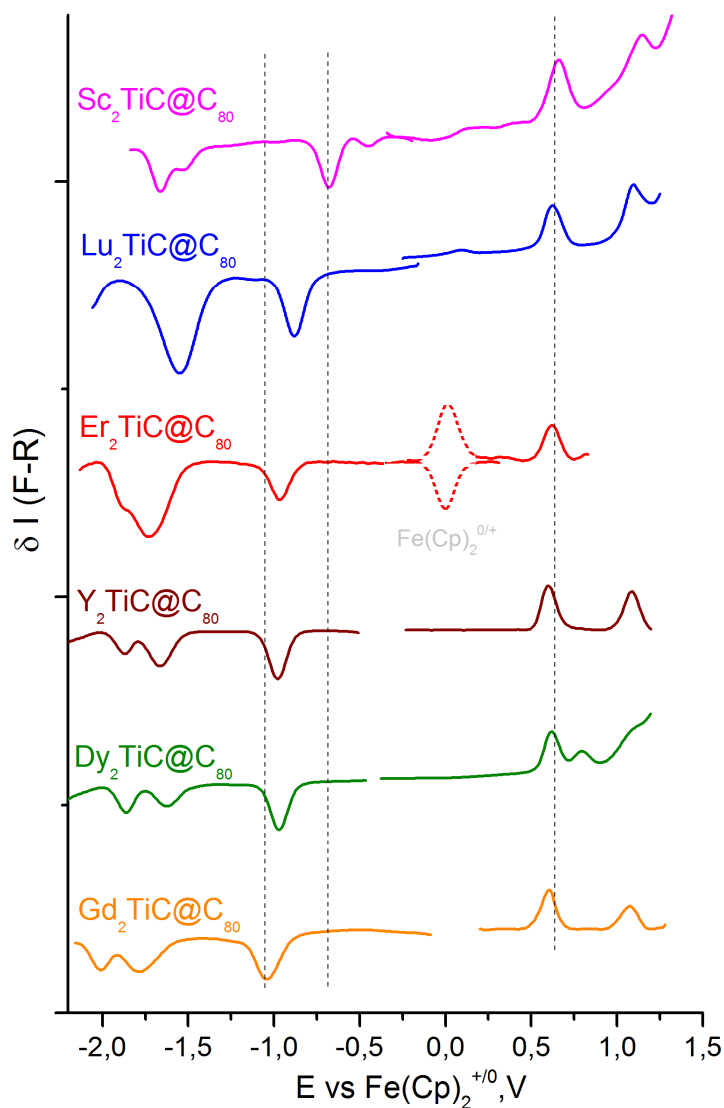


Figure 4.6. Square wave voltammetry of $M_2TiC@C_{80-Ih}$ compounds with different metals. Measurements are performed at room temperature in *o*-dichlorobenzene/TBAPF₄ with the scan rate 100 mV/s

The electrochemical behavior of the M_2TiC_2 -clusterfullerenes follows the same trend, with some deviations due to the difference in the MO distribution. The first oxidation potential of the $Sc_2TiC_2@C_{80-Ih}$ is shifted to the cathodic direction vs $Sc_2TiC@C_{80-Ih}$ due to the cluster contribution to the HOMO, but the shift is not dramatic (0.13 V), which also agrees with the distribution of the HOMO between the cluster and the cage. In case of Dy, the corresponding shift of the first oxidation potential is 0.15 V (see table 4.2)

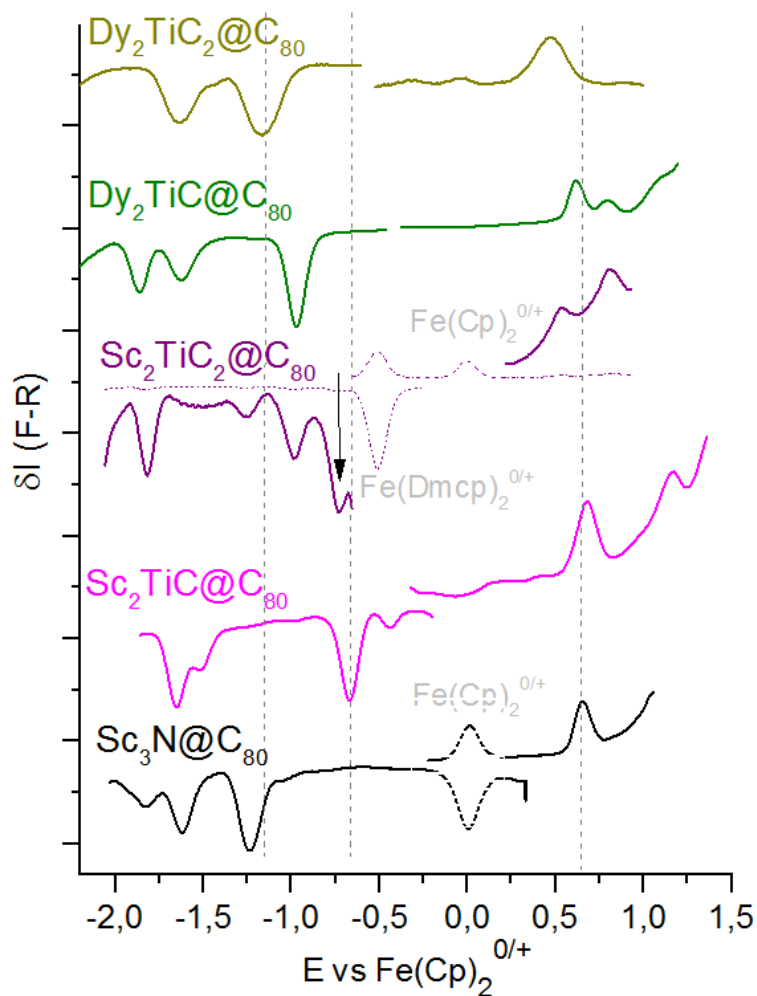


Figure 4.7. Square wave voltammetry of several M_2TiC and M_2TiC_2 -based EMFs. Measurements are performed at room temperature in *o*-dichlorobenzene/TBAPF₄ with the scan rate 100 mV/s

Reduction potentials of $Sc_2TiC_2@C_{80-I_h}$ and $Dy_2TiC_2@C_{80-I_h}$ are shifted negatively versus $Sc_2TiC@C_{80-I_h}$ and $Dy_2TiC@C_{80-I_h}$, and the shift is larger for $Dy_2TiC_2@C_{80-I_h}$ (see table 4.2). To explain this behavior we can use the same line of arguments as for M_2TiC -clusterfullerenes. So far as the LUMO of M_2TiC_2 -clusterfullerenes is similarly located on the internal cluster with high contribution of the Ti, the first reduction of the compound will be also accompanied by the cluster size increasing. The M_2TiC_2 -cluster is more sterically hindered than the M_2TiC -cluster with the same metal, so the reduction requires applying some extra negative potential. In case of bigger Dy^{3+} this difference is naturally more pronounced.

The above described dependence is valid not only in case of metal-titanium-carbide-EMFs: in the $TiM_2N@C_{80-I_h}$ family^{146,152,190}, the first reduction step is also a Ti-based process, and its potential was shown to be more negative in case of $TiY_2N@C_{80-I_h}$ than in $TiSc_2N@C_{80-I_h}$, because of the larger cluster size. Furthermore, in $TiM_2N@C_{80}$ the valence state of titanium is

Ti(III), and it becomes Ti(II) upon reduction. The ionic radius of Ti(II) is 0.86 Å, and therefore, the increase of the intrinsic cluster size in the Ti(III)/Ti(II) couple ($\Delta R(M^{3+/2+})=0.19$ Å) is more pronounced than in the Ti(IV)/Ti(III) couple ($\Delta R(M^{4+/3+})=0.06$ Å). That is why, the potential shift in case nitrides is also more pronounced. Furthermore, reduction potentials of the $\text{TiM}_2\text{N}@C_{80-I_h}$ clusterfullerene family are generally more negative than reduction potentials of their carbide counterparts $\text{M}_2\text{TiC}@C_{80-I_h}$. Thus, the variation of the potential of the internal Ti-based redox couple can act as a measure of the strain energy for different Ti-containing clusterfullerenes.

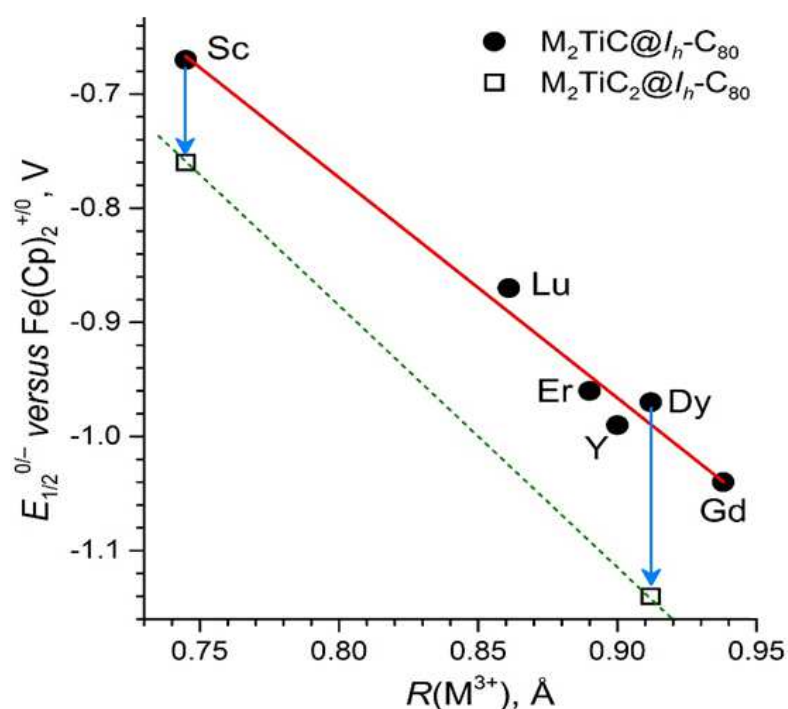


Figure 4.8. Correlation between the reduction potentials of $\text{M}_2\text{TiC}@C_{80-I_h}$ (dots) and $\text{M}_2\text{TiC}_2@C_{80-I_h}$ (squares) and the Shannon ionic radii of the metals, $R(M^{3+})$. The arrows denote negative shifts of the reduction potentials when going from M_2TiC - to M_2TiC_2 -clusterfullerenes.

It should be noted, that in 2013 similar correlation was also observed for the endohedral Ce(IV)/Ce(III) redox couple in $\text{CeM}_2\text{N}@C_{80-I_h}$ ($M=\text{Sc}, \text{Lu}, \text{Y}$).¹⁴⁴ In these EMFs, the first oxidation step is usually described as an oxidation of the trivalent Ce. Because the ionic radius of Ce(IV) is smaller than that of Ce(III), oxidation of Ce(III) results in a decrease of the size of the endohedral cluster. Authors demonstrated, that difference in inner strain of neutral molecules predetermines the difference in the first oxidation potential: bigger and more strained clusters can be oxidized at lower potentials.

Table 4.2. Redox potentials of selected Ti-based EMFs.

EMF	ox-I	red-I	red-II	red-III	gap _{EC}	link
Sc ₂ TiC@C ₈₀	+0.66	-0.67	-1.51	-1.66	1.33	t.w.
Sc ₂ TiC ₂ @C ₈₀	+0.53	-0.76	-1.01	-1.96	1.26	t.w.
Lu ₂ TiC@C ₈₀	+0.63	-0.87	-1.53	-	1.50	t.w.
Er ₂ TiC@C ₈₀	+0.62	-0.96	-1.72	-	1.58	t.w.
Y ₂ TiC@C ₈₀	+0.60	-0.99	-1.67	-1.89	1.59	t.w.
Dy ₂ TiC@C ₈₀	+0.61	-0.97	-1.62	-1.87	1.58	t.w.
Dy ₂ TiC ₂ @C ₈₀	0.47	-1.14	-1.58	-2.29	1.61	t.w.
Gd ₂ TiC@C ₈₀	+0.60	-1.04	-1.72	-1.91	1.64	t.w.
Sc ₃ N@C ₈₀	+0.63	-1.24	-1.73	-	1.78	t.w.
TiSc ₂ N@C ₈₀	0.16	-0.94	-1.58	-2.21	1.10	¹⁵²
TiY ₂ N@C ₈₀	0.00	-1.11	-1.79	-	1.11	¹⁴⁶

Potentials are listed in Volt versus the [Fe(Cp)₂]⁺⁰ pair, "ox" stands for oxidation, "red" stands for reduction, gap_{EC} is an electrochemical gap defined as the difference of the first reduction and oxidation potentials. All clusterfullerenes have I_h-cage. All potentials obtained in this work have been measured in the SWV experiment and can be slightly to that measured in the CV experiment.

4.3. Chapter summary

1. Electrochemical investigations of $M_2TiC@C_{80-I_h}$ and $M_2TiC_2@C_{80-I_h}$ EMF series have revealed, that the first reversible reduction of these fullerenes predominantly occurs on internal Ti and can be described as Ti^{IV}/Ti^{III} redox process.

2. Reduction potentials of endohedral $Ti(IV)/Ti(III)$ redox couples exhibits dramatic variation with the size of endohedral clusters. In particular, reduction potential in the $M_2TiC@C_{80-I_h}$ series correlates linearly with the ionic radius of non-Ti metals in M_2TiC cluster. The increase of the ionic radius of Ti upon reduction increases the strain of the whole fullerene molecule that is why to reduce EMFs with bigger (and hence more strained) more negative potential should be applied.

Chapter 5. Experimental details.

Synthesis of mixed Er-Sc EMFs

Two graphite rods of 10 cm length and 6 mm diameter were drilled 6-7 cm depth and filled with a mixture of metal oxides, graphite powder and guanidium thiocyanate in a molar ratio Er/Sc/GT/C=1:1:2.5:15). Then, the rods were fixed inside the fullerene generator on two electrodes, which were linked to an electric arc generator. The walls of the chamber and the electrodes were water cooled throughout the synthesis process. The chamber was pumped and filled with Helium up to the pressure of 200 mbar. Before arc-discharge evaporation start rods were brought into contact and preliminary heated for 10-15 minutes (the current was set as 15 A). During the arc-discharge evaporation the current was set in the form of square signal with 100A at the high point. Two rods were evaporated alternatively and there was a breaking between two impulses to let the generator cool down and stabilize. After the synthesis procedure the chamber was pumped again and cooled down for 1 hour, then the soot containing fullerene was collected from the reactor chamber to the cellulose extraction thimble and extracted with Acetone for 1h in a Soxhlet-Extractor to wash most of the non-fullerene products. This step was followed by the second over-night extraction with carbon disulfide to dissolve fullerenes. The CS₂ extract was distilled of and the residual fullerene mixture was then washed with acetone and redissolved in toluene. Every extract was analyzed with HPLC and laser desorption time-of-flight (LD-TOF) mass spectrometer (Biflex III Bruker, Germany) running in both positive and negative ion modes.

HPLC analysis and separation.

Individual EMFs and EMF derivatives were separated with multistep high performance liquid chromatography (HPLC). In the first stage, the soot extract was separated into several fractions by analytical single-run HPLC (Agilent, 1100 series, UV-absorbance *detection* at 320 nm), employing a linear combination of two analytical 4.6 mm x 250 mm Buckyprep columns (Nacalai Tesque, Japan), with flow rate of 1.6 mL/min and an injection volume of 800 µL.

Further isolation and purification of individual EMFs was performed by recycling HPLC (SunFlow 501, detector Sunchrom 100, UV-absorbance *detection* at 320 nm) with semi-preparative 10 x 250 mm Buckyprep or semi-preparative 10 x 250 mm Buckyprep –M column. (Nacalai Tesque, Japan), with a flow rate of 1.5-3 mL/min and an injection volume of 3-6 mL.

Fraction purity was controlled with laser desorption time-of-flight (LD-TOF) mass spectrometry, running in both positive and negative ion modes HPLC testruns were performed with analytical single-run HPLC (Agilent, 1100 series, UV-absorbance *detection* at 320 nm), employing a linear combination of two analytical 4.6 mm x 250 mm Buckyprep columns (Nacalai Tesque, Japan), with flow rate of 1.6 mL/min and an injection volume of 200 μ L. Pure toluene (99,8%, Spectronorm, VWR Prolabo) was used as an eluent at all steps of separation.

Spectroscopic and physicochemical measurements.

LDI mass-spectra were measured with a Bruker auto flex mass-spectrometer. The analyzer was calibrated before each measurement batch using the mixture of empty fullerenes with known composition. Mass distribution was analyzed with Isotope Pattern and Molecular Weight Calculator Software.

UV-vis-NIR absorption spectra were measured in toluene solution at room temperature with Shimadzu 3100 spectrophotometer. *Spectrophotometric measurements* of $\text{Er}_2@\text{C}_{82}\text{-C}_{3v}$ were performed with the same equipment. 0.8 mg of $\text{Er}_2@\text{C}_{82}\text{-C}_{3v}$ were first dissolved in 10 ml of toluene, than the solution was consistently diluted to the volume of 25 and 50 ml. The values of molar extinction coefficients at 379 nm, 477 nm and 899 nm were determined as averaged from three experiments with different concentrations.

Raman spectra were recorded at 78 K on a T 64000 triple spectrometer (JobinYvon) using 647 nm excitation wavelength of the Kr laser. For Raman measurements, the samples were drop-casted onto single-crystal KBr disks.

IR spectra were measured on KBr substrates using Vertex 80 FT-IR spectrometer (Bruker, Germany).

The 125 MHz ^{13}C *NMR spectra* were measured at room temperature with d^6 -acetone as a lock on an Avance 500 spectrometer (Bruker, Germany) using the multiprobe head PH 1152Z.

X-band EPR measurements were performed at Bruker EMXplusX EPR spectrometer with PremiumX Microwave Bridge and high sensitivity standard resonator (ER4119HS). For temperature dependent measurements internal variable temperature control unit (ER 4131VT) was used. The samples were dissolved in o-dichlorobenzene. In case of $\text{Sc}_2@\text{C}_{82}^+$, $\text{Y}_2@\text{C}_{80}(\text{CH}_2\text{Ph})^+$ and $\text{Y}_2@\text{C}_{80}(\text{CH}_2\text{Ph})^-$ experiments the reactions with redox-active agents were done in the glovebox, than the solution was put in the EPR tube, closed and covered with teflon

to prevent reactions with water and oxygen. EPR spectra simulation was performed with X-Soft and Easy Spin (Matlab) software.

Magnetization measurements were performed using a Quantum Design VSM MPMS3 magnetometer. The samples were drop-casted from either toluene ($\text{Er}_2\text{@C}_{82}$, $\text{Er}_2\text{S@C}_{82}$) or from o-dichlorobenzene ($[\text{Er}_2\text{@C}_{82}^+]\text{SbCl}_6^-$) into standard polypropylene capsules in the glovebox.

DFT-optimization of molecular structures was performed with PBE functional¹⁹² using Priroda code¹⁹³. The calculations employed original basis set of TZ2P-quality basis set, which comprised full-electron basis {6,3,2}/(11s,6p,2d) for C, N, and O atoms, and SBK-type effective core potential with {5,5,4}/(9s,9p,8d) valence part for Sc, Ti, Y and La atoms, and {5,5,3,4}/{10s,10p,9d,7f} valence part for Lu atoms. For visualization of molecular orbital and spin densities, single-point energy calculations were then performed using Orca suite¹⁹⁴, with PBE functional, ZORA scalar-relativistic correction, and full-electron TZVP basis set for all elements. Molecular structures and isosurfaces were visualized with VMD code¹⁹⁵.

Electrochemical measurements.

Cyclic Voltammetry experiments were performed in 0.1 M TBABF₄-o-dichlorobenzene in a glove box using potentiostat-galvanostat PARSTAT 4000A. A three-electrode system of original design employing platinum wires as working and a counter electrodes and a silver wire, covered with silver chloride as a pseudoreference electrode was used. The electrochemical cell (volume of 50 μl) was made from the standard NMR tube. Potentials were measured versus ferrocene-ferrocenium couple as an internal standard. Scan rate was set as 100 mV/s.

Square Wave Voltammetry experiments were performed at the same equipment with the following experimental parameters: pulse height of 40 mV, Step height of 10 mV, and frequency of 10 Hz, that resulted in scan rate of 100 mV/s.

For decontamination, working electrode and counter electrode were annealed in propane burner's flame after each experiment, while the pseudoreference electrode was washed several times with ethanol.

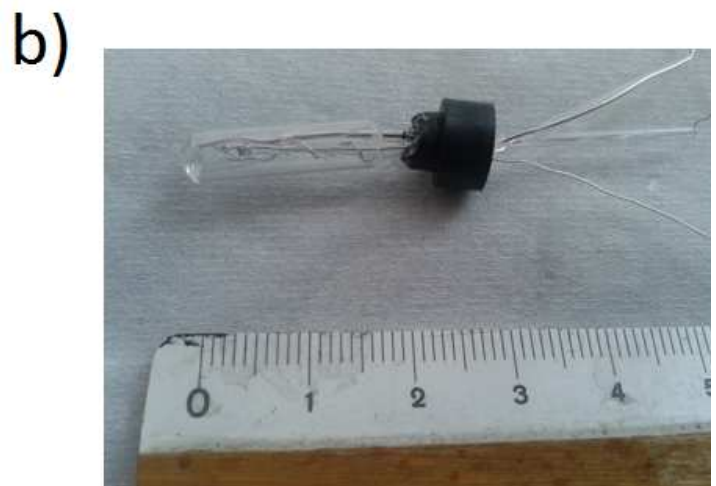
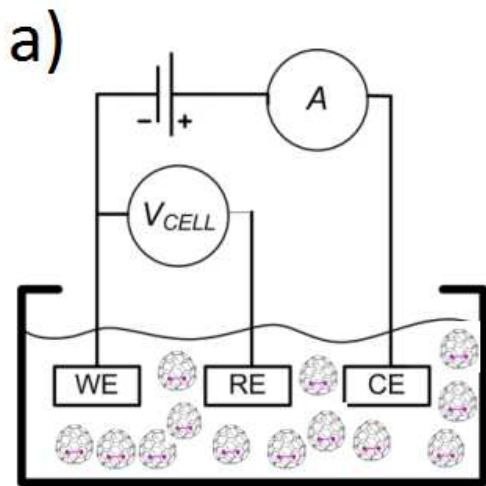


Figure 5.1. (a) Schematic image of three-electrode system, employing in the present work; (b) photo of electrochemical system together with empty cell.

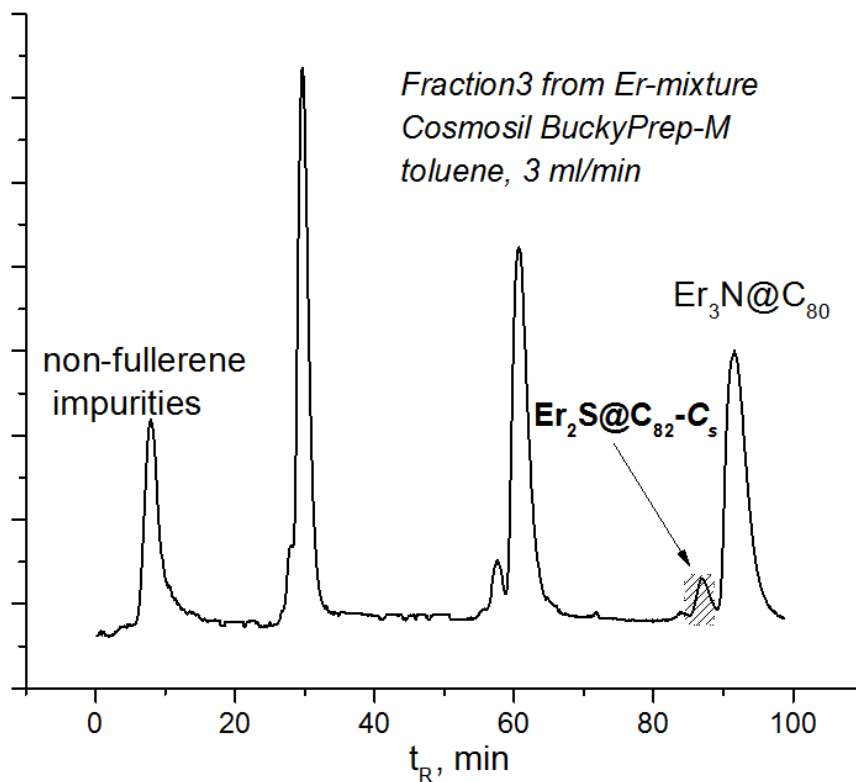


Figure 5.2a. Isolation of $Er_2S@C_{82}-C_s$ EMF (10×250 mm Buckyprep-M column; flow rate 1.5 ml/min; injection volume as 5 ml; toluene as eluent; room temperature).

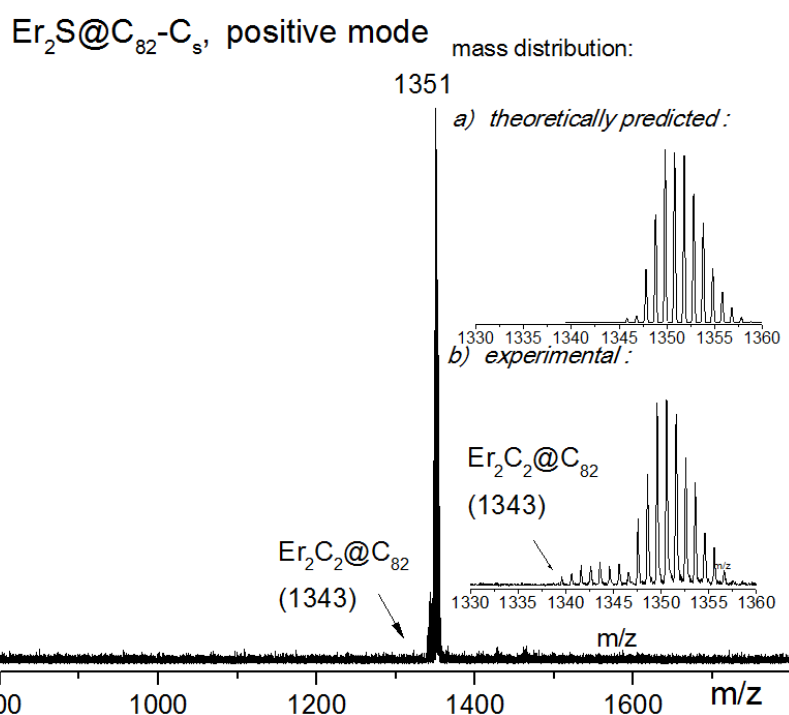


Figure 5.2b. Positive-ion mass spectrum of isolated $Er_2S@C_{82}-C_s$, the inset shows experimental mass distribution in comparison to the theoretical one.

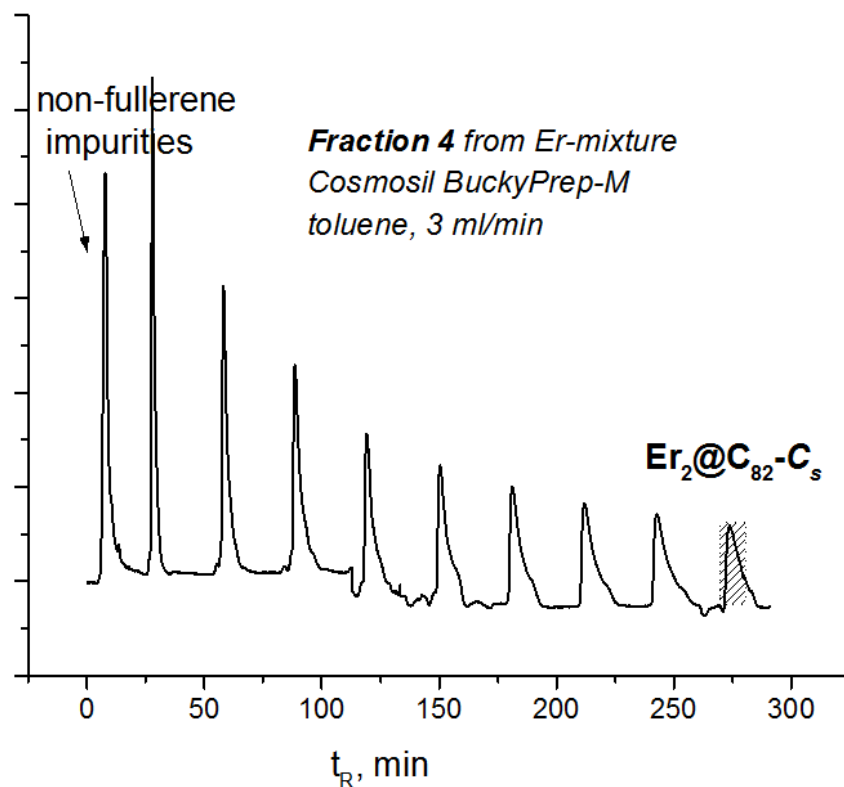


Figure 5.3a. Isolation of $Er_2@C_{82}-C_5$ EMF (10×250 mm Buckyprep-M column; flow rate 1.5ml/min; injection volume as 5 ml; toluene as eluent; room temperature).

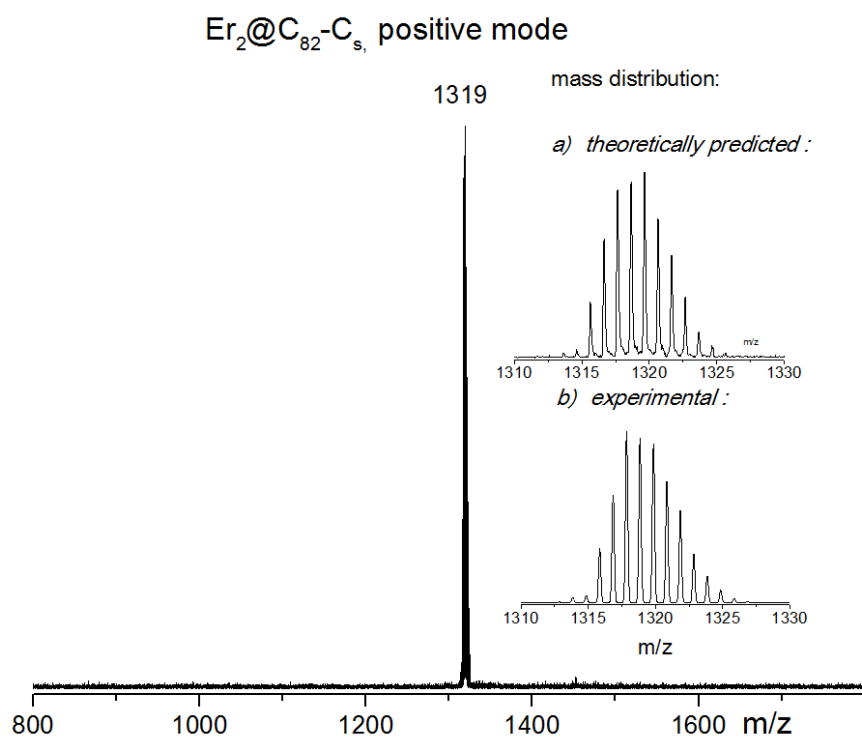


Figure 5.3b. Positive-ion mass spectrum of isolated $Er_2@C_{82}-C_5$, the inset shows experimental mass distribution in comparison to the theoretical one.

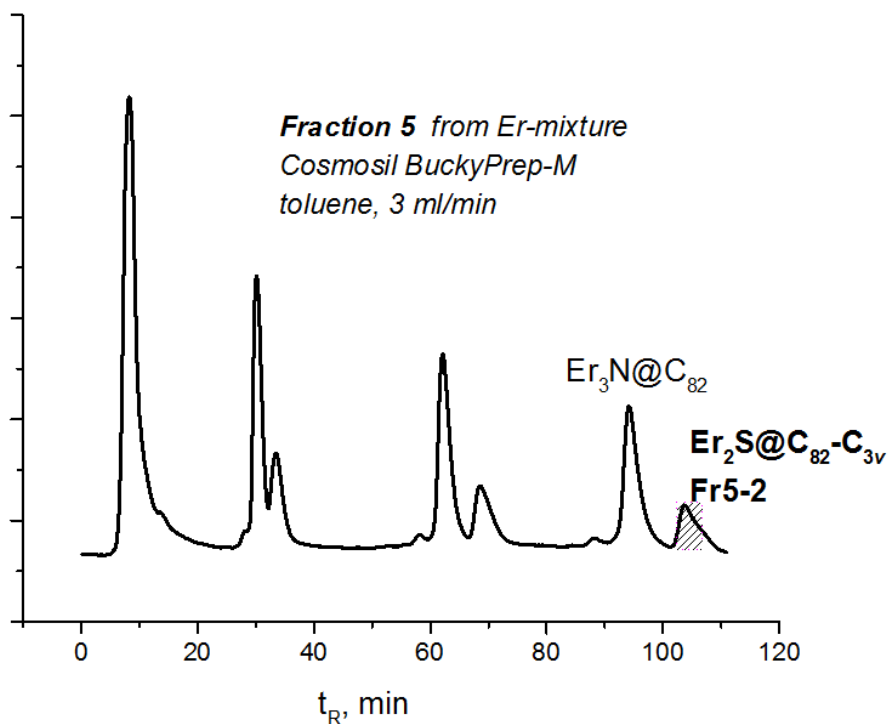


Figure 5.4a. Isolation of $Er_2S@C_{82}-C_{3v}$ EMF (10×250 mm Buckyprep-M column; flow rate 1.5 ml/min; injection volume as 5 ml; toluene as eluent; room temperature).

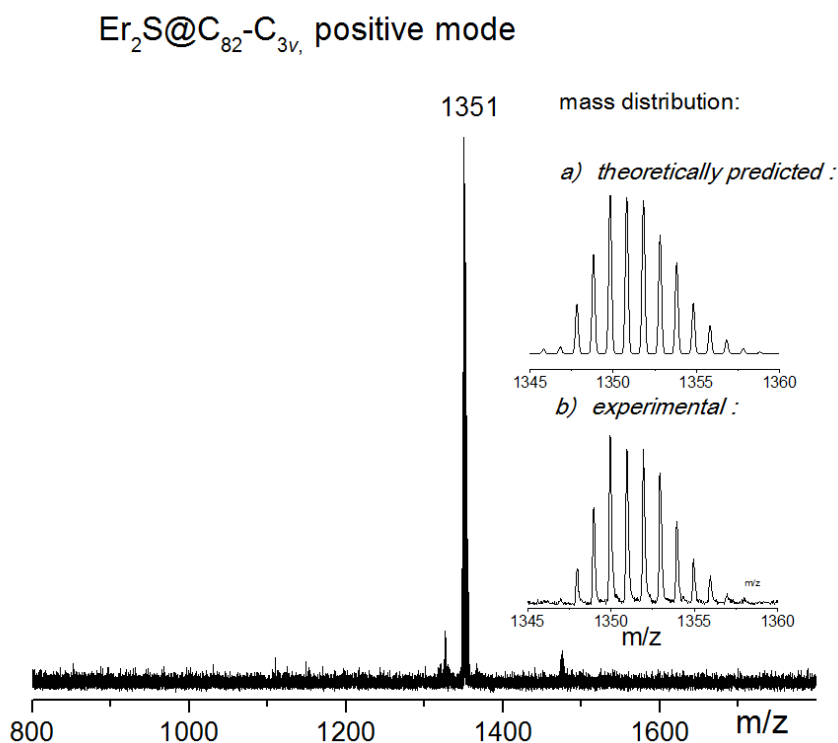


Figure 5.4b. Positive-ion mass spectrum of isolated $Er_2S@C_{82}-C_{3v}$, the inset shows experimental mass distribution in comparison to the theoretical one.

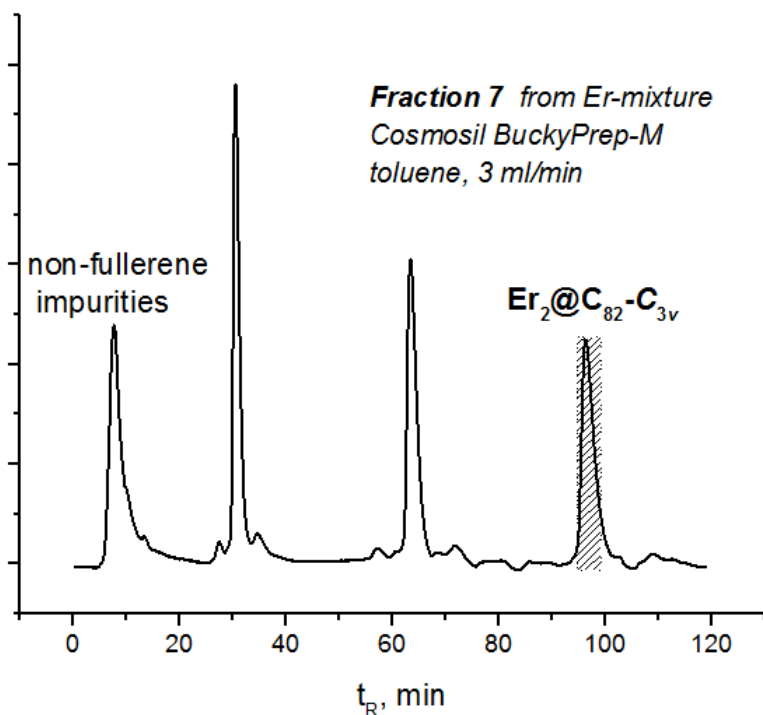


Figure 5.5a. Isolation of $Er_2@C_{82}-C_{3v}$ EMF (10×250 mm Buckyprep-M column; flow rate 1.5 ml/min; injection volume as 5 ml; toluene as eluent; room temperature).

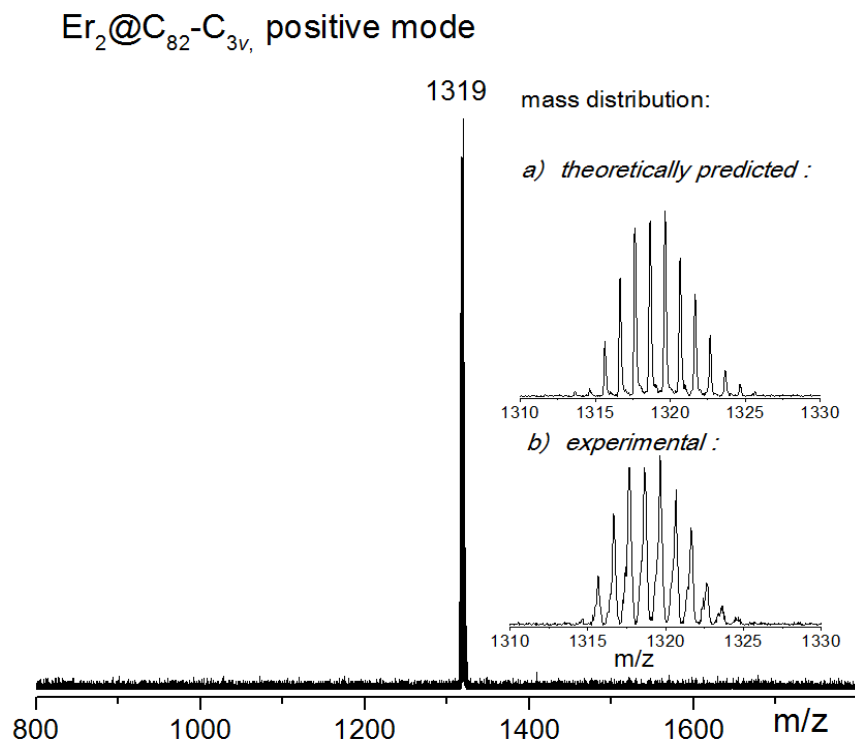


Figure 5.5b. Positive-ion mass spectrum of isolated $Er_2@C_{82}-C_{3v}$, the inset shows experimental mass distribution in comparison to the theoretical one.

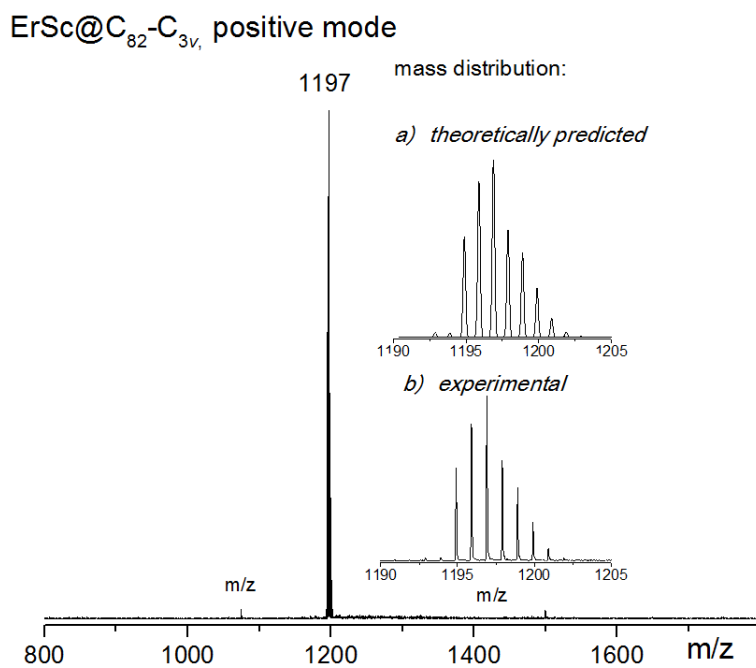


Figure 5.6. Positive-ion mass spectrum of isolated ErSc@C₈₂-C_{3v}, the inset shows experimental mass distribution in comparison to the theoretical one.

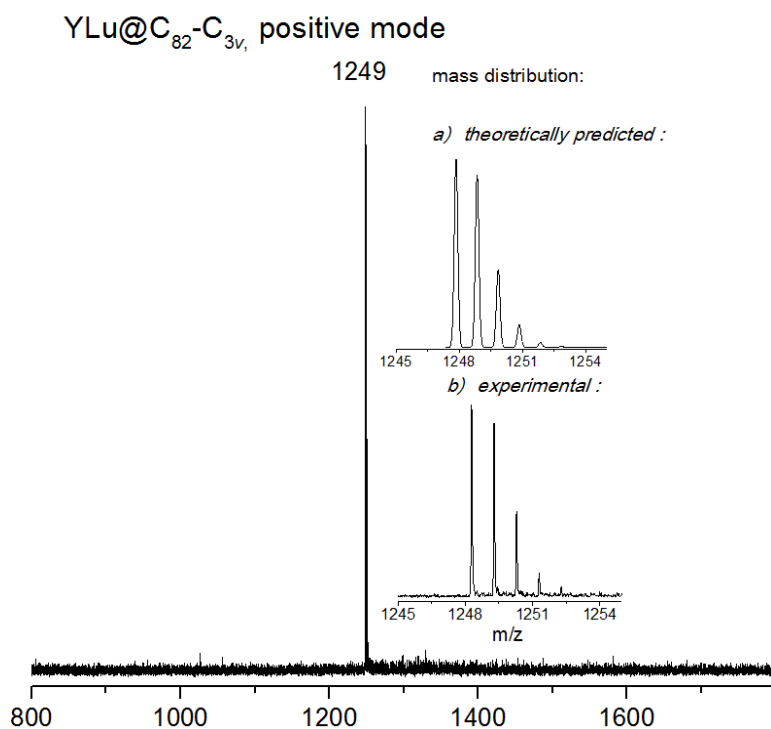


Figure 5.7. Positive-ion mass spectrum of isolated YLu@C₈₂-C_{3v}, the inset shows experimental mass distribution in comparison to the theoretical one

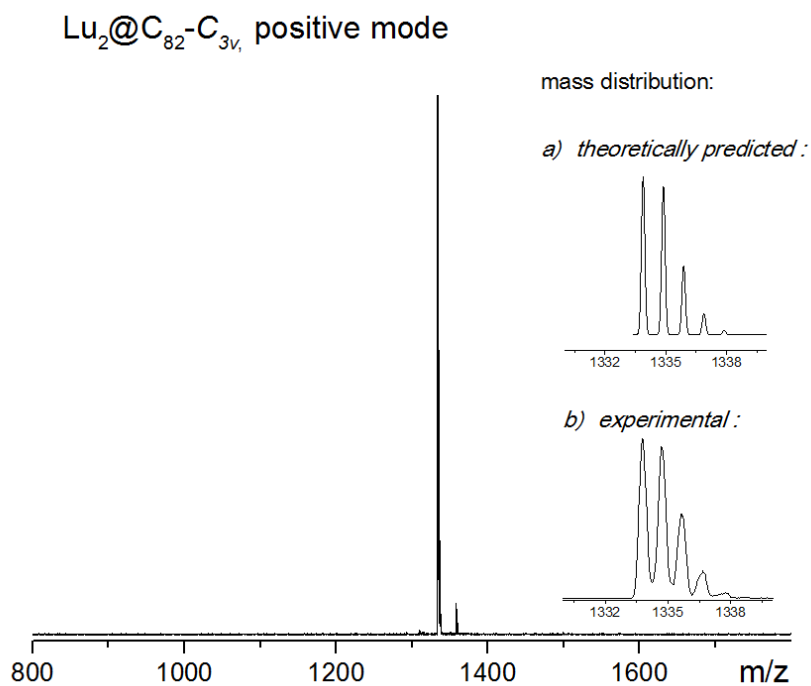


Figure 5.8. Positive-ion mass spectrum of isolated $\text{Er}_2@C_{82}-C_{3v}$, the inset shows experimental mass distribution in comparison to the theoretical one.

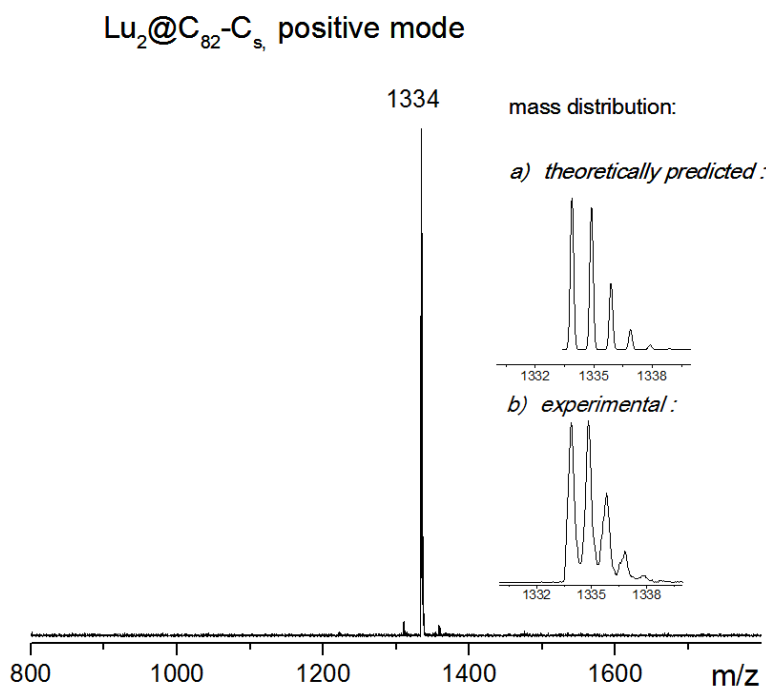


Figure 5.9. Positive-ion mass spectrum of isolated $\text{Lu}_2@C_{82}-C_s$, the inset shows experimental mass distribution in comparison to the theoretical one.

$\text{Sc}_2@C_{82}-C_{3v}$ positive mode

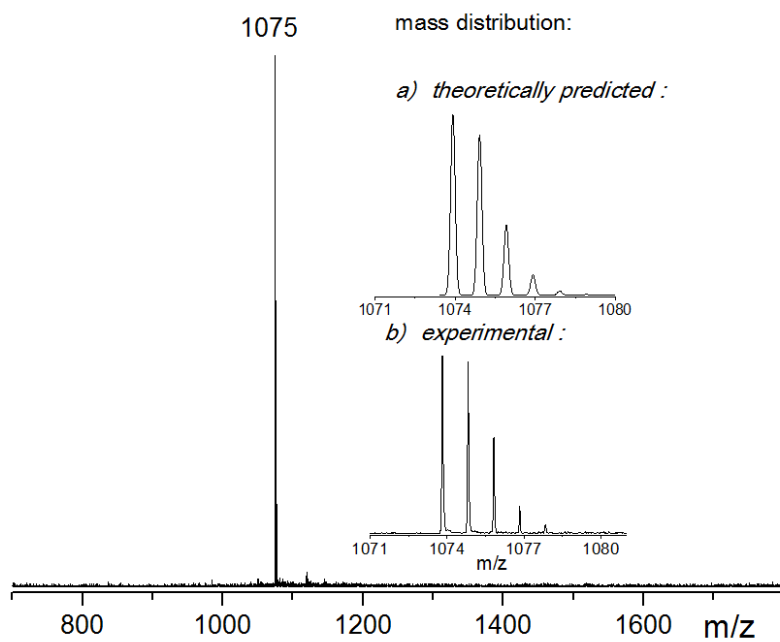


Figure 5.10. Positive-ion mass spectrum of isolated $\text{Lu}_2@C_{82}-C_{3v}$, the inset shows experimental mass distribution in comparison to the theoretical one.

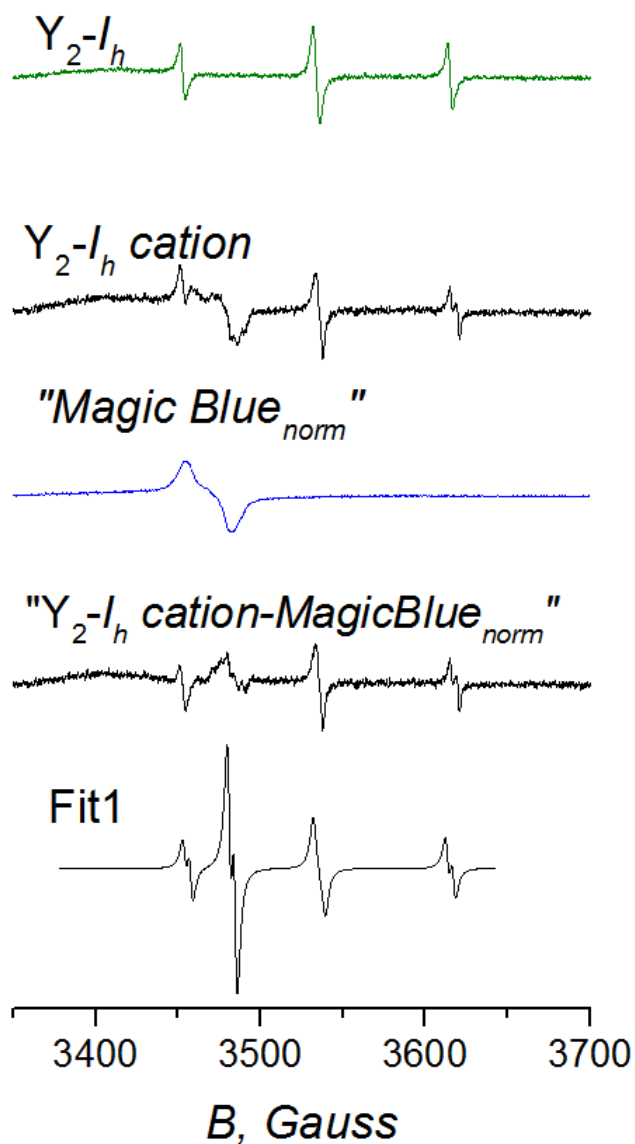


Figure 5.11. Processing of the EPR spectra of Y_2-I_h cation, synthesized in the reaction with the “Magic blue” oxidant. Top to bottom: EPR spectra of the parent Y_2-I_h , measured in the same conditions, EPR spectra of the parent Y_2-I_h cation with excess of “Magic blue”, normalized spectrum of the “Magic blue”, measured in the same conditions, result of the subtraction of the “Magic blue” spectrum from the cation spectrum, EPR simulation, obtained in the following conditions: $g=[1,962; 1,962; 1,998]$, $a=[208; 208; 242]$ MHz, $J=10$ MHz

Summary.

This thesis reports on the investigations of endohedral metallofullerenes (EMFs) with redox-active clusters inside.

Chapter 1 briefly reviews the families of endohedral clusterfullerenes, such as monometallofullerenes, dimetallofullerenes, nitride clusterfullerenes, carbide clusterfullerenes and sulfide clusterfullerenes, their synthesis, isolation and properties. Special attention is paid to electrochemical studies of EMFs, including several examples of cage-based and cluster-based redox activity of fullerene molecules.

Two next chapters are illustrating the concept of the metal-metal bonding in dimetallofullerenes. Recent DFT calculations demonstrate that such fullerenes must be considered as a combination of a carbon cage with enclosed metal dimers with a possibility of metal-metal bonding, rather than rather than a combination of carbon cage with two non-interacting metal atoms^{167,171}. Wherein the bonding appearance is determined by the energy matching between the frontier carbon cage orbitals and the M–M bonding metal dimer orbital.

Chapter 2 describes spectroscopic and electrochemical studies of $M_2@C_{82-C_{3v}}$ and $M_2@C_{82-C_5}$ dimetallofullerenes (M = Sc, Lu, Er, as well as their combinations)¹⁹⁶. Electrochemical studies have demonstrated, that the $M^{2+}-M^{2+}$ bonding orbital is the HOMO orbital of the dimetallofullerene molecule, which strongly influences the oxidation behavior of dimetallofullerenes in comparison with corresponding isomers of sulfide- and carbide clusterfullerenes $M_2S@C_{82}$ and $M_2C_2@C_{82}$, respectively. $M_2@C_{82}$ cations have an unpaired electron on the metal-metal bonding orbital, which results in a strong interaction between unpaired electron and nuclei spins or localized magnetic moments of metal atoms. In particular, the EPR spectrum of $Sc_2@C_{82}^+$ cation radical exhibits a giant isotropic ⁴⁵Sc hyperfine coupling constant of 199.2 G due to the large contribution of 4s atomic orbitals of Sc to the Sc–Sc bonding MO in $Sc_2@C_{82}$. For $Er_2@C_{82}$, SQUID magnetometry showed that the cation $Er_2@C_{82}^+$ has substantially different magnetic properties than the pristine neutral form.

Chapter 3, logically following the previous one, describes another family of compounds with metal-metal bonding: dimetallofullerene derivatives $M_2@C_{80}(CH_2Ph)$ with C_{80-I_h} and $C_{80-D_{5h}}$ cages (M = Y, Tb, Dy), that have been recently synthesized in our group¹⁸⁷. These EMFs have very interesting electronic structure with single-occupied molecular orbital in the ground state

that is proved with help of EPR spectroscopy. Cyclic voltammetry experiments have demonstrated, that unoccupied component of the single-occupied MO acts as the LUMO of the molecule, while occupied component of SOMO is not redox active. The spin structure of $Y_2@C_{80}(CH_2Ph)$ with C_{80-I_h} is changed upon redox reactions, that can be seen in comparison of EPR spectra of oxidized and reduced forms with that of the neutral one. The first oxidation turns parent $Y_2@C_{80}(CH_2Ph)$ radical to a biradical particle with one unpaired electron at the metal-bonding SOMO and another one – at the fullerene cage. The first reduction leads to the two-fold occupation of the M-M bonding MO, resulting in the diamagnetic EPR-silent anion.

The last research topic addressed in the Chapter 4 of this work concerns the new $M_2TiC@C_{80-I_h}$ EMFs with double $Ti(IV)=(\mu_3-C)$ bonding inside the carbon cage. Electrochemical investigations of $M_2TiC@C_{80-I_h}$ and $M_2TiC_2@C_{80-I_h}$ EMF series with different metals such as Sc, Y, Lu, Dy and Gd have revealed, that the first reversible reduction of these fullerenes predominantly occurs on internal Ti atom and can be described as the Ti^{IV}/Ti^{III} redox process. Reduction potential of the endohedral Ti^{IV}/Ti^{III} redox couple is dramatically dependent on the size of endohedral clusters. In particular, reduction potential in the $M_2TiC@C_{80-I_h}$ series correlates linearly with the ionic radius of non-Ti metal atom in the M_2TiC cluster. The increase of the ionic radius of Ti upon reduction leads to the growth of the strain energy of the whole fullerene molecule. For this reason, more negative potentials are required to reduce EMFs with bigger (more strained) clusters. This results are a part of research, made by Katrin Junghans during her PhD time in IFW^{164,197}.

Chapter 5 contains a detailed description of experiment procedures and the equipment used throughout the work. The chapter also describes HPLC-separation and Mass-spectroscopy results for several dimetallofullerenes, which are discussed in the Chapter 2.

References.

- (1) Kroto, H. W.; Heath, J. R.; O'Brien, S. C.; Curl, R. F.; Smalley, R. E. C₆₀: Buckminsterfullerene. *Nature* **1985**, *318*, 162.
- (2) Heath, J. R.; O'Brien, S. C.; Zhang, Q.; Liu, Y.; Curl, R. F.; Tittel, F. K.; Smalley, R. E. Lanthanum Complexes of Spheroidal Carbon Shells. *J. Am. Chem. Soc.* **1985**, *107* (25), 7779–7780.
- (3) Chai, Y.; Guo, T.; Jin, C.; Haufler, R. E.; Chibante, L. P. F.; Fure, J.; Wang, L.; Alford, J. M.; Smalley, R. E. Fullerenes with Metals inside. *J. Phys. Chem.* **1991**, *95* (20), 7564–7568.
- (4) Ioffe, I. N.; Chen, C.; Yang, S.; Sidorov, L. N.; Kemnitz, E.; Troyanov, S. I. Chlorination of C₈₆ to C₈₄Cl₃₂ with Nonclassical Heptagon-Containing Fullerene Cage Formed by Cage Shrinkage. *Angew. Chemie - Int. Ed.* **2010**, *49* (28), 4784–4787.
- (5) Troshin, P. A.; Avent, A. G.; Darwish, A. D.; Martsinovich, N.; Abdul-Sada, A. K.; Street, J. M.; Taylor, R. Isolation of Two Seven-Membered Ring C₅₈ Fullerene Derivatives: C₅₈F₁₇CF₃ and C₅₈F₁₈. *Science* **2005**, *309* (July), 278.
- (6) Troyanov, S. I. Ioffe I. N., Mazaleva O. N., Sidorov L. N., † Shangfeng Y., Wei T., Kemnitz E., and Troyanov S. I. **2013**, *90* (28), 13821–13823.
- (7) Zhang, Y.; Ghiassi, K. B.; Deng, Q.; Samoylova, N. A.; Olmstead, M. M.; Balch, A. L.; Popov, A. A. Synthesis and Structure of LaScN@C(hept)-C₈₀ with One Heptagon and Thirteen Pentagons. *Angew Chem Int Ed Engl* **2014**, 495–499.
- (8) Kroto, H. W. The Stability of the Fullerenes C_n, with N = 24,28,32,36,50,60 and 70. *Nature* **1987**, *329*, 529–531.
- (9) Stevenson, S.; Fowler, P. W.; Heine, T.; Duchamp, J. C.; Rice, G.; Glass, T.; Harich, K.; Hajdu, E.; Bible, R.; Dorn, H. C. A Stable Non-Classical Metallofullerene Family. *Nature* **2000**, *408* (November), 427–428.
- (10) Wang, C. R.; Kai, T.; Tomiyama, T.; Yoshida, T.; Kobayashi, Y.; Nishibori, E.; Takata, M.; Sakata, M.; Shinohara, H. C₆₆ Fullerene Encaging a Scandium Dimer. *Nature* **2000**, *408* (November), 426–427.
- (11) Chen, N.; Beavers, C. M.; Mulet-Gas, M.; Rodríguez-Forteza, A.; Munoz, E. J.; Li, Y. Y.; Olmstead, M. M.; Balch, A. L.; Poblet, J. M.; Echegoyen, L. Sc₂S@Cs(10528)-C₇₂: A Dimetallic Sulfide Endohedral Fullerene with a Non Isolated Pentagon Rule Cage. *J. Am. Chem. Soc.* **2012**, *134* (18), 7851–7860.

- (12) Yamada, M.; Wakahara, T.; Tsuchiya, T.; Maeda, Y.; Akasaka, T.; Mizorogi, N.; Nagase, S. Spectroscopic and Theoretical Study of Endohedral Dimetallofullerene Having a Non-IPR Fullerene Cage: Ce₂@C₇₂. *J. Phys. Chem. A* **2008**, *112* (33), 7627–7631.
- (13) Wakahara, T.; Nikawa, H.; Kikuchi, T.; Nakahodo, T.; Rahman, G. M. A.; Tsuchiya, T.; Maeda, Y.; Akasaka, T.; Yoza, K.; Horn, E.; Yamamoto, K.; Mizorogi, N.; Slanina, Z.; Nagase, S. La@C₇₂ Having a Non-IPR Carbon Cage. *J. Am. Chem. Soc.* **2006**, *128* (44), 14228–14229.
- (14) Yang, S.; Kalbac, M.; Popov, A.; Dunsch, L. A Facile Route to the Non-IPR Fullerene Sc₃N@C₆₈: Synthesis, Spectroscopic Characterization, and Density Functional Theory Computations (IPR = Isolated Pentagon Rule). *Chem. - A Eur. J.* **2006**, *12* (30), 7856–7863.
- (15) Yang, S.; Popov, A. A.; Dunsch, L. The Role of an Asymmetric Nitride Cluster on a Fullerene Cage: The Non-IPR Endohedral DySc₂N@C₇₆. *J. Phys. Chem. B* **2007**, *111* (49), 13659–13663.
- (16) Fowler, P.; Manolopoulos, D. E. An Atlas of Fullerenes. **2006**, 15–17, 51–58.
- (17) Godly, E. W.; Taylor, R. Nomenclature and Terminology of Fullerenes: A Preliminary Study. *Pure Appl. Chem.* **1997**, *69* (7), 1411–1434.
- (18) Schwerdtfeger, P.; Wirz, L. N.; Avery, J. The Topology of Fullerenes. *Wiley Interdiscip. Rev. Comput. Mol. Sci.* **2015**, *5* (1), 96–145.
- (19) Popov, A. A.; Shangfeng Yang; Lothar Dunsch. Chapter 2. Endohedral Fullerenes. *Chem. Rev.* **2013**, 5989–6113.
- (20) Wang, L. S.; Alford, J. M.; Chai, Y.; Diner, M.; Zhang, J.; McClure, S. M.; Guo, T.; Scuseria, G. E.; Smalley, R. E. The Electronic-Structure of Ca@C₆₀. *Chem. Phys. Lett.* **1992**, *207* (4–6), 354–359.
- (21) Johnson, R.; de Vries, M.; Salem, J.; Bethune, D. S.; Yannoni, C. S. Electron Paramagnetic Resonance Studies of Lanthanum-Containing C₈₂. *Nature* **1992**, *355*, 239–240.
- (22) Krätschmer, W.; Lamb, L.D.; Fostiropoulos, K.; Huffman, D. . Solid C₆₀: a New Form of Carbon. *Nature* **1990**, *347* (18), 354–358.
- (23) Bethune, D. S.; Johnson, R. D.; Salem, J. R.; de Vries, M. S.; Yannoni, C. S. Atoms in Carbon Cages: The Structure and Properties of Endohedral Fullerenes. *Nature* **1993**, *366* (6451), 123–128.
- (24) Funasaka, H.; Yamamoto, K.; Sakurai, K.; Ishiguro, T.; Sugiyama, K.; Takahashi, T.; Kishimoto, Y. Preparation of Fullerene Derivatives by Resistive Heating With Graphite Crucible. *Fuller. Sci. Technol.* **1993**, *1* (3), 437–448.

- (25) Kyesmen, P. I.; Onoja, A.; Amah, A. N. Fullerenes Synthesis by Combined Resistive Heating and Arc Discharge Techniques. *Springerplus* **2016**, *5* (1), 1–7.
- (26) Yoshie, K.; Kasuya, S.; Eguchi, K.; Yoshida, T. Novel Method for C₆₀ Synthesis: A Thermal Plasma at Atmospheric Pressure. *Appl. Phys. Lett.* **1992**, *61* (23), 2782.
- (27) Alexakis, T.; Tsantrizos, P. G.; Tsantrizos, Y. S.; Meunier, J.-L. Synthesis of Fullerenes via the Thermal Plasma Dissociation of Hydrocarbons. *Appl. Phys. Lett.* **1997**, *70* (16), 2102.
- (28) Tellgmann, R.; Krawez, N.; Lin, S.-H.; Hertel, I. V.; Campbell, E. E. B. Endohedral Fullerene Production. *Nature*. 1996, pp 407–408.
- (29) Shimshi, R.; Cross, R. J.; Saunders, M. Beam Implantation: A New Method for Preparing Cage Molecules Containing Atoms at High Incorporation Levels. *J. Am. Chem. Soc.* **1997**, *119* (5), 1163–1164.
- (30) Saunders, M.; Jimenezvazquez, H. A.; Cross, R. J.; Poreda, R. J. Stable Compounds of Helium and Neon - He@C₆₀ and Ne@C₆₀. *Science (80-.)*. **1993**, *259* (5100), 1428–1430.
- (31) Cooper, H. J.; Hendrickson, C. L.; Marshall, A. G. Direct Detection and Quantitation of He@C₆₀ by Ultrahigh-Resolution Fourier Transform Ion Cyclotron Resonance Mass Spectrometry. *J. Am. Soc. Mass Spectrom.* **2002**, *13* (11), 1349–1355.
- (32) Peng, R.-F.; Chu, S.-J.; Huang, Y.-M.; Yu, H.-J.; Wang, T.-S.; Jin, B.; Fu, Y.-B.; Wang, C.-R. Preparation of He@C₆₀ and He₂@C₆₀ by an Explosive Method. *J. Mater. Chem.* **2009**, *19* (22), 3602.
- (33) Rubin, Y. Organic Approaches to Endohedral Metallofullerenes: Cracking Open or Zipping up Carbon Shells? *Chem. - A Eur. J.* **1997**, *3* (7), 1009–1016.
- (34) Komatsu, K. Encapsulation of Molecular Hydrogen in Fullerene C₆₀ by Organic Synthesis. **2014**, *238* (2005), 0–3.
- (35) Xiao, J.; Savina, M. R.; Martin, G. B.; Francis, A. H.; Meyerhoff, M. E. 9341-9342 9341. **1994**, No. 14, 9341–9342.
- (36) Ding, J.; Yang, S. Efficient N, N -Dimethylformamide Extraction of Endohedral Metallofullerenes for HPLC Purification. *Chem. Mater.* **1996**, *4756* (1), 2824–2827.
- (37) Lian, Y.; Shi, Z.; Zhou, X.; Gu, Z. Different Extraction Behaviors between Divalent and Trivalent Endohedral Metallofullerenes. *Chem. Mater.* **2004**, *16* (9), 1704–1714.
- (38) Khodorkovskii, M. A.; Koltover, K.; Yagubskii, E. B. Novel Proficient Method for Isolation of

- Endometallofullerenes from Fullerene-Containing Soots by Two-Step O -Xylene– N , N - Dimethylformamide Extraction. *J. Mater. Chem.* **1998**, *8* (4), 893–895.
- (39) Sun, D.; Liu, Z.; Guo, X.; Xu, W.; Liu, S. High-Yield Extraction of Endohedral Rare-Earth Fullerenes. *J. Phys. Chem. B* **1997**, *101* (20), 3927–3930.
- (40) Wong, T. Solid Phase Extraction as a Simple Method for the Enrichment Endohedral Metallofullerenes. **1996**, *37* (51), 9249–9252.
- (41) Shinohara, H. Endohedral Metallofullerenes. *Reports Prog. Phys.* **2000**, *63* (6), 843–892.
- (42) Stevenson, S.; Rice, G.; Glass, T.; Harich, K.; Cromer, F.; Jordan, M. R.; Craft, J.; Dorn, H. C. Metallofullerenes in High Yield and Purity. *Nature* **1999**, *80*, 80–82.
- (43) Chaur, M. N.; Melin, F.; Ortiz, A. L.; Echegoyen, L. Chemical, Electrochemical, and Structural Properties of Endohedral Metallofullerenes. *Angewandte Chemie - International Edition*. 2009, pp 7514–7538.
- (44) Dunsch, L.; Georgi, P.; Ziegs, F.; Zöller, H. German Patent DE 10301722 A1., 2002.
- (45) Yang, S.; Zhang, L.; Zhang, W.; Dunsch, L. A Facile Route to Metal Nitride Clusterfullerenes by Using Guanidinium Salts: A Selective Organic Solid as the Nitrogen Source. *Chem. – A Eur. J.* **2010**, *16* (41), 12398–12405.
- (46) Svitova, A.; Braun, K.; Popov, A. A.; Dunsch, L. A Platform for Specific Delivery of Lanthanide-Scandium Mixed-Metal Cluster Fullerenes into Target Cells. *ChemistryOpen* **2012**, *1* (5), 207–210.
- (47) Yang, S.; Dunsch, L. A Large Family of Dysprosium-Based Trimetallic Nitride Endohedral Fullerenes: Dy₃N@C_{2n} (39 ≤ N ≤ 44). *J. Phys. Chem. B* **2005**, *109* (25), 12320–12328.
- (48) Melin, F.; Chaur, M. N.; Engmann, S.; Elliott, B.; Kumbhar, A.; Athans, A. J.; Echegoyen, L. The Large Nd₃N@C_{2n} (40 ≤ N ≤ 49) Cluster Fullerene Family: Preferential Templating of a C₈₈ Cage by a Trimetallic Nitride Cluster. *Angew. Chemie - Int. Ed.* **2007**, *46* (47), 9032–9035.
- (49) Chaur, M. N.; Melin, F.; Ashby, J.; Elliott, B.; Kumbhar, A.; Rao, A. M.; Echegoyen, L. Lanthanum Nitride Endohedral Fullerenes La₃N@C_{2n} (43 ≤ n ≤ 55): Preferential Formation of La₃N@C₉₆. *Chem. – A Eur. J.* **2008**, *14* (27), 8213–8219.
- (50) Yang, S.; Kalbac, M.; Popov, A.; Dunsch, L. Gadolinium-Based Mixed-Metal Nitride Clusterfullerenes GdxSc_{3-x}N@C₈₀ (x=1, 2). *ChemPhysChem* **2006**, *7* (9), 1990–1995.
- (51) Stevenson S, Coralie R. B, . Maslenikova J. S. , Villarreal J.R. Mackey M.A., Mercado B. Q, K. C. K.

- O. M. M. and B. A. L. Selective Synthesis, Isolation, and Crystallographic Characterization of $\text{LaSc}_2\text{N}@I_h\text{-C}_{80}$. *Inorg. Chem.* **2012**, 51, 13096-13102.
- (52) Svitova, A. L.; Ghiassi, K. B.; Schlesier, C.; Junghans, K.; Zhang, Y.; Olmstead, M. M.; Balch, a L.; Dunsch, L.; Popov, A. A. Endohedral Fullerene with μ_3 -Carbido Ligand and Titanium-Carbon Double Bond Stabilized inside a Carbon Cage. *Nat. Commun.* **2014**, 5, 3568.
- (53) Stevenson, S.; Rottinger, K. A. CuCl_2 for the Isolation of a Broad Array of Endohedral Fullerenes Containing Metallic, Metallic Carbide, Metallic Nitride, and Metallic Oxide Clusters, and Separation of Their Structural Isomers. *Inorg. Chem.* **2013**, 52 (16), 9606–9612.
- (54) Alvarez, M. M.; Gillan, E. G.; Holczer, K.; Kaner, R. B.; Min, K. S.; Whetten, R. L. Lanthanum carbide (La_2C_{80}): a soluble dimetallofullerene. *J Phys Chem* **1991**, 95 (26), 10561-10563.
- (55) Akasaka, T.; Nagase, S.; Kobayashi, K.; Walchli, M.; Yamamoto, K.; Kako, M.; Hoshino, T.; Erata, T. ^{13}C and ^{139}La NMR Studies of La_2C_{80} : First Evidence for Circular Motion of Metal Atoms in Endohedral Dimetallofullerenes. *Angew. Chem., Int. Ed.* **1997**, 36 (15), 1643–1645.
- (56) Ito, M.; Nagaoka, S.; Kodama, T.; Miyake, Y.; Suzuki, S. *Abstracts Fullerene, Nanotubes Gen. Symp.e*; 2008.
- (57) Ding, J.; Yang, S.; Bay, C. W.; Kong, H.; May, R. V. Isolation and Characterization of $\text{Pr}@\text{C}_{82}$ and Pr_2C_{80} . **1996**, 7863 (c), 11254–11257.
- (58) Din, J.; Yang, S. Isolation and Characterization of the Dimetallofullerene Ce_2C_{80} . *Angeu. Chem. Int. Ed. Engl.* **1996**, 19, 2234–2235.
- (59) Yamada, M.; Mizorogi, N.; Tsuchiya, T.; Akasaka, T.; Nagase, S. Synthesis and Characterization of the D_{5h} Isomer of the Endohedral Dimetallofullerene Ce_2C_{80} : Two-Dimensional Circulation of Encapsulated Metal Atoms Inside a Fullerene Cage. *Chem. – A Eur. J.* **2009**, 15 (37), 9486–9493.
- (60) Olmstead, M. M.; De Bettencourt-Dias, A.; Stevenson, S.; Dorn, H. C.; Balch, A. L. Crystallographic Characterization of the Structure of the Endohedral Fullerene $\{\text{Er}_2\text{C}_{82}$ Isomer I $\}$ with C_s Cage Symmetry and Multiple Sites for Erbium along a Band of Ten Contiguous Hexagons. *J. Am. Chem. Soc.* **2002**, 124 (16), 4172–4173.
- (61) Olmstead, M. M.; Lee, H. M.; Stevenson, S.; Dorn, H. C.; Balch, A. L. Crystallographic Characterization of Isomer 2 of Er_2C_{82} and Comparison with Isomer 1 of Er_2C_{82} . *Chem. Commun. (Camb)*. **2002**, 1 (22), 2688–2689.
- (62) Yasuhiro Ito, Toshiya Okazaki, Shingo Okubo, Masahiro Akachi, Yutaka Ohno, T. M.; Tetsuya

- Nakamura, Ryo Kitaura, Toshiki Sugai, and H. S. Enhanced 1520 Nm Photoluminescence from Er³⁺ Ions in Di-Erbium-Carbide. *ACS Nano* **2007**, *1* (5), 456–462.
- (63) Kikuchi, K.; Akiyama, K.; Sakaguchi, K.; Kodama, T.; Nishikawa, H.; Ikemoto, I.; Ishigaki, T.; Achiba, Y.; Sueki, K.; Nakahara, H. Production and Isolation of the Isomers of Dimetallofullerenes, HoTm@C₈₂ and Tm₂@C₈₂. *Chem. Phys. Lett.* **2000**, *319* (5–6), 472–476.
- (64) Wang, C.; Kai, T.; Tomiyama, T.; Yoshida, T.; Kobayashi, Y.; Nishibori, E.; Takata, M.; Sakata, M.; Shinohara, H. A Scandium Carbide Endohedral Metallofullerene: (Sc₂C₂)@C₈₄. *Angew. Chem. Int. Ed.* **2001**, *40*, 397–399.
- (65) Slanina, Z.; Tsuchiya, T.; Nagase, S.; Akasaka, T. X-Ray Structures of Sc₂C₂@C_{2n} (N = 40 – 42): In-Depth Understanding of the Core – Shell Interplay in Carbide Cluster Metallofullerenes. **2012**.
- (66) Inoue, T.; Tomiyama, T.; Sugai, T.; Okazaki, T.; Suematsu, T.; Fujii, N.; Utsumi, H.; Nojima, K.; Shinohara, H. Trapping a C₂ Radical in Endohedral Metallofullerenes: Synthesis and Structures of (Y₂C₂)@C₈₂ (Isomers I, II, and III). *J. Phys. Chem. B* **2004**, *108*, 7573–7579.
- (67) Nishibori, E.; Narioka, S.; Takata, M.; Sakata, M.; Inoue, T.; Shinohara, H. A C₂ Molecule Entrapped in the Pentagonal-Dodecahedral Y₂ Cage in Y₂C₂@C₈₂(III). *ChemPhysChem* **2006**, *7* (2), 345–348.
- (68) Iiduka, Y.; Wakahara, T.; Nakajima, K.; Tsuchiya, T.; Nakahodo, T.; Maeda, Y.; Akasaka, T.; Mizorogi, N.; Nagase, S. ¹³C NMR Spectroscopic Study of Scandium Dimetallofullerene, Sc₂@C₈₄ vs. Sc₂C₂@C₈₂. *Chem. Commun. (Camb)*. **2006**, No. 19, 2057–2059.
- (69) Nishibori, E.; Ishihara, M.; Takata, M.; Sakata, M.; Ito, Y.; Inoue, T.; Shinohara, H. Bent (metal)₂C₂ Clusters Encapsulated in (Sc₂C₂)@C₈₂(III) and (Y₂C₂)@C₈₂(III) Metallofullerenes. *Chem. Phys. Lett.* **2006**, *433* (1–3), 120–124.
- (70) Dunsch, L.; Yang, S.; Zhang, L.; Svitova, A.; Oswald, S.; Popov, A. A. Metal Sulfide in a C₈₂ Fullerene Cage: A New Form of Endohedral Clusterfullerenes. *J. Am. Chem. Soc.* **2010**, *132* (15), 5413–5421.
- (71) Chen, N.; Chaur, M. N.; Moore, C.; Pinzón, J. R.; Valencia, R.; Rodríguez-Forteza, A.; Poblet, J. M.; Echegoyen, L. Synthesis of a New Endohedral Fullerene Family, Sc₂S@C_{2n} (N = 40–50) by the Introduction of SO₂. *Chem. Commun. (Camb)*. **2010**, *46* (26), 4818–4820.
- (72) Mercado, B. Q.; Stuart, M. A.; Mackey, M. A.; Pickens, J. E.; Confait, B. S.; Stevenson, S.; Easterling, M. L.; Rodri, A.; Poblet, J. M.; Olmstead, M. M. Sc₂(μ₂-S) Trapped in a Fullerene

- Cage : The Isolation and Structural Characterization of Sc₂(μ₂-S)₂@Cs(6)-C₈₂ and the Relevance of the Thermal and Entropic Effects in Fullerene Isomer Selection. *J. Am. Chem. Soc.* **2010**, *2* (6), 12098–12105.
- (73) Fornstedt, T.; Forssén, P.; Westerlund, D. Basic HPLC Theory and Definitions: Retention, Thermodynamics, Selectivity, Zone Spreading, Kinetics, and Resolution. *Anal. Sep. Sci. 5 Vol. Set, Vol. 2* **2015**, 1–22.
- (74) Hirsch, A.; Brettreich, M. *Fullerenes: Chemistry and Reactions*; 2005; Vol. 127.
- (75) Karasuma, N. HPLC Column for Fullerene Separation. *www.nacalaiusa.com*.
- (76) Svitova, A. L.; Krupskaya, Y.; Samoylova, N.; Kraus, R.; Geck, J.; Dunsch, L.; Popov, A. A. Magnetic Moments and Exchange Coupling in Nitride Clusterfullerenes Gd_xSc_{3-x}N@C₈₀ (X = 1-3). *Dalt. Trans.* **2014**, *43* (20).
- (77) Zhang, Y.; Popov, A. A.; Schiemenz, S.; Dunsch, L. Synthesis, Isolation, and Spectroscopic Characterization of Holmium-Based Mixed-Metal Nitride Clusterfullerenes: Ho_xSc_{3-x}N@C₈₀ (x=1, 2). *Chem. - A Eur. J.* **2012**, *18* (31), 9691–9698.
- (78) Raebiger, J. W.; Bolskar, R. D. Improved Production and Separation Processes for Gadolinium Metallofullerenes. *J. Phys. Chem. C* **2008**, *112* (17), 6605–6612.
- (79) Diener, M. D.; Smith, C. A.; Veirs, D. K. Anaerobic Preparation and Solvent-Free Separation of Uranium Endohedral Metallofullerenes. *Chem. Mater.* **1997**, *9* (8), 1773–1777.
- (80) Liu, S.; Sun, S. Recent Progress in the Studies of Endohedral Metallofullerenes. *J. Organomet. Chem.* **2000**, *599* (1), 74–86.
- (81) Ge, Z.; Duchamp, J. C.; Cai, T.; Gibson, H. W.; Dorn, H. C. Purification of Endohedral Trimetallic Nitride Fullerenes in a Single, Facile Step. *J. Am. Chem. Soc.* **2005**, *127* (46), 16292–16298.
- (82) Angeli, C. D.; Cai, T.; Duchamp, J. C.; Reid, J. E.; Singer, E. S.; Gibson, H. W.; Dorn, H. C. Purification of Trimetallic Nitride Templated Endohedral Metallofullerenes by a Chemical Reaction of Congeners with Eutectic 9-Methylanthracene. *Chem. Mater.* **2008**, *20* (15), 4993–4997.
- (83) Wu, B.; Wang, T.; Zhang, Z.; Feng, Y.; Gan, L.; Jiang, L.; Wang, C. An Effective Retro-Cycloaddition of M₃N@C₈₀ (M = Sc, Lu, Ho) Metallofulleropyrrolidines. *Chem. Commun.* **2013**, *49* (89), 10489.
- (84) Alford, J. M.; Diener, M. D. Isolation and Properties of Small-Bandgap Fullerenes. *Nature* **1998**,

393 (6686), 668–671.

- (85) Tshuchiya, T.; Wakahara, T.; Shirakura, S.; Maeda, Y.; Akasaka, T.; Kobayashi, K.; Nagase, S.; Kato, T.; Kadish, K. M. Reduction of Endohedral Metallofullerenes: A Convenient Method for Isolation. *Chem. Mater.* **2004**, *16* (12), 4343–4346.
- (86) Fuchs, D.; Rietschel, H.; Michel, R. H.; Fischer, A.; Weis, P.; Kappes, M. M. Extraction and Chromatographic Elution Behavior of Endohedral Metallofullerenes: Inferences Regarding Effective Dipole Moments. *J. Phys. Chem.* **1996**, *100* (2), 725–729.
- (87) Vol, C. S.; Science, E.; Britain, G. Synthesis, Extraction and Electronic Structure of Ce@C_{2n}. *Pergamon* **2000**, *58* (I), 1873–1876.
- (88) Anderson, M. R.; Dorn, H. C.; Stevenson, S. A. Making Connections between Metallofullerenes and Fullerenes: Electrochemical Investigations. *Carbon N. Y.* **2000**, *38* (11), 1663–1670.
- (89) Kubozono, Y.; Maeda, H.; Takabayashi, Y.; Hiraoka, K.; Nakai, T.; Kashino, S.; Emura, S.; Ukita, S.; Sogabe, T. Extractions of Y@C₆₀, Ba@C₆₀, La@C₆₀, Ce@C₆₀, Pr@C₆₀, Nd@C₆₀ and Gd@C₆₀ with Aniline. *J. Am. Chem. Soc.* **2000**, *7863* (96), 6998–6999.
- (90) Kareev, I. E.; Bubnov, V. P.; Laukhina, E. E.; Dodonov, A. F.; Kozlovski, V. I.; Yagubskii, E. B. Experimental Evidence in Support of the Formation of Anionic Endohedral Metallofullerenes During Their Extraction with N, N-Dimethylformamide. *Fullerenes, Nanotub. Carbon Nanostructures* **2005**, *12* (1–2), 65–69.
- (91) Tsuchiya, T.; Wakahara, T.; Lian, Y.; Maeda, Y.; Akasaka, T.; Kato, T.; Mizorogi, N.; Nagase, S. Selective Extraction and Purification of Endohedral Metallofullerene from Carbon Soot. *J. Phys. Chem. B* **2006**, *110* (45), 22517–22520.
- (92) Bolskar, R. D.; Alford, J. M. Chemical Oxidation of Endohedral Metallofullerenes: Identification and Separation of Distinct Classes. *Chem. Commun. (Camb)*. **2003**, *72* (11), 1292–1293.
- (93) Elliott, B.; Yu, L.; Echegoyen, L. A Simple Isomeric Separation of D_{5h} and I_h Sc₃N@C₈₀ by Selective Chemical Oxidation. *J. Am. Chem. Soc.* **2005**, *127* (31), 10885–10888.
- (94) Cerón, M. R.; Li, F.-F.; Echegoyen, L. An Efficient Method to Separate Sc₃N@C₈₀ I_h and D_{5h} Isomers and Sc₃N@C₇₈ by Selective Oxidation with Acetylferrocenium [Fe(COCH₃C₅H₄)Cp]⁺. *Chemistry* **2013**, *19* (23), 7410–7415.
- (95) Aoyagi, S.; Nishibori, E.; Sawa, H.; Sugimoto, K.; Takata, M.; Miyata, Y.; Kitaura, R.; Shinohara, H.; Okada, H.; Sakai, T.; Ono, Y.; Kawachi, K.; Yokoo, K.; Ono, S.; Omote, K.; Kasama, Y.; Ishikawa, S.; Komuro, T.; Tobita, H. A Layered Ionic Crystal of Polar Li@C₆₀ Superatoms. *Nat.*

- Chem.* **2010**, 2 (8), 678–683.
- (96) Stevenson, S.; Harich, K.; Yu, H.; Stephen, R. R.; Heaps, D.; Coumbe, C.; Phillips, J. P. Nonchromatographic “Stir and Filter Approach” (SAFA) for Isolating Sc₃N@C₈₀ Metallofullerenes. *Sci. Technol.* **2006**, No. 12, 8829–8835.
- (97) Stevenson, S.; Mackey, M. A.; Coumbe, C. E.; Phillips, J. P.; Elliott, B.; Echegoyen, L. Rapid Removal of D_{5h} Isomer Using the “Stir and Filter Approach” and Isolation of Large Quantities of Isomerically Pure Sc₃N@C₈₀ Metallic Nitride Fullerenes. *J. Am. Chem. Soc.* **2007**, 129 (19), 6072–6073.
- (98) Stevenson, S.; Rottinger, K. a; Field, J. S. Fractionation of Rare-Earth Metallofullerenes via Reversible Uptake and Release from Reactive Silica. *Dalton Trans.* **2014**, 43 (20), 7435–7441.
- (99) Olah, G. A.; Bucsi, I.; Lambert, C.; Aniszfeld, R.; Trivedi, N. J.; Sensharma, D. K. Polyarenefullerenes, Ca(H-Ar)_n, Obtained by Acid-Catalyzed Fullerenation of Aromaticd. *Biochemistry* **1991**, No. 17, 9387–9388.
- (100) Bucsi, I.; Aniszfeld, R.; Shamma, T.; Prakash, G. K.; Olah, G. a. Convenient Separation of High-Purity C₆₀ from Crude Fullerene Extract by Selective Complexation with AlCl₃. *Proc. Natl. Acad. Sci.* **1994**, 91 (19), 9019–9021.
- (101) Stevenson, S.; Mackey, M. A.; Pickens, J. E.; Stuart, M. A.; Confait, B. S.; Phillips, J. P. Selective Complexation and Reactivity of Metallic Nitride and Oxometallic Fullerenes with Lewis Acids and Use as an Effective Purification Method. *Inorg. Chem.* **2009**, 48 (24), 11685–11690.
- (102) Alexey A. Popov, Ning Chen, Julio R. Pinzón, Steven Stevenson, Luis A. Echegoyen, and L. D. Redox-Active Scandium Oxide Cluster inside a Fullerene Cage: Spectroscopic, Voltammetric, Electron Spin Resonance Spectroelectrochemical, and Extended Density Functional Theory Study of Sc₄O₂@C₈₀ and Its Ion Radicals. *J. Am. Chem. Soc.* **2012**, 134 (48), 19607–19618.
- (103) Akiyama, K.; Hamano, T.; Nakanishi, Y.; Takeuchi, E.; Noda, S.; Wang, Z.; Kubuki, S.; Shinohara, H. Non-HPLC Rapid Separation of Metallofullerenes and Empty Cages with TiCl₄ Lewis Acid. *J. Am. Chem. Soc.* **2012**, 134 (23), 9762–9767.
- (104) Wang, Z.; Nakanishi, Y.; Noda, S.; Akiyama, K.; Shinohara, H. The Origin and Mechanism of Non-HPLC Purification of Metallofullerenes with TiCl₄. *J. Phys. Chem. C* **2012**, 116 (48), pp 25563–25567.
- (105) Cai, T.; Xu, L.; Shu, C.; Champion, H. A.; Reid, J. E.; Anklin, C.; Anderson, M. R.; Gibson, H. W.; Dorn, H. C. Selective Formation of a Symmetric Sc₃N@C₇₈ Bisadduct: Adduct Docking

- Controlled by an Internal Trimetallic Nitride Cluster. *J. Am. Chem. Soc.* **2008**, *130* (7), 2136–2137.
- (106) Yang, S.; Rapta, P.; Dunsch, L. The Spin State of a Charged Non-IPR Fullerene: The Stable Radical Cation of Sc₃N@C₆₈. *Chem. Commun. (Camb)*. **2007**, *80* (2), 189–191.
- (107) Cai, T.; Xu, L.; Anderson, M. R.; Ge, Z.; Zuo, T.; Wang, X.; Olmstead, M. M.; Balch, A. L.; Gibson, H. W.; Dorn, H. C. Structure and Enhanced Reactivity Rates of the D_{5h} Sc₃N@C₈₀ and Lu₃N@C₈₀ Metallofullerene Isomers : The Importance of the Pyracylene Motif. *J. Am. Chem. Soc.* **2006**, No. 128, 8581/8589.
- (108) Krause, M.; Dunsch, L. Isolation and Characterisation of Two Sc₃N@C₈₀ Isomers. *ChemPhysChem* **2004**, *5* (9), 1445–1449.
- (109) Stevenson, S.; Rottinger, K. A.; Fahim, M.; Field, J. S.; Martin, B. R.; Arvola, K. D. Tuning the Selectivity of Gd₃N Cluster Endohedral Metallofullerene Reactions with Lewis Acids. *Inorg. Chem.* **2014**, *53* (24), 12939–12946.
- (110) Chaur, M. N.; Melin, F.; Elliott, B.; Athans, A. J.; Walker, K.; Holloway, B. C.; Echegoyen, L. Gd₃N@C_{2n} (N = 40, 42, and 44): Remarkably Low HOMO-LUMO Gap and Unusual Electrochemical Reversibility of Gd₃N@C₈₈. *J. Am. Chem. Soc.* **2007**, *129* (47), 14826–14829.
- (111) Stevenson, S.; Arvola, K. D.; Fahim, M.; Martin, B. R.; Ghiassi, K. B.; Olmstead, M. M.; Balch, A. L. Isolation and Crystallographic Characterization of Gd₃N@D₂(35)-C₈₈ through Non-Chromatographic Methods. *Inorg. Chem.*, **2016**, *55* (1), 62–67
- (112) Brownson, D. A. C.; Banks, C. E. *Interpreting Electrochemistry*; 2014.
- (113) Connelly, N. G.; Geiger, W. E. Chemical Redox Agents for Organometallic Chemistry. *Chem. Rev.* **1996**, *96* (2), 877–910.
- (114) Suzuki, Toshiyasu, et al. Electrochemical Properties of La@C₈₂. *J. Am. Chem. Soc.* **1993**, *115*.23, 1106–1107.
- (115) Suzuki T, Kikuchi K, O. F. Electrochemical Properties of Fullerenolanthanides. *Tetrahedron* **1996**, No. 52 (14), 4973–4982.
- (116) Qingshan X., Perez-Cordero E., Echegoyen L. Electrochemical Detection of (C₆₀)⁶⁻ and (C₇₀)⁶⁻: Enhanced Stability of Fullerides in Solution. *J. Am. Chem. Soc.* **1992**, *114*, 10, 3978–3980.
- (117) Zalibera, M.; Popov, A. A.; Kalbac, M.; Rapta, P.; Dunsch, L. The Extended View on the Empty C₂(3)-C₈₂ Fullerene: Isolation, Spectroscopic, Electrochemical, and Spectroelectrochemical

- Characterization and DFT Calculations. *Chem. – A Eur. J.* **2008**, *14* (32), 9960–9967.
- (118) Gao, X.; Caemelbecke, E. Van; Kadish, K. M. Visible and Near-Infrared Absorption Spectra of Singly and Doubly Reduced C₇₆ Fullerene Anions. *Electrochem. Solid-State Lett.* **1998**, *1* (5), 222–223.
- (119) Zalibera, M.; Rapta, P.; Popov, A. A.; Dunsch, L. Charged States of Four Isomers of C₈₄ Fullerene : In Situ ESR and Vis - NIR Spectroelectrochemistry and DFT Calculations. *J. Phys. Chem. C* **2009**, *113*, 5141–5149.
- (120) Reed, C. a; Bolskar, R. D. Discrete Fulleride Anions and Fullerenium Cations. *Chem. Rev.* **2000**, *100* (3), 1075–1120.
- (121) Zhang, Y.; Popov, A. A. Transition-Metal and Rare-Earth-Metal Redox Couples inside Carbon Cages: Fullerenes Acting as Innocent Ligands. *Organometallics* **2014**, *33* (18), 4537–4549.
- (122) Aoyagi S, Nishibori E, S. H. A Layered Ionic Crystal of Polar Li@C₆₀ Superatoms. *Nat Chem* **2010**, *2* (8), 678–683.
- (123) Okada, H.; Komuro, T.; Sakai, T.; Matsuo, Y.; Ono, Y.; Omote, K.; Yokoo, K.; Kawachi, K.; Kasama, Y.; Ono, S.; Hatakeyama, R.; Kaneko, T.; Tobita, H. Preparation of Endohedral Fullerene Containing Lithium (Li@C₆₀) and Isolation as Pure Hexafluorophosphate Salt ([Li+@C₆₀][PF₆-]). *RSC Adv.* **2012**, *2* (28), 10624.
- (124) Lu, X.; Slanina, Z.; Akasaka, T.; Tsuchiya, T.; Mizorogi, N.; Nagase, S. Yb@C_{2n} (N = 40, 41, 42): New Fullerene Allotropes with Unexplored Electrochemical Properties. *J. Am. Chem. Soc.* **2010**, *132* (16), 5896–5905.
- (125) Hu, Z.; Hao, Y.; Slanina, Z.; Gu, Z.; Shi, Z.; Uhl'ik, F.; Zhao, Y.; Feng, L. Popular C₈₂ Fullerene Cage Encapsulating a Divalent Metal Ion Sm²⁺: Structure and Electrochemistry. *Inorg. Chem.* **2015**, *54* (5), 2103–2108.
- (126) Xu, W.; Niu, B.; Feng, L.; Shi, Z.; Lian, Y. Access to an Unexplored Chiral C₈₂ Cage by Encaging a Divalent Metal: Structural Elucidation and Electrochemical Studies of Sm@C₂(5)-C₈₂. *Chem. – A Eur. J.* **2012**, *18* (45), 14246–14249.
- (127) Cao, B.; Wakahara, T.; Tsuchiya, T.; Kondo, M.; Maeda, Y.; Aminur Rahman, G. M.; Akasaka, T.; Kobayashi, K.; Nagase, S.; Yamamoto, K. Isolation, Characterization, and Theoretical Study of La₂@C₇₈. *J. Am. Chem. Soc.* **2004**, *126* (30), 9164–9165.
- (128) Suzuki, T.; Maruyama, Y.; Kato, T.; Kikuchi, K.; Nakao, Y.; Achiba, Y.; Kobayashi, K.; Nagase, S. Electrochemistry and Ab Initio Study of the Dimetallofullerene La₂@C₈₀. *Angew. Chemie Int.*

Ed. English **1995**, 34 (10), 1094–1096.

- (129) Yamada, M.; Nakahodo, T.; Wakahara, T.; Tsuchiya, T.; Maeda, Y.; Akasaka, T.; Kako, M.; Yoza, K.; Horn, E.; Mizorogi, N.; Kobayashi, K.; Nagase, S. Positional Control of Encapsulated Atoms inside a Fullerene Cage by Exohedral Addition. *J. Am. Chem. Soc.* **2005**, 127 (42), 14570–14571.
- (130) Kurihara, H.; Lu, X.; Iiduka, Y.; Mizorogi, N.; Slanina, Z.; Tsuchiya, T.; Nagase, S.; Akasaka, T. Sc₂@C_{3v}(8)-C₈₂ vs. Sc₂C₂@C_{3v}(8)-C₈₂: Drastic Effect of C₂ Capture on the Redox Properties of Scandium Metallofullerenes. *Chem. Commun. (Camb)*. **2012**, 48 (9), 1290–1292.
- (131) Suzuki T, Kikuchi K, O. F. et al. Electrochemical Properties of Fullerenolanthanides. *Tetrahedron* **1996**, 52 (14), :4973–4982.
- (132) Cao, B.; Wakahara, T.; Tsuchiya, T.; Kondo, M.; Maeda, Y.; Rahman, G. M. A.; Akasaka, T.; Kobayashi, K.; Nagase, S.; Yamamoto, K. Isolation, Characterization, and Theoretical Study of La₂@C₇₈. *J. Am. Chem. Soc.* **2004**, 126 (30), 9164–9165.
- (133) Yamada, M.; Wakahara, T.; Tsuchiya, T.; Maeda, Y.; Kako, M.; Akasaka, T.; Yoza, K.; Horn, E.; Mizorogi, N.; Nagase, S. Location of the Metal Atoms in Ce₂@C₇₈ and Its Bis-Silylated Derivative. *Chem. Commun. (Camb)*. **2008**, 36 (5), 558–560.
- (134) Cardona, C. M.; Elliott, B.; Echegoyen, L. Unexpected Chemical and Electrochemical Properties of M₃N@C₈₀ (M = Sc, Y, Er). *J. Am. Chem. Soc.* **2006**, 128 (19), 6480–6485.
- (135) Jakes, P.; Dinse, K.-P. Chemically Induced Spin Transfer to an Encased Molecular Cluster: An EPR Study of Sc₃N@C₈₀ Radical Anions. *J. Am. Chem. Soc.* **2001**, 123 (7), 8854–8855.
- (136) Yang, S.; Zalibera, M.; Rapta, P.; Dunsch, L. Charge-Induced Reversible Rearrangement of Endohedral Fullerenes: Electrochemistry of Tridysprosium Nitride Clusterfullerenes Dy₃N@C_{2n} (2n=78, 80). *Chem. – A Eur. J.* **2006**, 12 (30), 7848–7855.
- (137) Wei, T.; Wang, S.; Liu, F.; Tan, Y.; Zhu, X.; Xie, S.; Yang, S. Capturing the Long-Sought Small-Bandgap Endohedral Fullerene Sc₃N@C₈₂ with Low Kinetic Stability. *J. Am. Chem. Soc.* **2015**, 137 (8), 3119–3123.
- (138) Chaur, M. N.; Melin, F.; Elliott, B.; Kumbhar, A.; Athans, A. J.; Echegoyen, L. New M₃N@C_{2n} Endohedral Metallofullerene Families (M=Nd, Pr, Ce; n=40–53): Expanding the Preferential Templating of the C₈₈ Cage and Approaching the C₉₆ Cage. *Chem. – A Eur. J.* **2008**, 14 (15), 4594–4599.
- (139) Chaur, M. N.; Valencia, R.; Rodríguez-Forteza, A.; Poblet, J. M.; Echegoyen, L. Trimetallic Nitride Endohedral Fullerenes: Experimental and Theoretical Evidence for the M₃N⁶⁺@C_{2n}⁶⁻ Model.

Angew. Chemie Int. Ed. **2009**, *48* (8), 1425–1428.

- (140) Chaur, M. N.; Aparicio-Anglès, X.; Mercado, B. Q.; Elliott, B.; Rodríguez-Forteza, A.; Clotet, A.; Olmstead, M. M.; Balch, A. L.; Poblet, J. M.; Echegoyen, L. Structural and Electrochemical Property Correlations of Metallic Nitride Endohedral Metallofullerenes. *J. Phys. Chem. C* **2010**, *114* (30), 13003–13009.
- (141) Robinson, J. R.; Qiao, Y.; Gu, J.; Carroll, P.; Walsh, P.; Schelter, E. J. The Role of Dynamic Ligand Exchange in the Oxidation Chemistry of Cerium(III). *Chem. Sci.* **2016**, *0*, 1–11.
- (142) Vargová, A.; Popov, A.; Rapta, P.; Sun, B.; Zhang, L.; Dunsch, L. Electrochemical Tuning of Spin States of the Endohedral Metallofullerene Y@C₈₂ as Probed by ESR Spectroelectrochemistry. *Chemphyschem* **2010**, *11* (8), 1650–1653.
- (143) Sc, C. C. N. C. M.; Zhang, Y.; Schiemenz, S.; Popov, A. A.; Dunsch, L. Strain-Driven Endohedral Redox Couple CeIV/CeIII in Nitride. *J. Phys. Chem. Lett* **2013**, *4*, 2404–2409.
- (144) Zhang, Y.; Popov, A. A.; Dunsch, L. Endohedral Metal or a Fullerene Cage Based Oxidation? Redox Duality of Nitride Clusterfullerenes Ce_xM_{3-x}N@C₇₈₋₈₈ (x=1,2; M = Sc and Y) Dictated by the Encaged Metals and the Carbon Cage Size. *Nanoscale* **2014**, *6* (2), 1038–1048.
- (145) Wei, T.; Wang, S.; Lu, X.; Tan, Y.; Huang, J.; Liu, F.; Li, Q.; Xie, S.; Yang, S. Entrapping a Group-VB Transition Metal, Vanadium, within an Endohedral Metallofullerene: V_xSc_{3-x}N@Ih-C₈₀ (x = 1, 2). *J. Am. Chem. Soc.* **2016**, *138* (1), 207–214.
- (146) Chen, C.; Liu, F.; Li, S.; Wang, N.; Popov, A. A.; Jiao, M.; Wei, T.; Li, Q.; Dunsch, L.; Yang, S. Titanium/yttrium Mixed Metal Nitride Clusterfullerene TiY₂N@C₈₀: Synthesis, Isolation, and Effect of the Group-III Metal. *Inorg. Chem.* **2012**, *51* (5), 3039–3045.
- (147) Junghans, K.; Rosenkranz, M.; Popov, A. A. Sc₃CH@C₈₀ : Selective ¹³C Enrichment of the Central Carbon Atom. *Chem. Commun.* **2016**, *52*, 6561–6564.
- (148) Feng, Y.; Wang, T.; Wu, J.; Zhang, Z.; Jiang, L.; Han, H.; Wang, C. Electron-Spin Excitation by Implanting Hydrogen into Metallofullerene: The Synthesis and Spectroscopic Characterization of Sc₄C₂H@Ih-C₈₀. *Chem. Commun.* **2014**, *50* (81), 12166–12168.
- (149) Tang Q., Abella L, Hao Y., Li X., Wan Y, Rodríguez-Forteza A., Poblet J.M., i Feng Lai, and C. N. Sc₂O@C_{3v}(8)-C₈₂: A Missing Isomer of Sc₂O@C₈₂. *Inorg. Chem.* **2016**, *55* (4), 1926–1933.
- (150) Iiduka, Y.; Wakahara, T.; Nakajima, K.; Nakahodo, T.; Tsuchiya, T.; Maeda, Y.; Akasaka, T.; Yoza, K.; Liu, M. T. H.; Mizorogi, N.; Nagase, S. Experimental and Theoretical Studies of the Scandium Carbide Endohedral Metallofullerene Sc₂C₂@C₈₂ and Its Carbene Derivative. *Angew. Chemie*

- 2007**, *119* (29), 5658–5660.
- (151) Chaur, M. N.; Athans, A. J.; Echegoyen, L. Metallic Nitride Endohedral Fullerenes: Synthesis and Electrochemical Properties. *Tetrahedron* **2008**, *64* (50), 11387–11393.
- (152) Popov, A. A.; Chen, C.; Yang, S.; Lipps, F.; Dunsch, L. Spin-Flow Vibrational Spectroscopy of Molecules with Flexible Spin Density : *ACS Nano* **2010**, *4* (8), 4857–4871.
- (153) Stoll, S.; Schweiger, A. EasySpin: Simulating Cw ESR Spectra. *Biol. Magn. Reson.* **2007**, *27*, 299–321.
- (154) Seifert, G.; Bartl, A.; Dunsch, L.; Ayuela, A.; Rockenbauer, A. Electron Spin Resonance Spectra: Geometrical and Electronic Structure of Endohedral Fullerenes. *Appl. Phys. A Mater. Sci. Process.* **1998**, *66* (3), 265–271.
- (155) Zuo, T.; Xu, L.; Beavers, C. M.; Olmstead, M. M.; Fu, W.; Crawford, T. D.; Balch, A. L.; Dorn, H. C. M₂@C₇₉N (M = Y, Tb): Isolation and Characterization of Stable Endohedral Metallofullerenes Exhibiting M-M Bonding Interactions inside aza[80]fullerene Cages. *J. Am. Chem. Soc.* **2008**, *130* (39), 12992–12997.
- (156) Shinohara, H.; Sato, H.; Ohkohchi, M.; Ando, Y.; Kodama, T.; Shida, T.; Kato, T.; Saito, Y. *Nature* **1992**, *357*, 52-54.
- (157) Yannoni, C. S.; Hoinkis, M.; de Vries, M. S.; Bethune, D. S.; Salem, J. R.; Crowder, M. S.; Johnson, R. D. Scandium Clusters in Fullerene Cages. *Science* (80-.). **1992**, *256* (April), 1191–1192.
- (158) Yamada, M.; Kurihara, H.; Suzuki, M.; Guo, J. D.; Waelchli, M.; Olmstead, M. M.; Balch, A. L.; Nagase, S.; Maeda, Y.; Hasegawa, T.; Lu, X.; Akasaka, T. Sc₂@C₆₆ Revisited: An Endohedral Fullerene with Scandium Ions Nestled within Two Unsaturated Linear Triquinanes. *J. Am. Chem. Soc.* **2014**, *136* (21), 7611–7614.
- (159) Kato, T. Metal Dimer and Trimer within Spherical Carbon Cage. *J. Mol. Struct.* **2007**, *838* (1–3), 84–88.
- (160) Wang, T.; Wu, J.; Feng, Y.; Ma, Y.; Jiang, L.; Shu, C.; Wang, C. Preparation and ESR Study of Sc₃C₂@C₈₀ Bis-Addition Fulleropyrrolidines. *Dalt. Trans.* **2012**, *41* (9), 2567.
- (161) Ma, Y.; Wang, T.; Wu, J.; Feng, Y.; Jiang, L.; Shu, C.; Wang, C. Susceptible Electron Spin Adhering to an Yttrium Cluster inside an Azafullerene C₇₉N. *Chem. Commun.* **2012**, *48* (94), 11570–11572.
- (162) Morton, J. J. L.; Tiwari, A.; Dantelle, G.; Porfyrakis, K.; Ardavan, A.; Briggs, G. A. D. Switchable

- ErSc₂N Rotor within a C₈₀ Fullerene Cage: An Electron Paramagnetic Resonance and Photoluminescence Excitation Studies. *Phys. Rev. Lett.* **2008**, *101* (1), 13002.
- (163) Yang, S.; Popov, A. A.; Dunsch, L. Carbon Pyramidalization in Fullerene Cages Induced by the Endohedral Cluster: Non-Scandium Mixed Metal Nitride Clusterfullerenes. *Angew. Chemie - Int. Ed.* **2008**, *47* (43), 8196–8200.
- (164) Junghans, K.; Schlesier, C.; Kostanyan, A.; Samoylova, N. A.; Deng, Q.; Rosenkranz, M.; Schiemenz, S.; Westerström, R.; Greber, T.; Büchner, B.; Popov, A. A. Methane as a Selectivity Booster in the Arc-Discharge Synthesis of Endohedral Fullerenes: Selective Synthesis of the Single-Molecule Magnet Dy₂TiC@C₈₀ and Its Congener Dy₂TiC₂@C₈₀. *Angew. Chemie - Int. Ed.* **2015**, *54* (45), 13411–13415.
- (165) Kong, H. Systematic Isolation of Endohedral Fullerenes Containing. **1997**, *58* (li), 1661–1667.
- (166) Okazaki, T.; Lian, Y.; Gu, Z.; Suenaga, K.; Hisanori Shinohara. Isolation and Spectroscopic Characterization of Sm-Containing Metallofullerenes. *Chem. Phys. Lett.* **2000**, *320* (5–6), 435–440.
- (167) Popov, A. A.; Avdoshenko, S. M.; Pendás, A. M.; Dunsch, L. Bonding between Strongly Repulsive Metal Atoms: An Oxymoron Made Real in a Confined Space of Endohedral Metallofullerenes. *Chem. Commun.* **2012**, *48*, 8031.
- (168) Valencia, R.; Rodríguez-Forteza, A.; Poblet, J. M. Understanding the Stabilization of Metal Carbide Endohedral Fullerenes M₂C₂@C₈₂ and Related Systems. *J. Phys. Chem. A* **2008**, *112* (20), 4550–4555.
- (169) Popov, A. A. Metal-Cage Bonding, Molecular Structures and Vibrational Spectra of Endohedral Fullerenes: Bridging Experiment and Theory. *Journal of Computational and Theoretical Nanoscience*. 2009, 292–317.
- (170) Okazaki, T.; Suenaga, K.; Lian, Y.; Gu, Z.; Shinohara, H. Intrafullerene Electron Transfers in Sm-Containing Metallofullerenes : Sm@C_{2n}. *Journal of Molecular Graphics and Modelling* **2001**, *3263* (0), 244–251.
- (171) A., P. A.; Dunsch, L. Bonding in Endohedral Metallofullerenes as Studied by Quantum Theory of Atoms in Molecules. *Chem. – A Eur. J.* **2009**, *15* (38), 9707–9729.
- (172) Kalemou, A.; Kaplan, I. G.; Mavridis, A. The Sc₂ Dimer Revisited. *J. Chem. Phys.* **2010**, *132* (2), 1–7.
- (173) Cao, X.; Dolg, M. Pseudopotential Study of Lanthanum and Lutetium Dimers. *Theor. Chem. Acc.*

- 2002, 108 (3), 143–149.
- (174) Y. Ralchenko, A. E. K. and J. R. NIST Atomic Database. *Natl. Inst. Stand. Technol. Gaithersbg.* **2011**.
- (175) Huang, Z.; Ye, L.; Yang, Z.; Xie, X. Interaction between Er Atoms and the Carbon Cage C82. *Phys. Rev. B* **2000**, 61 (19), 12786–12791.
- (176) Popov, A.; Zhang, L.; Dunsch, L.; Plasmon-Enhanced Photoemission from a Single Y3N@C80 Fullerene *ACS Nano*. **2010**, 4 (2), 7444–7447.
- (177) Yang, T.; Zhao, X.; Osawa, E. Can a Metal–Metal Bond Hop in the Fullerene Cage? *Chem. – A Eur. J.* **2011**, 17 (37), 10230–10234.
- (178) Wang, J.; Irle, S. No Title. *ECS Meeting Abstracts*. 2011, p 1782.
- (179) Lu, X.; Nakajima, K.; Iiduka, Y.; Nikawa, H.; Mizorogi, N.; Slanina, Z.; Tsuchiya, T.; Nagase, S.; Akasaka, T. Structural Elucidation and Regioselective Functionalization of An Unexplored Carbide Cluster Metallofullerene Sc2C2@Cs(6)-C82. **2011**, No. 6, 19553–19558.
- (180) Weltner, W.; McLeod, D.; Kasai, P. H. ESR and Optical Spectroscopy of ScO, YO, and LaO in Neon and Argon Matrices; Establishment of Their Ground Electronic States. *J. Chem. Phys.* **1967**, 46, 3172–3184.
- (181) Rieger, P. H. *Electron Spin Resonance Analysis and Interpretation*; 2007.
- (182) Wang, Z.; Kitaura, R.; Shinohara, H. Metal-Dependent Stability of Pristine and Functionalized Unconventional Dimetallofullerene M2@Ih-C80. *J. Phys. Chem. C* **2014**, 118 (25), 13953–13958.
- (183) Tagmatarchis, N.; Shinohara, H. Production, Separation, Isolation, and Spectroscopic Study of Dysprosium Endohedral Metallofullerenes. *Chem. Mater.* **2000**, 12 (10), 3222–3226.
- (184) Kareev I. E., Bubnov V.P., Y. E. B. Endohedral Gadolinium-Containing Metallofullerenes in the Trifluoromethylation Reaction. *Russ Chem Bull* **2008**, 57, 1486–1491.
- (185) Kareev, I. E.; Lebedkin, S. F.; Bubnov, V. P.; Yagubskii, E. B.; Ioffe, I. N.; Khavrel, P. A.; Kuvychko, I. V.; Strauss, S. H.; Boltalina, O. V. Trifluoromethylated Endohedral Metallofullerenes: Synthesis and Characterization of Y@C82(CF3)5. *Angew. Chemie - Int. Ed.* **2005**, 44 (12), 1846–1849.
- (186) Yamada, M.; Kurihara, H.; Suzuki, M.; Saito, M.; Slanina, Z.; Uhlik, F.; Aizawa, T.; Kato, T.; Olmstead, M. M.; Balch, A. L.; Maeda, Y.; Nagase, S.; Lu, X.; Akasaka, T. Hiding and Recovering Electrons in a Dimetallic Endohedral Fullerene: Air-Stable Products from Radical Additions. *J. Am. Chem. Soc.* **2015**, 137 (1), 232–238.

- (187) Liu F.; Krylov, D.; Spree, L.; Avdoshenko, S.; Samoylova, N.; Kostanyan, A.; Greber, T.; Wolter A.U.B.; Büchner, B.; Popov, A. A. High Blocking Temperature in Fullerene Molecule Magnet with Giant Exchange Coupling between Covalently-Bonded Lanthanide Ions. *Nat. Comm., In Press*.
- (188) Bao, L.; Chen, M.; Pan, C.; Yamaguchi, T.; Kato, T.; Olmstead, M. M.; Balch, A. L.; Akasaka, T.; Lu, X. Crystallographic Evidence for Direct Metal-Metal Bonding in a Stable Open-Shell La₂@Ih-C80 Derivative. *Angew. Chemie - Int. Ed.* **2016**, *55* (13), 4242–4246.
- (189) Iiduka, Y.; Wakahara, T.; Nakahodo, T.; Tsuchiya, T.; Sakuraba, A.; Maeda, Y.; Akasaka, T.; Yoza, K.; Horn, E.; Kato, T.; Liu, M. T. H.; Mizorogi, N.; Kobayashi, K.; Nagase, S. Structural Determination of Metallofullerene: A Surprising Finding. *J. Am. Chem. Soc.* **2005**, *127* (36), 12500–12501.
- (190) Yang, S.; Chen, C.; Popov, A. A.; Zhang, W.; Liu, F.; Dunsch, L. An Endohedral Titanium(III) in a Clusterfullerene: Putting a Non-Group-III Metal Nitride into the C80-Ih Fullerene Cage. *Chem. Commun.* **2009**, *2* (42), 6391.
- (191) Shannon, R. D. Revised Effective Ionic Radii and Systematic Studies of Interatomic Distances in Halides and Chalcogenides. *Acta Crystallogr. Sect. A* **1976**, *32* (5), 751–767.
- (192) Perdew, J. P.; Burke, K.; Ernzerhof, M. Generalized Gradient Approximation Made Simple. *Phys. Rev. Lett.* **1996**, *77* (18), 3865–3868.
- (193) Laikov, D. N. Fast Evaluation of Density Functional Exchange-Correlation Terms Using the Expansion of the Electron Density in Auxiliary Basis Sets. *Chem. Phys. Lett.* **1997**, *281* (1), 151–156.
- (194) Neese, F. The ORCA Program System. *Wiley Interdiscip. Rev. Comput. Mol. Sci.* **2012**, *2* (1), 73–78.
- (195) Humphrey, W.; Dalke, A.; Schulten, K. VMD: Visual Molecular Dynamics. *Journal of Molecular Graphics*. 1996, pp 33–38.
- (196) Samoylova, N. A.; Avdoshenko, S. M.; Krylov, D. S.; Thompson, H. R.; Kirkhorn, A. C.; Rosenkranz, M.; Schiemenz, S.; Ziegls, F.; Wolter, A. U. B.; Yang, S.; Stevenson, S.; Popov, A. A. Confining the Spin between Two Metal Atoms within the Carbon Cage: Redox-Active Metal-Metal Bonds in Dimetallofullerenes and Their Stable Cation Radicals. *Nanoscale, In press*.
- (197) Junghans, K.; Ghiassi, K. B.; Samoylova, N. A.; Deng, Q.; Rosenkranz, M.; Olmstead, M. M.; Balch, A. L.; Popov, A. A. Synthesis and Isolation of the Titanium–Scandium Endohedral Fullerenes—Sc₂TiC@IhC80, Sc₂TiC@D5h-C80 and Sc₂TiC₂@Ih-C80: Metal Size Tuning of the.

Chem. Eur. J. **2016**, *22* (37).

List of Publications.

1. [6,6]-Open and [6,6]-closed isomers of $C_{70}(CF_2)$: Synthesis, electrochemical and quantum chemical investigation. N. Samoylova, N. Belov, V. Brotsman, I. Ioffe, N. Lukonina, V. Markov, A. Ruff, A. Rybalchenko, P. Schuler, O. Semivrazhskaya, B. Speiser, S. I. Troyanov, T. V. Magdesieva, A. A. Goryunkov, *Chem. Eur. J.* 2013, 19(52), 17969–17979 DOI: 10.1002/chem.201302946.

2. Magnetic moments and exchange coupling in nitride clusterfullerenes $Gd_xSc_{3-x}N@C_{80}$ ($x = 1-3$). A. Svitova, Y. Krupskaya, N. Samoylova, R. Kraus, J. Geck, L. Dunsch, A. A. Popov. *Dalton Trans.* 2014, 43, 7387-7390. DOI: 10.1039/C3DT53367K

3. Synthesis and Structure of $LaSc_2N@Cs(\text{hept})-C_{80}$ with One Heptagon and Thirteen Pentagons. Y. Zhang, K. B. Ghiassi, Q. Deng, N. Samoylova, M. M. Olmstead, A. L. Balch, A. A. Popov. *Angew. Chem. Int. Ed.* 2015, 54 (2), 495-499. DOI: 10.1002/anie.201409094

4. Methane as a selectivity booster in the synthesis of endohedral fullerenes: towards selective synthesis of the single molecule magnet $Dy_2TiC@C_{80}$ and its congener $Dy_2TiC_2@C_{80}$. K. Junghans, C. Schlesier, A. Kostanyan, N. A. Samoylova, Q. Deng, M. Rosenkranz, S. Schiemenz, R. Westerström, T. Greber, B. Büchner, A. A. Popov. *Angew. Chem. Int. Ed.* 2015, 54 (45), 13411-13415, DOI: 10.1002/anie.201505870

5. Synthesis and Isolation of the Titanium–Scandium Endohedral Fullerenes— $Sc_2TiC@Ih-C_{80}$, $Sc_2TiC@D_{5h}-C_{80}$ and $Sc_2TiC_2@Ih-C_{80}$: Metal Size Tuning of the TiIV/TiIII Redox Potentials. K. Junghans, K. B. Ghiassi, N. A. Samoylova, Q. Deng, M. Rosenkranz, M. M. Olmstead, A. L. Balch, A. A. Popov. *Chem. Eur. J.* 2016, 22 (37), 13098-13107. DOI: 10.1002/chem.201601655 .

6. Confining the Spin between Two Metal Atoms within the Carbon Cage: Redox-Active Metal-Metal Bonds in Dimetallofullerenes and Their Stable Cation Radicals. N. A. Samoylova, S. M. Avdoshenko, D. S. Krylov, H. R. Thompson, A. C. Kirkhorn, M. Rosenkranz, S. Schiemenz, F. Ziegls, A. U. B. Wolter, S. Yang, S. Stevenson, A. A. Popov. *Nanoscale*, In Press, DOI: 10.1039/C7NR02288C

7. High Blocking Temperature in Fullerene Molecule Magnet with Giant Exchange Coupling between Covalently-Bonded Lanthanide Ions. F. Liu, D. Krylov, L. Spree, S. Avdoshenko, N. Samoylova, A. Kostanyan, T. Greber, A.U. Wolter, B. Buchner, A. A. Popov In Press.

8. "Non-Chromatographic Separation of Endohedral Metallofullerenes by Utilizing Their Redox Properties" as a chapter in book "Endohedral Fullerenes: Electron Transfer and Spin" by Alexey A. Popov, S. Stevenson, N. Samoylova, A. A. Popov. Nanostructure Science and Technology by *Springer International Publishing*, 2017. In Press. DOI 10.1007/978-3-319-47049-8

Acknowledgements

Foremost, I would like to thank my supervisor, Dr. Alexey A. Popov, for his advices and suggestions during the planning and development of this research work. Also I would like to thank him for theoretical support during my studies. I deeply appreciate his guidance and contribution to my work.

I would like to express my sincere gratitude to Prof. Dr. Gotthard Seifert, Prof. Dr. Biprajit Sarkar and Prof. Dr. Bernd Büchner. Meanwhile, I would like to thank all the members of my dissertation committee.

I am very grateful to Sandra Schiemenz for IR and Raman measurements, to Dr. Stanislav Avdoshenko for DFT calculations, to Marco Rosenkranz for NMR and low-temperature EPR measurements and to Denis Krylov for the magnetic measurements. My special thanks go to Dr. Fupin Liu and Katrin Junghans for their interesting samples that they have kindly provided to me.

I would like to acknowledge several colleagues from our department, which includes Lukas Spree, Dr. Chia-Hsiang Chen, Dr. Peter Machata, Qingming Deng, Dr. Evgenia Dmitrieva, Dr. Yang Zhang, Denis Krylov, Ariane Brandenburg and Kristina Ditte. My special thanks are extended to the technician team: Sandra Schiemenz, Marco Rosenkranz, Alexander Berger and Frank Ziegs. The scientific and technical knowledge I have learnt from them, I will appreciate during the rest of my scientific career.

Also I would like to acknowledge Prof. Dr. Steven Stevenson, Hannah R. Thompson and Amelia C. Kirkhorn from the Indiana-Purdue University Fort Wayne for our fruitful collaboration in the $M_2@C_{82}$ research.

Finally, I would like to thank Prof. Dr. Lev. N. Sidorov and Dr. Alexey A. Goryunkov from Moscow State University for introducing me to the world of fullerenes many years ago.

I herewith declare that I have produced this paper without the prohibited assistance of third parties and without making use of aids other than those specified; notions taken over directly or indirectly from other sources have been identified as such. This paper has not previously been presented in identical or similar form to any other German or foreign examination board.
17.05.2017, Dresden

(N. Samoylova)